

UNIVERSIDAD NACIONAL AUTÓNOMA DE MÉXICO

POSGRADO EN CIENCIAS BIOLÓGICAS

FACULTAD DE MEDICINA

LA ACETOGENINA LAHERRADURINA Y EL ALCALOIDE LIRIODENINA PROMUEVEN LA INDUCCIÓN DE APOPTOSIS Y AUTOFAGIA MEDIANTE LA DESREGULACIÓN DE LA DINÁMICA MITOCONDRIAL EN CÁNCER COLORRECTAL *IN VITRO*

TESIS

QUE PARA OPTAR POR EL GRADO DE:

DOCTORA EN CIENCIAS

PRESENTA:

DELGADO WALDO ROCIO IZAMARY

DRA. NADIA JUDITH JACOBO HERRERA
INSTITUTO NACIONAL DE CIENCIAS MEDICAS Y NUTRICIÓN SALVADOR ZUBIRÁN.
DR. CARLOS GUADALUPE PERÉZ PLASENCIA
INSTUTITO NACIONAL DE CANCEROLOGÍA
DR. MARIANO MARTÍNEZ VÁZQUEZ
FACULTAD DE QUIMICA, UNAM

CIUDAD UNIVERSITARIA, CD. MX. DICIEMBRE, 2024.

Universidad Nacional Autónoma de México
UNAM
Biblioteca Central
Dirección General de Bibliotecas de la UNAM

UNAM – Dirección General de Bibliotecas
Tesis Digitales
Restricciones de uso

DERECHOS RESERVADOS ©
PROHIBIDA SU REPRODUCCIÓN TOTAL O PARCIAL

Todo el material contenido en esta tesis esta protegido por la Ley Federal del Derecho de Autor (LFDA) de los Estados Unidos Mexicanos (México).

El uso de imágenes, fragmentos de videos, y demás material que sea objeto de protección de los derechos de autor, será exclusivamente para fines educativos e informativos y deberá citar la fuente donde la obtuvo mencionando el autor o autores. Cualquier uso distinto como el lucro, reproducción, edición o modificación, será perseguido y sancionado por el respectivo titular de los Derechos de Autor.

PROTESTA UNIVERSITARIA DE INTEGRIDAD Y

HONESTIDAD ACADÉMICA Y PROFESIONAL

(Graduación con trabajo escrito)

De conformidad con lo dispuesto en los artículos 87, fracción V, del Estatuto General, 68, primer párrafo, del Reglamento General de Estudios Universitarios y 26, fracción I, y 35 del Reglamento General de Exámenes, me comprometo en todo tiempo a honrar a la institución y a cumplir con los principios establecidos en el Código de Ética de la Universidad Nacional Autónoma de México, especialmente con los de integridad y honestidad académica.

De acuerdo a lo anterior, manifiesto que el trabajo escrito titulado:

La acetogenina laherradurina y el alcaloide liriodenina promueven la inducción de apoptosis y autofagia mediante la desregulación de la dinámica mitocondrial en cáncer colorrectal *in vitro*

Que presenté para obtener el grado de DOCTOR(A) EN CIENCIAS, es original, de mí autoría y lo realicé con rigor metodológico exigido por el Programa de Posgrado en Ciencias Biológicas, citando las fuentes de ideas, textos, imágenes, gráficos u otro tipo de obras empleadas para su desarrollo.

En consecuencia, acepto que la falta de cumplimiento de las disposiciones reglamentarias y normativas de la Universidad, en particular las ya referenciadas en el Código de Ética, llevará a la nulidad de los actos de carácter académico administrativo del proceso de obtención de mi grado académico.

Atentamente



DELGADO WALDO ROCIO IZAMARY
No. de cuenta UNAM: 308076178



UNIVERSIDAD NACIONAL AUTÓNOMA DE MÉXICO

POSGRADO EN CIENCIAS BIOLÓGICAS

FACULTAD DE MEDICINA

LA ACETOGENINA LAHERRADURINA Y EL ALCALOIDE LIRIODENINA PROMUEVEN LA INDUCCIÓN DE APOPTOSIS Y AUTOFAGIA MEDIANTE LA DESREGULACIÓN DE LA DINÁMICA MITOCONDRIAL EN CÁNCER COLORRECTAL *IN VITRO*

TESIS

QUE PARA OPTAR POR EL GRADO DE:

DOCTORA EN CIENCIAS

PRESENTA:

DELGADO WALDO ROCIO IZAMARY

DRA. NADIA JUDITH JACOBO HERRERA
INSTITUTO NACIONAL DE CIENCIAS MEDICAS Y NUTRICIÓN SALVADOR ZUBIRÁN.
DR. CARLOS GUADALUPE PERÉZ PLASENCIA
INSTUTITO NACIONAL DE CANCEROLOGÍA
DR. MARIANO MARTÍNEZ VÁZQUEZ
FACULTAD DE QUIMICA, UNAM

CIUDAD UNIVERSITARIA, CD. MX. DICIEMBRE, 2024.

COORDINACIÓN GENERAL DE ESTUDIOS DE POSGRADO
COORDINACIÓN DEL POSGRADO EN CIENCIAS BIOLÓGICAS
ENTIDAD (FACULTAD DE MEDICINA)
OFICIO: CGEP/CPCB/FMED/0800/2024
ASUNTO: Oficio de Jurado

M. en C. Ivonne Ramírez Wence
Directora General de Administración Escolar, UNAM
P r e s e n t e

Me permito informar a usted que en la reunión ordinaria del Comité Académico del Posgrado en Ciencias Biológicas, celebrada el día **7 de octubre de 2024** se aprobó el siguiente jurado para el examen de grado de **DOCTORA EN CIENCIAS** de la estudiante **DELGADO WALDO ROCÍO IZAMARY** con número de cuenta **308076178** con la tesis titulada **"LA ACETOGENINA LAHERRADURINA Y EL ALCALOIDE LIRIODENINA PROMUEVEN LA INDUCCIÓN DE APOPTOSIS Y AUTOFAGIA MEDIANTE LA DESREGULACIÓN DE LA DINÁMICA MITOCONDRIAL EN CÁNCER COLORRECTAL *IN VITRO*",** realizada bajo la dirección de la **DRA. NADIA JUDITH JACOBO HERRERA,** quedando integrado de la siguiente manera:

Presidente:	DRA. VILMA ARACELI MALDONADO LAGUNAS
Vocal:	DR. ALEJANDRO ZENTELLA DEHESA
Vocal:	DRA. GISELA CEBALLOS CANCINO
Vocal:	DRA. MARÍA CONCEPCIÓN GUTIÉRREZ RUIZ
Secretario:	DR. MARIANO MARTÍNEZ VÁZQUEZ

Sin otro particular, me es grato enviarle un cordial saludo.

A T E N T A M E N T E
"POR MI RAZA HABLARÁ EL ESPÍRITU"
Ciudad Universitaria, Cd. Mx., a 29 de octubre de 2024

COORDINADOR DEL PROGRAMA

DR. ARTURO CARLOS II BECERRA BRACHO

c. c. p. Expediente del alumno

ACBB/RCHT/EARR/rcht

Agradecimientos institucionales

Al Posgrado en Ciencias Biológicas de la *Universidad Nacional Autónoma de México* (UNAM), mi querida alma mater, (me prome= que regresaría a esta casa de estudios y lo logré) por haberme brindado la oportunidad de formarme y desarrollarme académicamente durante el transcurso de mis estudios de doctorado, además me permiEó expandir mis horizontes y ver el mundo desde otra perspecEva. Por haberme apoyado con becas para realizar estancias en el extranjero, donde pude desenvolverme en nuevos ambientes, crecer cien=ficamente, aprender nuevas cosas y mejorar en otras, además de mejorar mi inglés y comenzar a fortalecer mi francés. Sin el posgrado, nada de esto hubiera sido posible, y por ello siempre le estaré profundamente agradecida.

Agradezco también *Consejo Nacional de Humanidades, Ciencias y Tecnologías (CONAHCyT)*, México, por la beca otorgada con el número de registro 779672, y al apoyo brindado por *CONAHCyT* con número de proyecto CB-2016-285884, que fueron esenciales para la conEnuación de mi trabajo experimental. Estos recursos no solo facilitaron mi invesEgación, sino que también me permiEeron seguir soñando y conEnuar mi camino en la ciencia.

Finalmente, mi más profundo agradecimiento a mis tutores, quienes no solo fueron mentores académicos, sino también pilares fundamentales en mi vida durante estos años. **A la Dra. Nadia, Dr. Carlos y Dr. Mariano**, no tengo palabras suficientes para expresar lo agradecida que estoy por todo lo que hicieron por mí. Ustedes me cobijaron, no solo como estudiante, sino como a una hija. Nunca me dejaron sola en los momentos di[ciles, siempre estuvieron ahí para ofrecerme su apoyo incondicional, su guía, su comprensión, y me dieron la confianza necesaria para seguir adelante. Me dieron mucho más que conocimientos; me dieron su cariño y eso es algo que llevaré conmigo toda la vida. A los demás miembros que formaron parte de mi jurado, también les agradezco por sus valiosas aportaciones, comentarios y sugerencias que contribuyeron a mi formación como invesEgadora y como persona.

Si no se reproduce automáticamente el audio. Dale play al botón de abajo o escanea este QR y escucha la canción adjunta mientras lees esta hoja.

Agradecimientos a título personal

¿Alguna vez has oído hablar del efecto mariposa? 🦋

Este concepto describe cómo pequeños cambios en las condiciones iniciales pueden tener un impacto significativo en el futuro. Es como ***el aleteo de una mariposa*** en Brasil provocará un tornado en Texas.

¿Por qué tiene sentido este primer párrafo en los agradecimientos de mi tesis? 🖨️

Porque cada detalle, cada momento y cada decisión te han llevado al instante en que lees estas líneas. Como dice una de mis películas favoritas 🎬y cito: ***"Sometimes we're on a collision course, and we just don't know it. Whether it's by accident or by design, there's not a thing we can do about it."*** (The curious case of benjamin button).

¿Qué pasaría si, por leer esta tesis, llegas cinco minutos tarde a tu destino? 🙄



Tal vez pierdas el metro, llegues tarde a tu destino, donde conocerás a una persona que solo iba a estar en ese preciso momento que tu llegaste, no antes, y esa persona cambiará tu vida 😱. O quizá no notes el impacto inmediato y solo veas los efectos años después. Tal vez te seguirás preguntando, ¿esto qué tiene que ver? 🙄 Pues justamente eso me paso a mí.

No haré tan larga la historia, pero resulta que una decisión tan pequeña puede cambiar totalmente el rumbo de las cosas. De eso se trata el efecto mariposa pues, ¿no?, como el hecho de encontrar una motivación para hacer una estancia en otro país. ***"Pos no que no tronabas pistolita"*** 🙈eso me dijeron porque yo no quería ir para allá, estaba negada a irme a otro país, ya sabes muchas cosas involucradas… mi zona de confort, mi familia, mi México, mis amigos, etc.

Pero dije ***"Chsm"*** 🤭 (nótese que es una abreviación de una mala palabra, coloquialmente dicha en México para decir "si lo hare"), ¿qué puede salir mal?

Debo de decir que no fue fácil, para empezar, no era solo decir ***"si quiero"*** y ya. Debía de hacer entrevistas con la Dra en Francia, planificar experimentos con mis tutores en México, estudiar para pasar mi candidatura en el posgrado, ordenar mis clases 🤓, resolver los experimentos fallidos 👩‍🔬, estudiar artículos, y tenía que tener en mente otras cosas como: dinero, deudas, papeles, vuelos, hospedaje, inglés, francés. En fin, todo eso debía tener en orden para poder ir a las Francias 🥹.

Hubo días que simplemente me quería rendir, es muy tormentoso todo esto de la burocracia en México, así como otras piedritas que se atravesaron en mi camino. En ese momento estuve a punto de tirar la toalla por lo difícil que se ponía y llegué a llorar de la desesperación 😭, porque no hay un instructivo que debas seguir para saber que tienes que hacer. Pero con lágrimas en los ojos, y cansada de todo, seguí. Y como decimos acá en México, ***"por un pelo de rana calva"*** (dícese de algo que por poco y pasa) y no lo logro 😔. Pero ya sabrán como va esta historia, lo logré y aquí ando.

Esta es solo una parte de todo lo que viví en ese año. Sería imposible resumirlo todo aquí. Ahora sí, ***"a lo que te truje Chencha"*** (es decir, vamos a lo importante). En esos momentos ***"soliloquiando"*** 🤪en Francia, me pregunté: ¿Qué habría pasado si no hubiera encontrado la motivación para ir? ¿Qué habría sido de mí si no hubiera luchado contra mis miedos? ¿Dónde estaría hoy? ¿Mi presente sería diferente? 🤔

Tal vez si, tal vez no, no lo sé. Pero ahora sabes a lo que me refería al inicio, cuando comencé a hablar del efecto mariposa, porque cada una de estas decisiones, no solo las tomadas por mí, si no las tomadas por otras personas, han repercutido en la vida de cada uno de nosotros, y me siento muy feliz en la manera en que han terminado para mí 😌.

Si no se reproduce automáticamente el audio. Dale play al botón de abajo o escanea este QR y escucha la canción adjunta mientras lees esta hoja.

Sabiendo ahora todo este discurso introductorio, no me queda más que decir gracias a todos los que de alguna manera han estado en mi vida, aunque sea unos segundos tan efímeros, o toda una temporada completa.

A mi familia: Mamá, Papá muchísimas gracias por siempre apoyarme en mis malas y buenas decisiones, por no dejarme "sola" y aunque sea en videollamada. Siempre se los he dicho, son mi más grande inspiración y los amo con toda mi alma ❤️. A mis hermanos, a Edén y Smaquenci bebé 🐶los rete amo, neta muchas gracias por darme fuerzas y apoyo motivacional para hacer lo que hice; por esos mensajes que me hacen mis días en nuestro chat de whats 💬.

A Hanxiao y Zhenrui, amigas, muchas gracias por las pláticas en el laboratorio. Me encantaba hablar de nuestros choques culturales y siempre la pasé genial con ustedes "– Iza: Hey, hru? 🤔 – Hanxiao: Tired. 😪 – Iza: What are you gonna do? – Hanxiao (singing): Work, work, work. – Iza (singing and laughing): Work, work, work! 🎶

A Yahir, porque es una personita que realmente admiro mucho. Amigo sin ti, nada de esto hubiera sido posible, y cada vez que te veo me dan muchas ganas de crecer como tú, no solo en lo laboral, ¡si no en lo personal también! 😌.

A la Dra. Svetlana, muchas gracias por haberme dado la oportunidad de ser parte de su laboratorio en Francia 🇫🇷. Gracias a usted me di cuenta de que realmente tengo un gran potencial en la ciencia, y su manera de expresarse sobre mi trabajo me ha motivado a querer seguir desarrollándome en este campo 🔬. Siempre recordaré su amabilidad y su comprensión cuando aún nos costaba expresarnos en inglés. Su apoyo ha sido invaluable en mi formación y en mi confianza como investigadora.

A mis amigos del laboratorio!!, Jossi bebé, mi hermano del alma, como en cada tesis te lo digo, y esta no será la excepción, eres mi ejemplo a seguir, te amo!. Eduardo bebesin! Muchas gracias por ser ese apoyo emocional que necesité, obvio también por toda la ayuda que me diste en el laboratorio, te quiero. ¡¡Rebeca bebé, te extraño mucho Amix!!: A mis demás amigos del lab: Oli, Sam, Fri, Janis 🫗🔬👩‍🔬🧪, los quiero, ¡están en mi cocoro! A todos los demás que, aunque no los mencioné saben que los quiero, los llevo en mi corazón y gracias por todo.

A mis amigos incondicionales del alma, Mauricio y Cecy 🤠, no tengo palabras para agradecerles enormemente por apoyarme en mis crisis de ansiedad, sin ustedes me habría derrumbado. Y que no importa cuantas veces la cague 💩, siempre van a estar ahí, escuchando mis 20 min de audios, o leyendo miles de líneas, los amo 🤗.

Finalmente, esta tesis está *súper, hiper, mega* dedicada a la persona más importante para mí. Porque sin cada decisión que esa persona tomó, no habría surgido esa cadena interminable de *efecto mariposa* que me trajo hasta aquí. Nada de esto habría sido posible sin ti: Izamary 😎

Por cada ***"ne mams, que chingón"*** (conjunto de malas palabras que expresan emoción) por cada experimento logrado 😎, cada ***"ptm"*** 😤 (abreviación de una mala palabra para expresar enojo) por los experimentos fallidos, por cada día haciendo las figuras, cada hora analizando datos 👩‍💻, cada minuto en el laboratorio en México y en Francia. Cada segundo esperando el resultado del experimento, cada ***"córrele wey, porque si no vas a perder el avión"***, cada paso hacia ese avión que me llevaba a una nueva aventura, cada ***"milla"*** recorrida en los aviones 🛫, cada kilómetro en los trenes 🚅, cada copo de nieve que caía en mi cara ❄️, cada todo. ***¡¡Porque nada de esto tendría sentido sin mi!!.***

Iza querida de mi corazón ❤️sabes lo que te ha costado, sigue así y derrumbaras todo a tu paso 💣 Te amo.

Gracias a todos por acompañarme en este viaje.

Nos vemos la siguiente temporada.

Índice

Índice de figuras

1. Resumen 1

2. Abstract 2

3. Introducción: 3

3.1 Descripción general del cáncer 3

3.2 Cáncer Colorrectal 4

3.3 Epidemiologia, Factores de Riesgo y tratamientos 5

4. Metabolitos Derivados de Plantas como Agentes Terapéuticos Potenciales 6

5. Red Central de Moléculas Involucradas en el Desarrollo del CCR 9

5.1 Papel de la Vía de Señalización PI3K/AKT/mTOR en el Cáncer 9

5.2 Dinámica Mitocondrial en la Progresión del Cáncer 10

5.3 Crosstalk de la Autofagia y la Apoptosis en Células Cancerosas 11

6. Estrategias Terapéuticas: ACGs y LIR en el tratamiento del CCR 13

6.1 Potencial Terapéutico de las ACGs en el Tratamiento del Cáncer 13

6.2 Potencial Terapéutico de LIR en el Tratamiento del Cáncer 14

7. Justificación 14

8. Hipótesis 14

9. Objetivos 14

9.1 General 14

9.2 Particulares 15

10. Metodología 15

10.1 Cultivo Celular 15

10.2 Reactivos 16

10.3 IC_{50} de las líneas celulares de cáncer colorrectal 16

10.4 Western Blot (WB) 17

10.5 Medición de los niveles de ATP 17

10.6 Medición de la respiración mitocondrial mediante análisis de flujo extracelular 18

10.7 Potencial de la membrana mitocondrial 18

10.8 Análisis de la morfología mitocondrial 19

10.9 Medición del contenido de masa mitocondrial 19

10.10 Immunofluoresencia 20

10.11 Análisis estadístico 21

11. Resultados 21

11.1 Evaluación Citotóxica de los compuestos 21

11.2 Análisis de los complejos de la ETC 22

11.3 Análisis de cambios en el estado energético mediante cuantificación de ATP 24

11.4 Análisis de la tasa de glucólisis mediante la medición del eflujo de protones 25

11.5 Análisis del potencial de membrana mitocondrial 26

11.6 Medición de la respiración mitocondrial mediante análisis de flujo extracelular 28

11.7 Análisis de la dinámica mitocondrial 30

11.8 Medición del contenido de masa mitocondrial 32

11.9 Analisis de proteínas involucradas en la dinámica mitocondrial 33

11.10 Análisis de marcadores moleculares de la vía mTOR mediante detección de proteínas .. 34

11.11 Análisis de autofagia 35

11.12 Análisis de daño a DNA 37

11.13 Detección de proteínas involucradas en la apoptosis. 38

12. Discusión 39

13. Conclusión 48

14. Referencias bibliográficas 50

15. Anexo I (Artículo requisito para la obtención del grado) 61

16. Anexo II (Artículos adicionales realizados durante los estudios de doctorado) 83

Índice de figuras

Figura 1: Características distintivas del cáncer 3
Figura 2: Mecanismos del desarrollo del CCR 5
Figura 3: Estadísticas del cáncer colorrectal 6
Figura 4: Estructura química de LIR 7
Figura 5: Estructura química de LAH 8
Figura 6: Vía de señalización PI3K/AKT/mTOR en el desarrollo del cáncer 10
Figura 7: La compleja interacción entre la apoptosis y la autofagia 12
Figura 8: Viabilidad celular en células de CRC y células no tumorales 22
Figura 9: Expresión de complejos de OXPHOS en mitocondrias de células de CRC y no tumorales 23
Figura 10: Disminución en los niveles de ATP Inducido por los LAH y LIR 24
Figura 11: Análisis del flujo glucolítico en células de CRC y no tumorales 26
Figura 12: Disrupción de $\Delta\Psi_M$ y alteraciones bioenergéticas. 28
Figura 13: Análisis del flujo metabólico de células de CRC y no tumorales 30
Figura 14: Los compuestos naturales inducen fragmentación mitocondrial 31
Figura 15: Contenido de masa mitocondrial en células de CRC y no tumorales. 32
Figura 16: Detección de proteínas involucradas en la dinámica mitocondrial 34
Figura 17: Detección de 4E-BP1, sustrato de mTOR 35
Figura 18: Inducción de autofagia por compuestos naturales. 36
Figura 19: Detección de proteínas involucradas en la autofagia 37
Figura 20: Inducción de focos de γ-H2AX por compuestos naturales 38
Figura 21: Detección de proteínas involucradas en la apoptosis 39
Figura 22: Mecanismo propuesto de acción de LAH y LIR 49

1. Resumen

El cáncer colorrectal (CCR) se encuentra entre las neoplasias más comunes a nivel mundial, con México registrando anualmente 16,802 casos y 8,603 muertes. A pesar de las opciones de tratamiento disponibles, como la cirugía, quimioterapia y radioterapia, la exposición prolongada a agentes quimioterapéuticos convencionales a menudo conlleva toxicidad o resistencia a los fármacos. Los compuestos naturales, como las acetogeninas anonáceas (ACGs) y los alcaloides, ofrecen alternativas prometedoras. En este estudio, se investigó el efecto de Laherradurina (LAH) y Liriodenina (LIR), dos compuestos derivados de plantas, en el CCR. LAH inhibidor del complejo I de la cadena de transporte de electrones, y LIR inhibidor de la topoisomerasa II. Ambos compuestos inducen apoptosis y autofagia en células de CCR, modulando la dinámica mitocondrial y la vía de señalización mTOR. Se observó que LAH y LIR alteran la función mitocondrial, aumentando la glucólisis y fragmentando las mitocondrias, lo que condujo al deterioramiento de la fosforilación oxidativa, contribuyendo a la inducción de apoptosis celular. Además, se desreguló la vía de señalización mTOR, afectando la proliferación celular y aumentando la sensibilidad de las células de CCR a la autofagia. Estos hallazgos destacan el potencial terapéutico de LAH y LIR en el tratamiento del CCR, así como la necesidad de investigar más a fondo sus mecanismos de acción para desarrollar terapias más efectivas contra esta enfermedad.

2. Abstract

Colorectal cancer (CRC) ranks among the most common neoplasms worldwide, with Mexico annually reporting 16,802 cases and 8,603 deaths. Despite available treatment options such as surgery, chemotherapy, and radiation therapy, prolonged exposure to conventional chemotherapeutic agents often leads to drug toxicity or resistance. Natural compounds like Annonaceous Acetogenins (ACGs) and alkaloids offer promising alternatives. This study investigated the effect on CRC of Laherradurin (LAH) and Liriodenine (LIR), two plant-derived compounds. LAH inhibits complex I of the electron transport chain, while LIR inhibits topoisomerase II. Both compounds induce apoptosis and autophagy in CRC cells by modulating mitochondrial dynamics and the mTOR signaling pathway. Moreover, LAH and LIR alter mitochondrial function, increase glycolysis and mitochondria fragmentation, leading to impaired oxidative phosphorylation and contributing to apoptosis induction. Additionally, after treatment the mTOR signaling pathway is also dysregulated, affecting cell proliferation, and increasing autophagy in CRC cells. These findings highlight the therapeutic potential of LAH and LIR in CRC treatment, emphasizing the need for further investigation into their mechanisms of action to develop more effective therapies against colorectal cancer.

3. Introducción:

3.1 Descripción general del cáncer

El cáncer comprende una serie de enfermedades caracterizadas por mutaciones sucesivas en genes supresores de tumores y la activación de oncogenes. Esto conduce a alteraciones en la señalización proliferativa, vías de muerte celular, adquisición de inmortalidad replicativa, inducción de angiogénesis y metástasis (1), así como a la inestabilidad genómica, la evasión de la respuesta inmunitaria, la inflamación sostenida y desregulación del metabolismo energético (2). Estos eventos son reconocidos como "hallmarks del cáncer", los cuales las células normales adquieren durante su progresión hacia la malignidad. Recientemente, se han identificado características adicionales como el desbloqueo de la plasticidad fenotípica, la reprogramación epigenética no mutacional, los microbiomas polimórficos y las células senescentes (3) (Fig. 1). Los tipos más comunes de cáncer, que contribuyen al mayor número de muertes anualmente en todo el mundo, incluyen el cáncer de pulmón, de mama, de hígado y colorrectal (4).

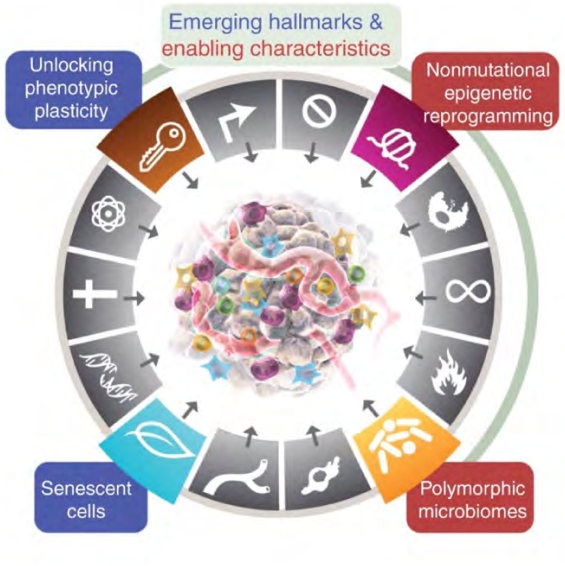


Figura 1: Características distintivas del cáncer

Las características distintivas del cáncer abarcan ocho capacidades distintas y dos características habilitadoras. Características emergentes como la reprogramación del metabolismo celular, la evasión de la destrucción inmunitaria, la inflamación que promueve el tumor, y la inestabilidad genómica y mutación contribuyen aún más al crecimiento y progresión del tumor al activar estas capacidades funcionales. Se han identificado elementos adicionales que contribuyen como, el desbloqueo de la plasticidad fenotípica, la reprogramación epigenética no mutacional, los microbiomas polimórficos y las células senescentes. Fuente: Hallmarks of Cancer: New Dimensions by Hanahan, 2022 (3).

3.2 Cáncer Colorrectal

El cáncer colorrectal (CCR) se caracteriza por la proliferación anormal de células epiteliales glandulares en el colon o recto (5). El CCR típicamente comienza como una lesión precancerosa, denominada adenoma intermedio, y progresa hacia un carcinoma invasivo (adenocarcinoma) (6) que puede extenderse a diferentes órganos distantes y dar lugar a lesiones metastásicas, siendo el hígado el órgano más frecuentemente afectado (7). El CCR abarca tres tipos principales: esporádico, hereditario y asociado a colitis.

La progresión del CCR, conocida como "carcinogénesis colorrectal", implica la acumulación de mutaciones genéticas germinales (heredadas) y/o somáticas (adquiridas) a lo largo de un período de 10-15 años. Este proceso se desarrolla en cuatro etapas principales: iniciación, promoción, progresión y metástasis (8) (Fig. 2).

La iniciación ocurre cuando factores genéticos, metabólicos y carcinogénicos dañan la molécula de ácido desoxirribonucleico (ADN), predisponiendo a las células afectadas a una transformación neoplásica (6). La inducción del CCR está asociada con tres vías moleculares (9), la menos común de las cuales es la inestabilidad microsatélite (MSI), caracterizada por cambios en las repeticiones cortas de microsatélites debido a genes deficientes en reparación de desajustes (MMR), (10). Además, la hipermetilación del ADN CpG activa o silencia la expresión de genes específicos (11). La vía más prevalente, observada en el 70% de los casos, es la inestabilidad cromosómica, marcada por mutaciones en oncogenes y/o genes supresores de tumores como APC, KRAS, PIK3CA (Fig. 2), BRAF, SMAD4 o TP53 (12).

Durante la etapa de promoción, las células experimentan una expansión clonal debido a las mutaciones, lo que conduce a la sobreactivación de la vía de señalización Wnt/β-catenina (13). Este evento inicia la proliferación celular desregulada y la formación de adenomas, acompañada de la adquisición de mutaciones adicionales como KRAS (14), CMYC (15), o BRAF (16). Posteriormente, en la etapa de progresión, los factores de crecimiento derivados del microambiente tumoral (TME) alimentan aún más el crecimiento celular al desregular genes como HIF1- α (17–19) y p53 (20), culminando en

la transformación de estos clones en tumores malignos (Fig. 2). Mutaciones adicionales y alteraciones en el proceso de transición epitelial-mesenquimal (EMT) facilitan la posterior metástasis a órganos distantes (9,12).

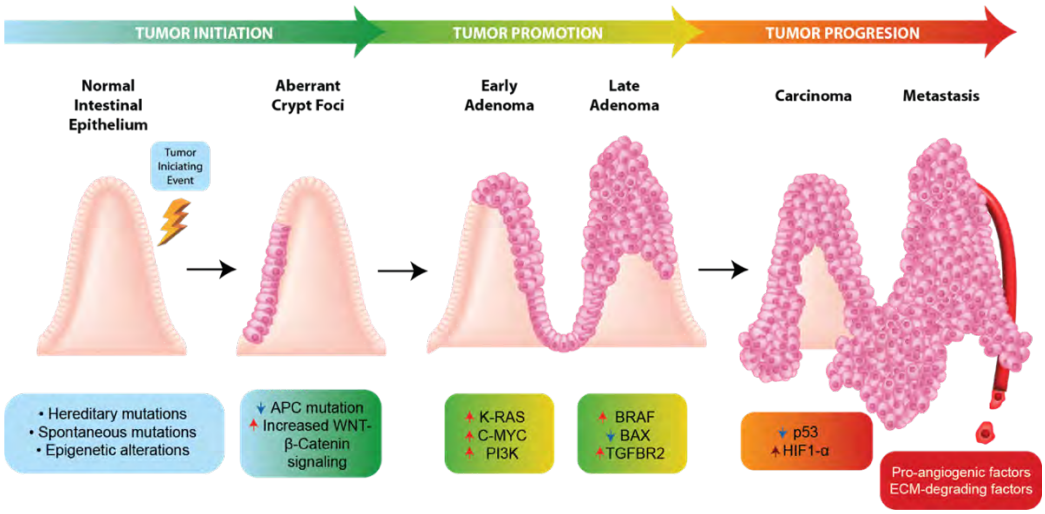


Figura 2: Mecanismos del desarrollo del CCR

El CCR surge de una compleja interacción de mutaciones genéticas, que afectan predominantemente a oncogenes y genes supresores de tumores. Esta cascada de alteraciones genéticas impulsa la evolución de las células normales hacia lesiones preneoplásicas, como focos aberrantes de criptas, que progresan hacia adenomas y finalmente culminan en carcinoma colorrectal. Adaptado de: Inflammation and Colon Cancer by Terzic, 2010 (21).

3.3 Epidemiologia, Factores de Riesgo y tratamientos

El CCR ocupa el tercer lugar como neoplasia más común en todo el mundo en ambos sexos, mientras que en México se reportan anualmente 16 802 casos y 8 603 muertes, destacando su impacto en la salud pública (4) (Fig. 3).

El CCR está influenciado por una combinación de factores ambientales y genéticos (22). Factores ambientales como la inactividad física, obesidad, edad, inflamación crónica (8) y ciertos hábitos dietéticos (consumo de carnes rojas o procesadas y alcohol) se han relacionado positivamente con el CCR (23). Estos factores contribuyen a la disfunción metabólica, la inflamación, el estrés oxidativo, la disbiosis bacteriana y la integridad comprometida de la barrera intestinal (24).

En el factor genético (25), los síndromes hereditarios como el síndrome de Lynch (síndrome de cáncer colorrectal no polipósico hereditario o HNPCC) y la poliposis

adenomatosa familiar, están asociados con un riesgo significativamente aumentado de desarrollar CCR (26). Mientras que los CCR hereditarios representan aproximadamente el 5% de todos los casos de CCR (6), representan aquellos con una susceptibilidad elevada a la enfermedad.

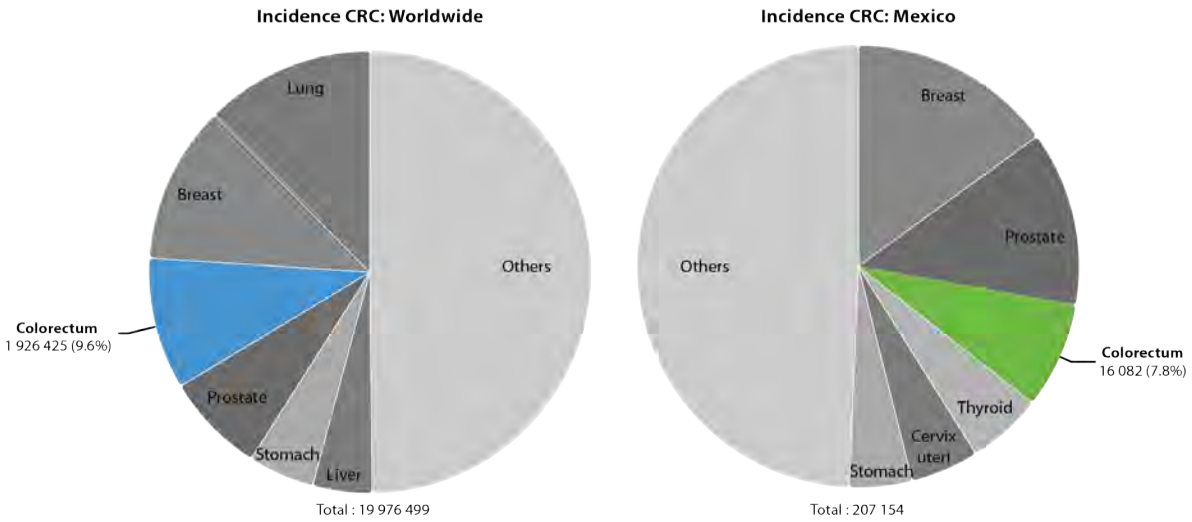


Figura 3: Estadísticas del cáncer colorrectal

Estimaciones y proporción de casos incidentes de CCR en el mundo en 2022 y en México. Fuente: GLOBOCAN 2022 (4).

El tratamiento para el CCR varía según la localización del tumor y la etapa del diagnóstico. Las terapias actuales incluyen cirugía, quimioterapia (5-fluorouracilo [5-FU] y oxaliplatino en etapas 1 y 2, y Cetuximab, Panitumumab y Bevacizumab en etapas 3 y 4), y radioterapia (27). Sin embargo, la exposición prolongada a estos agentes quimioterapéuticos puede llevar a una mayor toxicidad para el paciente o resistencia a los medicamentos.

4. Metabolitos Derivados de Plantas como Agentes Terapéuticos Potenciales

En los últimos años, ha habido una búsqueda de nuevos compuestos con mayor eficacia, menor toxicidad y menos efectos secundarios en comparación con las terapias convencionales de primera línea contra el cáncer. Estos compuestos a menudo se dirigen a las vías de señalización involucradas en la progresión del cáncer (28), y los metabolitos derivados de plantas están ganando atención por sus diversas funciones biológicas, incluidas actividades anticancerígenas (29).

Los metabolitos secundarios (o especializados) de las plantas constituyen una variedad estructuralmente diversa de compuestos orgánicos (30) que desempeñan roles cruciales en el crecimiento, desarrollo y la interacción de las plantas con el medio ambiente (31). Estos metabolitos se categorizan en múltiples grupos según la clasificación de la British Nutrition Foundation, incluyendo terpenoides, compuestos que contienen nitrógeno, compuestos que contienen azufre, compuestos fenólicos y policétidos (32).

4.1.1 Alcaloides

Los alcaloides, un grupo diverso de compuestos nitrogenados, son los productos naturales más abundantes, encontrados predominantemente en las plantas. El término "alcaloide" está vinculado a sus propiedades básicas (alcalinizantes), atribuidas a la presencia de uno o más átomos de nitrógeno, como aminas primarias, secundarias o terciarias, que a menudo se encuentran en heterociclos (33).

4.1.1.1 Liriodenina

Liriodenina (LIR), un alcaloide oxoporfínico natural, se deriva de la 1-azabenzantrona y comprende un anillo de quinolina unido a una unidad de tetralona, formando un compuesto aromático (34). Su estructura plana facilita su intercalación en el ADN (Fig. 4) (35).

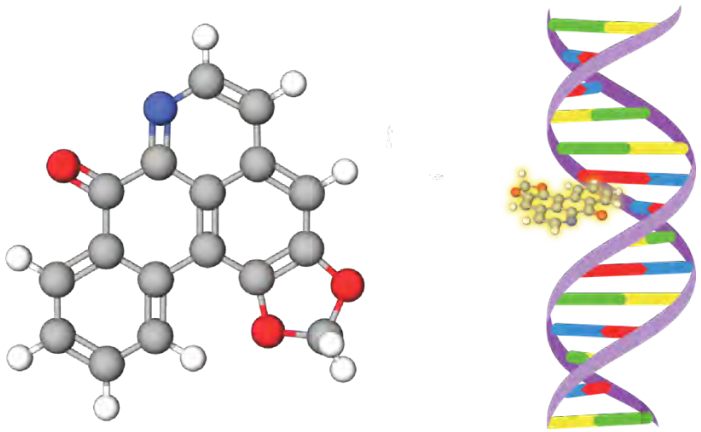


Figura 4: Estructura química de LIR

Estructura molecular 3D de LIR. Creada por el software MolView 3D. Fuente: PubChem

La actividad antitumoral de LIR se deriva de su estructura aromática planar, que le permite intercalarse entre los pares de bases de la doble hélice del ADN (Fig. 4) (36). Además, LIR actúa como inhibidor catalítico de la topoisomerasa II (TOPII), impidiendo la síntesis del ADN (37). Esta inhibición induce el arresto del ciclo celular en la fase G1 y promueve la regulación al alza del supresor tumoral p53 (38,39).

4.1.2 Acetogeninas Annonáceas

Las acetogeninas annonáceas (ACG) son metabolitos derivados de la vía del policétido y aislados de la familia Annonaceae. La estructura química de las ACG se caracteriza por la presencia de 35 a 37 átomos de carbono, organizados en cuatro regiones distintas: el anillo α, una γ-lactona β-insaturada, de uno a tres anillos de tetrahidrofuranos (THF) flanqueados por grupos hidroxilo (OH), una larga cadena alquilada y un espaciador alquilado que conecta el anillo de γ-lactona con el anillo THF (Fig. 5) (40).

4.1.2.1 Laherradurina

Laherradurina (LAH), un producto natural extraído de las semillas de Annona cherimolia, se destaca como un compuesto bioactivo significativo dentro de la familia Annonaceae. LAH se caracteriza por la presencia de dos anillos de tetrahidrofuranos adyacentes (bis-THF adyacente) y una γ-lactona β-hidroxilada saturada. Una distancia de 13 átomos entre el carbono que enlaza el sistema de anillos THF y la lactona γ-insaturada contribuye a sus propiedades antitumorales (Fig. 5).

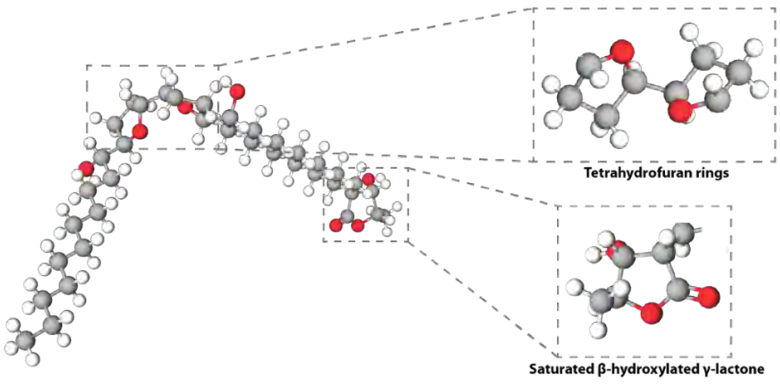


Figura 5: Estructura química de LAH

Estructura molecular 3D de LAH. Creada por el software MolView 3D. Fuente: PubChem.

LAH ha demostrado la capacidad de inducir la inhibición del crecimiento celular tanto en modelos *in vitro* como *in vivo* de CCR (41). El mecanismo de acción de las ACGs implica la inhibición de la NADH-ubiquinona oxidoreductasa, también conocida como complejo I, que cataliza la oxidación de NADH y genera el gradiente electroquímico de protones necesario para la síntesis de adenosín trifosfato (ATP). Esta inhibición se logra mediante la unión del anillo γ-lactona en la cuarta y quinta hélice transmembrana en la subunidad ND1 del complejo I (42). Además, las ACGs han mostrado potencial como inhibidores de la NADH oxidasa de membrana plasmática (NOX) en células cancerosas, lo que conduce a la disminución de los niveles de ATP y posterior arresto del ciclo celular en la fase G1 (43). Las ACG actúan como inhibidores efectivos cuando los segmentos de γ-lactona y THF están unidos por un espaciador alquílico largo de 13 carbonos (44). La selectividad de las ACGs por las células tumorales surge de sus niveles más altos de NADH oxidasa y una mayor demanda de ATP (45).

Tanto el complejo I como NOX sirven como las principales fuentes de especies reactivas de oxígeno (ROS) (46). El estrés oxidativo generado por estos complejos activa la vía de señalización PI3K/AKT/mTOR al tiempo que inhibe la actividad de PTEN (47).

5. Red Central de Moléculas Involucradas en el Desarrollo del CCR

5.1 Papel de la Vía de Señalización PI3K/AKT/mTOR en el Cáncer

La vía de señalización PI3K/AKT/mTOR destaca como una de las vías intracelulares más cruciales, que regula el crecimiento celular, la motilidad, la supervivencia, el metabolismo y la angiogénesis, y se encuentra frecuentemente desregulada en varios tipos de cáncer (48). La activación de esta vía comienza con la unión de un factor de crecimiento a los receptores tirosina quinasas (RTKs), promoviendo el reclutamiento de fosfatidilinositol-3-cinasa (PI3K). Las PI3Ks fosforilan la fosfatidilinositol-(4,5) bifosfato (PIP2) a fosfatidilinositol (3,4,5)-trifosfato (PIP3), reclutando y fosforilando a PDK1. Posteriormente, PDK1 y el objetivo de la rapamicina, complejo 2 (mTORC2) fosforilan y activan AKT en treonina 308 y serina 473, respectivamente (47). El AKT fosforilado, a su vez, activa el objetivo de la rapamicina complejo 1 (mTORC1), iniciando así la síntesis de proteínas, nucleótidos y lípidos, y la biogénesis ribosomal (49), al mismo tiempo que

inhibe la apoptosis y la autofagia de manera concurrente (Fig. 6). Además, regula el metabolismo energético al aumentar la actividad de enzimas metabólicas como el coactivador 1-α del receptor activado por proliferadores de peroxisomas-γ (PGC-1α), una enzima crucial involucrada en la regulación del metabolismo oxidativo mitocondrial (50).

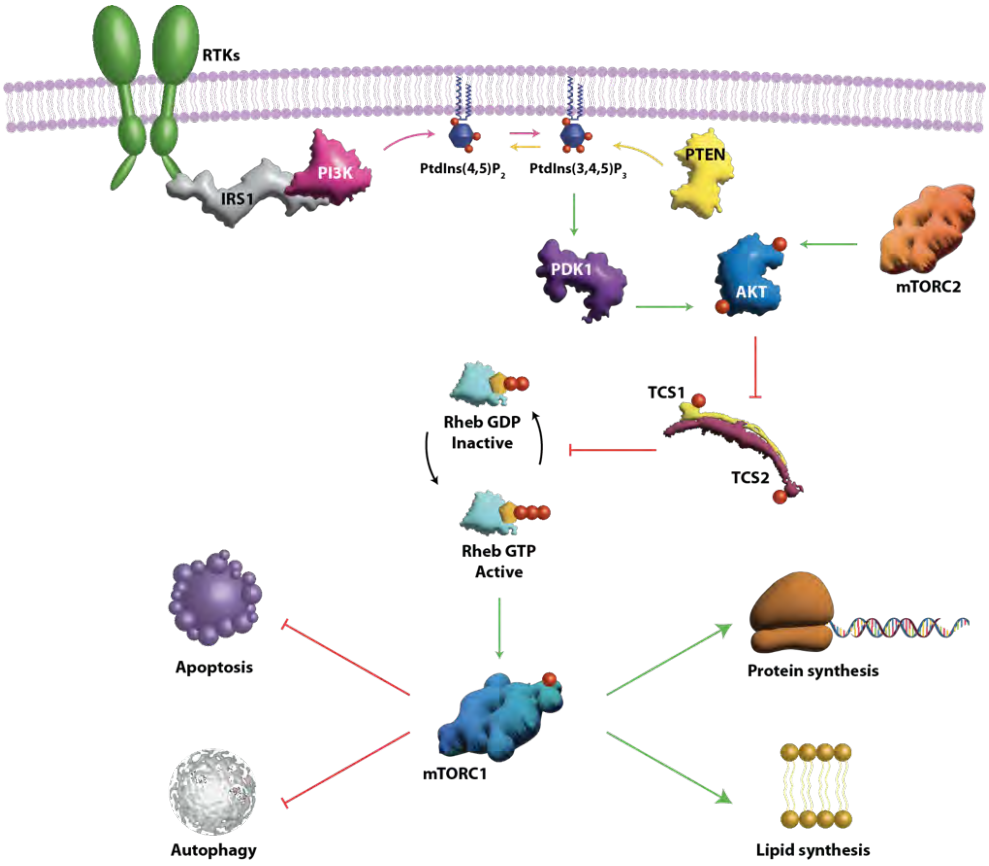


Figura 6: Vía de señalización PI3K/AKT/mTOR en el desarrollo del cáncer

El proceso comienza con la autofosforilación de PI3K, lo que desencadena la activación de AKT mediante la conversión de PIP2 a PIP3. Esta activación, junto con mTORC1, alimenta el crecimiento tumoral y facilita el almacenamiento de energía en las células cancerosas. Además, la regulación al alza de AKT conduce a la fosforilación de genes y proteínas diana, inhibiendo la apoptosis y la autofagia. Además, las miARNs desreguladas desempeñan un papel en la promoción de la proliferación celular del cáncer. Adaptado de: mTOR signaling at a glance por Laplante (51).

5.2 Dinámica Mitocondrial en la Progresión del Cáncer

Las mitocondrias, organelos centrales para el metabolismo celular, experimentan fusión, fisión y movimiento continuo a lo largo del citoesqueleto, formando una red dinámica regulada por las guanosinas trifosfatasas (GTPasas) relacionadas con dinamina (52). Esta interacción dinámica está estrechamente vinculada al metabolismo celular,

influenciando la producción de energía y los mecanismos de control de calidad mitocondrial. La disfunción de la dinámica mitocondrial puede alterar el fenotipo metabólico de las células cancerosas, contribuyendo al efecto Warburg y promoviendo el crecimiento y la supervivencia tumoral. Además, las alteraciones en la dinámica mitocondrial pueden afectar los mecanismos de control de calidad mitocondrial, lo que lleva a la acumulación de mitocondrias dañadas y promoviendo la inestabilidad genómica y la progresión del cáncer. Es importante destacar que los cambios dinámicos en la morfología y distribución mitocondrial han sido implicados en la invasión y metástasis de células cancerosas, influenciando la motilidad celular y el fenotipo invasivo (53). La dinámica mitocondrial es un objetivo prometedor para inducir selectivamente la apoptosis en células cancerosas mientras se preservan las células normales, proporcionando un posible tratamiento del cáncer. Además, la mitofagia, el proceso de eliminación de mitocondrias dañadas ha surgido como un enfoque prometedor para eliminar selectivamente las células cancerosas con defectos mitocondriales. Comprender la interacción entre la dinámica mitocondrial y la biología del cáncer puede llevar al descubrimiento de nuevos objetivos terapéuticos y estrategias para combatir la progresión del cáncer.

5.3 Crosstalk de la Autofagia y la Apoptosis en Células Cancerosas

La autofagia representa un proceso conservado evolutivamente crucial para mantener el equilibrio de las fuentes de energía celular en condiciones de desarrollo críticas y en respuesta al estrés nutricional (54). Este proceso implica la formación de una vesícula de doble membrana llamada autofagosoma, que está regulada por genes relacionados con la autofagia (ATGs) (55). Estos ATGs, incluido el componente clave la proteína asociada a microtúbulos de cadena ligera 3B (LC3), facilitan el reclutamiento de organelos dañados en el autofagosoma, donde interactúan con lisosomas para su degradación, evitando así la progresión celular (Fig. 7, lado derecho). LC3, desempeña un papel fundamental en la biogénesis y maduración del autofagosoma, sirviendo como marcador de las membranas autofágicas. Por otro lado, la apoptosis, otro proceso vital, dirige la muerte celular programada y está regulada por la familia de proteasas cisteína-aspartato (caspasas) (56). Estos zimógenos se activan mediante la escisión por

caspasas y se regulan a través de dos vías de señalización: la vía extrínseca y la vía intrínseca o mitocondrial. Ambas vías convergen para activar caspasas efectoras como la caspasa 3, lo que finalmente conduce a la fragmentación del ADN y la muerte celular (Fig. 7, lado izquierdo) (57).

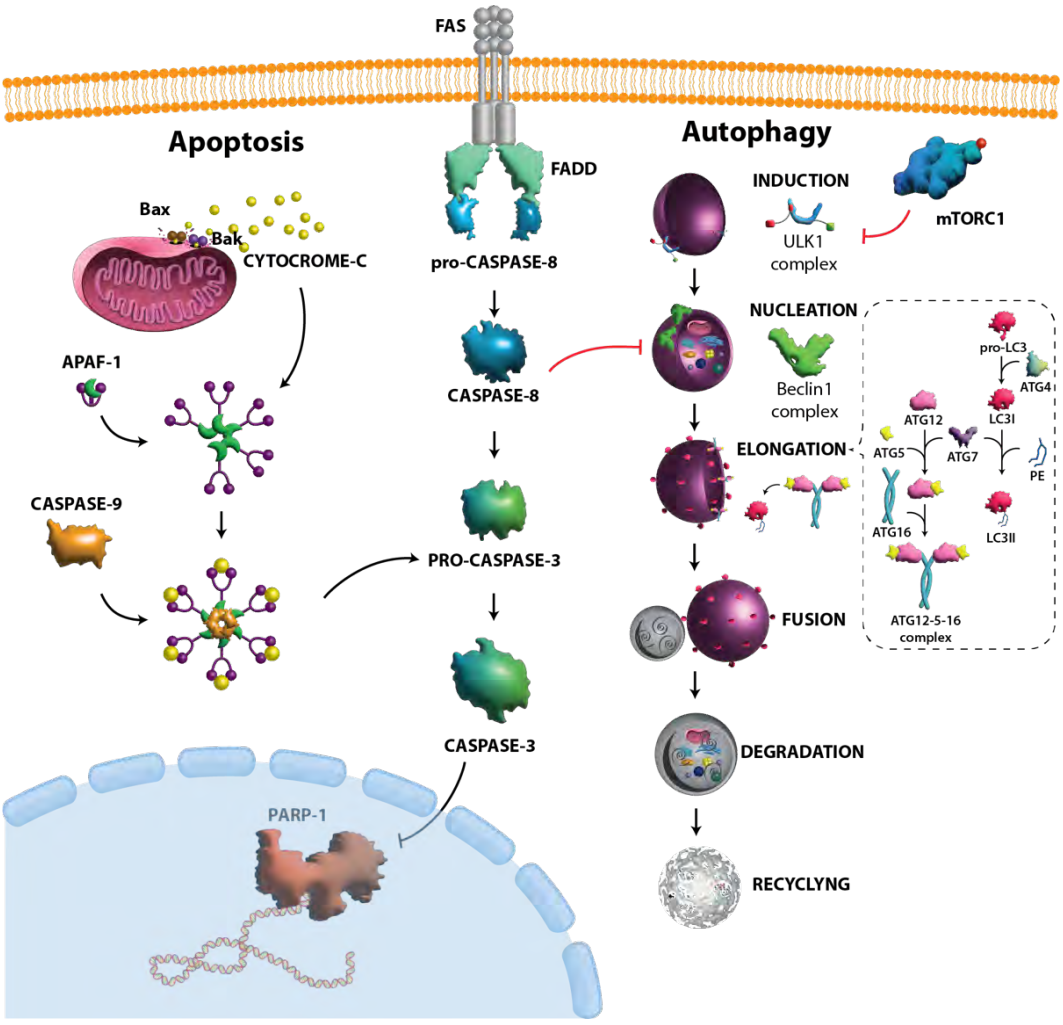


Figura 7: La compleja interacción entre la apoptosis y la autofagia

La apoptosis, activada por las vías extrínseca e intrínseca, implica la unión de ligandos a receptores de muerte, desencadenando la caspasa-8 y posteriormente la caspasa-3 y 7. Simultáneamente, la vía intrínseca es controlada por dímeros BAX/BAK que inducen la formación de poros mitocondriales, liberando citocromo C para activar la caspasa-9, conduciendo a la muerte celular apoptótica mediada por la caspasa-3. Paralelamente, la autofagia comienza con la activación del complejo ULK, iniciando la formación del autofagosoma. El complejo Beclin1 luego facilita la elongación del autofagosoma a través de los sistemas de lipoidación Atg12 y LC3. El complejo Atg5-Atg12-Atg16L1 ayuda a mantener la estructura del autofagosoma, permitiendo que LC3B-II se ancle y forme autofagolisosomas para la degradación del contenido, crucial para la homeostasis celular y la adaptación al estrés.

6. Estrategias Terapéuticas: ACGs y LIR en el tratamiento del CCR

6.1 Potencial Terapéutico de las ACGs en el Tratamiento del Cáncer

Varias ACGs han demostrado inducir apoptosis y autofagia (58). Un análogo de bullatacin llamado AA005, con sustitución de anillos THF por un éter de etilenglicol, mostró actividad antitumoral superior a la de la bullatacina. Este análogo (AA005) fue probado recientemente en líneas celulares de cáncer colorrectal (CCR), donde indujo la autofagia mediante un aumento en la detección de LC3II en respuesta a la depleción de ATP, aumentando la actividad de la proteína quinasa activada por AMP (AMPK) y suprimiendo la vía de señalización mTORC1, lo que llevó a la inhibición del crecimiento tumoral (59). Esto sugiere que la represión de mTOR puede estar estrechamente relacionada con la inducción de apoptosis de la muerte celular (60), similar a informes anteriores donde la evaluación del extracto de acetato de etilo que contiene Annomuricina E indujo apoptosis mediante la regulación negativa de Bcl-2 y la regulación positiva de Bax. Además, Annomuricina E exhibió una citotoxicidad ligeramente menor en comparación con 5-FU en líneas celulares de cáncer de colon, lo que proporciona evidencia de la selectividad de los AGCs para las líneas celulares de cáncer (61). La selectividad antiproliferativa de AGC se debió a los anillos de THF en modelos in vitro e in vivo de carcinoma nasofaríngeo humano, provocando arresto del ciclo celular en la fase G2/M, daño mitocondrial, aumento del Ca2+ citosólico y mitocondrial que resultó en la inducción de apoptosis en respuesta al estrés del retículo endoplásmico (62). Estos datos son consistentes con informes anteriores donde los extractos de ACG de Annona coriacea se utilizaron para tratar líneas celulares de cáncer cervical y una línea celular de queratinocitos normales. Los AGC fueron más selectivos en la disminución de la proliferación celular solo en líneas celulares derivadas de cáncer mediante el aumento de la expresión de γ-H2AX fosforilada que indica daño en el ADN, la proteína p21 y el arresto del ciclo celular en la fase G2/M y eventual apoptosis (63). Tres ACGs de Annona cherimolia (cherimolina-1, motrilina y LAH) indujeron apoptosis en la línea celular de hepatocarcinoma HepG2. LAH causó la muerte celular por apoptosis mediante la pérdida del potencial de membrana mitocondrial (MMP o $\Delta\Psi_M$), promoviendo la liberación de citocromo c y la activación subsiguiente de caspasas (64).

6.2 Potencial Terapéutico de LIR en el Tratamiento del Cáncer

Estudios *in vitro* indican que LIR tiene actividad citotóxica en líneas celulares de cáncer de hígado (HepG2 y SK-Hep), induciendo arresto del ciclo celular en la fase G1 e inhibiendo la síntesis de ADN (65). LIR también muestra una actividad potente en el cáncer de colon, e inhibe el ciclo celular en células SW480 a través de una vía de arresto en la fase G1/S dependiente del óxido nítrico y de p53 (66). Estos estudios indican el gran potencial de LIR como agente terapéutico para varios tipos de cáncer.

7. Justificación

Se considera que la inducción de la autofagia y apoptosis mediante la inhibición de mTOR, promoviendo la alteración de la dinámica mitocondrial en las células tumorales con metabolitos secundarios derivados de plantas, puede ser un enfoque terapéutico prometedor para el tratamiento del CCR, con la capacidad de reducir efectos secundarios y mejorar la calidad de vida de los pacientes.

8. Hipótesis

En este estudio, se plantea que LAH, un inhibidor del complejo I de la cadena de transporte de electrones (ETC), y LIR, un inhibidor de la topoisomerasa II (TOPII), interrumpirán procesos celulares cruciales para la supervivencia de las células cancerosas e inducirán apoptosis y autofagia en células de CCR mediante la disfunción mitocondrial y la inhibición de la vía mTOR. El modelo *in vitro* de CCR proporcionará conocimientos valiosos sobre el potencial terapéutico de estos compuestos y su impacto en la función mitocondrial y las vías de supervivencia celular.

9. Objetivos

9.1 General

Identificar los mecanismos moleculares que modifican la función mitocondrial y regulan la activación de apoptosis y autofagia en modelos in vitro de CCR tratados con LAH y LIR.

9.2 Particulares

- Evaluar la citotoxicidad de los compuestos en líneas celulares de CCR
- Investigar los cambios inducidos por los compuestos en los complejos de la ETC
- Cuantificar las alteraciones en el estado energético de las células de CCR mediante la medición de ATP después del tratamiento con compuestos
- Medir cambios en el flujo glucolítico de las células de CCR con tratamientos a través de la cuantificación de la tasa de acidificación extracelular
- Examinar el estado del potencial de la membrana mitocondrial post-tratamiento
- Examinar el estado del metabolismo energético mediante la evaluación de la tasa de consumo de oxígeno inducida por los compuestos
- Validar la condición de la red mitocondrial utilizando MitoTracker y evaluar marcadores moleculares asociados con la dinámica mitocondrial.
- Cuantificar el contenido de masa mitocondrial utilizando NaO
- Analizar los marcadores moleculares asociados con la vía de señalización mTOR alterada por los tratamientos a través de la detección de proteínas
- Analizar la formación de autofagosomas usando el marcaje de mCherryGFP-LC3
- Validar la inducción de apoptosis y autofagia mediante la detección de proteínas de marcadores moleculares
- Determinar la formación de focos de daño en el ADN positivos para γ-H2AX

10. Metodología

10.1 Cultivo Celular

Las líneas celulares derivadas de CCR (HCT116, SW620) y no tumorales CRL-1790 fueron proporcionadas por el Instituto Nacional de Cancerología en la Ciudad de México. Estas líneas celulares se sembraron en cajas de cultivo de 100 x 15 mm con medio DMEM/F-12 GIBCO® suplementado con 10% de suero fetal bovino (FBS) (CORNING) y se mantuvieron en una incubadora (Thermo Scientific) a 37°C con 5% de CO_2. Una vez alcanzado el 80% de confluencia, las líneas celulares fueron expuestas a los tratamientos. Todos los experimentos se realizaron bajo estas condiciones.

10.2 Reactivos

LAH fue extraída de las semillas de *Annona diversifolia Saff (Annonaceae)*, recolectadas en Copoya, Chiapas, México, e identificado en el Herbario Eizi Matuda de la Universidad de Ciencias y Artes de Chiapas, México. Los controles adicionales incluyeron Rapamicina (RAP) a 1 μM (TO-R001, Euromedex, Souffelweyersheim, Francia), Sulfato de Hidroxicloroquina (HCQ) a 50 μM (HY-B1370, MedChemExpress, Monmouth Junction, NJ, EE.UU.), TORIN-1 a 1 μM (HY-13003, MedChemExpress, Monmouth Junction, NJ, EE.UU.), Oligomicina A a 10 μM (HY-16589, MedChemExpress, Monmouth Junction, NJ, EE.UU.), CCCP a 100 μM (C2759, Sigma-Aldrich, St. Louis, MO, EE.UU.), Antimicina A a 2.5 μM (A8674, Sigma-Aldrich, St. Louis, MO, EE.UU.), glucosa a 20 mM (103577-100, Agilent Technologies, Santa Clara, CA, EE.UU.) y 2-DG a 20 nM (103344-100, Agilent Technologies, Santa Clara, CA, EE.UU.).

10.3 IC_{50} de las líneas celulares de cáncer colorrectal

La concentración inhibitoria 50 (IC_{50}) para LAH se determinó mediante un ensayo colorimétrico de Sulforrodamina B (SRB), siguiendo el protocolo establecido en 2006 (67). Las células se sembraron en placas de 96 pozos a una densidad de 1×10^4 células por pozo, se dejaron adherir durante la noche y se trataron con varias dosis de LAH durante 24 h. Tras la fijación con ácido tricloroacético al 10% y la tinción con SRB al 0.5% (S9012, Sigma-Aldrich, St. Louis, MO, EE.UU.), se midió la densidad óptica (OD) a 510 nm utilizando un espectrofotómetro de microplacas Epoch (BioTek, Winooski, VT, EE.UU.). Las curvas de dosis-respuesta y la viabilidad celular se analizaron con el software GraphPad Prism versión 8.0.2, realizando los experimentos por triplicado.

Para LIR, la viabilidad celular se determinó mediante el ensayo de bromuro de tetrazolio (MTT), siguiendo el protocolo establecido en 2018 (68), La OD se midió espectrofotométricamente a 490 nm utilizando un lector de microplacas Infinite 200 PRO (Tecan, Männedorf, Suiza), y la tasa de supervivencia celular se expresó como porcentaje del control. Las curvas de dosis-respuesta y los valores de viabilidad celular se obtuvieron utilizando el software GraphPad Prism.

10.4 Western Blot (WB)

Las líneas celulares fueron expuestas a tratamientos específicos para evaluar la expresión de proteínas, luego los pellets celulares se resuspendieron en un tampón de lisis NETN, y se determinaron las concentraciones de proteínas. Las muestras se cargaron en geles de Tris-Glicina al 4–12% y se transfirieron a membranas de PVDF (IPVH00010, Millipore, Burlington, MA, EE.UU.). Después de bloquear las membranas en 5% de leche en TBS-T, se incubaron con anticuerpos primarios durante la noche a 4 °C, y luego se lavaron las membranas 3 veces con TBS-T, seguido de la incubación con un anticuerpo secundario apropiado durante una hora a temperatura ambiente. Las bandas de proteínas se visualizaron utilizando un sustrato de quimioluminiscencia (WBKLS0500, Millipore, Burlington, MA, EE.UU.). Se utilizaron los siguientes anticuerpos: cóctel de anticuerpos total OXPHOS humano WB (ab110411, Abcam, Cambridge, Reino Unido); anti-β-actina (C4) (sc-47778, Santa Cruz Biotechnology, Dallas, TX, EE.UU.); anti-caspasa-8 (AM46, Millipore, Burlington, MA, EE.UU.); anti-mitofusina 1 (14739S); anti-fosfo-DRP1 (Ser637) (6319S); anti-DRP1 (8570); anti-fosfo-4E-BP1 (Thr37/46) (2855S); anti-4E-BP1 (9644S); anti-ULK1 (8054S); anti-fosfo-ULK1 (Ser757) (14202); anti-P62 (5114S); anti-LC3B (2775); anti-PARP1 (9542); anti-PARP cortada (9541); anti-AIF (5318); anti-caspasa-3 (9662); anti-GAPDH (51332S); anti-IgG de ratón, HRP-conjugado (7076); anti-IgG de conejo, HRP-conjugado (7074), todos de Cell Signaling Technology, Danvers, MA, EE.UU.

10.5 Medición de los niveles de ATP

Las concentraciones de ATP se midieron por triplicado utilizando el kit del Sistema de Ensayo de Quimioluminiscencia ATPlite 1step (6016736, PerkinElmer, Waltham, MA, EE.UU.), siguiendo el protocolo del fabricante. La luminiscencia total se midió utilizando un lector de microplacas de 96 pozos. Los niveles de ATP se expresaron como un porcentaje del control no tratado.

10.6 Medición de la respiración mitocondrial mediante análisis de flujo extracelular

El análisis de flujo extracelular se realizó en el analizador de flujo extracelular Seahorse XF96 (Agilent Technologies, Santa Clara, CA, EE.UU.). Las células se sembraron a una densidad de $0.8x10^4$ (HCT116, CRL1790) y $1x10^4$ (SW620) en una microplaca de cultivo celular Seahorse XF96 (101085-004, Agilent Technologies, Santa Clara, CA, EE.UU) con medio RPMI al 10% de FBS, 1% P/S a 37°C en un incubador humidificado. Tras la exposición a los tratamientos, las células se lavaron e incubaron con medio XF RPMI. Los compuestos del Kit de Prueba de Estrés Mitocondrial Seahorse XF Cell (103015-100, Agilent Technologies, Santa Clara, CA, EE.UU.) y del Kit de Ensayo de Tasa Glucolítica Seahorse XF (103344-100, Agilent Technologies, Santa Clara, CA, EE.UU.) se cargaron en la microplaca, y las mediciones se realizaron utilizando el software Seahorse Wave versión 2.6.3.5. Los datos se normalizaron en función de la intensidad de fluorescencia con tinción de Hoechst.

10.7 Potencial de la membrana mitocondrial

Para evaluar el MMP ($\Delta\Psi_M$), se sembraron $2.5x10^5$ células de CCR en una placa de 6 pocitos. Después de 24 h de adherencia, las células fueron tratadas. Después del tiempo de exposición, las células fueron lavadas con RPMI tibio sin FBS, tratadas con tripsina, los pellets celulares se resuspendieron en medio DMEM al 1% de FBS con 100 nM de tetrametilrodamina metil éster (TMRM) (T5428, Sigma-Aldrich, St. Louis, MO, EE.UU.), e incubados durante 10 minutos a 37°C en la oscuridad. La intensidad de fluorescencia se adquirió en el nivel basal utilizando el detector FL2 en un citómetro de flujo BD Accuri™ C6 Plus (BD Biosciences, Franklin Lakes, NJ, EE.UU.). Se analizaron un total de $1x10^4$ células por condición. La intensidad relativa de TMRM se calculó utilizando el software FlowJo X versión 10.8.1. Los niveles basales de TMRM se determinaron de manera independiente para cada línea celular y estos niveles se utilizaron para la normalización. Para validar el potencial de membrana mitocondrial, las células se trataron con 10 µM de Oligomicina A como control positivo y 10 µM de CCCP como control negativo.

10.8 Análisis de la morfología mitocondrial

Para visualizar las mitocondrias, se sembraron $3x10^4$ células en portaobjetos tratados previamente con 0.1 mg/mL de poli-D-lisina (Sigma, A-003-E) en una placa de 6 pocitos. Después de 24 h, las células fueron expuestas a LAH y LIR. Una vez finalizado el tiempo de exposición, el medio se reemplazó con RPMI al 1% de FBS conteniendo 100 nM de MitoTracker Orange CMTMRos (M7510, Thermo Fisher Scientific, Waltham, MA, EE.UU) e incubado en oscuridad durante 45 minutos a 37°C. Después de la incubación, las células fueron lavadas 3 veces con PBS tibio durante 5 minutos, una vez con H_2O, y fijadas con 4% de paraformaldehído (PFA) durante 20 minutos. Después de la fijación, las células fueron lavadas 3 veces con PBS tibio durante 5 minutos y una vez con H_2O. Los portaobjetos se montaron en un portaobjetos de vidrio con medio de montaje Fluoroshield con DAPI (Sigma, F6057). Para DAPI (F6057, Sigma-Aldrich, St. Louis, MO, EE.UU) y MitoTracker, las imágenes se observaron a 405 nm y 561 nm, respectivamente. Las imágenes se adquirieron en un microscopio confocal Leica SPE DM4000B (Leica Microsystems, Wetzlar, Alemania) con un objetivo de inmersión en aceite de 63x.

10.9 Medición del contenido de masa mitocondrial

Se sembraron $2.5x10^5$ células de CCR en una placa de 6 pocitos y se trataron con LAH. Después del tratamiento, las células fueron incubadas con medio RPMI al 10% de FBS que contenía 100 nM de 10-N-nonil acridina naranja (NaO) (A1301, Invitrogen, Waltham, MA, EE.UU.) durante 10 minutos a 37 °C en la oscuridad. La intensidad de fluorescencia se midió utilizando un citómetro de flujo BD Accuri™ C6 Plus (BD Biosciences, Franklin Lakes, NJ, EE.UU.), analizando 1 × 10^4 células por condición. La intensidad relativa de NaO se calculó utilizando el software FlowJo X versión 10.8.1; los niveles basales de NaO se determinaron de manera independiente para cada línea celular, y estos niveles se utilizaron para la normalización. Se usaron Oligomicina A y CCCP como controles positivo y negativo para el potencial de membrana mitocondrial, respectivamente.

10.10 Immunofluoresencia

Para localizar los autofagosomas, las células fueron transfectadas con el plásmido pBABE-puro-mCherry-EGFP-LC3B (22418, Addgene, Cambridge, MA, EE.UU). Las células se cultivaron en placas de 24 pocitos sobre cubreobjetos recubiertos con 0.1 mg/mL de polidilisina (A-003-E, Sigma-Aldrich, St. Louis, MO, EE.UU.) a una densidad de $4x10^4$ células por pocito y se permitió que se adhirieran durante la noche a 37 °C. Posteriormente, las células fueron transfectadas con 1 µg de ADN de plásmido utilizando Lipofectamine 2000 (11668019, Thermo Fisher Scientific, Waltham, MA, EE.UU.) y se sometieron a LAH durante 24 h. Las células fueron fijadas con PFA al 4% durante 30 min y permeabilizadas con Triton X-100 al 0.1% en solución salina tamponada con fosfato (PBS-T: 137 mM NaCl, 2.7 mM KCl, 10 mM Na2HPO4, 2 mM KH2PO4, pH 7.4) durante 5 min. Los cubreobjetos se bloquearon con suero bovino albumina (BSA) al 1% en PBS-T durante 1 h. Para la inmunotinción, los cubreobjetos se incubaron durante la noche con el anticuerpo primario contra la alfa-tubulina (DM1A, 1:100, Cell Signaling Technology, Danvers, MA, EE.UU.). Después de lavar con PBS-T, los cubreobjetos se incubaron con el anticuerpo secundario conjugado con Alexa Fluor 568 (ab175473, 1:100, Abcam, Cambridge, Reino Unido) en 1% BSA en PBS-T durante 1 h a temperatura ambiente. Después de tres lavados con PBS-T, los cubreobjetos se incubaron durante 5 min con PBS-T que contenía 10 µM DAPI. Finalmente, los cubreobjetos se montaron con Vectashield Vibrance (H-1700, Vector Laboratories, Burlingame, CA, EE.UU.) en portaobjetos y se sellaron con esmalte. Las imágenes digitales se capturaron utilizando un microscopio invertido Zeiss LSM 880 con un objetivo de inmersión en aceite de 63× a la longitud de onda adecuada (excitación a 587 nm para mCherry, excitación a 568 nm para tubulina y excitación a 405 nm para DAPI) y se analizaron utilizando el software FIJI 1.53.

Para detectar γ-H2AX, se realizaron todas las técnicas como se describió anteriormente (sin transfección de plásmido y utilizando faloidina para teñir el citoesqueleto). Se utilizó anti-γ-H2AX (D17A3) (Cell Signaling Technology, Danvers, MA, EE.UU.) (1:100) como anticuerpo primario, y se utilizó un anticuerpo secundario conjugado con Cy2 de anti-goat-rabbit (ab6940, Abcam, Cambridge, Reino Unido). Las imágenes digitales se

adquirieron utilizando un microscopio invertido Zeiss LSM 880 con un objetivo de inmersión en aceite de 60×. Las señales de fluorescencia se detectaron con Cy2 (para γ-H2AX) a una longitud de onda de excitación de 490 nm y una longitud de onda de emisión de 525 nm, y con DAPI a una longitud de onda de excitación de 405 nm y una longitud de onda de emisión de 461 nm. Todas las imágenes fueron procesadas utilizando el software FIJI 1.53.

10.11 Análisis estadístico

Las curvas de dosis-respuesta para estimar la viabilidad celular se trazaron tomando los logaritmos de las concentraciones del compuesto a lo largo del eje X y la viabilidad celular a lo largo del eje Y. Utilizando el software GraphPad Prism 8.0.2 (Inc., La Jolla, California, EE. UU.), se eligió el parámetro "Log (inhibidor) vs. respuesta normalizada" para estimar el valor de IC_{50} (concentración de un fármaco que produce una respuesta inhibitoria máxima del 50%). Los resultados se expresan como media ± error estándar (SD) o error estándar de la media (SEM). Se utilizó GraphPad Prism 8.0.2 para el análisis estadístico. Las diferencias entre dos grupos se analizaron mediante ANOVA de una vía, y las diferencias entre grupos se analizaron mediante ANOVA de dos vías con las pruebas de comparación múltiple de Dunnett y Tukey. La significancia estadística se indica de la siguiente manera: * $p < 0.05$, ** $p < 0.01$, *** $p < 0.001$ y **** $p < 0.0001$.

11. Resultados

11.1 Evaluación Citotóxica de los compuestos

Se observó un efecto dependiente de la dosis en el porcentaje de inhibición celular de LAH y LIR a medida que aumentaba la concentración del medicamento, así como en el tiempo de exposición al tratamiento.

La IC_{50} para LAH se estableció después de 24 h de tratamiento a concentraciones de 7.184 μM y 20.35 μM en las líneas celulares HCT116 (Fig. 8A) y SW620 (Fig. 8B), respectivamente. Para LIR, la IC_{50} después de 24 h de tratamiento se estableció a concentraciones de 22.76 μM, 29.12 μM para las líneas celulares HCT116 (Fig. 8D), y SW620 (Fig. 8E), respectivamente. La concentración de LAH en la línea celular no

tumoral (CRL1790) (Fig. 8C) no se definió después de 24 h de tratamiento, sugiriendo que probablemente se necesite una concentración más alta para establecer el IC_{50}. Mientras tanto, para LIR, la IC_{50} fue de 47.27 µM (Fig. 8F), lo que indica un mayor porcentaje de inhibición del crecimiento celular en comparación con las células tumorales, sugiriendo una mayor resistencia. Además, la línea celular SW620 mostró un mayor porcentaje de inhibición en comparación con la línea celular HCT116 con ambos compuestos. Estos resultados sugieren que los tratamientos pueden ser selectivos para las células cancerosas.

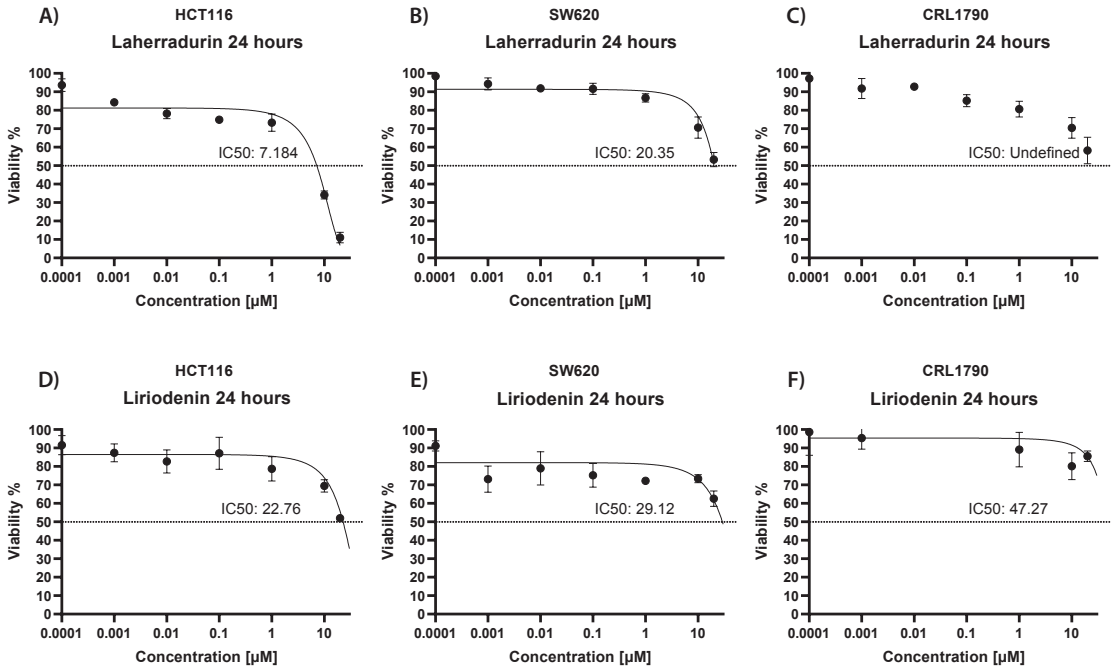


Figura 8: Viabilidad celular en células de CRC y células no tumorales

Curvas de dosis-respuesta que muestran los valores de IC_{50} de células tratadas con LAH (A-C) y LIR (D-F) durante una exposición de 24 h, evaluadas mediante ensayo de SRB y MTT. Los datos se presentan como la media ± SEM de experimentos biológicos realizados por triplicado.

11.2 Análisis de los complejos de la ETC

Para investigar si LAH y LIR inhiben la ETC, particularmente el complejo I, en las líneas celulares HCT116, SW620 y CRL1790, se llevó a cabo la inmunodetección de los complejos de fosforilación oxidativa (OXPHOS) utilizando WB. La Fig. 9A muestra que tanto LAH como LIR exhiben una reducción en la expresión de los complejos I (Fig. 9B),

IV (Fig. 9C) y II (Fig. 9D). Sin embargo, no se observan cambios significativos en la detección de los complejos III (Fig. 9E) y V (Fig. 9F). Por lo tanto, LAH y LIR inhiben la ETC.

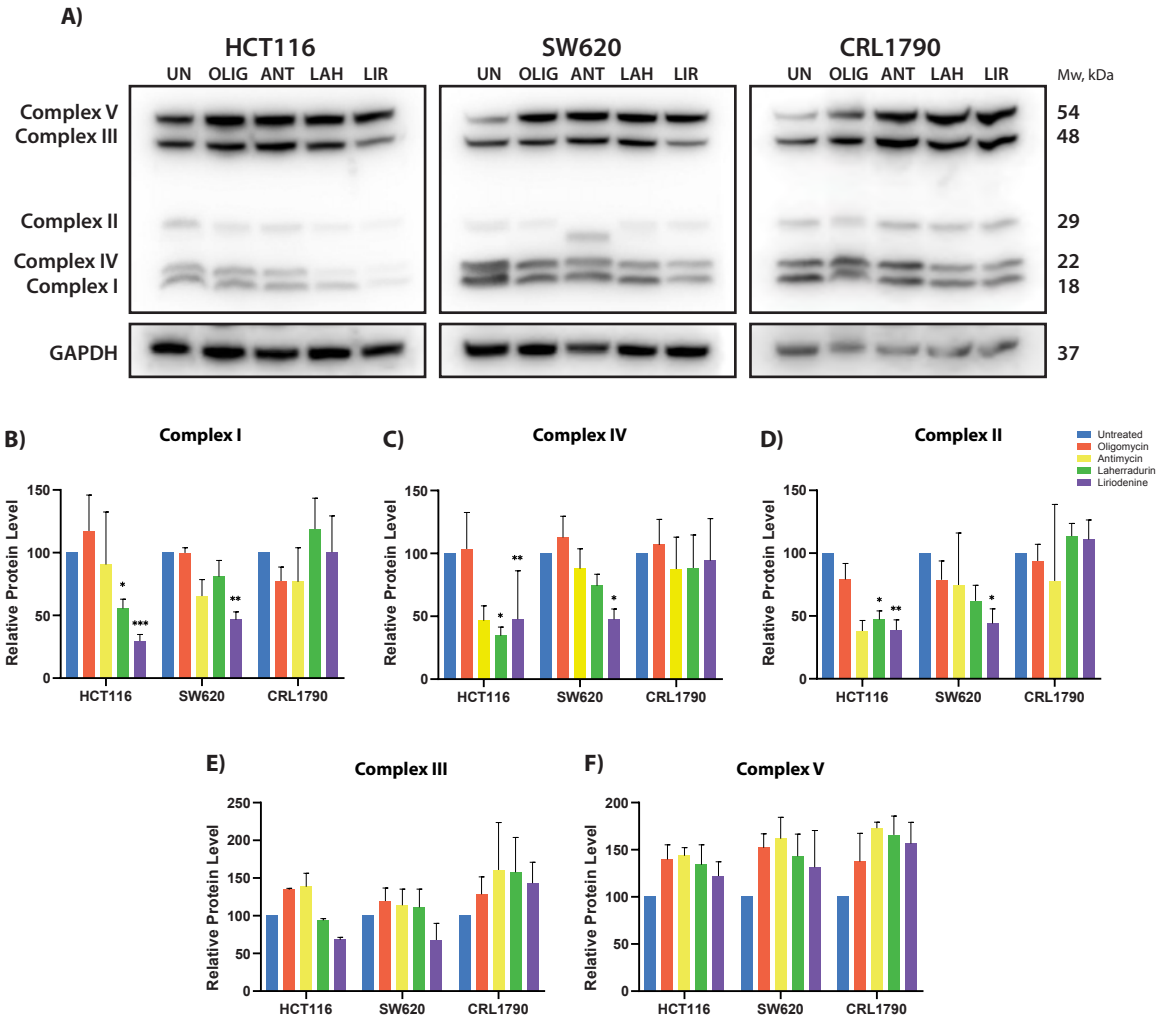


Figura 9: Expresión de complejos de OXPHOS en mitocondrias de células de CRC y no tumorales

*Se utilizó un cóctel de anticuerpos dirigidos a proteínas que representan los cinco complejos de OXPHOS mitocondrial para evaluar la expresión de proteínas mitocondriales en líneas celulares de CRC: HCT116, SW620 y CRL1790 (A), bajo las siguientes condiciones experimentales: Sin Tratamiento (UN), Oligomicina, Antimicina A (ANT), LAH y LIR. GAPDH se utilizó como control de carga. El cóctel de anticuerpos incluyó los siguientes blancos: subunidad NDUFB8 del complejo I (B), subunidad SDHB del complejo II (D), subunidad UQCR2 del complejo III (E), subunidad MTCO1 del complejo IV (C) y subunidad ATP5A del complejo V (F). El WB se replicó técnicamente tres veces en total, demostrando un blot representativo. Los valores se expresan como media ± SEM normalizada en relación con su control respectivo y luego se presentan como cambio relativo al tratamiento; ***P < 0.01, **P < 0.05, *P < 0.1. Se aplicó una prueba de ANOVA de dos vías con prueba de comparaciones múltiples de Dunnett.*

11.3 Análisis de cambios en el estado energético mediante cuantificación de ATP

Dado el efecto inhibitorio de LAH y LIR sobre la OXPHOS, procedimos a investigar los niveles de ATP, los cuales podrían indicar alteraciones metabólicas en las células de CRC. Para ello, empleamos tratamientos con oligomicina, glucosa y 2-desoxi-D-glucosa (2-DG). La oligomicina inhibe la ATP sintasa, mientras que la glucosa proporciona sustrato para la glucólisis y el 2-DG la inhibe. Como se muestra en la Fig. 10, observamos una disminución en los niveles de ATP después del tratamiento con oligomicina y 2-DG, indicando su efectividad en la interrupción de las vías de producción de energía. No hubo cambios significativos en los niveles de ATP en las células tratadas con glucosa en comparación con el control. Como era de esperar, se observó una notable disminución en los niveles de ATP después del tratamiento con LAH y LIR, lo que sugiere una interrupción potencial de las vías de producción de energía y una reprogramación metabólica en las células de CRC. Esto destaca el impacto de LAH y LIR en la función mitocondrial y el metabolismo glucolítico. Para verificar esta información, se realizó el perfil bioenergético de estas células utilizando la plataforma Seahorse XF-Bioanalyzer.

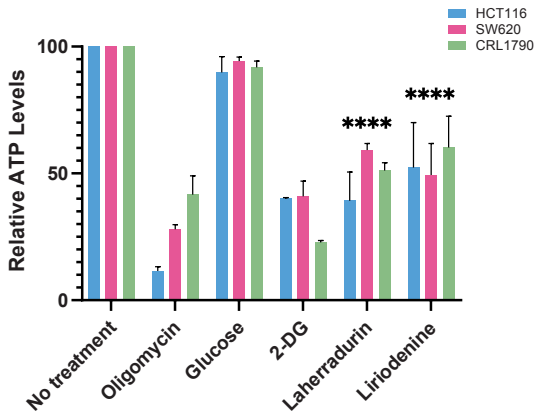


Figura 10: Disminución en los niveles de ATP Inducido por los LAH y LIR

*Niveles relativos de ATP de las células a las 24 h de tratamiento. Los grupos de tratamiento incluyeron: Sin tratamiento, Oligomicina, Glucosa, 2-DG, LAH y LIR. Los resultados se presentan como la media ± SE de tres experimentos independientes. La significancia estadística se determinó mediante una prueba de ANOVA de dos vías con la prueba de comparaciones múltiples de Tukey (****P < 0.001).*

11.4 Análisis de la tasa de glucólisis mediante la medición del eflujo de protones

La producción de energía en las células ocurre a través de dos vías: la glucólisis y la respiración mitocondrial. Para demostrar la inhibición de la ETC, se evaluó la tasa glucolítica mediante la medición de la tasa de acidificación extracelular (ECAR) y la tasa de consumo de oxígeno (OCR), indicadores de glucólisis y OXPHOS, respectivamente.

Durante la glucólisis, la conversión de glucosa a lactato conduce a la producción neta y expulsión de protones hacia el medio extracelular. Además, el CO_2 derivado de las mitocondrias puede contribuir a la acidificación extracelular. Para calcular la acidificación atribuida a las mitocondrias y al CO_2, se midió el consumo de oxígeno por parte de la célula y se restó de la tasa total de eflujo de protones (PER) (Fig. 11A).

El valor resultante, glicoPER, representa la tasa de protones extruidos durante la glucólisis. Las Figs. 11B-D ilustran que las líneas celulares tratadas con rapamicina (RAP) (incluida debido a su papel en la inhibición de mTOR y la regulación metabólica) y las células no tratadas, que exhiben una baja tasa glucolítica basal, mientras que LAH y LIR muestran una tasa glucolítica más alta en comparación con los controles. Este aumento se atribuye a la inhibición de la OXPHOS, lo que conduce a niveles elevados de glucólisis. Las Figs. 11E-G muestran que la RAP mostró valores similares al control no tratado en la tasa basal de eflujo de protones, indicando que no hubo alteraciones significativas en el ETC o en el estado glucolítico. En contraste, los tratamientos con LAH y LIR indujeron cambios significativos, evidenciados por un aumento en la tasa basal de eflujo de protones, destacando su impacto distintivo en las vías metabólicas celulares de las células de CRC. La Fig. 11H muestra que LAH y LIR resultaron en una tasa total de eflujo de protones un 50% más alta que la de las células no tratadas y tratadas con RAP. Estas observaciones sugieren fuertemente una mayor glucólisis en las células de CRC tratadas con estos compuestos.

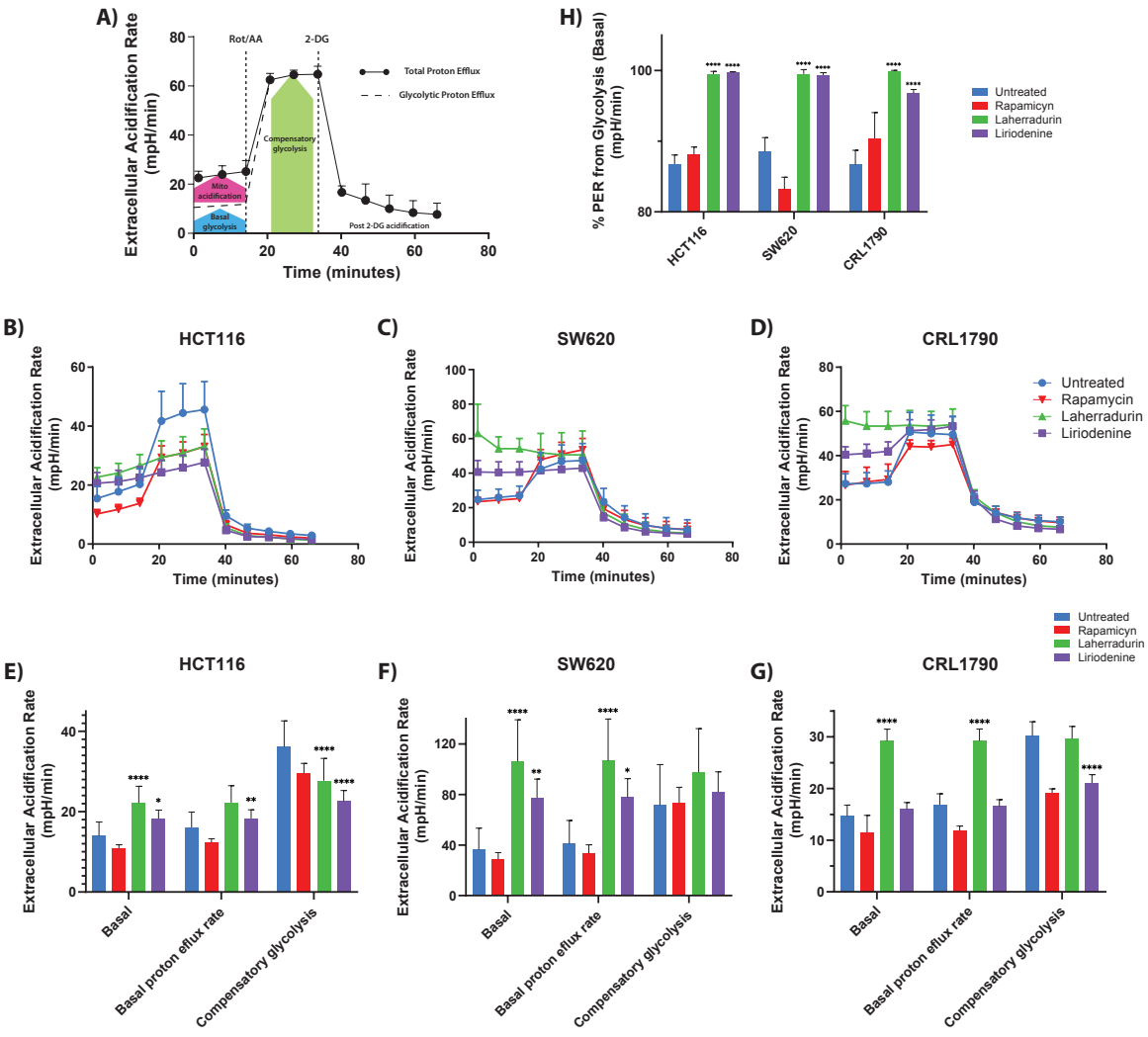


Figura 11: Análisis del flujo glucolítico en células de CRC y no tumorales

*(A) Análisis de flujo extracelular que muestra la tasa de eflujo de protones. (B-D) ECAR después de la adición secuencial de diferentes moduladores de la función glucolítica (Rotenona/Antimicina A y 2-DG) se determinó utilizando un analizador Seahorse XF96. Las células fueron tratadas con LAH y LIR durante 24 h. (E-G) Perfil bioenergético de parámetros glucolíticos. Basal: respiración basal. Tasa de eflujo de protones basal: (glicoPER) tasa basal de glucólisis. Glucólisis compensatoria: la capacidad de la célula para compensar la producción de energía a través de la glucólisis después del bloqueo de la producción de ATP mitocondrial. (H) % PER de glucólisis representa la contribución de la vía glucolítica a la acidificación extracelular total. Los resultados representan al menos tres experimentos biológicos independientes, cada uno de los cuales consistió en la siembra independiente de células en ocho pozos de microplacas Seahorse. Los datos se presentan como media ± SE. ****P < 0.001, ***P < 0.01, **P < 0.05, *P < 0.1, en relación con el control mediante una prueba de ANOVA de dos vías con la prueba de comparaciones múltiples de Dunnett.*

11.5 Análisis del potencial de membrana mitocondrial

Las mitocondrias funcionan como reguladores cruciales en diversas vías celulares que conducen a la apoptosis o autofagia (69). El daño celular desencadena un aumento en ROS, que a su vez provoca alteraciones en el transporte de electrones, la producción de

ATP y el MMP, culminando en la liberación de proteínas señalizadoras de muerte celular en el citosol (70). El MMP es fundamental para la OXPHOS y desempeña un papel pivotal en el proceso de almacenamiento de energía, siendo esencial para la síntesis de ATP. Además, el MMP participa en la activación de componentes señalizadores de muerte celular. El MMP se genera principalmente por bombas de protones, con los complejos I, III y IV. Mantener el MMP en un nivel estable es crucial para la función celular normal (71) (72).

Para evaluar el MMP en células de CRC tratadas o no con LAH y LIR, se realizó tinción con TMRM. TMRM es un tinte lipofílico catiónico (+ cargado), de color naranja-rojo, permeable a las células. Debido al potencial de membrana negativo de las mitocondrias, el TMRE es captado por estas a través de una diferencia de potencial transmembrana. Una vez dentro, se oxida y emite fluorescencia. LAH puede inducir apoptosis y autofagia, procesos asociados con alteraciones en el MMP. Las células no fluorescentes (histograma rojo) no muestran señal, pero al añadir el fluoróforo, se emiten señales de TMRM (histograma azul). En presencia tanto de LAH como de LIR, se observa un aumento significativo en la intensidad de la señal de TMRM en las tres líneas celulares (histogramas verde bosque y morado) (Fig. 12A-C), sugiriendo un incremento en $\Delta\Psi_M$ (Fig. 12D). Esto probablemente desencadena la inhibición de la OXPHOS y la acumulación subsiguiente de protones, lo que conduce a un aumento en la glucólisis, así como a la regulación al alza de ROS.

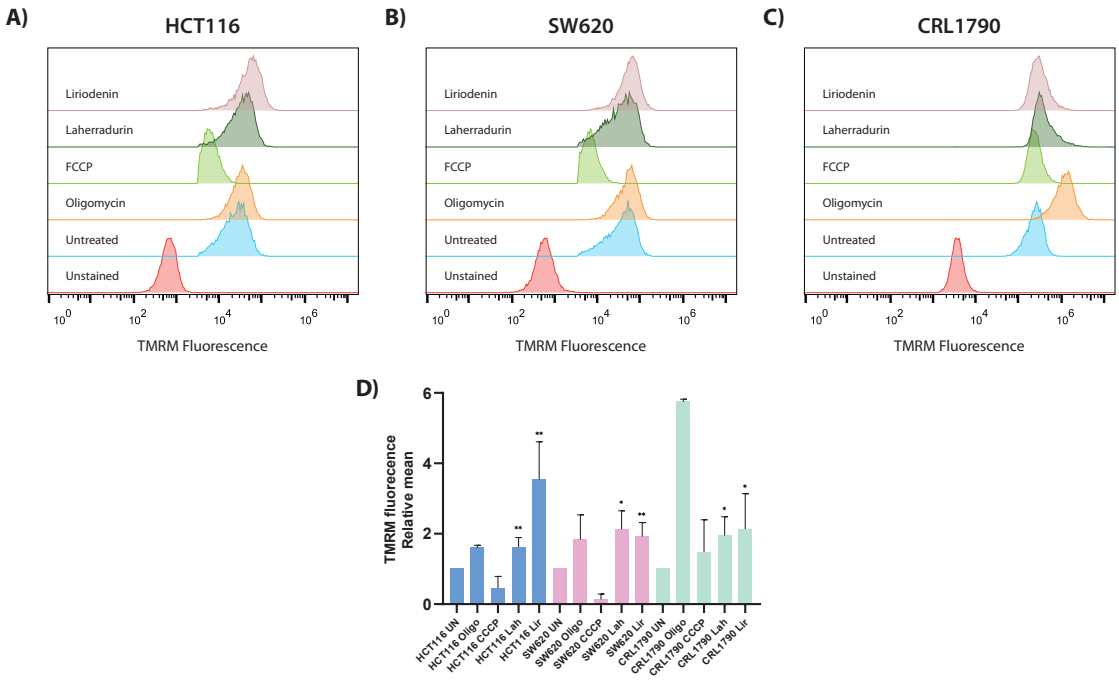


Figura 12: Disrupción de $\Delta\Psi_M$ y alteraciones bioenergéticas.

*(A-B) Citogramas representativos que muestran la intensidad relativa de TMRM en células de cáncer colorrectal (CRC) y en células no tumorales (C) tratadas con LAH durante 24 h. (D) El gráfico de barras muestra la intensidad relativa de TMRM en células de CRC tratadas con LAH a las 24 h. Los resultados representan al menos tres experimentos biológicos independientes. La significancia estadística en relación con el control se determinó mediante una prueba t de una muestra. **p < 0.05, *p < 0.1*

11.6 Medición de la respiración mitocondrial mediante análisis de flujo extracelular

The Seahorse XF Cell Mito Stress Assay, que examina seis parámetros bioenergéticos de la respiración mitocondrial (Fig. 13A). Inicialmente, se midió la respiración basal, reflejando el consumo inicial de oxígeno utilizado por las células para satisfacer la demanda de ATP. Posteriormente, se introdujo el inhibidor de la ATP sintasa, Oligomicina, para inhibir la producción de ATP, proporcionando información sobre la respiración ligada a ATP. Luego se evaluó la fuga de protones, indicando daño mitocondrial, como una disminución en el consumo de oxígeno debido al desacoplamiento del MMP (Fig. 13A). Después del tratamiento con oligomicina, se añadió el cianuro 4-(trifluorometoxi)fenilhidrazona (FCCP), un desacoplador de la OXPHOS, para medir la capacidad respiratoria de reserva. Este parámetro evalúa el ATP adicional que puede ser producido por la OXPHOS bajo demandas energéticas aumentadas. También se midió

la respiración máxima, que representa la tasa máxima de consumo de oxígeno alcanzada al estimular la cadena respiratoria, durante la administración de FCCP. Finalmente, se administró rotenona, un inhibidor del complejo I, para observar cambios en el consumo de oxígeno y la respiración no mitocondrial. La evaluación precisa de la respiración mitocondrial es crucial para comprender la bioenergética celular.

El análisis reveló que el tratamiento con RAP (incluido debido a sus efectos en las vías de señalización de mTOR, que pueden influir en el metabolismo celular y la función mitocondrial) mostró una ligera reducción en los valores de OCR en comparación con el control, aunque no tan pronunciada como se observó con los tratamientos LAH y LIR. Desde el principio, hubo una reducción significativa en el OCR mitocondrial basal en las tres líneas celulares en comparación con los controles no tratados (Fig. 13B-D). El patrón observado persistió con el OCR mitocondrial manteniéndose sensible al inhibidor de la ATPasa, Oligomicina; sin embargo, el tratamiento con RAP mostró una ligera disminución en el OCR, mientras que los compuestos disminuyeron notablemente los valores. Además, el OCR asociado con la producción de ATP en las tres líneas celulares tratadas con los compuestos fue menor en comparación con las células no tratadas o tratadas con RAP. Además, tras la inyección del segundo compuesto, FCCP, para permeabilizar la membrana interna y revelar la capacidad respiratoria mitocondrial máxima, no se observó un aumento en la respuesta de OCR en las mitocondrias tratadas con los compuestos, a diferencia de las células de control y las tratadas con RAP. Estos hallazgos sugieren un daño bioenergético mitocondrial significativo en las tres líneas celulares (Fig. 13E-G).

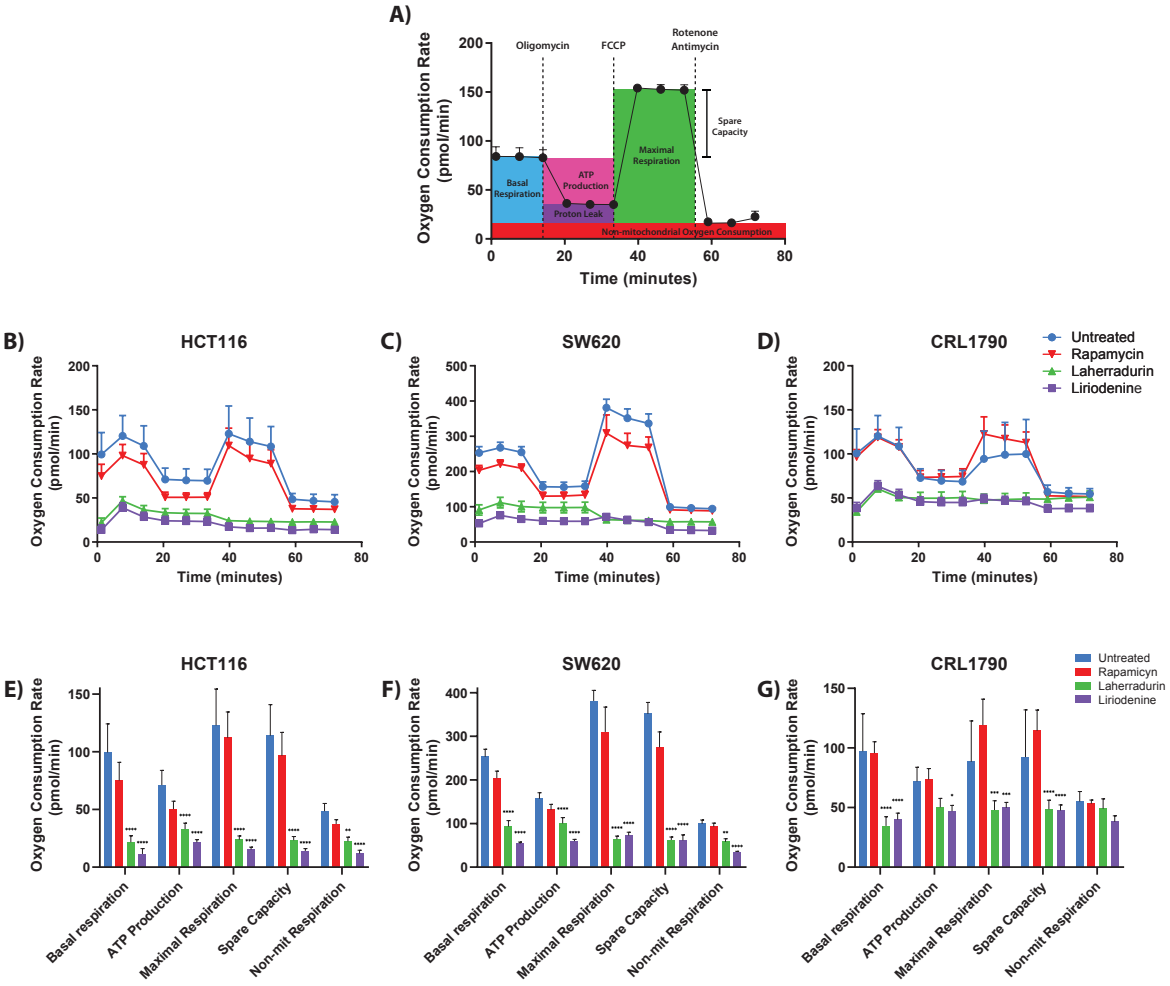


Figura 13: Análisis del flujo metabólico de células de CRC y no tumorales

*(A) Representación esquemática que ilustra el consumo de oxígeno medido mediante análisis de flujo extracelular, destacando los parámetros calculables. (B-D) OCR después de la adición secuencial de varios moduladores de la función mitocondrial (Oligomicina, FCCP y Rotenona/Antimicina A) se determinó utilizando un analizador Seahorse XF96. Las células fueron tratadas con LAH y LIR individualmente durante 24 h. (E-G) Perfil bioenergético que comprende seis parámetros de respiración: Respiración basal, respiración relacionada al ATP, capacidad respiratoria máxima, capacidad respiratoria libre y respiración no mitocondrial. Los resultados se muestran de tres experimentos biológicos independientes, cada uno de ellos involucrando siembras de células independientes en ocho pozos de microplacas de Seahorse. Los datos se presentan como media ± SE. La significancia estadística en relación con el control se indica de la siguiente manera: ****P < 0.001, ***P < 0.01, **P < 0.05, *P < 0.1, según lo determinado por ANOVA de dos vías con prueba de comparaciones múltiples de Dunett.*

11.7 Análisis de la dinámica mitocondrial

Se utilizó tinción con Mitotracker para evaluar si los tratamientos con LAH y LIR afectaron el MMP y posteriormente alteraron la dinámica mitocondrial de las células de CRC tratadas.

Mitotracker, posee un grupo clorometilo reactivo a tiol para el marcaje mitocondrial, funciona como un colorante lipofílico catiónico (+). Dado el MMP negativo, los colorantes lipofílicos catiónicos pueden penetrar la membrana celular y acumularse en la matriz mitocondrial a través del gradiente de MMP.

Las observaciones revelan una red mitocondrial altamente dinámica en el control negativo (células no tratadas) (Fig. 14), indicando fisión mitocondrial y asociado con una mayor producción de ATP. A continuación, se trataron las células de CRC con dos inhibidores como controles: Cloroquina (CQ) y RAP. La CQ, un inhibidor de la autofagia impide la fusión de autofagosomas y lisosomas al afectar el pH lisosomal. Después del tratamiento con 50 µM de CQ, las mitocondrias mostraron morfología esférica, alargadas en forma de varilla, o en disposiciones filamentosas, similares a las observadas en las células no tratadas (73) (Fig. 14). Esto indica que no se observaron eventos de mitofagia, sugiriendo que la CQ inhibió exitosamente el proceso de unión de autofagosomas y lisosomas. Por otro lado, el RAP inhibe la señalización de mTOR e induce la privación de nutrientes, lo que conduce a la fusión mitocondrial. Esto resulta en elongación mitocondrial (hiperfusión) (74), protegiéndolas de la degradación (75). Mientras que el tratamiento con LAH y LIR resulta en fragmentación mitocondrial (Fig. 14). Esta fragmentación está estrechamente vinculada con el deterioro de la OXPHOS, daño en el ADN mitocondrial y producción de ROS.

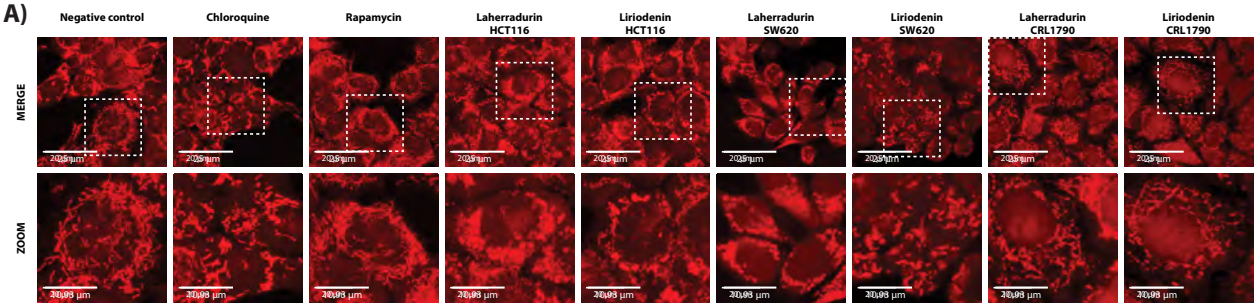


Figura 14: Los compuestos naturales inducen fragmentación mitocondrial

Morfología de las mitocondrias teñidas con MitoTracker Rojo en células de CRC y no tumorales. Imágenes de fluorescencia tomadas con microscopía confocal LEICA a 63× con MitoTracker, DAPI y ZOOM con tratamientos: No tratado, RAP, CQ, LAH, LIR a 24 h de exposición. Las fotos son representativas de al menos tres experimentos independientes. Barra de escala: 25 µm, zoom: 10.93 µm.

11.8 Medición del contenido de masa mitocondrial

LAH y LIR inducen la fragmentación mitocondrial, posiblemente relacionada con el aumento de la masa mitocondrial. Para medir la masa mitocondrial, se utilizó la tinción con NaO, que se incorpora en las membranas mitocondriales internas y se une a la cardiolipina. La intensidad de la tinción de NaO es independiente del MMP.

Se observó que la masa mitocondrial aumenta con los tratamientos en las tres líneas celulares después de 24 horas, probablemente debido a la fragmentación causada por los compuestos. Las células sin fluorescencia (histograma rojo) no muestran señal; cuando se agrega la etiqueta de fluoróforo, se emiten señales de NaO (histograma azul). Sin embargo, en presencia de los compuestos, la intensidad de la señal de NaO aumentó en las tres líneas celulares, indicando un aumento en el contenido de masa mitocondrial (Fig. 15).

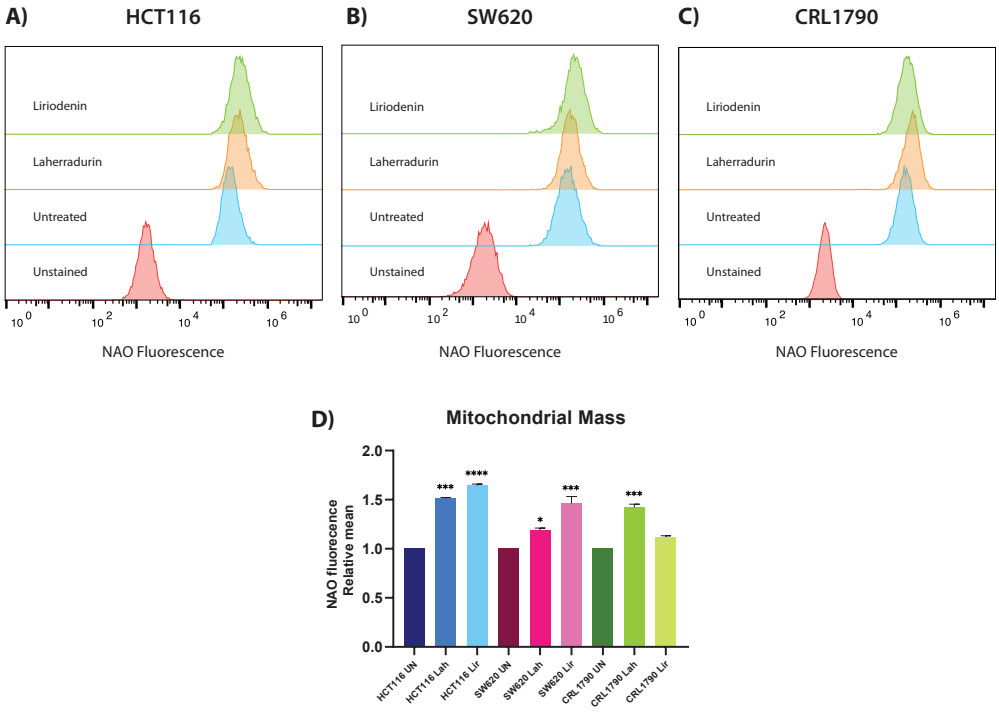


Figura 15: Contenido de masa mitocondrial en células de CRC y no tumorales.

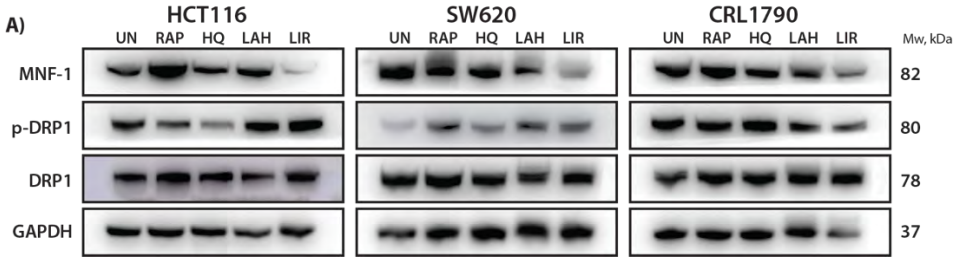
(A-B) Citogramas representativos que muestran la intensidad relativa de NaO en células de cáncer colorrectal (CRC) y en células no tumorales (C) tratadas con LAH durante 24 h. (D) El gráfico de barras ilustra la intensidad relativa de NaO de las células de CRC tratadas con LAH y LIR durante 24 h. Los resultados representan datos de al menos tres experimentos biológicos independientes y se presentan como media ± SE. La significancia estadística se determinó

*utilizando ANOVA de una vía con prueba de comparaciones múltiples de Tukey, con ****P < 0.001, ***P < 0.01 y *P < 0.1, en relación con el control.*

11.9 Analisis de proteínas involucradas en la dinámica mitocondrial

Para validar la inducción de daño y fisión mitocondrial por los compuestos en las líneas celulares HCT116, SW620 y CRL1790, se realizó un análisis de WB para analizar el comportamiento de las proteínas asociadas con la dinámica mitocondrial, específicamente la mitofusina 1 (MFN1) y la proteína relacionada con la dinamina 1 (DRP1), el regulador principal de la fisión mitocondrial, una proteína citosólica de la familia de las GTPasas. La fisión mitocondrial se activará cuando CDK1 fosforile receptores de la membrana externa, como la proteína de fisión mitocondrial 1 (FIS1), el factor de fisión mitocondrial (MFF) y MiD49/51, que reclutan y polimerizan DRP1. Esta polimerización ocurre en espirales alrededor de las mitocondrias y, mediante la hidrólisis de trifosfato de guanosina (GTP), constriñe las mitocondrias provocando la ruptura de la membrana.

Se observa disminución significativa en la expresión de la proteína MFN1, particularmente en el tratamiento con LIR de las líneas celulares HCT116 y CRL1790 (Fig. 16A), mientras que ambos tratamientos resultan en niveles disminuidos de MFN1 en la línea celular SW620 (Fig. 16B). Por el contrario, se observa aumento significativo en la detección de DRP1 fosforilado en las líneas celulares de CCR con ambos tratamientos, lo que sugiere que los compuestos pueden inducir la fisión mitocondrial. No se observan cambios significativos en la línea celular no tumoral (Fig. 16C). No se observan cambios significativos en la detección de DRP1 total en las tres líneas celulares (Fig. 16D).



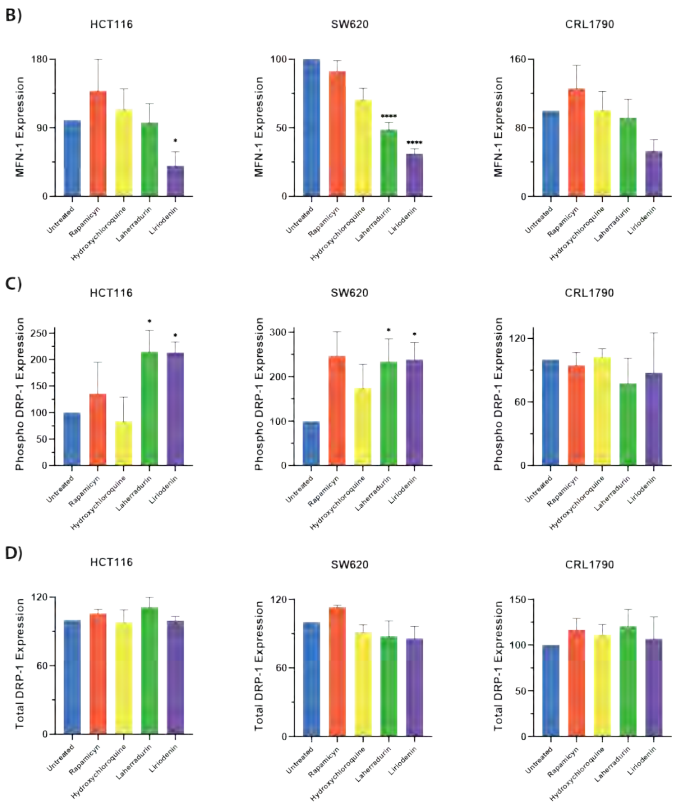


Figura 16: Detección de proteínas involucradas en la dinámica mitocondrial

*Imágenes representativas de tres experimentos independientes y cuantificación de los niveles de expresión de las proteínas MFN1, p-DRP1 y DRP1, GAPDH utilizado como control de carga. Los valores se expresan como media ± SE, normalizados en relación con el control. La significancia estadística se determinó utilizando una prueba ANOVA de una vía, seguida de la prueba de comparaciones múltiples de Dunnett, con ***P < 0.01, **P < 0.05 y *P < 0.1 indicando significancia.*

11.10 Análisis de marcadores moleculares de la vía mTOR mediante detección de proteínas

La vía de señalización de mTOR se destaca como una de las principales vías desreguladas en el CRC, promoviendo el metabolismo energético a través de una mayor actividad de las enzimas metabólicas. Para demostrar la función de la vía mTOR, se realizó la inmunodetección de proteínas mediante WB para la proteína de unión al factor de iniciación eucariótico 4E (4E-BP1), tanto en sus formas total como fosforilada, que son sustratos de mTORC1. La Fig. 17A ilustra una disminución en la forma fosforilada (Fig. 17B) y total de 4E-BP1 (Fig. 17C), sugiriendo una posible inhibición de mTOR por los compuestos.

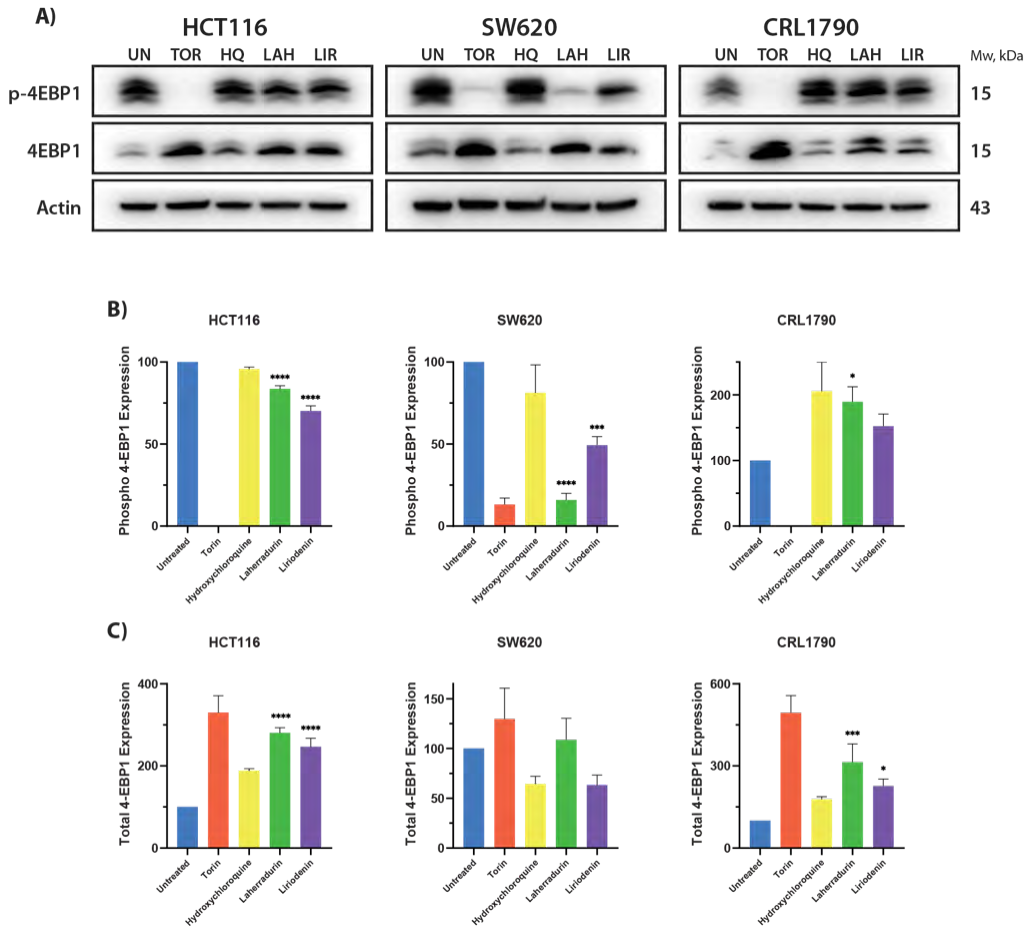


Figura 17: Detección de 4E-BP1, sustrato de mTOR

*Imágenes representativas y cuantificación gráfica de los niveles de expresión de las proteínas p-4E-BP1 y 4E-BP1. GAPDH se utilizó como control de carga. Las réplicas se realizaron un total de tres veces. Los valores se expresan como media ± SE, normalizados en relación con el control. La significancia estadística se determinó utilizando una prueba ANOVA de una vía, seguida de la prueba de comparaciones múltiples de Dunnett, con ***P < 0.01, **P < 0.05 y *P < 0.1 indicando significancia.*

11.11 Análisis de autofagia

Dado que LAH y LIR inhiben la fosforilación de 4E-BP1, es probable que mTORC1 se vea afectado, lo que potencialmente impacta el flujo autofágico. Para explorar esto, se evaluó la inducción de autofagia mediante detección fluorescente. Las células fueron transfectadas con el plásmido mCherry-eGFP-LC3B y tratadas con Torin 1, HCQ y LAH durante 24 h. Este ensayo permite visualizar los autolisosomas como puntos rojos, marcando así la actividad autofágica.

El tratamiento con Torin 1 (un inhibidor de mTORC1 y promotor de la autofagia), HCQ y LAH resultó en la formación de puntos positivos para mCherry (Fig. 18). Es importante destacar que, aunque tanto Torin 1 como HCQ generaron puntos positivos para mCherry, sus mecanismos de acción son distintos. Torin 1 promueve la autofagia al inhibir mTORC1, lo que provoca un aumento en la formación de autofagosomas, mientras que HCQ bloquea la fusión de los autofagosomas con lisosomas, causando la acumulación de vacuolas autofágicas. Esta diferencia subraya los variados efectos de los tratamientos en la regulación de la autofagia.

En el tratamiento con LAH y LIR se observó un aumento en la formación de puntos autofágicos, lo que sugiere un reclutamiento de LC3 y la subsecuente formación de autofagolisosomas, promoviendo así la degradación celular. Sin embargo, en la línea celular no tumoral no se detectó la formación de puntos LC3, lo que indica que la autofagia no fue inducida por estos tratamientos.

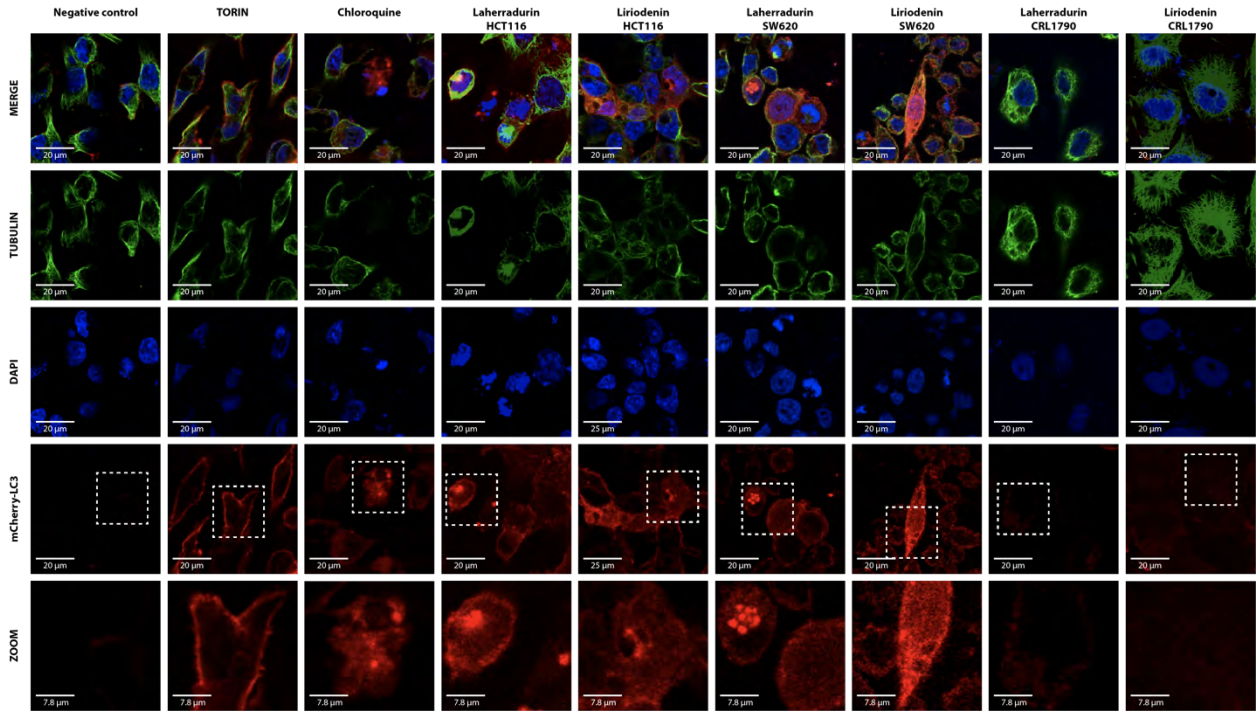


Figura 18: Inducción de autofagia por compuestos naturales.

Autofagosomas teñidos con mCherry en células de CRC y no tumorales. Imágenes de fluorescencia capturadas con microscopía confocal Zeiss LSM 880 a 63×. Se muestran mCherry-LC3, Tubulina, DAPI y ZOOM con tratamientos: Sin tratar, TOR, CQ, LAH, LIR durante 24 horas de exposición. Las fotos son representativas de al menos tres experimentos independientes. Barra de escala: 20 µm, zoom: 7.8 µm.

Para explorar más a fondo el impacto de LAH y LIR en la autofagia en las líneas celulares HCT116 y SW620, se realizó un análisis por WB para observar la expresión de proteínas asociadas con la autofagia: ULK1, p-ULK1, ATG12, LC3I y LC3II. Ambas líneas celulares tumorales mostraron un notable aumento en la detección de fosfo-ULK1. Mientras que las células SW620 exhibieron una regulación al alza de ULK1 total, no se observaron cambios similares en las otras líneas celulares (Fig. 19A). Además, el tratamiento con LAH condujo a un aumento dependiente del tiempo en los niveles de ATG12 en las líneas celulares tumorales, en contraste con los niveles invariables en las células no tumorales. De manera similar, la detección de LC3II aumentó con el tiempo en ambas líneas celulares tumorales, mientras que no se observó tal tendencia en la línea celular no tumoral (Fig. 19B). Estos hallazgos subrayan el potencial de LAH y LIR para inducir selectivamente la autofagia en células tumorales.

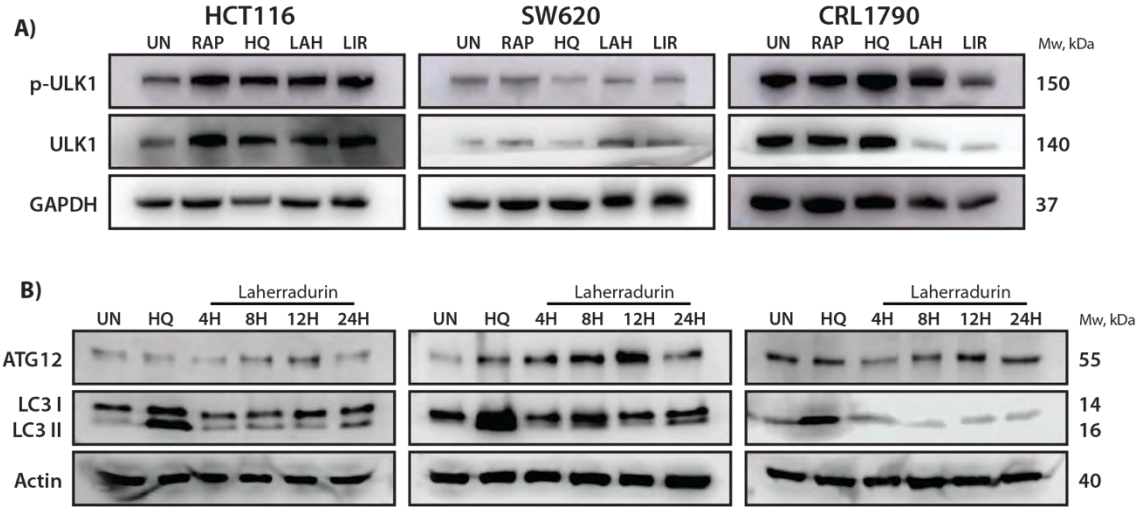


Figura 19: Detección de proteínas involucradas en la autofagia

Imágenes representativas de los niveles de expresión de las proteínas ATG5, ATG12, LC3-I y LC3-II. Actina fue utilizada como control de carga. Se realizaron tres réplicas del experimento.

11.12 Análisis de daño a DNA

Las roturas de doble cadena del ADN (DSBs) se examinaron mediante inmunotinción para fosfo-serina 139 histona 2AX (γ-H2AX), un marcador de DSBs del ADN (Fig. 20). La inducción de los focos de γ-H2AX, como se demuestra mediante inmunotinción, corresponde a los sitios donde se localizan enzimas implicadas en la reparación o

apoptosis. Como se muestra en la Fig. 20, los tratamientos con LAH y LIR en líneas celulares de CRC inducen la producción de γ-H2AX. Esto sugiere que una fracción significativa de la histona γ-H2AX está fosforilada en la cromatina de estas células, señalando la alteración de las estructuras del ADN.

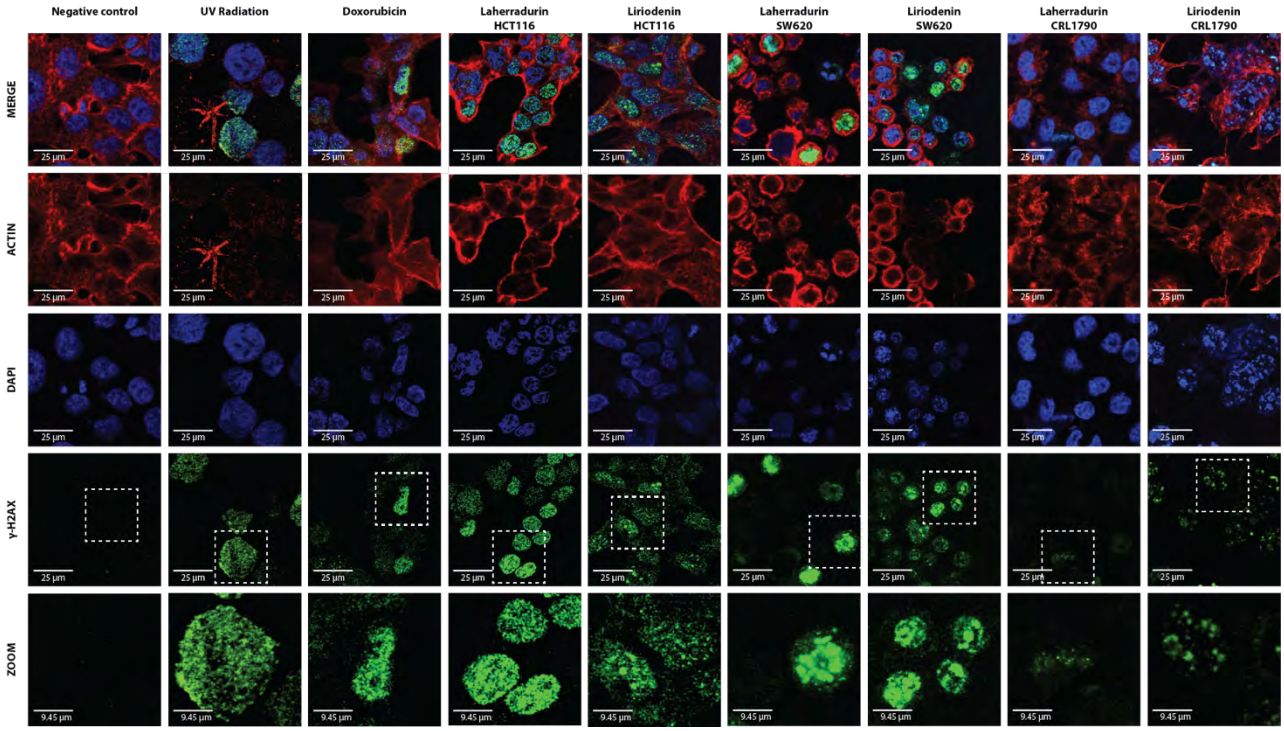


Figura 20: Inducción de focos de γ-H2AX por compuestos naturales

Detección de focos de H2AX en células de CRC y no tumorales. Imágenes de fluorescencia tomadas con microscopía confocal Zeiss LSM 880 a 63×. γ-H2AX, DAPI, ACTINA y ZOOM con tratamientos: Sin tratar, radiación UV, Doxorrubicina, LAH, LIR con exposición de 24 h. Las fotos son representativas de al menos tres experimentos independientes. Barra de escala: 25 µm, zoom: 9.45 µm.

11.13 Detección de proteínas involucradas en la apoptosis.

Para evaluar los efectos apoptóticos de los compuestos en líneas celulares de cáncer colorrectal y no tumoral, se realizó un análisis de WB dirigido a proteínas asociadas con la apoptosis: poli(ADP-Ribosa) polimerasa 1 (PARP-1), factor inductor de apoptosis (AIF), caspasa-8 y caspasa-3. Se observó PARP-1 escindido en ambos tratamientos en las líneas celulares HCT116 y CRL1790, mientras que la esición fue evidente solo en el tratamiento con LIR en las células SW620. Además, los niveles de AIF aumentaron en las tres líneas celulares tras el tratamiento. No hubo cambios evidentes en la detección

de caspasa-8 en HCT116, pero se observó disminución en SW620 y aumento en la línea CRL1790. La caspasa-3 escindida se mostró exclusivamente en las líneas celulares HCT116 y SW620, sin detectarse dicha esición en la línea celular no tumoral (Fig. 21). Estos hallazgos concuerdan con la detección de γ-H2AX, lo que sugiere que el daño en el ADN inducido por los tratamientos no puede ser reparado (Fig. 20), desencadenando así respuestas apoptóticas en líneas celulares de CRC.

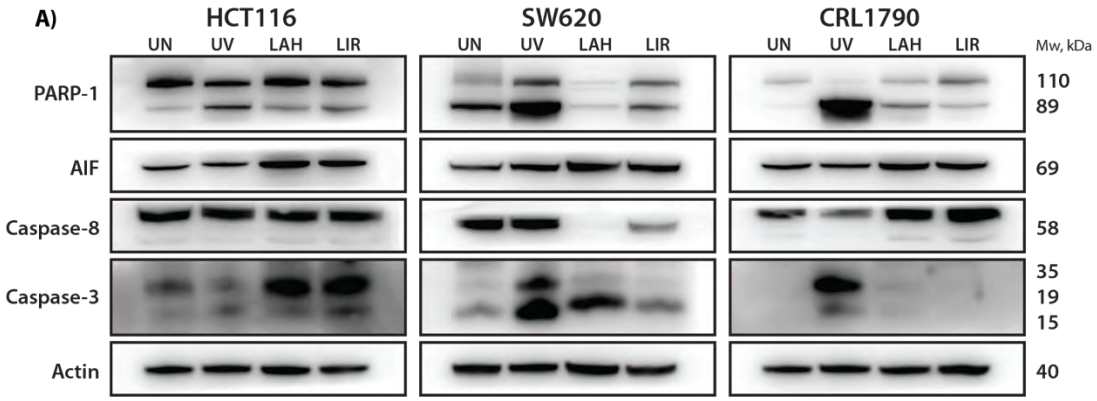


Figura 21: Detección de proteínas involucradas en la apoptosis

Imágenes representativas de los niveles de expresión de las proteínas PARP-1, ATF, Caspasa-8 y Caspasa-3. Actina fue utilizada como control de carga. Se realizaron tres réplicas en total.

12. Discusión

El estudio de los efectos de LAH y LIR en el CCR se extiende más allá de la citotoxicidad y abarca alteraciones en la energética celular. Es ampliamente reconocido que LAH disminuye la función mitocondrial en varios tipos de cáncer, un resultado esperado. Sin embargo, el impacto de LIR en el metabolismo celular del CCR y su influencia en la función mitocondrial deteriorada siguen siendo poco explorados. En este trabajo se presenta, por primera vez, los efectos de estos compuestos naturales en la función mitocondrial y las vías metabólicas, revelando información sobre la interacción entre el metabolismo energético y la progresión del cáncer.

Hace décadas, Otto Warburg descubrió que las células tumorales exhibían una mayor actividad glucolítica en comparación con las células normales, lo que llevó a la hipótesis de daño mitocondrial e inhibición de la OXPHOS en las células tumorales (76). Sin embargo, estudios recientes han discutido este planteamiento, sugiriendo que la función

respiratoria mitocondrial permanece intacta en la mayoría de las células tumorales. De hecho, la actividad de la OXPHOS se incrementa en ciertos tipos de cáncer, desempeñando un papel crucial en la proliferación celular, la metástasis tumoral y la resistencia a la terapia (77). Por ejemplo, Ren et al. (2023) demostraron que la regulación al alza de prohibitina 2 (PHB2) estabiliza el complejo I mitocondrial y aumenta su actividad, lo que resulta en niveles de OXPHOS altamente regulados al alza, promoviendo así la proliferación celular y la tumorigénesis del CCR. Por el contrario, la eliminación de PHB2 reduce significativamente los niveles de OXPHOS mitocondrial en células de CCR (78). Tomando como base estos resultados, se procedió a determinar los niveles de OXPHOS, por lo que se midió el OCR utilizando el kit Mitostres en un Bioenergizador Seahorse (Seahorse Bioscience), que se usa como un indicador de la actividad de la OXPHOS mitocondrial (79). Las células de CRC mostraron un OCR elevado, lo que sugiere que pueden producir más ATP al aumentar su OXPHOS mitocondrial que mediante la glucólisis.

Con base en la comprensión de la función mitocondrial en las células cancerosas, en este trabajo se investigaron los efectos de LAH y LIR en la bioenergética celular. Los compuestos afectaron la función mitocondrial, caracterizada por la reducción en la detección de complejos de OXPHOS, estudios previos han indicado que LAH inhibe el complejo I (44,64); sin embargo, no hay reportes que mencionen la participación de LIR en la inhibición de la OXPHOS. En este estudio, se reveló que LIR contribuye a la alteración de esta cadena; sin embargo, sigue sin estar claro si esta participación es directa o indirecta. La reducción en la detección de estos complejos conduce a la disminución de ATP (80) y a la alteración de la dinámica mitocondrial, destacando el impacto significativo de estos compuestos en el metabolismo celular. Dado el papel fundamental de las mitocondrias en el metabolismo energético, su disfunción contribuye a la patogénesis del CCR (53). Además, estos resultados sugieren que las células de CCR exhiben adaptaciones metabólicas para compensar la OXPHOS deteriorada.

Quian et al. (2010) señalaron que la disfunción en la OXPHOS reduce la generación de ATP mitocondrial, lo que lleva a un aumento compensatorio en la producción total de ATP intracelular en la glucólisis (79). Los resultados de este trabajo coinciden con esta

observación, ya que se demostró Los valores porcentuales de los niveles de ATP representados en la Fig. 10 indican el aporte correspondiente tanto de la mitocondria como de la glucólisis a la producción total de ATP, en comparación con las observaciones de la Fig. 13, en la que sólo se evaluó el ATP generado por la mitocondria. En este trabajo también reveló un deterioro significativo en la respiración mitocondrial máxima, con la capacidad respiratoria reservada disminuida en las células tratadas, lo que indica deterioro de la función mitocondrial. Los resultados se asemejan estrechamente a los de varios estudios que involucran diversos compuestos naturales, que también interrumpen la respiración mitocondrial e inducen una glucólisis compensatoria en diferentes tipos de cáncer (81–83).

Comprender la estrecha relación entre el metabolismo energético y la dinámica mitocondrial es crucial en la biología del cáncer (84). La inducción de la fragmentación mitocondrial y un aumento en el contenido de masa mitocondrial sugieren una interacción compleja entre estas dinámicas y las respuestas metabólicas desencadenadas por LAH y LIR. La fragmentación mitocondrial, frecuentemente asociada con mitocondrias disfuncionales (85) y una mayor producción de ROS, puede contribuir al estrés celular y la apoptosis, en consonancia con los resultados de estudios previos (86).

Las mitocondrias mantienen un equilibrio continuo entre fusión y fisión, un proceso llamado dinámica mitocondrial (87), que es crucial para preservar la morfología mitocondrial y facilitar el intercambio eficiente de contenidos mitocondriales (88). La fusión mitocondrial acelera el intercambio de materiales en las mitocondrias para compensar la función mitocondrial (84), mientras que la fisión mitocondrial elimina las mitocondrias dañadas a través de la mitofagia. El equilibrio en la fusión-fisión mitocondrial está controlado por varios reguladores (86). La fusión mitocondrial en la membrana mitocondrial externa está mediada por MFN1 y mitofusina 2 (MFN2), mientras que la fusión en la membrana mitocondrial interna está mediada por la proteína de atrofia óptica 1 (OPA1) (89). La fisión mitocondrial está mediada por DRP1, FIS1 y MFF (84).

Previamente, se reportó que las células dependientes de OXPHOS exhiben niveles elevados de MFN1/2 (90). Por el contrario, la deficiencia de MFN1/2 resulta en

morfología mitocondrial aberrante, caracterizada por fragmentación pronunciada de la red (91). Los resultados indican que LIR reduce los niveles de MFN1, sugiriendo disrupción de la fusión de la membrana mitocondrial externa, consistente con los resultados en este trabajo de MitoTracker que muestran la fragmentación de la red mitocondrial inducida por LIR. Sin embargo, con el tratamiento de LAH, no se observa reducción en los niveles de MFN1 a nivel de proteína. Esta discrepancia puede atribuirse al posible papel compensatorio de MFN2, que puede sustituir a MFN1 (92) en mitocondrias que carecen de MFN1 debido a su similitud estructural (91).

Por otro lado, Li et al. (2017) demostraron que la polifilina I, un compuesto natural extraído de los rizomas de Paris polyphylla, induce la translocación mitocondrial de DRP1, lo que conduce a la fisión mitocondrial, la liberación de citocromo c de las mitocondrias al citosol y, en última instancia, la apoptosis (93). En este estudio, se observó aumento en la fisión mitocondrial, como lo demuestran los niveles elevados de la proteína p-Drp1 en células de CRC expuestas a los tratamientos, pero no en la línea no tumoral. Estos resultados son consistentes con el marcaje de MitoTracker, donde se observa que los tratamientos inducen la fragmentación mitocondrial en líneas celulares de CCR.

Esta fragmentación mitocondrial se atribuye a la disfunción celular (94), el deterioro de OXPHOS (95), el daño de mtDNA (96), y la producción de ROS (97). Además, la fragmentación mitocondrial facilita la eliminación autofágica de las mitocondrias dañadas y está estrechamente asociada con la fisión mitocondrial (98). En contraste, los resultados revelan que las células no tratadas exhiben una extensa matriz mitocondrial tubular, que se extiende por todo el citosol e interactúa estrechamente con el núcleo y el retículo endoplásmico (99). Las redes mitocondriales altamente dinámicas oscilan entre un estado fragmentado y un continuo tubular, reflejando un equilibrio entre la fusión y la fisión mitocondrial, promoviendo así una mayor producción de ATP (100). Bajo condiciones de estrés metabólico o depleción de nutrientes, ocurre una elongación rápida y transitoria de la red mitocondrial, denominada hiperfusión mitocondrial inducida por estrés (101). Se ha observado hiperfusión mitocondrial en respuesta a tratamientos como

RAP e CQ (102). Mientras que los compuestos resultan en mitocondrias fragmentadas, sugiriendo una posible fisión mitocondrial.

Asimismo, las alteraciones dinámicas en la energía mitocondrial se han relacionado con la desregulación del MMP (71). $\Delta\Psi_M$ sirve como un indicador crucial de la función mitocondrial. $\Delta\Psi_M$ se origina del bombeo de protones a través de la membrana mitocondrial interna, simultáneamente con el transporte de electrones. (103). Este proceso impulsa varias funciones mitocondriales esenciales, como la síntesis de ATP, la acumulación de calcio y el mantenimiento de gradientes de iones (71). Estudios previos de Isenberg et al. (2000) informaron reducción del 20% en $\Delta\Psi_M$ en células HepG2 tras el tratamiento con rotenona, un inhibidor del complejo I de OXPHOS (104). Mientras que de Pedro et al. (2000) informaron una disminución gradual en $\Delta\Psi_M$ en células HepG2 tras la exposición a LAH (64), Aquí se presentan datos contrastantes. Se observó aumento en $\Delta\Psi_M$ en células de CRC tratadas con los compuestos en las tres líneas celulares. Sin embargo, solo se observaron diferencias significativas con el tratamiento de LIR en células HCT116. Este aumento en $\Delta\Psi_M$ puede contribuir a disminuir la producción de ATP y promover la generación de ROS. Los cambios en $\Delta\Psi_M$ pueden influir en alteraciones en el metabolismo energético.

Además de las alteraciones observadas en la dinámica mitocondrial y el metabolismo energético, este estudio aporta datos sobre la participación de procesos celulares clave como la señalización de mTOR, apoptosis y autofagia en la respuesta al tratamiento con LAH y LIR. La desregulación de la señalización de mTOR se ha implicado en varios tipos de cáncer, incluido el CRC, donde desempeña un papel crucial en la promoción del crecimiento y la proliferación celular (105–108).

mTORC1 sirve como un regulador clave de la síntesis de proteínas, esencial para el crecimiento celular, al modular varios efectores rio abajo (109). A través de la fosforilación, mTORC1 activa la proteína 1 de unión al factor de iniciación eucariótico 4E (4E-BP1) y la quinasa 1 del ribosoma S6 (S6K1), promoviendo la síntesis de proteínas (110). La fosforilación de 4E-BP1 impide la unión a eIF4E, facilitando la traducción dependiente del cap, mientras que la activación de S6K1 conduce a la biogénesis

mejorada del ARNm y la elongación de la traducción (111). La proteína eIF4E, junto con otros factores de iniciación, media el reclutamiento de ribosomas y la iniciación de la traducción. Sin embargo, 4E-BP1 compite con estos factores al unirse a eIF4E, inhibiendo así la traducción (112).

En un estudio realizado por Liu et al. (2017), se demostró que los kavalactones (yangonin, flavokawain A y docetaxel), compuestos presentes en las raíces de la kava (Piper methysticum Forst), ejercen efectos inhibitorios sobre la vía mTOR rio arriba. Esto culmina en la inhibición de p70S6K y 4E-BP1, sustratos de la vía mTOR involucrados en la síntesis de proteínas, en líneas celulares de cáncer de vejiga (113). De manera similar, Alayev et al. (2020) investigaron las propiedades anticancerígenas del resveratrol en líneas celulares de cáncer de mama. Sus resultados revelaron que el resveratrol afecta a AKT, lo que conduce a la inhibición de mTORC1, así como de sus efectores p70S6K y 4E-BP1, que son cruciales para la regulación de la síntesis de proteínas (114).

En este estudio, se observa disminución en la 4E-BP1 fosforilada y aumento en su forma total después del tratamiento, lo que indica la inhibición de mTOR. En consecuencia, 4E-BP1 se une a eIF1, obstaculizando así la traducción de enzimas reguladoras metabólicas.

La inhibición de mTORC1 ha demostrado promover apoptosis y autofagia. Para analizar la autofagia, utilizamos el sistema mCherry-GFP-LC3, donde GFP-LC3 se usa comúnmente como marcador de imagen para autofagosomas. El GFP sensible al ácido se degrada en ambientes ácidos, lo que lo hace inadecuado para detectar autolisosomas. En contraste, mCherry es estable en ambientes ácidos, lo que le permite persistir en vesículas ácidas (115). En las células de CRC que expresan mCherry-GFP-LC3, la ausencia de una señal roja en nuestros controles indica la falta de autofagosomas fusionados con lisosomas, sugiriendo la falta de inducción de autofagia. Por el contrario, el tratamiento con LAH y LIR llevó a un aumento en la señal de mCherry, indicando la formación de autofagolisosomas e inducción de autofagia en líneas celulares de CRC, mientras que no se observó tal efecto en la línea celular no tumoral. Además, el

tratamiento con Torin 1 y CQ, conocidos inductores de autofagia, promovió la fusión de autofagosomas con lisosomas.

En informes anteriores, Liu et al. (2000) demostraron que el análogo de acetogenina AA005 induce la autofagia a través de la activación de AMPK, bloqueando así la vía de mTOR y llevando a un aumento en la detección de LC3 (59). Estos datos están estrechamente relacionados con los resultados de este trabajo, donde se observó la regulación al alza de ATG12 y LC3II, sugiriendo un aumento en la formación del conjugado ATG12-ATG5, un paso fundamental en la biogénesis de los autofagosomas. Además, se encontraron niveles aumentados de LC3II, la forma hiper-lipidada de LC3, lo que indica una mayor incorporación de LC3 a las membranas autofagósomales, indicativo de la iniciación y progresión de la autofagia. Esta serie de eventos demuestra aún más la inducción de autofagia por nuestros compuestos. Hasta la fecha, no se han reportado otros estudios que demuestren el potencial de los ACGs o LIR en la inducción de autofagia. Por lo tanto, estos resultados subrayan el notable potencial de nuestros compuestos para desencadenar la autofagia, como lo evidencian la regulación al alza de genes clave relacionados con la autofagia.

Bajo condiciones de estrés prolongado, la autofagia también puede contribuir a la muerte celular programada. La inducción de apoptosis por ACGs y LIR ha sido objeto de estudio, aunque no de manera exhaustiva. Existe información insuficiente respecto a LAH. Por el contrario, hay datos suficientes disponibles sobre otras ACGs, que han demostrado inducir la detención del ciclo celular en la fase G1/S (63,116,117) mediante la desregulación de diversas vías como MAPK (118) o Notch (119). Estas vías pueden aumentar los niveles de ROS (117), alterar el metabolismo energético (120), y, en última instancia, inducir la apoptosis, ya sea de manera dependiente de caspasas o independiente de caspasas (121,122). Además, se ha observado que LIR induce apoptosis mediante la desregulación de la fase G1/S en diferentes tipos de cáncer (37–39,66,123).

Este trabajo sobre las vías apoptóticas revela inducción significativa de la muerte celular programada en células de CRC tras el tratamiento con LAH y LIR. La apoptosis, un

proceso controlado crucial para mantener la homeostasis tisular, a menudo está desregulada en el cáncer, lo que permite que las células malignas evadan las señales de muerte y proliferen sin control (124). Aquí se demuestra que la LAH y LIR desencadenan la apoptosis en células de CRC a través de múltiples mecanismos. En primer lugar, se observó aumento pronunciado en las DSBs de ADN, como lo demuestra la regulación al alza de γ-H2AX fosforilado, un marcador bien establecido de daño en el ADN y un componente clave de la vía de respuesta al daño en el ADN (DDR) (125). La formación de γ-H2AX ocurre rápidamente en sitios de DSBs de ADN, donde sirve como plataforma de reclutamiento para varias proteínas DDR involucradas en procesos de reparación y señalización (126).

Previamente Chen et al, (2017) mostró que el compuesto natural ampliamente conocido resveratrol, el cual inhibe el complejo I de la ETC (127), sensibilizó a las células de cáncer de próstata radioresistentes al incrementar la fosforilación de ATM y su proteína objetivo γ-H2AX, provocando la detención del ciclo celular y, posteriormente, la muerte celular (128).

Por otro lado, Chien-Yi et al, (2015) demostraron que el compuesto natural curcumina un polifenol que reduce el estrés oxidativo mitocondrial (129), redujo la expresión de proteínas reparadoras del ADN como la proteína 14-3-3 sigma (14-3-3σ), la O6-metilguanina-ADN metiltransferasa (MGMT), el gen de susceptibilidad al cáncer de mama 1 (BRCA1) y el mediador del punto de control del daño del ADN 1 (MDC1). La curcumina también aumentó la fosforilación de p53 y la formación de focos de histona γ-H2AX (S140) en los núcleos de las células NCI-H460 de cáncer de pulmón (130). Esto sugiere que el aumento de la histona γ-H2AX en la cromatina, está alterando las estructuras de ADN en todo el núcleo, así como el arresto global de la replicación y el colapso de horquillas dentro del núcleo. Disminuyendo las proteínas reparadoras del ADN y conduciendo a la muerte celular (131).

Ebba et al, (2004) mostró que la doxorrubicina induce la fosforilación de la histona γ-H2AX de forma dependiente e independiente de ATM. Se mostró la formación pan nuclear de la fosforilación de la histona γ-H2AX en la serina 139 tanto en el núcleo como

en el citoplasma de la célula (132), lo que podría indicar letalidad celular inducida por estrés de replicación (133).

Similarmente, la detección de niveles elevados de γ-H2AX después del tratamiento con LAH y LIR indica una activación amplia de la vía DDR en respuesta al daño en el ADN inducido por estos compuestos. Esta activación inicia una cascada de eventos destinados a reparar el ADN dañado o a desencadenar la muerte celular apoptótica si la reparación no es factible. La señal de γ-H2AX aumentada observada en este estudio refleja la respuesta celular al estrés genotóxico infligido por la LAH y LIR, resaltando la efectividad de estos compuestos para inducir daño en el ADN y activar vías apoptóticas en células de CRC. Esta idea mecánica proporciona información valiosa para comprender los efectos citotóxicos de la LAH y LIR y subraya su potencial como agentes terapéuticos prometedores para combatir el CRC.

Además, este estudio reveló una cascada de eventos después de la inducción de DSBs de ADN, como la activación de la cascada de caspasas, incluida la caspasa-3, un efector central de la vía apoptótica. La caspasa-3, una vez activada, desempeña un papel crucial en la ejecución de la muerte celular apoptótica al dividir sustratos celulares clave involucrados en el mantenimiento de la integridad y función celular. El aumento observado en la activación de caspasas-3 corrobora la iniciación de vías de señalización apoptótica desencadenadas por el daño en el ADN inducido por la LAH y LIR. Esta respuesta coordinada subraya la potencia de estos compuestos para inducir la muerte celular apoptótica en células de CRC a través de la activación tanto de la respuesta al daño en el ADN como de las vías apoptóticas. Estos resultados son similares a los reportados por Rendón et al. (2024), donde demuestran que la LAH induce la muerte celular por apoptosis a través del ensayo TUNEL, correlacionando estos resultados con una disminución en la migración y una reducción en el volumen y el número de tumores (134). De manera similar, Schlie et al. (2009) en 2024 demuestra, en un modelo *in vivo*, que la LAH exhibe una mayor eficacia en la disminución del volumen tumoral en comparación con la doxorrubicina, lo que sugiere que este efecto puede atribuirse a la inducción de apoptosis (41). En este estudio, se detectó aumento en la activación de la cascada de caspasas, mediadores clave de la señalización apoptótica, lo que sugiere la

participación de vías apoptóticas intrínseca, como lo demuestra la detección intensificada de caspasa-3. Además, como se observó previamente, los tratamientos indujeron disfunción mitocondrial, caracterizada por una alteración en la integridad de la membrana y la liberación de citocromo c, amplificando aún más la señalización apoptótica. Estos datos remarcan los efectos pro-apoptóticos potentes de la LAH y LIR en células de CRC, destacando su potencial como agentes terapéuticos prometedores para inducir la muerte celular tumoral y suprimir el crecimiento tumoral.

La LAH y LIR ejercen efectos multifacéticos en células de CRC, que abarcan alteraciones en la función mitocondrial, reprogramación metabólica e inducción apoptótica. La elucidación de estas interacciones intrincadas proporciona información valiosa sobre el potencial terapéutico de estos compuestos en el tratamiento del CRC. Estudios futuros que exploren los mecanismos precisos subyacentes a sus efectos en la energética celular, así como su eficacia en modelos *in vivo* y en entornos clínicos, serán fundamentales para avanzar en el desarrollo como nuevos agentes anticancerígenos que se dirijan a las vulnerabilidades metabólicas en el CRC.

13. Conclusión

En conclusión, nuestro estudio proporciona evidencia convincente del potencial terapéutico de LAH y LIR en el tratamiento del CRC al elucidar los mecanismos de acción a nivel molecular. Estos resultados revelan que LAH y LIR ejercen sus efectos anticancerígenos mediante la alteración de la función mitocondrial mediante la inhibición de los complejos de OXPHOS, lo que conduce a un metabolismo energético desregulado caracterizado por un aumento de la glucólisis y la fragmentación mitocondrial. La alteración de la dinámica mitocondrial y la bioenergética contribuye al estrés celular y la inducción de apoptosis, como se evidencia por DSBs de ADN y la activación de vías apoptóticas. Además, LAH y LIR regulan a la baja la vía de señalización mTOR, alterando la homeostasis metabólica e inhibiendo la proliferación celular, sensibilizando aún más a las células de CRC al flujo autofágico. En conjunto, LAH y LIR emergen como prometedores agentes terapéuticos contra el CRC al dirigirse a múltiples vías interconectadas críticas para la supervivencia y proliferación celular cancerosa. Sus

mecanismos de acción multifacéticos subrayan su potencial como agentes anticancerígenos efectivos con la capacidad de superar la resistencia terapéutica y mejorar los resultados del paciente en el tratamiento del CRC. La elucidación adicional de los mecanismos moleculares precisos subyacentes a sus efectos, junto con su validación en entornos preclínicos y clínicos, será crucial para su traducción en la práctica clínica y el desarrollo de estrategias terapéuticas personalizadas para pacientes con CRC.

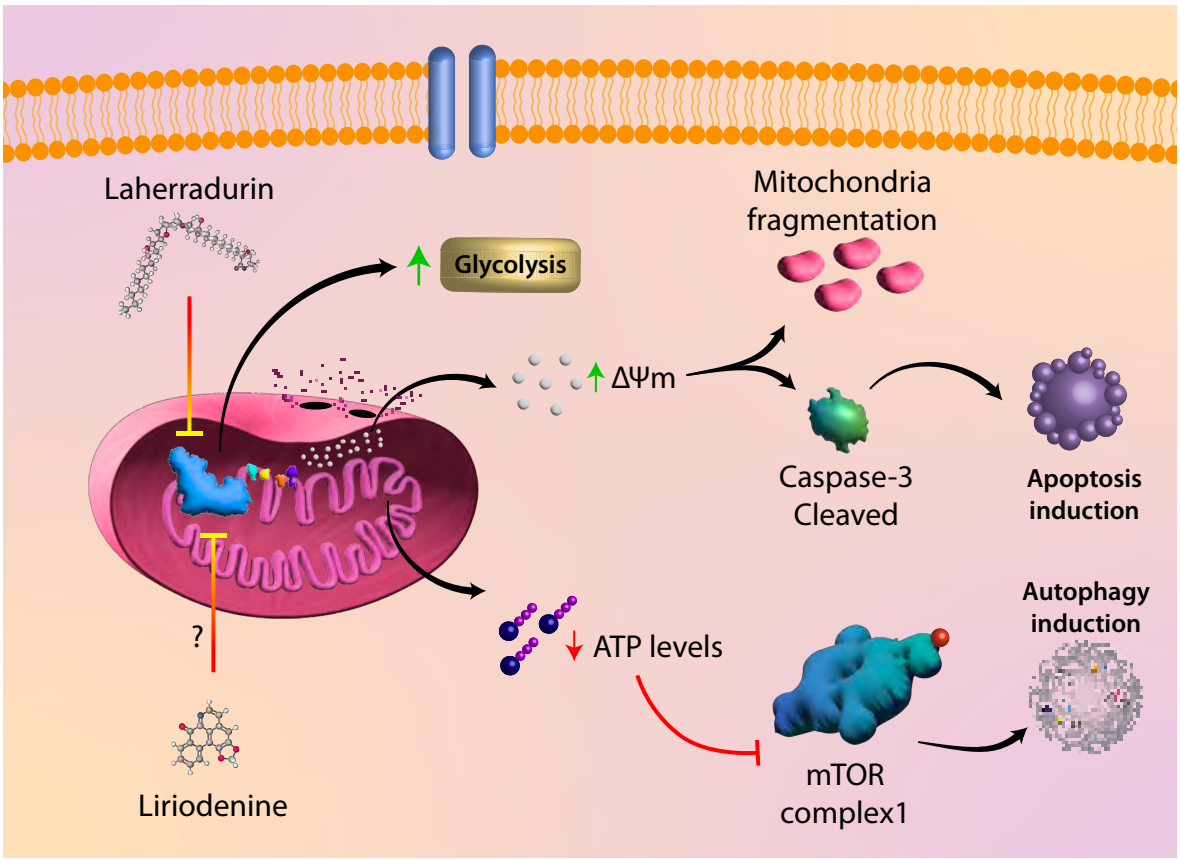


Figura 22: Mecanismo propuesto de acción de LAH y LIR

Mecanismo propuesto de acción de LAH y LIR: LAH y LIR actúan inhibiendo la ETC, lo cual resulta en la acumulación de protones en el espacio intermembranoso. Esta acumulación conduce a un aumento en la glucólisis, disminución en los niveles de ATP, y aumento del Potencial de la Membrana Mitocondrial (MMP). Estas alteraciones posteriormente inducen la fragmentación mitocondrial y pueden inhibir mTORC1, un complejo crucial en la regulación de la biogénesis de ribosomas y la síntesis de lípidos. En consecuencia, esta cascada de eventos conduce a la célula hacia la autofagia y principalmente la apoptosis, caracterizada por la inducción de la caspasa-3.

14. Referencias bibliográficas

1. Hanahan D, Weinberg RA. The hallmarks of cancer. Cell. 2000 Jan 7;100(1):57–70.
2. Hanahan D, Weinberg RA. Hallmarks of cancer: The next generation. Cell. 2011 Mar 4;144(5):646–74.
3. Hanahan D. Hallmarks of Cancer: New Dimensions. Cancer Discov [Internet]. 2022 Jan 1 [cited 2024 Feb 27];12(1):31–46. Available from: /cancerdiscovery/article/12/1/31/675608/Hallmarks-of-Cancer-New-DimensionsHallmarks-of
4. Bray F, Laversanne M, Sung H, Ferlay J, Siegel RL, Soerjomataram I, et al. Global cancer statistics 2022: GLOBOCAN estimates of incidence and mortality worldwide for 36 cancers in 185 countries. CA Cancer J Clin [Internet]. 2024 Apr 4 [cited 2024 May 2]; Available from: https://onlinelibrary.wiley.com/doi/full/10.3322/caac.21834
5. Hossain MS, Karuniawati H, Jairoun AA, Urbi Z, Ooi DJ, John A, et al. Colorectal Cancer: A Review of Carcinogenesis, Global Epidemiology, Current Challenges, Risk Factors, Preventive and Treatment Strategies. Cancers (Basel) [Internet]. 2022 Apr 1 [cited 2024 Feb 26];14(7):1732. Available from: /pmc/articles/PMC8996939/
6. Alzahrani SM, Al Doghaither HA, Al-Ghafar AB. General insight into cancer: An overview of colorectal cancer (Review). Mol Clin Oncol [Internet]. 2021 Dec 1 [cited 2024 Feb 26];15(6). Available from: /pmc/articles/PMC8591689/
7. Knowlton CA, Mackay MK, Speer TW, Vera RB, Arthur DW, Wazer DE, et al. Colon Cancer. Encyclopedia of Radiation Oncology [Internet]. 2023 Jun 3 [cited 2024 Feb 26];77–77. Available from: https://www.ncbi.nlm.nih.gov/books/NBK470380/
8. Keum NN, Giovannucci E. Global burden of colorectal cancer: emerging trends, risk factors and prevention strategies. Nature Reviews Gastroenterology & Hepatology 2019 16:12 [Internet]. 2019 Aug 27 [cited 2024 Feb 26];16(12):713–32. Available from: https://www.nature.com/articles/s41575-019-0189-8
9. Huang Z, Yang M. Molecular Network of Colorectal Cancer and Current Therapeutic Options. Front Oncol [Internet]. 2022 Apr 6 [cited 2024 Feb 26];12:852927. Available from: www.frontiersin.org
10. Li K, Luo H, Huang L, Luo H, Zhu X. Microsatellite instability: A review of what the oncologist should know. Cancer Cell Int [Internet]. 2020 Jan 13 [cited 2024 Feb 26];20(1):1–13. Available from: https://cancerci.biomedcentral.com/articles/10.1186/s12935-019-1091-8
11. Tapial S, Olmedillas-López S, Rueda D, Arriba M, García JL, Vivas A, et al. Cimp-Positive Status is More Representative in Multiple Colorectal Cancers than in Unique Primary Colorectal Cancers. Scientific Reports 2019 9:1 [Internet]. 2019 Jul 19 [cited 2024 Feb 26];9(1):1–11. Available from: https://www.nature.com/articles/s41598-019-47014-w
12. Schmitt M, Greten FR. The inflammatory pathogenesis of colorectal cancer. Nature Reviews Immunology 2021 21:10 [Internet]. 2021 Apr 28 [cited 2024 Feb 26];21(10):653–67. Available from: https://www-nature-com.pbidi.unam.mx:2443/articles/s41577-021-00534-x
13. Zhao H, Ming T, Tang S, Ren S, Yang H, Liu M, et al. Wnt signaling in colorectal cancer: pathogenic role and therapeutic target. Molecular Cancer 2022 21:1 [Internet]. 2022 Jul 14

[cited 2024 Feb 26];21(1):1–34. Available from: https://molecular-cancer.biomedcentral.com/articles/10.1186/s12943-022-01616-7
14. Bteich F, Mohammadi M, Li T, Bhat MA, Sofianidi A, Wei N, et al. Targeting KRAS in Colorectal Cancer: A Bench to Bedside Review. Int J Mol Sci [Internet]. 2023 Aug 1 [cited 2024 Feb 26];24(15). Available from: /pmc/articles/PMC10418782/
15. Tan L, Peng D, Cheng Y. Significant position of C-myc in colorectal cancer: a promising therapeutic target. Clin Transl Oncol [Internet]. 2022 Dec 1 [cited 2024 Feb 26];24(12):2295–304. Available from: https://pubmed.ncbi.nlm.nih.gov/35972682/
16. Nakayama I, Hirota T, Shinozaki E. BRAF Mutation in Colorectal Cancers: From Prognostic Marker to Targetable Mutation. Cancers (Basel) [Internet]. 2020 Nov 1 [cited 2024 Feb 26];12(11):1–29. Available from: /pmc/articles/PMC7694028/
17. Ioannou M, Paraskeva E, Baxevanidou K, Simos G, Papamichali R, Papacharalambous C, et al. HIF-1α in colorectal carcinoma: review of the literature. [cited 2024 Feb 26]; Available from: www.jbuon.com
18. Kuwai T, Kitadai Y, Tanaka S, Onogawa S, Matsutani N, Kaio E, et al. Expression of hypoxia-inducible factor-1α is associated with tumor vascularization in human colorectal carcinoma. Int J Cancer. 2003 Jun 10;105(2):176–81.
19. Zhang C, Liu J, Wang J, Zhang T, Xu D, Hu W, et al. The Interplay Between Tumor Suppressor p53 and Hypoxia Signaling Pathways in Cancer. Front Cell Dev Biol [Internet]. 2021 Feb 18 [cited 2024 Feb 26];9. Available from: /pmc/articles/PMC7930565/
20. Liebl MC, Hofmann TG. The role of p53 signaling in colorectal cancer. Cancers (Basel) [Internet]. 2021 May 1 [cited 2024 Feb 26];13(9). Available from: /pmc/articles/PMC8125348/
21. Terzić J, Grivennikov S, Karin E, Karin M. Inflammation and colon cancer. Gastroenterology [Internet]. 2010 [cited 2024 Feb 27];138(6). Available from: https://pubmed.ncbi.nlm.nih.gov/20420949/
22. Rawla P, Sunkara T, Barsouk A. Epidemiology of colorectal cancer: Incidence, mortality, survival, and risk factors. Prz Gastroenterol. 2019;14(2):89–103.
23. Sawicki T, Ruszkowska M, Danielewicz A, Niedźwiedzka E, Arłukowicz T, Przybyłowicz KE. A Review of Colorectal Cancer in Terms of Epidemiology, Risk Factors, Development, Symptoms and Diagnosis. Cancers (Basel) [Internet]. 2021 May 1 [cited 2024 Feb 26];13(9). Available from: /pmc/articles/PMC8122718/
24. Murphy N, Moreno V, Hughes DJ, Vodicka L, Vodicka P, Aglago EK, et al. Lifestyle and dietary environmental factors in colorectal cancer susceptibility. Mol Aspects Med. 2019 Oct 1;69:2–9.
25. Valle L, Vilar E, Tavtigian S V., Stoffel EM. Genetic predisposition to colorectal cancer: syndromes, genes, classification of genetic variants and implications for precision medicine. Journal of Pathology. 2019 Apr 1;247(5):574–88.
26. Shussman N, Wexner SD. Colorectal polyps and polyposis syndromes. Gastroenterol Rep (Oxf). 2014 Feb 1;2(1):1–15.
27. Wolpin BM, Mayer RJ. Systemic Treatment of Colorectal Cancer. Gastroenterology [Internet]. 2008 [cited 2022 Aug 27];134(5):1296. Available from: /pmc/articles/PMC2528832/

28. Fakhri S, Moradi SZ, Farzaei MH, Bishayee A. Modulation of dysregulated cancer metabolism by plant secondary metabolites: A mechanistic review. Semin Cancer Biol. 2022 May 1;80:276–305.
29. Shin SA, Moon SY, Kim WY, Paek SM, Park HH, Lee CS. Structure-Based Classification and Anti-Cancer Effects of Plant Metabolites. Int J Mol Sci [Internet]. 2018 Sep 6 [cited 2022 Aug 27];19(9). Available from: https://pubmed.ncbi.nlm.nih.gov/30200668/
30. Teoh ES. Secondary Metabolites of Plants. Medicinal Orchids of Asia [Internet]. 2016 [cited 2024 Apr 10];59–73. Available from: https://link.springer.com/chapter/10.1007/978-3-319-24274-3_5
31. Pott DM, Osorio S, Vallarino JG. From Central to Specialized Metabolism: An Overview of Some Secondary Compounds Derived From the Primary Metabolism for Their Role in Conferring Nutritional and Organoleptic Characteristics to Fruit. Front Plant Sci [Internet]. 2019 May 31 [cited 2022 Aug 27];10:835. Available from: /pmc/articles/PMC6609884/
32. Ahmed E, Arshad M, Zakriyya Khan M, Shoaib Amjad M, Mehreen Sadaf H, Riaz I, et al. Secondary metabolites and their multidimensional prospective in plant life. ~ 205 ~ Journal of Pharmacognosy and Phytochemistry. 2017;6(2):205–14.
33. Heinrich M, Mah J, Amirkia V. Alkaloids Used as Medicines: Structural Phytochemistry Meets Biodiversity—An Update and Forward Look. Molecules [Internet]. 2021 Apr 1 [cited 2023 May 21];26(7). Available from: /pmc/articles/PMC8036335/
34. Rodríguez-Arce E, Cancino P, Arias-Calderón M, Silva-Matus P, Saldías M. Oxoisoaporphines and Aporphines: Versatile Molecules with Anticancer Effects. Molecules [Internet]. 2020 [cited 2023 May 21];25(1). Available from: /pmc/articles/PMC6983244/
35. Li L, Xu Y, Wang B. Liriodenine induces the apoptosis of human laryngocarcinoma cells via the upregulation of p53 expression. Oncol Lett [Internet]. 2015 Mar 1 [cited 2023 May 21];9(3):1121. Available from: /pmc/articles/PMC4314988/
36. Chen CY, Wu HM, Chao WY, Lee CH. Review on pharmacological activities of liriodenine. Afr J Pharm Pharmacol [Internet]. 2013 May 15 [cited 2024 Feb 27];7(18):1067–70. Available from: https://academicjournals.org/journal/AJPP/article-abstract/597C37834167
37. Li YL, Qin QP, Liu YC, Chen ZF, Liang H. A platinum(II) complex of liriodenine from traditional Chinese medicine (TCM): Cell cycle arrest, cell apoptosis induction and telomerase inhibition activity via G-quadruplex DNA stabilization. J Inorg Biochem [Internet]. 2014 [cited 2024 Feb 27];137:12–21. Available from: https://pubmed.ncbi.nlm.nih.gov/24798373/
38. Hsieh TJ, Liu TZ, Chern CL, Tsao DA, Lu FJ, Syu YH, et al. Liriodenine inhibits the proliferation of human hepatoma cell lines by blocking cell cycle progression and nitric oxide-mediated activation of p53 expression. Food Chem Toxicol [Internet]. 2005 [cited 2024 Feb 27];43(7):1117–26. Available from: https://pubmed.ncbi.nlm.nih.gov/15833387/
39. Li L, Xu Y, Wang B. Liriodenine induces the apoptosis of human laryngocarcinoma cells via the upregulation of p53 expression. Oncol Lett [Internet]. 2015 Mar 1 [cited 2024 Feb 27];9(3):1121–7. Available from: https://pubmed.ncbi.nlm.nih.gov/25663867/
40. Di Toto Blessing L, Ramos J, Diaz S, Ben Altabef A, Bardón A, Brovetto M, et al. Insecticidal Properties of Annonaceous Acetogenins and Their Analogues. Interaction with Lipid Membranes: https://doi.org/101177/1934578X1200700929 [Internet]. 2012 Sep 1 [cited

2022 Aug 27];7(9):1215–8. Available from: https://journals.sagepub.com/doi/abs/10.1177/1934578X1200700929

41. Schlie-Guzmán MA, García-Carrancá A, González-Esquinca AR. In vitro and in vivo antiproliferative activity of laherradurin and cherimolin-2 of Annona diversifolia Saff. Phytother Res [Internet]. 2009 Aug [cited 2022 Aug 27];23(8):1128–33. Available from: https://pubmed.ncbi.nlm.nih.gov/19170140/
42. Nakanishi S, Abe M, Yamamoto S, Murai M, Miyoshi H. Bis-THF motif of acetogenin binds to the third matrix-side loop of ND1 subunit in mitochondrial NADH-ubiquinone oxidoreductase. Biochim Biophys Acta [Internet]. 2011 Sep [cited 2022 Aug 27];1807(9):1170–6. Available from: https://pubmed.ncbi.nlm.nih.gov/21616052/
43. Ruiz Hidalgo J, Gilabert M, Cabedo N, Cortes D, Neske A. Montanacin-L and montanacin-K two previously non-described acetogenins from Annona montana twigs and leaves. Phytochem Lett. 2020 Aug 1;38:78–83.
44. Kojima N, Abe M, Suga Y, Ohtsuki K, Tanaka T, Iwasaki H, et al. Critical role of a methyl group on the γ-lactone ring of annonaceous acetogenins in the potent inhibition of mitochondrial complex I. Bioorg Med Chem Lett [Internet]. 2013 Mar 1 [cited 2022 Aug 27];23(5):1217–9. Available from: https://pubmed.ncbi.nlm.nih.gov/23375227/
45. Agu KC, Okolie NP, Falodun A, Engel-Lutz N. In vitro anticancer assessments of Annona muricata fractions and in vitro antioxidant profile of fractions and isolated acetogenin (15-acetyl guanacone). Journal of Cancer Research and Practice. 2018 Jun 1;5(2):53–66.
46. Fukai T, Ushio-Fukai M. Cross-Talk between NADPH Oxidase and Mitochondria: Role in ROS Signaling and Angiogenesis. Cells [Internet]. 2020 Aug 6 [cited 2022 Aug 27];9(8). Available from: /pmc/articles/PMC7466096/
47. Koundouros N, Poulogiannis G. Phosphoinositide 3-Kinase/Akt Signaling and Redox Metabolism in Cancer. Front Oncol [Internet]. 2018 May 15 [cited 2022 Aug 27];8(MAY). Available from: https://pubmed.ncbi.nlm.nih.gov/29868481/
48. Yang J, Nie J, Ma X, Wei Y, Peng Y, Wei X. Targeting PI3K in cancer: mechanisms and advances in clinical trials. Molecular Cancer 2019 18:1 [Internet]. 2019 Feb 19 [cited 2022 Aug 27];18(1):1–28. Available from: https://molecular-cancer.biomedcentral.com/articles/10.1186/s12943-019-0954-x
49. Porstmann T, Santos CR, Griffiths B, Cully M, Wu M, Leevers S, et al. SREBP Activity Is Regulated by mTORC1 and Contributes to Akt-Dependent Cell Growth. Cell Metab [Internet]. 2008 Sep 9 [cited 2022 Aug 27];8(3–3):224. Available from: /pmc/articles/PMC2593919/
50. de la Cruz López KG, Toledo Guzmán ME, Sánchez EO, García Carrancá A. mTORC1 as a Regulator of Mitochondrial Functions and a Therapeutic Target in Cancer. Front Oncol. 2019 Dec 13;9:1373.
51. Laplante M, Sabatini DM. mTOR signaling at a glance. J Cell Sci [Internet]. 2009 Oct 10 [cited 2024 May 2];122(20):3589. Available from: /pmc/articles/PMC2758797/
52. Tagaya M, Arasaki K. Regulation of mitochondrial dynamics and autophagy by the mitochondria-associated membrane. Adv Exp Med Biol [Internet]. 2017 [cited 2023 May 7];997:33–47. Available from: https://link.springer.com/chapter/10.1007/978-981-10-4567-7_3

53. Liu Y, Sun Y, Guo Y, Shi X, Chen X, Feng W, et al. An Overview: The Diversified Role of Mitochondria in Cancer Metabolism. Int J Biol Sci [Internet]. 2023 [cited 2024 Mar 24];19(3):897. Available from: /pmc/articles/PMC9910000/
54. Gómez-Virgilio L, Silva-Lucero MDC, Flores-Morelos DS, Gallardo-Nieto J, Lopez-Toledo G, Abarca-Fernandez AM, et al. Autophagy: A Key Regulator of Homeostasis and Disease: An Overview of Molecular Mechanisms and Modulators. Cells [Internet]. 2022 Aug 1 [cited 2024 Apr 10];11(15). Available from: /pmc/articles/PMC9329718/
55. Li X, He S, Ma B. Autophagy and autophagy-related proteins in cancer. Molecular Cancer 2020 19:1 [Internet]. 2020 Jan 22 [cited 2023 Jun 14];19(1):1–16. Available from: https://molecular-cancer.biomedcentral.com/articles/10.1186/s12943-020-1138-4
56. De Almagro MC, Vucic D. THE INHIBITOR OF APOPTOSIS (IAP) PROTEINS ARE CRITICAL REGULATORS OF SIGNALING PATHWAYS AND TARGETS FOR ANTI-CANCER THERAPY. Exp Oncol. 34.
57. Portt L, Norman G, Clapp C, Greenwood M, Greenwood MT. Anti-apoptosis and cell survival: a review. Biochim Biophys Acta [Internet]. 2011 Jan [cited 2022 Aug 27];1813(1):238–59. Available from: https://pubmed.ncbi.nlm.nih.gov/20969895/
58. Xiao Q, Liu Y, Qiu Y, Yao Z, Zhou G, Yao ZJ, et al. Design, synthesis of symmetrical bivalent mimetics of annonaceous acetogenins and their cytotoxicities. Bioorg Med Chem Lett [Internet]. 2011 Jun 15 [cited 2022 Aug 27];21(12):3613–5. Available from: https://pubmed.ncbi.nlm.nih.gov/21570285/
59. Liu YQ, Cheng X, Guo LX, Mao C, Chen YJ, Liu HX, et al. Identification of an annonaceous acetogenin mimetic, AA005, as an AMPK activator and autophagy inducer in colon cancer cells. PLoS One [Internet]. 2012 Oct 8 [cited 2022 Aug 27];7(10). Available from: https://pubmed.ncbi.nlm.nih.gov/23056575/
60. Zou Z, Tao T, Li H, Zhu X. MTOR signaling pathway and mTOR inhibitors in cancer: Progress and challenges. Cell Biosci [Internet]. 2020 Mar 10 [cited 2023 May 22];10(1):1–11. Available from: https://cellandbioscience.biomedcentral.com/articles/10.1186/s13578-020-00396-1
61. Moghadamtousi SZ, Rouhollahi E, Karimian H, Fadaeinasab M, Firoozinia M, Abdulla MA, et al. The chemopotential effect of Annona muricata leaves against azoxymethane-induced colonic aberrant crypt foci in rats and the apoptotic effect of Acetogenin Annomuricin E in HT-29 cells: a bioassay-guided approach. PLoS One [Internet]. 2015 Apr 10 [cited 2022 Aug 27];10(4). Available from: https://pubmed.ncbi.nlm.nih.gov/25860620/
62. Juang SH, Chiang CY, Liang FP, Chan HH, Yang JS, Wang SH, et al. Mechanistic Study of Tetrahydrofuran- acetogenins In Triggering Endoplasmic Reticulum Stress Response-apotoposis in Human Nasopharyngeal Carcinoma. Scientific Reports 2016 6:1 [Internet]. 2016 Dec 21 [cited 2022 Aug 27];6(1):1–13. Available from: https://www.nature.com/articles/srep39251
63. Faria Gomes IN, Silva-Oliveira RJ, Oliveira Silva VA, Rosa MN, Vital PS, Barbosa MCS, et al. Annona coriacea Mart. Fractions Promote Cell Cycle Arrest and Inhibit Autophagic Flux in Human Cervical Cancer Cell Lines. Molecules [Internet]. 2019 [cited 2022 Aug 27];24(21). Available from: https://pubmed.ncbi.nlm.nih.gov/31683835/
64. De Pedro N, Cautain B, Melguizo A, Vicente F, Genilloud O, Peláez F, et al. Mitochondrial complex I inhibitors, acetogenins, induce HepG2 cell death through the induction of the

complete apoptotic mitochondrial pathway. J Bioenerg Biomembr [Internet]. 2013 Feb [cited 2022 Aug 27];45(1–2):153–64. Available from: https://pubmed.ncbi.nlm.nih.gov/23180140/
65. Hsieh TJ, Liu TZ, Chern CL, Tsao DA, Lu FJ, Syu YH, et al. Liriodenine inhibits the proliferation of human hepatoma cell lines by blocking cell cycle progression and nitric oxide-mediated activation of p53 expression. Food Chem Toxicol [Internet]. 2005 [cited 2023 May 7];43(7):1117–26. Available from: https://pubmed.ncbi.nlm.nih.gov/15833387/
66. Chen CY, Chen SY, Chen CH. Liriodenine induces G1/S cell cycle arrest in human colon cancer cells via nitric oxide- and p53-mediated pathway. Process Biochemistry. 2012 Oct 1;47(10):1460–8.
67. Vichai V, Kirtikara K. Sulforhodamine B colorimetric assay for cytotoxicity screening. Nat Protoc [Internet]. 2006 Aug [cited 2022 Aug 27];1(3):1112–6. Available from: https://pubmed.ncbi.nlm.nih.gov/17406391/
68. Kumar P, Nagarajan A, Uchil PD. Analysis of Cell Viability by the MTT Assay. Cold Spring Harb Protoc [Internet]. 2018 Jun 1 [cited 2024 May 7];2018(6):469–71. Available from: https://pubmed.ncbi.nlm.nih.gov/29858338/
69. Abate M, Festa A, Falco M, Lombardi A, Luce A, Grimaldi A, et al. Mitochondria as playmakers of apoptosis, autophagy and senescence. Semin Cell Dev Biol [Internet]. 2020 Feb 1 [cited 2024 May 6];98:139–53. Available from: https://pubmed.ncbi.nlm.nih.gov/31154010/
70. Chen W, Zhao H, Li Y. Mitochondrial dynamics in health and disease: mechanisms and potential targets. Signal Transduction and Targeted Therapy 2023 8:1 [Internet]. 2023 Sep 6 [cited 2024 May 6];8(1):1–25. Available from: https://www.nature.com/articles/s41392-023-01547-9
71. Zorova LD, Popkov VA, Plotnikov EY, Silachev DN, Pevzner IB, Jankauskas SS, et al. Mitochondrial membrane potential. Anal Biochem. 2018 Jul 1;552:50–9.
72. Zorova LD, Popkov VA, Plotnikov EJ, Silachev DN, Pevzner IB, Jankauskas SS, et al. Functional Significance of the Mitochondrial Membrane Potential. Biochem (Mosc) Suppl Ser A Membr Cell Biol [Internet]. 2018 Jan 1 [cited 2024 May 6];12(1):20–6. Available from: https://link.springer.com/article/10.1134/S1990747818010129
73. Chen Q, Shao X, Tian Z, Chen Y, Mondal P, Liu F, et al. Nanoscale monitoring of mitochondria and lysosome interactions for drug screening and discovery. Nano Res. 2019 May 1;12(5):1009–15.
74. Abstract G. mTOR Controls Mitochondrial Dynamics and Cell Survival via MTFP1. Mol Cell [Internet]. 2017 [cited 2024 Jul 3];67:922-935.e5. Available from: http://dx.doi.org/10.1016/j.molcel.2017.08.013
75. Bravo-Sagua R, López-Crisosto C, Parra V, Rodriguez-Peña M, Rothermel BA, Quest AFG, et al. mTORC1 inhibitor rapamycin and ER stressor tunicamycin induce differential patterns of ER-mitochondria coupling. Scientific Reports 2016 6:1 [Internet]. 2016 Nov 3 [cited 2024 Jul 3];6(1):1–12. Available from: https://www.nature.com/articles/srep36394
76. Alberghina L. The Warburg Effect Explained: Integration of Enhanced Glycolysis with Heterogeneous Mitochondria to Promote Cancer Cell Proliferation. Int J Mol Sci [Internet]. 2023 Nov 1 [cited 2024 Mar 27];24(21):15787. Available from: /pmc/articles/PMC10648413/

77. Ashton TM, Gillies McKenna W, Kunz-Schughart LA, Higgins GS. Oxidative Phosphorylation as an Emerging Target in Cancer Therapy. Clin Cancer Res [Internet]. 2018 Jun 1 [cited 2024 Mar 27];24(11):2482–90. Available from: https://pubmed.ncbi.nlm.nih.gov/29420223/
78. Ren L, Meng L, Gao J, Lu M, Guo C, Li Y, et al. PHB2 promotes colorectal cancer cell proliferation and tumorigenesis through NDUFS1-mediated oxidative phosphorylation. Cell Death & Disease 2023 14:1 [Internet]. 2023 Jan 20 [cited 2024 Mar 24];14(1):1–11. Available from: https://www.nature.com/articles/s41419-023-05575-9
79. Qian W, Van Houten B. Alterations in bioenergetics due to changes in mitochondrial DNA copy number. Methods. 2010 Aug 1;51(4):452–7.
80. Greene J, Segaran A, Lord S. Targeting OXPHOS and the electron transport chain in cancer; Molecular and therapeutic implications. Semin Cancer Biol. 2022 Nov 1;86:851–9.
81. Ozsvari B, Sotgia F, Simmons K, Trowbridge R, Foster R, Lisanti MP. Mitoketoscins: Novel mitochondrial inhibitors for targeting ketone metabolism in cancer stem cells (CSCs). Oncotarget. 2017;8(45):78340–50.
82. Cheng G, Zielonka J, McAllister DM, Mackinnon AC, Joseph J, Dwinell MB, et al. Mitochondria-targeted vitamin E analogs inhibit breast cancer cell energy metabolism and promote cell death. BMC Cancer. 2013 Jun 13;13.
83. Zhao F, Vakhrusheva O, Markowitsch SD, Slade KS, Tsaur I, Cinatl J, et al. Artesunate impairs growth in cisplatin-resistant bladder cancer cells by cell cycle arrest, apoptosis and autophagy induction. Cells. 2020 Dec 1;9(12):1–19.
84. Wu Z, Xiao C, Long J, Huang W, You F, Li X. Mitochondrial dynamics and colorectal cancer biology: mechanisms and potential targets. Cell Communication and Signaling [Internet]. 2024 Dec 1 [cited 2024 Mar 25];22(1):1–14. Available from: https://biosignaling.biomedcentral.com/articles/10.1186/s12964-024-01490-4
85. Kim I, Rodriguez-Enriquez S, Lemasters JJ. Selective degradation of mitochondria by mitophagy. Arch Biochem Biophys [Internet]. 2007 Jun 15 [cited 2024 Mar 27];462(2):245–53. Available from: https://pubmed.ncbi.nlm.nih.gov/17475204/
86. Adebayo M, Singh S, Singh AP, Dasgupta S. Mitochondrial Fusion and Fission: The fine-tune balance for cellular homeostasis. FASEB J [Internet]. 2021 Jun 1 [cited 2024 Mar 26];35(6):e21620. Available from: /pmc/articles/PMC8415099/
87. Chen W, Zhao H, Li Y. Mitochondrial dynamics in health and disease: mechanisms and potential targets. Signal Transduction and Targeted Therapy 2023 8:1 [Internet]. 2023 Sep 6 [cited 2024 Mar 26];8(1):1–25. Available from: https://www.nature.com/articles/s41392-023-01547-9
88. Wang S, Tan J, Miao Y, Zhang Q. Mitochondrial Dynamics, Mitophagy, and Mitochondria–Endoplasmic Reticulum Contact Sites Crosstalk Under Hypoxia. Front Cell Dev Biol. 2022 Feb 25;10:848214.
89. Boulton DP, Caino MC. Mitochondrial Fission and Fusion in Tumor Progression to Metastasis. Front Cell Dev Biol. 2022 Mar 9;10:849962.
90. Xie L, Zhou T, Xie Y, Bode AM, Cao Y. Mitochondria-Shaping Proteins and Chemotherapy. Front Oncol [Internet]. 2021 Nov 18 [cited 2024 Mar 25];11:769036. Available from: www.frontiersin.org

91. Filadi R, Pendin Di, Pizzo P. Mitofusin 2: from functions to disease. Cell Death & Disease 2018 9:3 [Internet]. 2018 Feb 28 [cited 2024 Mar 26];9(3):1–13. Available from: https://www.nature.com/articles/s41419-017-0023-6
92. Wang H, Luo W, Chen H, Cai Z, Xu G. Mitochondrial dynamics and mitochondrial autophagy: Molecular structure, orchestrating mechanism and related disorders. Mitochondrion. 2024 Mar 1;75:101847.
93. Li GB, Fu RQ, Shen HM, Zhou J, Hu XY, Liu YX, et al. Polyphyllin I induces mitophagic and apoptotic cell death in human breast cancer cells by increasing mitochondrial PINK1 levels. Oncotarget [Internet]. 2017 Feb 2 [cited 2024 Mar 25];8(6):10359. Available from: /pmc/articles/PMC5354664/
94. Fu W, Liu Y, Yin H. Mitochondrial Dynamics: Biogenesis, Fission, Fusion, and Mitophagy in the Regulation of Stem Cell Behaviors. Stem Cells Int [Internet]. 2019 [cited 2024 Mar 26];2019. Available from: https://pubmed.ncbi.nlm.nih.gov/31089338/
95. Punter KB, Chu C, Chan EYW. Mitochondrial dynamics and oxidative phosphorylation as critical targets in cancer. Endocr Relat Cancer [Internet]. 2023 Jan 1 [cited 2024 Mar 26];30(1). Available from: https://erc.bioscientifica.com/view/journals/erc/30/1/ERC-22-0229.xml
96. Cao K, Riley JS, Heilig R, Montes-Gómez AE, Vringer E, Berthenet K, et al. Mitochondrial dynamics regulate genome stability via control of caspase-dependent DNA damage. Dev Cell. 2022 May 23;57(10):1211-1225.e6.
97. Ježek J, Cooper KF, Strich R. Reactive Oxygen Species and Mitochondrial Dynamics: The Yin and Yang of Mitochondrial Dysfunction and Cancer Progression. Antioxidants [Internet]. 2018 Mar 1 [cited 2024 Mar 26];7(1). Available from: /pmc/articles/PMC5789323/
98. Huang Q, Zhan L, Cao H, Li J, Lyu Y, Guo X, et al. Increased mitochondrial fission promotes autophagy and hepatocellular carcinoma cell survival through the ROS-modulated coordinated regulation of the NFKB and TP53 pathways. Autophagy [Internet]. 2016 Jun 2 [cited 2024 Mar 26];12(6):999. Available from: /pmc/articles/PMC4922447/
99. Bernard G, Bellance N, James D, Parrone P, Fernandez H, Letellier T, et al. Mitochondrial bioenergetics and structural network organization. J Cell Sci [Internet]. 2007 Mar 1 [cited 2024 Mar 27];120(5):838–48. Available from: https://dx.doi.org/10.1242/jcs.03381
100. Wai T, Langer T. Mitochondrial Dynamics and Metabolic Regulation. Trends in Endocrinology & Metabolism. 2016 Feb 1;27(2):105–17.
101. Das R, Chakrabarti O. Mitochondrial hyperfusion: a friend or a foe. Biochem Soc Trans [Internet]. 2020 Apr 29 [cited 2024 Mar 27];48(2):631–44. Available from: /biochemsoctrans/article/48/2/631/222499/Mitochondrial-hyperfusion-a-friend-or-a-foe
102. Morita M, Prudent J, Basu K, Goyon V, Katsumura S, Hulea L, et al. mTOR Controls Mitochondrial Dynamics and Cell Survival via MTFP1. Mol Cell. 2017 Sep 21;67(6):922-935.e5.
103. Sukumar M, Liu J, Mehta GU, Patel SJ, Roychoudhuri R, Crompton JG, et al. Mitochondrial Membrane Potential Identifies Cells with Enhanced Stemness for Cellular Therapy. Cell Metab. 2016 Jan 12;23(1):63–76.
104. Isenberg JS, Klaunig JE. Role of the mitochondrial membrane permeability transition (MPT) in rotenone-induced apoptosis in liver cells. Toxicol Sci [Internet]. 2000 [cited 2024 Mar 27];53(2):340–51. Available from: https://pubmed.ncbi.nlm.nih.gov/10696782/

105. Francipane MG, Lagasse E. mTOR pathway in colorectal cancer: an update. Oncotarget [Internet]. 2014 [cited 2024 Mar 27];5(1):49. Available from: /pmc/articles/PMC3960188/
106. Wang XW, Zhang YJ. Targeting mTOR network in colorectal cancer therapy. World Journal of Gastroenterology : WJG [Internet]. 2014 Apr 4 [cited 2024 Mar 27];20(15):4178. Available from: /pmc/articles/PMC3989954/
107. Leiphrakpam PD, Are C. PI3K/Akt/mTOR Signaling Pathway as a Target for Colorectal Cancer Treatment. International Journal of Molecular Sciences 2024, Vol 25, Page 3178 [Internet]. 2024 Mar 9 [cited 2024 Mar 27];25(6):3178. Available from: https://www.mdpi.com/1422-0067/25/6/3178/htm
108. Panwar V, Singh A, Bhatt M, Tonk RK, Azizov S, Raza AS, et al. Multifaceted role of mTOR (mammalian target of rapamycin) signaling pathway in human health and disease. Signal Transduction and Targeted Therapy 2023 8:1 [Internet]. 2023 Oct 2 [cited 2024 Mar 27];8(1):1–25. Available from: https://www.nature.com/articles/s41392-023-01608-z
109. Condon KJ, Sabatini DM. Nutrient regulation of mTORC1 at a glance. J Cell Sci [Internet]. 2019 Nov 11 [cited 2024 Mar 27];132(21). Available from: /pmc/articles/PMC6857595/
110. Maracci C, Motta S, Romagnoli A, Costantino M, Perego P, Di Marino D. The mTOR/4E-BP1/eIF4E Signalling Pathway as a Source of Cancer Drug Targets. Curr Med Chem [Internet]. 2022 Feb 25 [cited 2024 Mar 27];29(20):3501–29. Available from: https://pubmed.ncbi.nlm.nih.gov/35209811/
111. Modrak-Wojcik A, Gorka M, Niedzwiecka K, Zdanowski K, Zuberek J, Niedzwiecka A, et al. Eukaryotic translation initiation is controlled by cooperativity effects within ternary complexes of 4E-BP1, eIF4E, and the mRNA 5′ cap. FEBS Lett. 2013 Dec 11;587(24):3928–34.
112. Qin X, Jiang B, Zhang Y. 4E-BP1, a multifactor regulated multifunctional protein. Cell Cycle [Internet]. 2016 Mar 18 [cited 2024 Mar 27];15(6):781. Available from: /pmc/articles/PMC4845917/
113. Liu Z, Ha US, Yu K, Wu C, Yokoyama N, Zi X. Kavalactone yangonin induces autophagy and sensitizes bladder cancer cells to flavokawain A and docetaxel via inhibition of the mTOR pathway. J Biomed Res [Internet]. 2017 [cited 2024 Mar 27];31(5):408. Available from: /pmc/articles/PMC5706433/
114. Alayev A, Salamon RS, Schwartz NS, Berman AY, Wiener SL, Holz MK. Combination of Rapamycin and Resveratrol for Treatment of Bladder Cancer. J Cell Physiol [Internet]. 2017 Feb 1 [cited 2024 Mar 27];232(2):436–46. Available from: https://onlinelibrary.wiley.com/doi/full/10.1002/jcp.25443
115. Hansen TE, Johansen T. Following autophagy step by step. BMC Biol. 2011 Jun 2;9.
116. Lee CC, Lin YH, Chang WH, Lin PC, Wu YC, Chang JG. Squamocin modulates histone H3 phosphorylation levels and induces G1 phase arrest and apoptosis in cancer cells. BMC Cancer [Internet]. 2011 Feb 8 [cited 2024 Mar 27];11. Available from: https://pubmed.ncbi.nlm.nih.gov/21299907/
117. Xue JY, Zhou GX, Chen T, Gao S, Choi MY, Wong YS. Desacetyluvaricin induces S phase arrest in SW480 colorectal cancer cells through superoxide overproduction. J Cell Biochem [Internet]. 2014 [cited 2024 Mar 27];115(3):464–75. Available from: https://pubmed.ncbi.nlm.nih.gov/24591255/

118. Yuan F, Bai G, Miao Y, Chen Y, Li X, Chen J. Annosquacin B induces mitochondrial apoptosis in multidrug resistant human breast cancer cell line MCF-7/ADR through selectively modulating MAPKs pathways. Pharm Biol [Internet]. 2016 Dec 1 [cited 2024 Mar 27];54(12):3040–5. Available from: https://pubmed.ncbi.nlm.nih.gov/27450387/
119. Li Y, Ye J, Chen Z, Wen J, Li F, Su P, et al. Annonaceous acetogenins mediated up-regulation of Notch2 exerts growth inhibition in human gastric cancer cells in vitro. Oncotarget [Internet]. 2017 [cited 2024 Mar 27];8(13):21140–52. Available from: https://pubmed.ncbi.nlm.nih.gov/28416750/
120. Yu BB, Yuan H, Chen YC, Zhou DX, Gan ZJ, Wang J, et al. Annonaceous Acetogenin Mimic AA005 Inhibits the Growth of TNBC MDA-MB-468 Cells by Altering Cell Energy Metabolism. Chembiochem [Internet]. 2022 Aug 17 [cited 2024 Mar 27];23(16). Available from: https://pubmed.ncbi.nlm.nih.gov/35676240/
121. Han B, Wang TD, Shen SM, Yu Y, Mao C, Yao ZJ, et al. Annonaceous acetogenin mimic AA005 induces cancer cell death via apoptosis inducing factor through a caspase-3-independent mechanism. BMC Cancer [Internet]. 2015 Mar 18 [cited 2024 Mar 27];15(1). Available from: /pmc/articles/PMC4379763/
122. Han B, Cao Y xia, Li Z ming, Wu Z xia, Mao Y qin, Chen H ling, et al. Annonaceous acetogenin mimic AA005 suppresses human colon cancer cell growth in vivo through downregulation of Mcl-1. Acta Pharmacol Sin [Internet]. 2019 Feb 1 [cited 2024 Mar 27];40(2):231–42. Available from: https://pubmed.ncbi.nlm.nih.gov/29921883/
123. Nordin N, Majid NA, Hashim NM, Rahman MA, Hassan Z, Ali HM. Liriodenine, an aporphine alkaloid from Enicosanthellum pulchrum, inhibits proliferation of human ovarian cancer cells through induction of apoptosis via the mitochondrial signaling pathway and blocking cell cycle progression. Drug Des Devel Ther [Internet]. 2015 Mar 10 [cited 2023 May 7];9:1437. Available from: /pmc/articles/PMC4362660/
124. Morana O, Wood W, Gregory CD. The Apoptosis Paradox in Cancer. International Journal of Molecular Sciences 2022, Vol 23, Page 1328 [Internet]. 2022 Jan 25 [cited 2024 May 7];23(3):1328. Available from: https://www.mdpi.com/1422-0067/23/3/1328/htm
125. Collins PL, Purman C, Porter SI, Nganga V, Saini A, Hayer KE, et al. DNA double-strand breaks induce H2Ax phosphorylation domains in a contact-dependent manner. Nat Commun [Internet]. 2020 Dec 1 [cited 2024 May 7];11(1). Available from: https://pubmed.ncbi.nlm.nih.gov/32572033/
126. Firsanov D V., Solovjeva L V., Svetlova MP. H2AX phosphorylation at the sites of DNA double-strand breaks in cultivated mammalian cells and tissues. Clin Epigenetics [Internet]. 2011 Aug [cited 2024 May 7];2(2):283. Available from: /pmc/articles/PMC3365398/
127. Desquiret-Dumas V, Gueguen N, Leman G, Baron S, Nivet-Antoine V, Chupin S, et al. Resveratrol Induces a Mitochondrial Complex I-dependent Increase in NADH Oxidation Responsible for Sirtuin Activation in Liver Cells. Journal of Biological Chemistry. 2013 Dec 20;288(51):36662–75.
128. Chen YA, Lien HM, Kao MC, Lo UG, Lin LC, Lin CJ, et al. Sensitization of Radioresistant Prostate Cancer Cells by Resveratrol Isolated from Arachis hypogaea Stems. PLoS One [Internet]. 2017 Jan 1 [cited 2024 May 7];12(1). Available from: /pmc/articles/PMC5231355/

129. Sathyabhama M, Priya Dharshini LC, Karthikeyan A, Kalaiselvi S, Min T. The Credible Role of Curcumin in Oxidative Stress-Mediated Mitochondrial Dysfunction in Mammals. Biomolecules [Internet]. 2022 Oct 1 [cited 2024 May 7];12(10). Available from: /pmc/articles/PMC9599178/
130. Chien-Yi Ting, Hsin-Ell Wang, Chien-Chih Yu, Hsin-Chung Liu, Yu-Chang Liu, I-Tsang Chiang. Curcumin Triggers DNA Damage and Inhibits Expression of DNA Repair Proteins in Human Lung Cancer Cells. Anticancer Res [Internet]. 2015 [cited 2024 May 7];35(7):3867–73. Available from: https://www.researchgate.net/publication/279629714_Curcumin_Triggers_DNA_Damage_and_Inhibits_Expression_of_DNA_Repair_Proteins_in_Human_Lung_Cancer_Cells
131. Liu Y, Parry JA, Chin A, Duensing S, Duensing A. Soluble histone H2AX is induced by DNA replication stress and sensitizes cells to undergo apoptosis. Mol Cancer [Internet]. 2008 Jul 10 [cited 2024 May 7];7(1):1–10. Available from: https://molecular-cancer.biomedcentral.com/articles/10.1186/1476-4598-7-61
132. Kurz EU, Douglas P, Lees-Miller SP. Doxorubicin activates ATM-dependent phosphorylation of multiple downstream targets in part through the generation of reactive oxygen species. J Biol Chem [Internet]. 2004 Dec 17 [cited 2024 May 7];279(51):53272–81. Available from: https://pubmed.ncbi.nlm.nih.gov/15489221/
133. Moeglin E, Desplancq D, Conic S, Oulad-Abdelghani M, Stoessel A, Chiper M, et al. Uniform Widespread Nuclear Phosphorylation of Histone H2AX Is an Indicator of Lethal DNA Replication Stress. Cancers (Basel) [Internet]. 2019 Mar 1 [cited 2024 May 7];11(3). Available from: https://pubmed.ncbi.nlm.nih.gov/30871194/
134. Rendón-Barrón MJ, Pérez-Arteaga E, Delgado-Waldo I, Coronel-Hernández J, Pérez-Plasencia C, Rodríguez-Izquierdo F, et al. Laherradurin Inhibits Tumor Growth in an Azoxymethane/Dextran Sulfate Sodium Colorectal Cancer Model In Vivo. Cancers (Basel) [Internet]. 2024 Feb 1 [cited 2024 Mar 27];16(3). Available from: /pmc/articles/PMC10854818/

15. Anexo I (Artículo requisito para la obtención del grado)

Nota: El artículo presentado en esta tesis se incluye en su versión completa, ya que la revista en la que fue publicado no tiene restricciones de publicación que impidan su reproducción en este documento.

cells

MDPI

Article

Laherradurin Inhibits Colorectal Cancer Cell Growth by Induction of Mitochondrial Dysfunction and Autophagy Induction

Izamary Delgado-Waldo [1,2], Svetlana Dokudovskaya [3], Yahir A. Loissell-Baltazar [3], Eduardo Pérez-Arteaga [1], Jossimar Coronel-Hernández [4], Mariano Martínez-Vázquez [5], Eloy Andrés Pérez-Yépez [4], Alejandro Lopez-Saavedra [6,7], Nadia Jacobo-Herrera [1,*] and Carlos Pérez Plasencia [4,8,*]

[1] Unidad de Bioquímica, Instituto Nacional de Ciencias Médicas y Nutrición Salvador Zubiran, Av. Vasco de Quiroga 15, Col. Belisario Domínguez Sección XVI, Tlalpan, Ciudad de México 14080, Mexico; izz.waldo11@gmail.com (I.D.-W.); epa.biol@outlook.es (E.P.-A.)
[2] Posgrado en Ciencias Biológicas, Universidad Nacional Autónoma de México, Copilco Universidad, Coyoacán, Ciudad de México 04510, Mexico
[3] CNRS UMR9018, Institut Gustave Roussy, Université Paris-Saclay, Villejuif 94805, France; svetlana.dokudovskaya@gustaveroussy.fr (S.D.); y.loissell@gmail.com (Y.A.L.-B.)
[4] Laboratorio de Genómica, Instituto Nacional de Cancerología, Instituto Nacional Nacional de Cancerología, Av. San Fernando 22, Belisario Domínguez Secc 16, Tlalpan, Ciudad de México 14080, Mexico; jossithunders@gmail.com (J.C.-H.); eperezy2306@gmail.com (E.A.P.-Y.)
[5] Instituto de Química, Universidad Nacional Autónoma de México, C. Exterior, C. Universitaria, Coyoacán, Ciudad de México 04510, CDMX, Mexico; marvaz@unam.mx
[6] Advanced Microscopy Applications Unit (ADMIRA)-Instituto Nacional de Cancerología, San Fernando 22. Col. Sección XVI, Tlalpan, Ciudad de México 14080, Mexico; alex@admiramicro.com
[7] Escuela de Medicina y Ciencias de la Salud, Tecnológico de Monterrey Ciudad de Mexico, C. Puente #222, Coapa, Arboledas del Sur, Tlalpan, Ciudad de Mexico 14380, Mexico
[8] Laboratorio de Genómica Funcional, Unidad de Biomedicina, Facultad de Estudios Superiores Iztacala, UNAM, Tlalnepantla Estado de México 54090, Mexico
* Correspondence: nadia.jacobo@gmail.com or nadia.jacoboh@incmnsz.mx (N.J.-H.); carlos.pplas@gmail.com (C.P.P.); Tel.: +52-(55)-5623-1333 (ext. 39807) (N.J.-H. & C. P.-P.)

Citation: Delgado-Waldo, I.; Dokudovskaya, S.; Loissell-Baltazar, Y.A.; Pérez-Arteaga, E.; Coronel-Hernández, J.; Martínez-Vázquez, M.; Pérez-Yépez, E.A.; Lopez-Saavedra, A.; Jacobo-Herrera, N.; Plasencia, C.P. Laherradurin Inhibits Colorectal Cancer Cell Growth by Induction of Mitochondrial Dysfunction and Autophagy Induction. *Cells* **2024**, *13*, 1649. https://doi.org/10.3390/cells13191649

Academic Editor: Steve Shnyder

Received: 9 September 2024
Revised: 27 September 2024
Accepted: 30 September 2024
Published: 3 October 2024

Copyright: © 2024 by the authors. Licensee MDPI, Basel, Switzerland. This article is an open access article distributed under the terms and conditions of the Creative Commons Attribution (CC BY) license (https://creativecommons.org/licenses/by/4.0/).

Abstract: LAH, an acetogenin from the Annonaceae family, has demonstrated antitumor activity in several cancer cell lines and in vivo models, where it reduced the tumor size and induced programmed cell death. We focused on the effects of LAH on mitochondrial dynamics, mTOR signaling, autophagy, and apoptosis in colorectal cancer (CRC) cells to explore its anticancer potential. Methods: CRC cells were treated with LAH, and its effects on mitochondrial respiration and glycolysis were measured using Seahorse XF technology. The changes in mitochondrial dynamics were observed through fluorescent imaging, while Western blot analysis was used to examine key autophagy and apoptosis markers. Results: LAH significantly inhibited mitochondrial complex I activity, inducing ATP depletion and a compensatory increase in glycolysis. This disruption caused mitochondrial fragmentation, a trigger for autophagy, as shown by increased LC3-II expression and mTOR suppression. Apoptosis was also confirmed through the cleavage of caspase-3, contributing to reduced cancer cell viability. Conclusions: LAH's anticancer effects in CRC cells are driven by its disruption of mitochondrial function, triggering both autophagy and apoptosis. These findings highlight its potential as a therapeutic compound for further exploration in cancer treatment.

Keywords: laherradurin; acetogenins; colon cancer; mitochondria; autophagy; apoptosis; glycolysis

1. Introduction

CRC is the third most prevalent malignant neoplasm worldwide, affecting individuals of both sexes. The treatment options for CRC vary depending on the tumor's location

and the stage at diagnosis, and may include surgery, chemotherapy, and radiation therapy [1]. One of the main issues with chemotherapeutic agents is their toxicity and the development of drug resistance. Consequently, there is a continuous effort to discover new compounds that offer enhanced efficacy and reduced toxicity compared to conventional treatments.

In cancer drug discovery, herbs are used frequently as a source of new molecules [2]. Plant metabolites, renowned for their structural diversity and bioactivity, have garnered significant attention for their anticancer properties [3]. Plant secondary metabolites, including phenanthrenes, phenols, flavonoids, bibenzyls, alkaloids, phenols, anthocyanins, and acetogenins, are bioactive molecules that may function as antioxidant, anti-inflammatory, antimicrobial, antiparasitic, anticoagulant, antidiabetic, and anticancer agents [4]. In this context, the first plant-derived antitumor agent approved by the FDA, vinicristine, is used to treat lymphoblastic leukemia [5], while other plant-derived drugs including but not limited to paclitaxel are applied for the treatment of breast, ovarian, and lung cancer [6], and omacetaxine mepesuccinate (homoharringtonine) is used for chronic myeloid leukemia [7], among others.

The annonaceous acetogenins (ACGs), obtained from the Annonaceae family, are a class of specialized metabolites with potential anticancer properties [8]. Notably, LAH (Figure 1A), an ACG extracted from the seeds of Annonaspecies, demonstrated significant cell growth inhibition in CRC models [9]. Previously our research group examined the antineoplasic effect of LAH in a colitis-associated tumor model in mice. We found that LAH reduced the tumor volume and number, suppressed cell migration in vitro, and induced cell death via apoptosis [10].

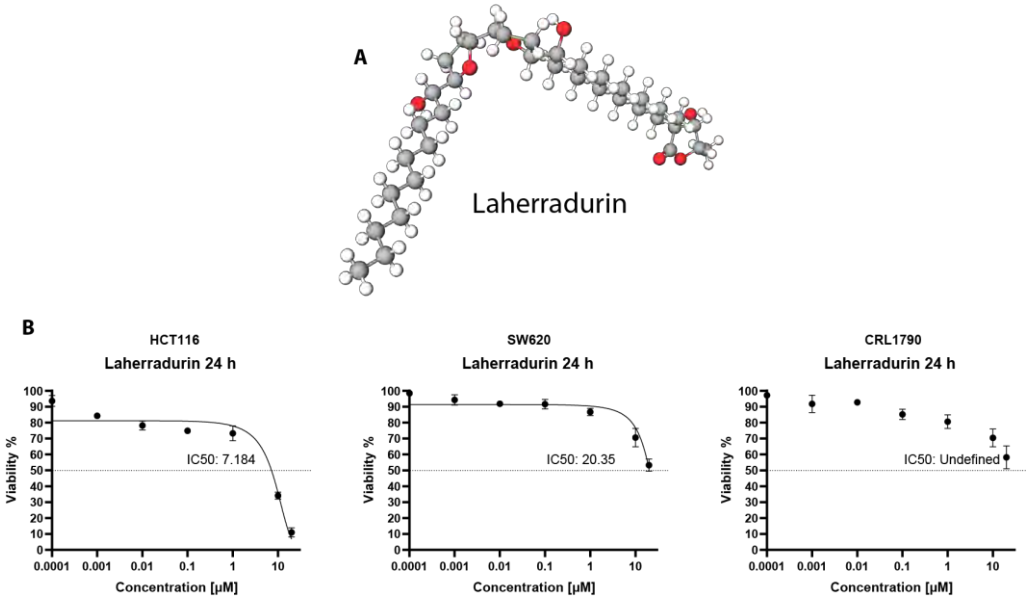


Figure 1. Dose-dependent effects of LAH on cellular inhibition. (**A**) Chemical 3D structure of LAH. Created by using MolView 3D software v2.4. Source: PubChem. (**B**) Dose–response curves showing IC_{50} values of CRC and non-tumoral cells treated with LAH during 24 h exposure, assessed via SRB. Curves represent triplicate biological repeats and are displayed as mean ± SEM (n = 3).

The principal molecular mechanism of ACGs involves the impairment of mitochondrial NADH-ubiquinone oxidoreductase (complex I), leading to adenosine triphosphate (ATP) depletion and cell cycle arrest [11]. Mitochondria are important for energy production, apoptosis regulation, metabolic reprogramming, and reactive oxygen species (ROS) generation. The dysregulation of mitochondrial dynamics, characterized by alterations in morphology, function, and signaling pathways, has been associated with cancer development [9]. In addition, mitochondrial dysfunction is related to cancer cell survival,

metastasis, and resistance to therapy, making them attractive targets for anticancer interventions [12]. The modulation of mitochondrial dynamics through plant-derived secondary metabolites represents a novel approach to induce apoptosis [13].

Recently, ACGs were shown to [13] induce autophagy in cancer cells [9,10,14–19]. Autophagy, a major catabolic process in the cells, is under the control of the PI3K/AKT/mTOR signaling pathway, a crucial regulator of cell proliferation and survival. The inhibition of mTOR complex 1 (mTORC1), leading to autophagy induction, has emerged as a novel anti-cancer strategy [20].

Our main goal was to evaluate the antitumor potential of LAH. To do so, we confirmed that it inhibits the electron transport chain complex. We found an increase in glycolysis and an oxidative phosphorylation (OXPHOS) activity reduction due to the inhibition of mitochondrial complex I at the metabolic level. We hypothesized that LAH induces damage at the mitochondrial level, which we demonstrated with a diminished mitochondrial membrane potential in addition to an elevation in mitochondrial mass due to mitochondrial fission and mitophagy induction. On the other hand, LAH, while affecting the glycolytic balance and OXPHOS, had a specific effect on autophagic flux in tumor cells in contrast to non-tumoral cells exposed to LAH. Finally, we demonstrated that these metabolic changes induce DNA damage leading to cell death via apoptosis

2. Materials and Methods

2.1. Reagents

LAH was extracted from the seeds of *Annona diversifolia* Saff (Annonaceae), collected in Copoya, Chiapas, México, and identified at the Eizi Matuda Herbarium of the Universidad de Ciencias y Artes de Chiapas, México. Additional controls included Rapamycin (RAP) at 1 μM (TO-R001, Euromedex, Souffelweyersheim, France), Hydroxychloroquine sulfate (HCQ) at 50 μM (HY-B1370, MedChemExpress, Monmouth Junction, NJ, USA), TORIN-1 at 1 μM (HY-13003, MedChemExpress, Monmouth Junction, NJ, USA), Oligomycin A at 10 μM (HY-16589, MedChemExpress, Monmouth Junction, NJ, USA), CCCP at 100 μM (C2759, Sigma-Aldrich, St. Louis, MO, USA), Antimycin A at 2.5 μM (A8674, Sigma-Aldrich, St. Louis, MO, USA), glucose at 20 mM (103577-100, Agilent Technologies, Santa Clara, CA, USA), and 2-DG at 20 nM (103344-100, Agilent Technologies, Santa Clara, CA, USA).

2.2. Cell Culture

The cell lines, HCT116 and SW620, and non-tumor cell line, CRL-1790, were provided by the National Cancer Institute in Mexico City, México. The cells were maintained in 100 × 15 mm culture dishes in DMEM/F-12 GIBCO® medium (Thermo Fisher Scientific, Waltham, MA, USA) supplemented with 10% fetal bovine serum (FBS, GIBCO®, Thermo Fisher Scientific, Waltham, MA, USA) at 37 °C with 5% CO_2. At 80% confluence, the cells were exposed to the treatments.

2.3. Cytotoxicity Assay

The IC_{50} value for LAH was determined via a Sulforhodamine B (SRB) colorimetric assay following the protocol established in 2006 [21]. Briefly, cells were seeded in 96-well plates at a density of 1×10^4 cells/well, allowed to adhere overnight and subsequently treated with different doses of LAH for 24 h. The cells were fixed with cold 10% trichloroacetic acid at 4° C for 1 h and washed four times with water, followed by staining with 100 μL of 0.5% SRB (S9012, Sigma-Aldrich, St. Louis, MO, USA) in 1% acetic acid for 30 min at room temperature. The excess of the stain was removed via washing four times with 1% acetic acid. The cells were resuspended in 200 mL of 10 mM Tris base at pH 10. The optical density at 510 nm was determined by using an Epoch microplate spectrophotometer (BioTek, Winooski, VT, USA). Dose–response curves and cellular viability values were

generated via GraphPad Prism software 8.0.2. All the experiments were performed in triplicate.

2.4. Western Blotting

Cell pellets were resuspended in NETN lysis buffer, and protein concentrations were determined. Samples were loaded onto 4–12% Tris-Glycine gels and transferred to PVDF membranes (IPVH00010, Millipore, Burlington, MA, USA). After blocking in 5% milk in TBS-T, membranes were incubated with primary antibody overnight at 4 °C, and membrane was washed 3 times with TBS-T followed by incubation with an appropriate secondary antibody for one hour at room temperature. Protein bands were visualized using an enhanced chemiluminescent substrate (WBKLS0500, Millipore, Burlington, MA, USA). The following antibodies were used: total OXPHOS human WB antibody cocktail (ab110411, Abcam, Cambridge, UK); anti-β-actin (C4) (sc-47778, Santa Cruz Biotechnology, Dallas, TX, USA); anti-caspase-8 (AM46, Millipore, Burlington, MA, USA); anti-mitofusin 1 (14739S), anti-phospho-DRP1 (Ser637) (6319S), anti-DRP1 (8570), anti-phospho-4E-BP1 (Thr37/46) (2855S), anti-4E-BP1 (9644S), anti-ULK1 (8054S), anti-phospho-ULK1 (Ser757) (14202), anti-P62 (5114S), anti-LC3B (2775), anti-PARP1 (9542), anti-cleaved PARP (9541), anti-AIF (5318), anti-caspase-3 (9662), anti-GAPDH (51332S), anti-mouse IgG, HRP-linked (7076), anti-rabbit IgG, HRP-linked (7074) were from Cell Signaling Technology, Danvers, MA, USA.

2.5. ATP Measurement

ATP concentrations were measured in triplicate using the ATPlite 1step Luminescence Assay System kit (6016736, PerkinElmer, Waltham, MA, USA) following the manufacturer's protocol. Total luminescence was measured using a 96-well microplate reader. ATP levels were expressed as a percentage of the untreated control.

2.6. Measurement of Mitochondrial Respiration

Mitochondrial respiration was assessed using the Seahorse XF96 extracellular flux analyzer (Agilent Technologies, Santa Clara, CA, USA). The cells were seeded in Seahorse XF96 cell culture microplates and allowed to adhere for 24 h. After exposure to the treatments, the cells were washed and incubated with XF RPMI medium. The compounds from the Seahorse XF Cell Mito Stress Test Kit (103015-100, Agilent Technologies, Santa Clara, CA, USA), and Seahorse XF Glycolytic Rate Assay Kit (103344-100, Agilent Technologies, Santa Clara, CA, USA) were loaded onto the microplate, and measurements were performed using Seahorse Wave software 2.6.3.5. The data were normalized based on the fluorescence intensity with Hoechst staining and the quantification of the total protein by using a bicinchoninic acid (BCA) assay (23227, Pierce BCA Protein Assay Kit, Thermo Fisher Scientific, Waltham, MA, USA).

2.7. Mitochondrial Membrane Potential Assessment

The mitochondrial transmembrane potential was assessed using Tetramethylrhodamine methyl ester (TMRM) (T5428, Sigma-Aldrich, St. Louis, MO, USA) fluorescence. CRC cells were seeded in 6-well plates and allowed to adhere for 24 h. Following the treatment with LAH, the cells were washed and incubated in DMEM containing 100 nM TMRM for 10 min at 37 °C in the dark. For flow cytometry analysis, TMRM fluorescence was excited at 549 nm and measured using a BD Accuri™ C6 Plus flow cytometer (BD Biosciences, Franklin Lakes, NJ, USA). A total of 1×10^4 cells were analyzed per condition. The relative TMRM intensity was calculated using FlowJo X software 10.8.1. Baseline TMRM levels were independently determined for each cell line, and these levels were used for normalization. To validate the mitochondrial membrane potential, the cells were treated with 10 μM Oligomycin A as a positive control and 10 μM CCCP as a negative control.

2.8. Analysis of Mitochondrial Morphology

The cells were seeded on poly-D-lysine-treated coverslips in 6-well plates and allowed to adhere for 24 h. After treatment with LAH, the cells were incubated with RPMI containing MitoTracker Orange CMTMRos (M7510, Thermo Fisher Scientific, Waltham, MA, USA) for 45 min at 37 °C in the dark. Following incubation, the cells were fixed with 4% paraformaldehyde (PFA), washed, and mounted on glass slides with Fluoroshield Mounting Media containing DAPI (F6057, Sigma-Aldrich, St. Louis, MO, USA). Images were captured at an excitation wavelength of 554 nm using a Confocal Leica SPE DM4000B microscope (Leica Microsystems, Wetzlar, Germany) with a 63× oil-immersion objective.

2.9. Mitochondrial Mass Measurement

The CRC cells were seeded in 6-well plates and treated with LAH. Following the treatment, the cells were incubated with 10% FBS RPMI medium containing 100 nM 10-N-nonyl acridine orange (NaO) (A1301, Invitrogen, Waltham, MA, USA) for 10 min at 37 °C in the dark. The fluorescence intensity was measured using a BD Accuri™ C6 Plus flow cytometer (BD Biosciences, Franklin Lakes, NJ, USA), with 1×10^4 cells analyzed per condition. The relative NaO intensity was calculated using FlowJo X software 10.8.1, baseline NaO levels were independently determined for each cell line, and these levels were used for normalization. Oligomycin A and CCCP were used as positive and negative controls for the mitochondrial membrane potential, respectively.

2.10. Immunofluorescence Staining

To localize autophagosomes, the cells were transfected with the pBABE-puro mCherry-EGFP-LC3B plasmid (22418, Addgene, Cambridge, MA, USA). The cells were cultured in 24-well plates on coverslips coated with 0.1 mg/mL poly-D-lysine (A-003-E, Sigma-Aldrich, St. Louis, MO, USA) at a density of 4×10^4 cells per well and allowed to adhere overnight at 37 °C. Subsequently, the cells were transfected with 1 μg of plasmid DNA using Lipofectamine 2000 (11668019, Thermo Fisher Scientific, Waltham, MA, USA) and subjected to drug treatment with LAH for 24 h. The cells were then fixed with 4% PFA for 30 min and permeabilized with 0.1% Triton X-100 in phosphate-buffered saline (PBS-T: 137 mM NaCl, 2.7 mM KCl, 10 mM Na_2HPO_4, 2 mM KH_2PO_4, pH 7.4) for 5 min. Coverslips were blocked with 1% bovine serum albumin (BSA) in PBS-T for 1 h. For immunostaining, the coverslips were incubated overnight with the primary antibody against alpha-tubulin (DM1A, 1:100, Cell Signaling Technology, Danvers, MA, USA). After washing with PBS-T, the coverslips were incubated with Alexa Fluor 568-conjugated mouse secondary antibody (ab175473, 1:100, Abcam, Cambridge, UK) in 1% BSA in PBS-T for 1 h at room temperature. After three washes with PBS-T, the coverslips were incubated for 5 min with PBS-T containing 10 μM DAPI. Finally, the coverslips were mounted with Vectashield Vibrance (H-1700, Vector Laboratories, Burlingame, CA, USA) on slides and sealed with nail polish. Digital images were captured using a Zeiss LSM 880 inverted microscope with a 63× oil-immersion objective at the appropriate wavelength (excitation at 587 nm for mCherry, excitation at 568 nm for tubulin, and excitation at 405 nm for DAPI) and analyzed using FIJI software 1.53. In order to detect γ-H2AX, all the manipulations were made as above (without plasmid transfection and using phalloidin to stain the cytoskeleton. Anti-γ-H2AX (D17A3) (Cell Signaling Technology, Danvers, MA, USA) (1:100) was used as a primary antibody, and goat-anti rabbit Cy2-conjugated was used as a secondary antibody (ab6940, Abcam, Cambridge, UK). Digital images were acquired using a Zeiss LSM 880 inverted microscope with a 60× oil-immersion objective. Fluorescence signals were detected with Cy2 (for γ-H2AX) at an excitation wavelength of 490 nm and an emission wavelength of 525 nm, and with DAPI at an excitation wavelength of 405 nm and an emission wavelength of 461 nm. All images were processed using FIJI software 1.53.

2.11. Statistical Analysis

Dose–response curves for estimating the cell viability were plotted by taking the logarithms of the concentrations of the compound along the X-axis and the cell viability along the Y-axis. Using GraphPad Prism Software 8.0.2, Inc., La Jolla, California, USA), the parameter "Log (inhibitor) vs. normalized response" was chosen to estimate the IC_{50} value (concentration of a drug giving a half-maximal inhibitory response). The results are expressed as mean ± standard error (SD) or standard error of the mean (SEM). GraphPad Prism Software 8.0.2 was used for statistical analysis. The differences between two groups were analyzed by using one-way ANOVA, and the differences between groups were analyzed by using two-way ANOVA with the Dunnett and Tukey multiple comparison tests. The statistical significance is indicated as follows: * $p < 0.05$, ** $p < 0.01$, *** $p < 0.001$, and **** $p < 0.0001$.

3. Results

3.1. LAH Inhibits Colon Cancer Cell Growth

The treatment with LAH of colon cancer cells demonstrated a marked increase in cellular inhibition with IC_{50} values of 7.184 μM and 20.35 μM for HCT116 and SW620, respectively, while remaining undetermined at 24 h in the non-tumoral CRL1790 cell line, suggesting the need for higher concentrations to achieve inhibition in non-tumor cells (Figure 1B, Figure S1). Such results suggest the potential selectivity depending on the cancer type and the potential therapeutic use of LAH for colon cancer. However, acetogenins, including LAH, have shown antiproliferative activity across various cancer types.

To understand how LAH affects cellular survival, we assessed its impact on the apoptosis in CRC and non-tumor cell lines by analyzing apoptosis-associated proteins through Western blotting. We observed an increase in the cleavage of PARP-1 in LAH-treated HCT116 and CRL-1790 cells but not in SW620 cells. The AIF levels increased in all three cell lines following the treatment, while caspase-8 showed variable expression: no change in HCT116, a decrease in SW620, and an increase in CRL-1790. The cleavage of caspase-3 (key proapoptotic protein) was observed in HCT116 and SW620 cells but was absent in the non-tumor CRL-1790 cell line (Figure 2A).

These findings highlight that LAH selectively induces apoptosis in cancer cells, as evidenced by caspase-3 cleavage, while sparing non-tumor cells. LAH is known for inhibiting mitochondrial complex I, which may initiate a cascade of events that trigger the apoptotic pathway. The disruption of mitochondrial function can lead to the release of pro-apoptotic factors and the activation of the caspase cascade, contributing to cell death. Additionally, mitochondrial dysfunction can result in the increased production of ROS, which may cause DNA damage and trigger γ-H2AX formation, an indicator of DNA double-strand breaks (DSBs).

Immunostaining for γ-H2AX clearly demonstrated that LAH treatment induces the formation of γ-H2AX foci in CRC cell lines (Figure 2B), which indicates the presence of DNA damage. This observation links mitochondrial inhibition, DNA damage, and apoptosis, suggesting that the impact of LAH on mitochondrial complex I may play a key role in initiating these downstream cellular processes, thereby enhancing its therapeutic potential against colon cancer. These findings contrast with those observed in the non-tumoral cell line, CRL1790. Further investigation is necessary to fully elucidate the intricate relationship between mitochondrial inhibition, DNA damage, and apoptosis in the mechanism of action of LAH.

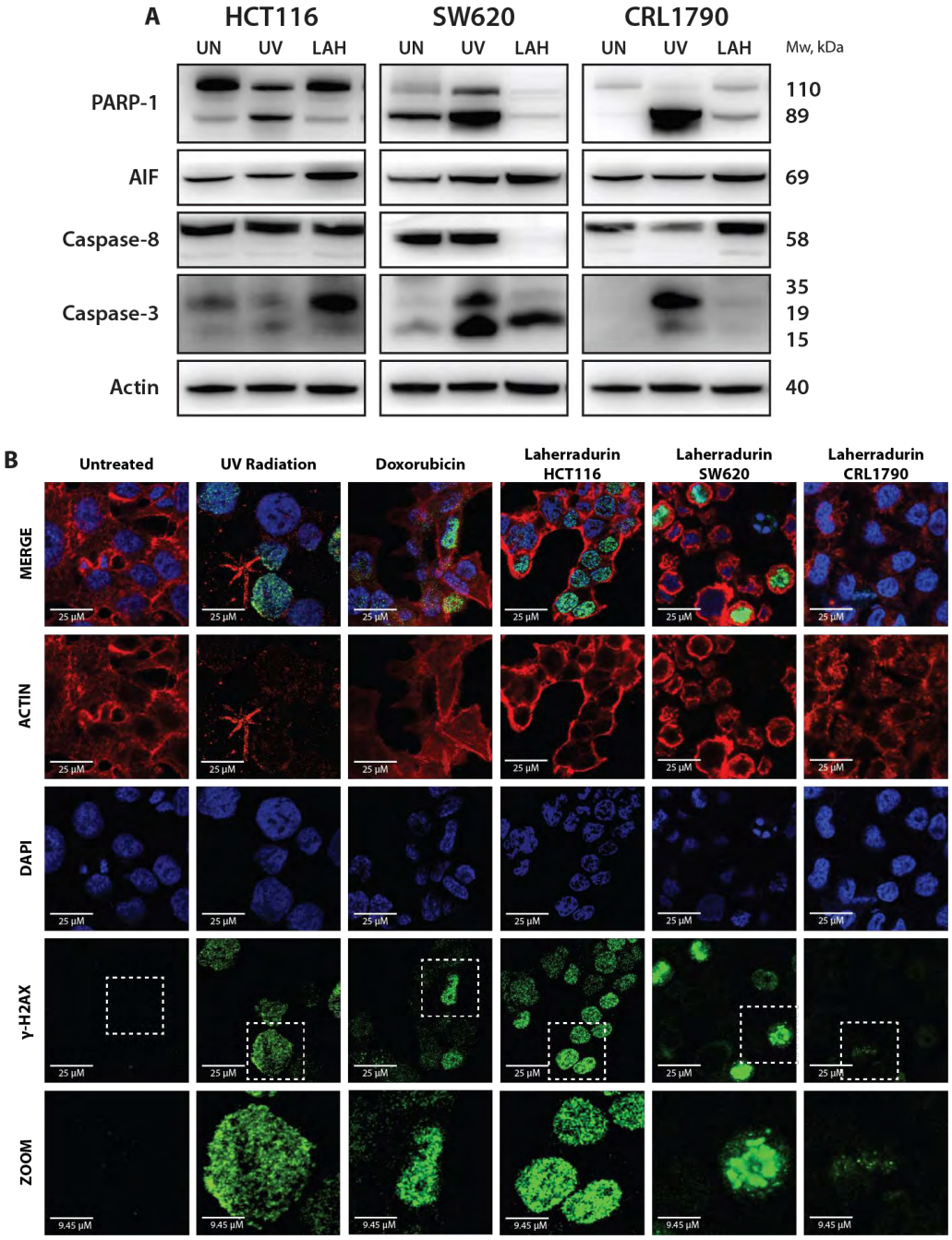


Figure 2. LAH induces apoptosis and DNA damage. (**A**) Representative images of protein expression levels of PARP-1, AIF, Caspase-8, and Caspase-3. GAPDH was used as loading control. Replicates were conducted three times in total. (**B**) H2AX foci detection in CRC and non-tumor cells. Fluorescence images taken with Zeiss LSM 880 confocal microscope at 63×. γ-H2AX, DAPI, ACTIN, and ZOOM with treatments: Untreated, UV radiation, Doxorubicin, LAH at 24 h exposure. The photos are representative of at least three independent experiments. Scale bar: 20 μm.

3.2. LAH Disrupts the Mitochondrial Function and Dynamics in Colon Cancer Cells, Leading to Bioenergetic Failure

LAH not only induces DNA damage and apoptosis but also disrupts the mitochondrial function and dynamics in colon cancer cells. Mitochondria, being central regulators of programmed cell death, respond to cellular stress by modulating reactive oxygen species (ROS) levels. This mitochondrial dysfunction affects critical processes such as electron transport chain (ETC) activity, ATP production, and mitochondrial membrane potential ($\Delta\Psi_M$ or MMP).

To investigate the specific effects of LAH on the mitochondrial function in colon cancer cells compared to non-tumorigenic cells, we assessed $\Delta\Psi_M$ as a key indicator of mitochondrial health using tetramethylrhodamine methyl ester (TMRM), a cationic, lipophilic dye that accumulates in active mitochondria with a high membrane potential. In untreated (non-fluorescent) cells, the red histogram shows no detectable signal. However, upon incubation with TMRM, a fluorescence signal is generated, shifting the histogram to the right (blue histogram), indicating an increase in MMP.

To ensure the validity of these results, we employed FCCP (carbonyl cyanide-p-trifluoromethoxyphenylhydrazone) and oligomycin as controls. FCCP, a known mitochondrial uncoupler, disrupts the proton gradient throughout the inner mitochondrial membrane, causing a shift in the TMRM signal to the left, consistent with decreased MMP. Conversely, oligomycin, an ATP synthase inhibitor, blocks the proton flow through the F_0F_1-ATPase, causing a shift further to the right, indicating increased MMP due to proton accumulation. In the presence of LAH, a substantial increase in TMRM fluorescence intensity was observed in all three cell lines (represented by the forest green histogram) (Figure 3A,B), signifying an elevation in $\Delta\Psi_M$. This heightened MMP likely reflects impaired oxidative phosphorylation (OXPHOS), leading to proton accumulation, increased glycolytic flux, and enhanced ROS production.

To further explore the impact of LAH on mitochondrial function, we employed the Seahorse XF Cell Mito Stress Assay to measure the key parameters of mitochondrial respiration, including basal respiration, ATP-linked respiration, proton leak, spare respiratory capacity, and maximal respiration (Figure 3C).

Our analysis revealed a significant reduction in the basal mitochondrial oxygen consumption rate (OCR) across all three cell lines treated with LAH, compared to the untreated controls (Figure 3D). This reduction suggests that LAH impairs the essential mitochondrial processes required for sustaining cellular energy production. Additionally, the OCR linked to ATP production was markedly lower in LAH-treated cells compared to both untreated and RAP-treated cells, further corroborating the impairment of mitochondrial ATP synthesis. Proton leak, a measure of protons escaping through the inner mitochondrial membrane without contributing to ATP synthesis, also increased in the LAH-treated cells, indicating mitochondrial dysfunction.

Upon the addition of FCCP, which uncouples the ETC to reveal maximal respiratory capacity, no significant increase in OCR was detected in the LAH-treated cells. This contrasts with the robust OCR increase seen in the control and RAP-treated cells, where FCCP stimulated maximal respiration. The lack of FCCP-induced OCR elevation in the LAH-treated cells signifies a depleted spare respiratory capacity, suggesting severe bioenergetic damage to mitochondria. The measurement of maximal respiration, after FCCP administration, was significantly impaired in the LAH-treated cells, a critical indicator of compromised mitochondrial function. This impairment suggests that LAH disrupts the mitochondria's ability to meet the energy demands under stress (Figure 3D).

In conclusion, LAH significantly disrupts mitochondrial respiration at multiple levels. The observed reductions in basal respiration, ATP-linked respiration, and maximal respiration, combined with the increased proton leak, underscore LAH's profound impact on mitochondrial integrity and bioenergetic capacity. These findings highlight the severe metabolic and bioenergetic deficits induced by LAH in colon cancer cells, providing further insight into its mechanism of action and potential as a therapeutic target.

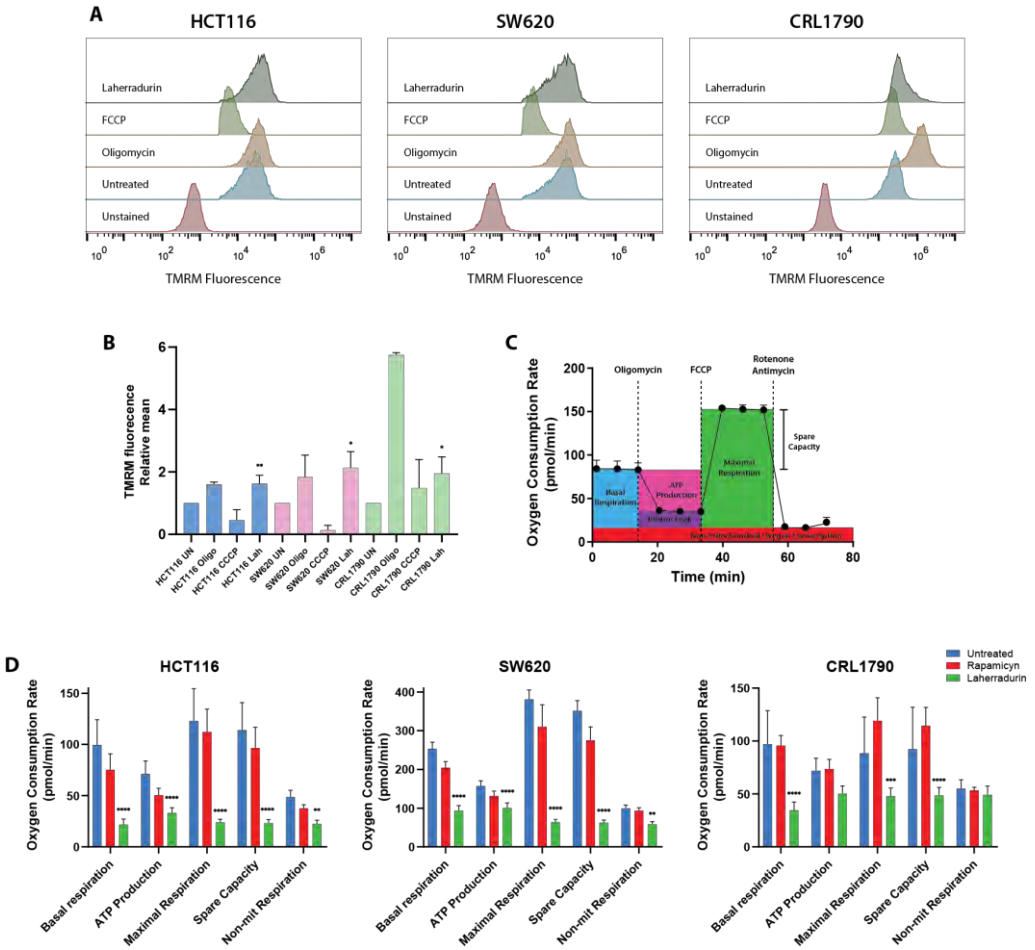


Figure 3. $\Delta\Psi_M$ Disruption and Bioenergetic Alterations. Cells were stained for TMRM (indicator $\Delta\Psi_M$) and analyzed in flow cytometry. (**A**) Representative cytograms depicting the relative intensity of TMRM in CRC cells and non-tumoral cells treated with LAH for 24 h. (**B**) Bar graph shows relative TMRM intensity of CRC cells treated with LAH at 24 h. Results represent at least three independent biological experiments. Statistical significance relative to the control was determined by one-sample t-test. $^{**}p < 0.05$, $^{*}p < 0.1$ (**C**) Schematic representation illustrating oxygen consumption measured through extracellular flux analysis, highlighting the calculable parameters. (**D**) Bioenergetic profile comprising five respiration parameters. OCR following sequential addition of various modulators of mitochondrial function (Oligomycin, FCCP, and Rotenone/Antimycin A) was determined using a Seahorse XF96 analyzer. Cells were treated with LAH individually for 24 h. The results are compiled from at least three independent biological experiments, each involving independent cell seeding in eight wells of Seahorse microplates. Data are presented as mean ± SE. Statistical significance relative to control is indicated as follows: $^{****}p < 0.001$, $^{***}p < 0.01$, $^{**}p < 0.05$, as determined by two-way ANOVA with Dunett's multiple comparisons test.

3.3. LAH-Induced Disruption of the Mitochondrial Electron Transport and Energy Production in CRC Cells

To further understand the impact of LAH on mitochondrial function, we analyzed the expression of OXPHOS proteins. OXPHOS complexes are integral to mitochondrial energy production and are directly affected by changes in MMP. In HCT116 cells, LAH treatment led to a reduction in the expression of complex I and complex IV, which are critical components of the mitochondrial electron transport chain (Figure 4A,B). This reduction in OXPHOS proteins correlates with the observed decrease in MMP, as disruption in the electron transport chain can lead to decreased $\Delta\Psi_M$ and impaired ATP production. In contrast, SW620 cells exhibited minimal changes in OXPHOS proteins and MMP, similar to non-tumor CRL-1790 cells, indicating that LAH's effect is more pronounced in

certain cancer cell types. In all the cell lines, no significant alterations were detected in complexes III and V upon LAH treatment (Figure S2).

The ATP levels, reflecting mitochondrial energy production, were significantly reduced in HCT116 cells following LAH treatment compared to SW620 and CRL-1790 cells (Figure 4C). This reduction is consistent with the observed decrease in MMP and OXPHOS protein expression, underscoring the impact of LAH on mitochondrial function and energy metabolism.

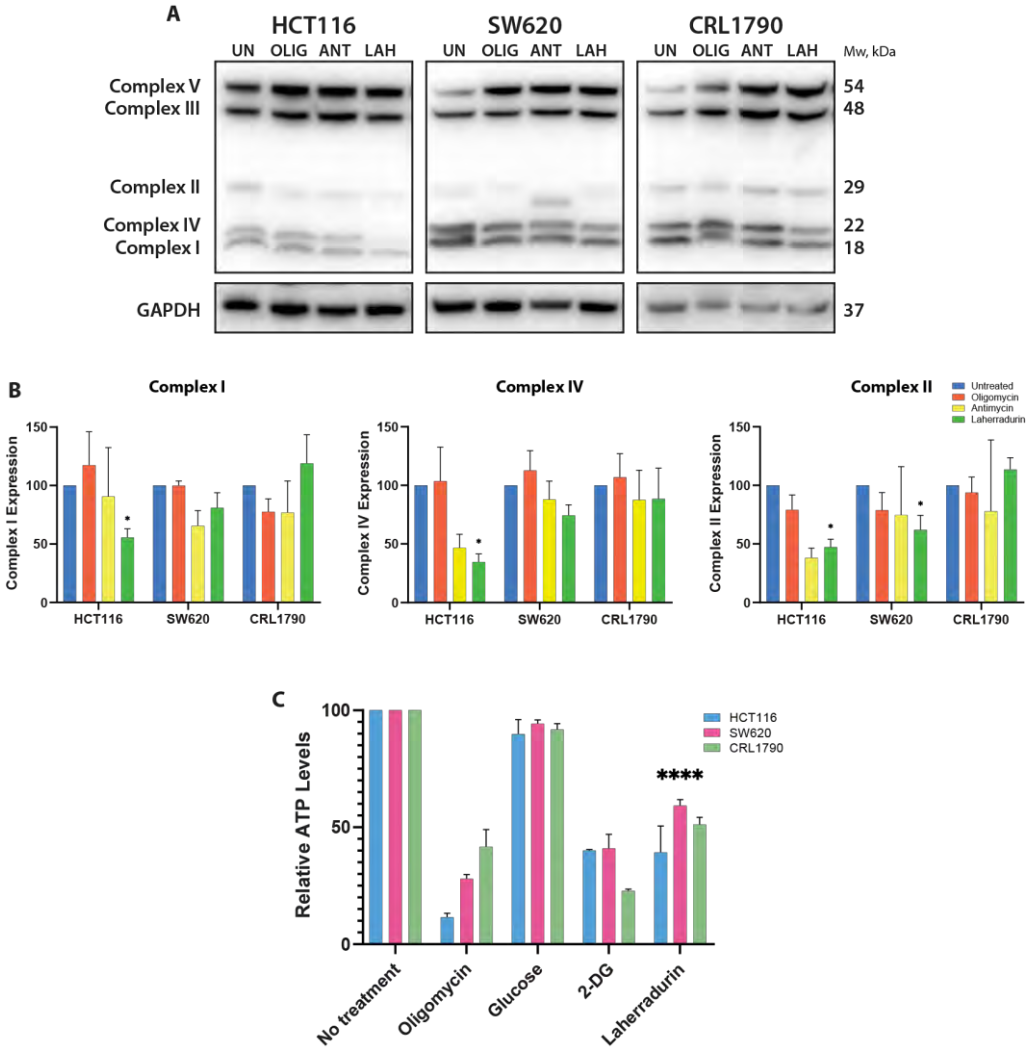


Figure 4. Expression of OXPHOS complexes in Mitochondria from CRC and Non-Tumor Cells. (**A**) A cocktail of antibodies targeting proteins representing the five mitochondrial OXPHOS complexes was utilized to assess the expression of mitochondrial proteins in CRC cell lines, under the following experimental conditions: Untreated (UN), Oligomycin, Antimycin A (ANT), and LAH. GAPDH was used as a loading control. (**B**) The antibody cocktail included the following targets: complex I subunit NDUFB8, complex II subunit SDHB, complex III subunit UQCR2, complex IV subunit MTCO1, and complex V subunit ATP5A. The WB was technically replicated three times in total, demonstrating a representative blot. Values are expressed as mean ± SEM normalized relative to their respective control and then presented as fold change relative to treatment: *$p < 0.1$. A two-way ANOVA test with Dunett's multiple comparisons test was applied. (**C**) Relative ATP levels of cells were measured at 24 h of treatment. Treatment groups included: No treatment, Oligomycin, Glucose, 2-DG, and LAH. Results are presented as the mean ± SE of three independent experiments. Statistical significance was determined by a two-way ANOVA with Tukey's multiple comparisons test (****$p < 0.001$).

3.4. LAH on the Glycolytic and Mitochondrial Function in Colon Cancer Cells

Next, we evaluated the glycolytic rate. To isolate the contribution of glycolysis to proton efflux, we measured cellular OCR and subtracted it from the total proton efflux rate (PER), resulting in the glycolytic proton efflux rate (glycoPER). This value reflects the rate of protons extruded during glycolysis. Figure 5A,B show that the rapamycin (RAP)-treated and untreated cell lines exhibited low basal glycolytic rates, whereas LAH treatment led to a significant increase in the glycolytic rate compared to the controls. This enhanced glycolysis is due to LAH's inhibition of OXPHOS, which forces cells to rely more on glycolysis for energy. The RAP-treated cells displayed similar basal proton efflux rates to the untreated controls, indicating a minimal impact on the ETC activity and glycolytic metabolism. In contrast, LAH treatment resulted in a significant rise in basal proton efflux, highlighting its pronounced effect on metabolic pathways. Figure 5C further demonstrates that LAH-induced proton efflux was approximately 50% higher than in the untreated and RAP-treated cells, indicating a substantial enhancement in glycolysis in CRC cells treated with LAH.

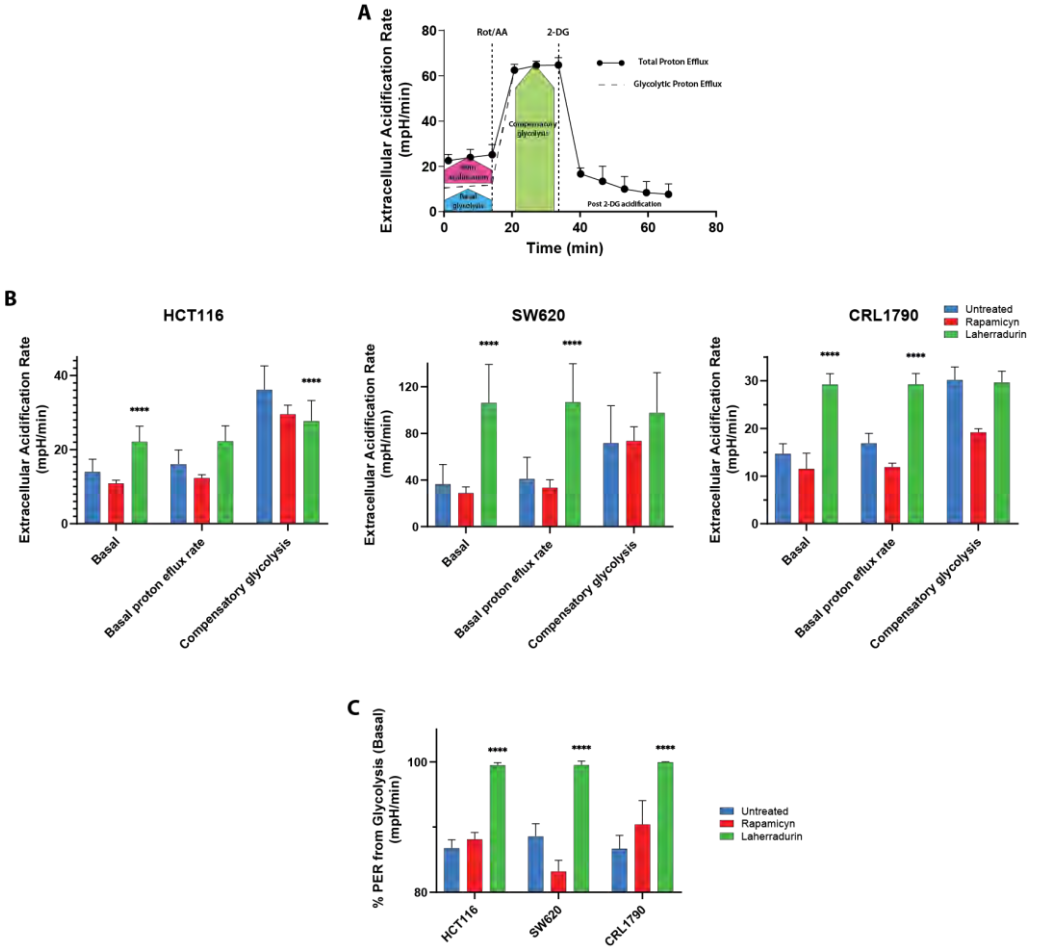


Figure 5. Analysis of glycolytic flux in CRC and non-tumor cells. (**A**) Schematic of proton efflux rate from extracellular flux analysis showing the calculable parameters. ECAR after sequential addition of different modulators of glycolytic function (Rotenone/Antimycin A and 2-DG) was determined using a Seahorse XF96 analyzer. (**B**) Bioenergetic profile of glycolytic parameters. Basal: basal respiration. Basal proton efflux rate: (glycoPER) glycolytic basal rate. Compensatory glycolysis: the ability of the cell to compensate for energy production through glycolysis following mitochondrial ATP production blockage. (**C**) % PER of glycolysis indicates the contribution of the glycolytic pathway to total extracellular acidification. Results represent at least three independent biological experiments, each of which consisted of independent seeding of cells in eight wells of Seahorse microplates. Data are presented as mean ± SE. ****$p < 0.001$, relative to control by two-way ANOVA with Dunett's multiple comparisons test.

3.5. Mitochondrial Dynamics and Function Altered by LAH

One of the reasons for the altered mitochondria function can be related to changes in the mitochondrial dynamics. We examined the mitochondrial dynamics using Mito-Tracker staining. Mito tracker, featuring a thiol-reactive chloromethyl group for mitochondrial labeling, is a cationic lipophilic dye. Its positive charge enables penetration through the cell membrane due to lipophilicity and accumulation within the mitochondrial matrix, facilitated by the negative mitochondrial membrane potential.

Observations of the untreated cells revealed a variety of mitochondrial shapes, including spherical, rod-shaped, and filamentous arrangements, indicative of mitochondrial dynamics and the associated increased ATP production (Figure 6A).

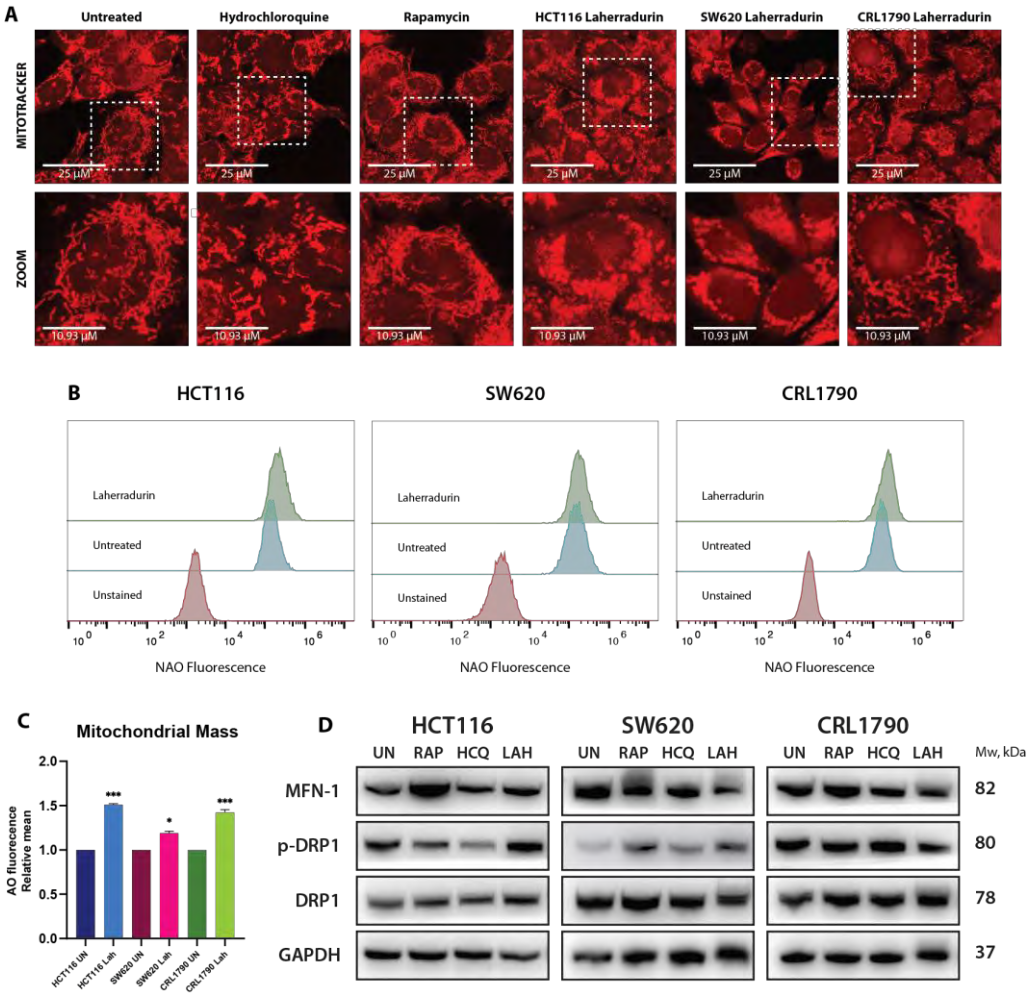


Figure 6. Effects of natural compounds on mitochondrial dynamics and function in CRC and non-tumor cells. (**A**) Fluorescence images of mitochondrial morphology stained with MitoTracker Red in CRC and non-tumor cells. Images were captured using LEICA confocal microscope at 63× magnification. Treatments include: Untreated, RAP, CQ, and LAH with 24 h exposure. Representative images from at least three independent experiments. Scale bar: 25 µm; zoom: 10.93 µm. (**B**) Representative cytograms depicting the relative intensity of NaO in CRC cells and non-tumoral cells treated with LAH for 24 h. (**C**) Bar graph illustrating the relative NaO intensity of CRC cells treated with LAH for 24 h. Cells were stained with NaO and analyzed via flow cytometry. Data represent at least three independent biological experiments, presented as mean ± SE. Statistical significance was assessed using one-sample t-test, with ***$p < 0.01$, and *$p < 0.1$, relative to the control. (**D**) Representative images and quantification of protein expression levels of MFN1, p-DRP1, and DRP1, normalized to GAPDH as a loading control.

We used HCQ and Rapamycin (RAP) as control treatments to understand the effects of LAH. HCQ, an autophagy inhibitor, affects lysosomal pH and prevents the fusion of autophagosomes and lysosomes. After treatment with 50 μM HCQ, mitochondria exhibited similar shapes to those observed in the untreated cells, suggesting that HCQ effectively inhibits mitophagy (Figure 6A). In contrast, RAP inhibits mTOR signaling and induces mitochondrial fusion, leading to elongated mitochondrial networks (hyperfusion), which protects mitochondria from degradation due to starvation effects (Figure 6A).

LAH treatment, however, resulted in significant mitochondrial fragmentation (Figure 6A). This fragmentation is associated with impaired OXPHOS, mtDNA damage, and increased ROS creation, as discussed earlier. Additionally, NaO staining revealed an increase in mitochondrial mass, suggesting that the fragmentation observed is related to alterations in mitochondrial network integrity and bioenergetic capacity, rather than a simple reduction in mitochondrial content (Figure 6B,C). This fragmentation can result from heightened mitochondrial biogenesis as a compensatory response to stress or damage, leading to a higher overall mitochondrial content.

These findings underscore the complex effects of LAH on mitochondrial morphology and function, contrasting with the effects of other treatments and highlighting the disruption of mitochondrial network integrity and bioenergetic function induced by LAH.

3.6. Association between Mitochondrial Fragmentation and Mass Increase

The results indicate an increase in the mitochondrial mass in all three cell lines after 24 h of LAH treatment, likely due to induced fragmentation. This fragmentation is associated with a compensatory increase in mitochondrial content. To further investigate, Western blot analysis was performed to assess the proteins involved in the mitochondrial dynamics, including mitofusin 1 (MFN1) and dynamin-related protein 1 (DRP1), a GTPase that modules mitochondrial fission upon phosphorylation. A significant decrease in MFN1 expression was observed in SW620 and CRL-1790 cells but not in HCT116 cells (Figure 6D, Figure S3). Conversely, a significant increase in phosphorylated DRP1 was detected in LAH-treated cancer cell lines, indicating enhanced mitochondrial fission. This suggests that LAH-induced fragmentation and the associated increase in mitochondrial mass are more pronounced in cancer cells compared to non-tumor cells, reflecting a selective impact on the mitochondrial dynamics in colon cancer cells. Thus, LAH had a profound impact on mitochondrial function and dynamics, which seems to be more specific for colon cancer cell lines and does not significantly disturb non-tumor cells.

3.7. mTORC1 Activity and Autophagy Induction Following LAH Treatment

To elucidate the effects of LAH on mTOR complex 1 activity, we analyzed the phosphorylation status of one of its key substrates, eukaryotic translation initiation factor 4E-binding protein 1 (4E-BP1). LAH treatment significantly reduced 4E-BP1 phosphorylation in HCT116 cells and SW620 in contrast to the non-tumoral cell line, CRL1790. The inhibition effects are similar to the downregulation observed with the mTORC1-specific inhibitor Torin 1 (Figure 7A, Figure S4). Interestingly, LAH did not significantly affect 4E-BP1 phosphorylation in HCT116 cells, which suggests that changes in 4E-BP1 activity might influence the mTORC1 activity in these cells. HCQ, an autophagy inhibitor that does not act on mTORC1, showed no impact on 4E-BP1 phosphorylation. We also examined other substrates, such as p70 S6 kinase (p70S6K) and transcription factor EB (TFEB); however, p70S6K did not show any significant changes following LAH treatment, and although TFEB expression diminished in their phosphorylated form, it did not reach statistical significance (data not shown). These findings suggest that the effects of LAH on mTORC1 signaling are specific to certain substrates, further highlighting the selective nature of its action.

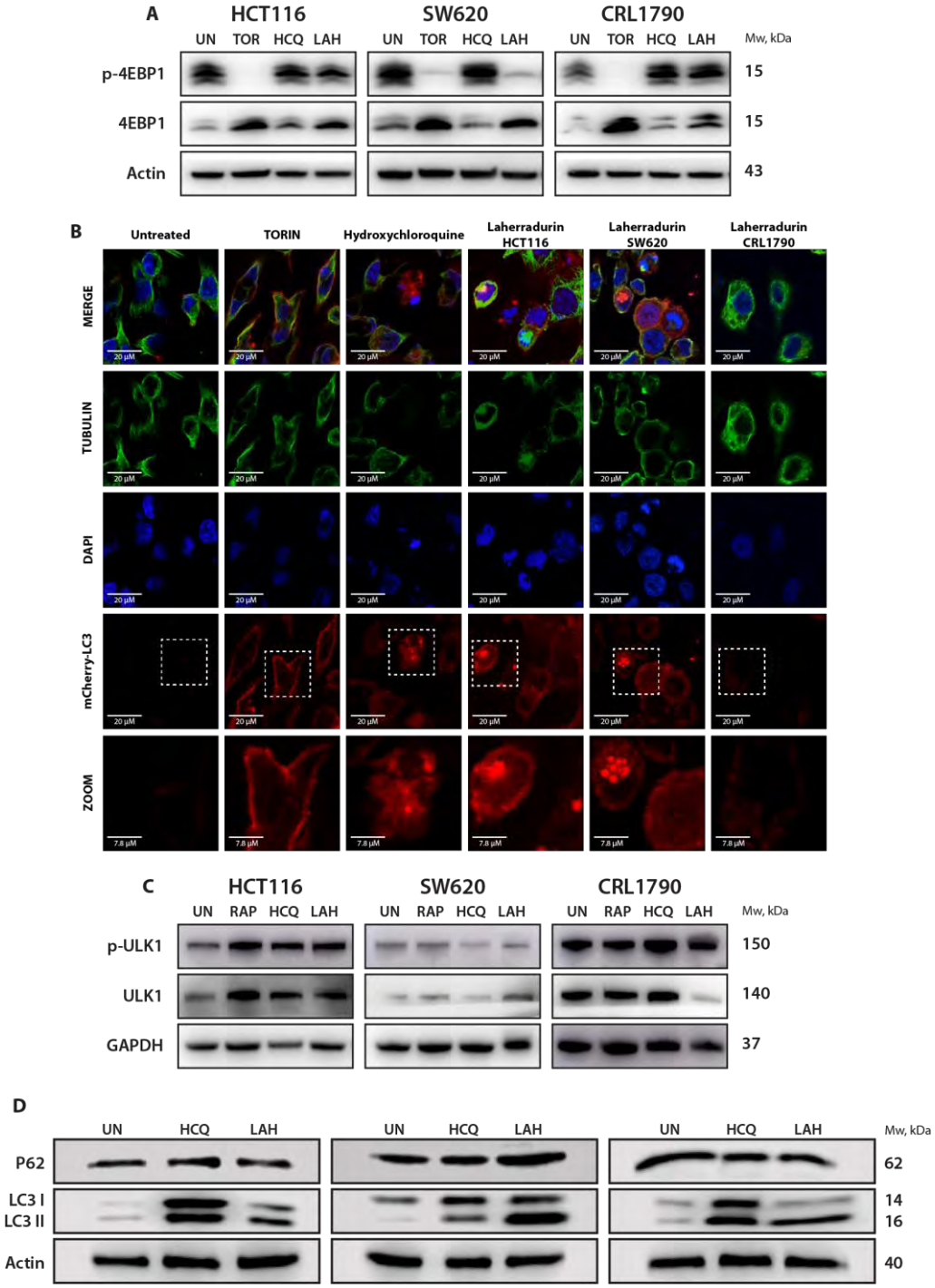


Figure 7. LAH modulates mTOR pathway and induces autophagy. (**A**) Representative images and graphical quantification of protein expression levels of p-4E-BP1, and 4E-BP1. (**B**) Autophagosome detection stained with mCherry in CRC and non-tumor cells. Fluorescence images taken with Zeiss LSM 880 confocal microscope at 63×. mCherry-LC3, Tubulin, DAPI, and ZOOM with treatments: Untreated, RAP, CQ, LAH at 24 h exposure. The photos are representative of at least three independent experiments. Scale bar: 20 μm. (**C,D**) Representative images of protein expression levels of p-ULK, ULK, P62, LC3-I, and LC3-II. GAPDH and actin were used as loading controls. Replicates were conducted three times in total.

3.8. Induction of Autophagy by LAH in Colon Cancer Cells

Since LAH inhibits phosphorylated 4E-BP1, it is plausible that it selectively targets mTORC1, potentially affecting autophagic flux. To investigate this, we assessed autophagy induction using fluorescent detection. The cells were transfected with the mCherry-

eGFP-LC3B plasmid and treated with Torin 1, HCQ, and LAH for 24 h. This assay visualizes autolysosomes as red dots, indicating autophagic activity.

Treatment with Torin 1 (an mTORC1 inhibitor and autophagy inducer), HCQ, and LAH resulted in the formation of mCherry-positive dots (Figure 7B). Notably, while both Torin 1 and HCQ induced mCherry-positive dots, their mechanisms differ. Torin 1 stimulates autophagy by inhibiting mTORC1, leading to increased autophagosome formation, whereas HCQ inhibits the fusion of autophagosomes with lysosomes, resulting in the accumulation of autophagic vacuoles. This distinction highlights the varied effects of the different treatments in autophagy regulation.

Further investigation into the impact of LAH on autophagy in the HCT116 and SW620 cell lines was conducted using Western blot analysis of autophagy-related proteins, including ULK1, P62, LC3I, and LC3II. ULK1 is a key kinase initiating autophagy, P62 is involved in the ubiquitinated cargo deliverance to autophagosomes, and LC3I and LC3II are crucial for autophagosomes, with LC3II serving as a marker for autophagosome formation.

The results showed a significant increase in the phospho-ULK1 levels in HCT116 cells, while a decrease was observed in the non-tumoral cell line. SW620 cells showed elevated total ULK1 levels, whereas no significant changes were noted in the HCT116 or non-tumor cells (Figure 7C, Figure S5). Additionally, LAH treatment increased the LC3II levels across all three cell lines, indicating autophagy induction; however, there were no significant changes in p62 detection (Figure 7D, Figure S5). These findings suggest that LAH induces autophagy in tumor cells, potentially through the induction of mitophagy.

4. Discussion

In this study, we explored the effects of a plant-derived metabolite, namely the acetogenin, LAH, on colon cancer cells, focusing on its impact on cellular energetics and mitochondrial dynamics. Our data revealed how LAH influences the mitochondrial function and metabolic pathways in CRC.

A hundred years ago, Otto Warburg discovered that tumor cells exhibit higher glycolytic activity than normal cells, suggesting mitochondrial damage and OXPHOS inhibition in tumors [22]. However, recent studies have challenged this view, showing intact mitochondrial function in most tumors and even increased OXPHOS activity in certain cancers, which supports cell proliferation, metastasis, and therapy resistance [23]. For instance, Ren et al. found that the upregulation of prohibitin 2 (PHB2) enhances mitochondrial complex I activity, boosting OXPHOS levels and promoting CRC tumorigenesis. PHB2 deletion reduces OXPHOS levels in CRC cells [24]. Similarly, in this study, we found elevated cellular OCR in CRC cells, indicating that these cells produce more ATP through upregulated mitochondrial OXPHOS rather than glycolysis.

LAH impaired mitochondrial function, characterized by the reduced detection of OXPHOS complexes [14,25]. This results in ATP depletion [26] and altered mitochondrial dynamics. This impairment significantly impacts cellular metabolism. Our findings demonstrate that LAH treatment leads to a notable decrease in the expression of OXPHOS complexes, critical for mitochondrial energy production. This reduction in OXPHOS proteins correlates with a decrease in $\Delta\Psi_M$ and a significant drop in ATP levels, confirming the disruption of mitochondrial function. Additionally, the observed changes in mitochondrial dynamics and metabolic shifts underscore LAH's profound effect on cellular energy production and the overall metabolic state.

OXPHOS dysfunction reduces mitochondrial ATP generation, leading to increased glycolysis [27]. Our study supports this, showing decreased ATP levels following LAH treatment (Figure 3 and Figure 4). Additionally, LAH significantly impaired mitochondrial respiration and decreased the reserved respiratory capacity, leading to severe mitochondrial dysfunction. These findings align with previous studies on various natural compounds that disrupt mitochondrial respiration and induce compensatory glycolysis in cancer cells [28–30].

Understanding the relationship between energy metabolism and mitochondrial dynamics is crucial in cancer biology [31]. Mitochondria maintain a continuous balance between fusion and fission [32]. Mitochondrial fusion hastens the exchange of materials in the mitochondria to compensate for mitochondrial function [31], and mitochondrial fission eliminates impaired mitochondria by way of mitophagy [33]. The induction of mitochondrial fragmentation and an increase in the mitochondrial mass suggest a complex interplay between these dynamics and the metabolic responses triggered by LAH. Mitochondrial fragmentation, often associated with dysfunctional mitochondria [34] and increased ROS production, may contribute to cellular stress and apoptosis [33].

The mitochondrial fusion at the outer mitochondrial membrane is mediated by MFN1 and mitofusin 2 (MFN2), whereas the fusion at the inner mitochondrial membrane is mediated by optic atrophy protein 1 (OPA1) [35]. Mitochondrial fission is mediated by DRP1, FIS1, and MFF (31). Under LAH treatment, we did not observe a reduction in MFN1 expression. This discrepancy may be attributed to the potential compensatory role of MFN2, which, to some extent, can substitute for MFN1 [36] in mitochondria lacking MFN1 due to their structural similarity [37].

Polyphilin I, a natural product obtained from Paris polyphylla rhizomes, induces the mitochondrial translocation of DRP1, leading to mitochondrial fission, the release of cytochrome c from the mitochondria to the cytosol, and eventual apoptosis [38]. We observed an increase in mitochondrial fission, as evidenced by the elevated levels of p-Drp1 protein in CRC cells exposed to LAH, but not in the non-tumor line. These findings accord with MitoTracker staining, where we observed that the LAH treatments induced mitochondrial fragmentation in the CRC cell lines. Mitochondrial fusion has been observed in response to treatments with RAP and HCQ [39].

This mitochondrial fragmentation is attributed to cellular dysfunction [40], OXPHOS impairment [41], mtDNA damage [42], and ROS production [43]. Moreover, mitochondrial fragmentation facilitates the autophagic elimination of damaged mitochondria and is closely associated with mitochondrial fission [44]. In contrast, our findings reveal that untreated cells typically exhibit a large tubular mitochondrial array, extending throughout the cytosol and closely interacting with the nucleus and endoplasmic reticulum [45]. The highly dynamic mitochondrial networks oscillate between a fragmented state and a tubular continuum, reflecting a balance between mitochondrial fusion and fission, thereby promoting increased ATP production [46]. Under the conditions of metabolic stress or nutrient depletion, the rapid and transient elongation of the mitochondrial network occurs, termed "stress-induced mitochondrial hyperfusion" [47]. Mitochondrial hyperfusion has been observed in response to treatments such as RAP and CQ [39], while LAH result in fragmented mitochondria, suggesting potential mitochondrial fission.

Additionally, the dynamic alterations in mitochondrial energy have been linked to dysregulation in MMP [48]. $\Delta\Psi_M$ serves as a crucial indicator of mitochondrial function, and $\Delta\Psi_M$ originates from proton pumping across the inner mitochondrial membrane concomitant with electron transport [49]. This process drives various essential mitochondrial functions, such as ATP synthesis, calcium accumulation, and the maintenance of ion gradients [48]. Previous studies reported a gradual decrease in $\Delta\Psi_M$ in HepG2 cells upon exposure to LAH [14]. Our results present contrasting data. We observed an increase in $\Delta\Psi_M$ in the CRC cells treated with LAH across all three cell lines. This increase in $\Delta\Psi_M$ may contribute to diminish ATP production and promote ROS generation. Changes in $\Delta\Psi_M$ can influence the alterations in energy metabolism.

In addition to the observed alterations in mitochondrial dynamics and energy metabolism, our study sheds light on the involvement of key cellular processes such as mTOR signaling, apoptosis, and autophagy in the response to treatment with LAH. The dysregulation of mTOR signaling has been associated with multiple types of cancer, including CRC, where it plays a central role in promoting cell growth and proliferation [50–53]. In our study, we observed a decrease in phosphorylated 4E-BP1 indicating mTOR inhibition.

mTOR inhibition has been shown to promote events such as apoptosis and autophagy. The acetogenin analogue, AA005, induces autophagy through the activation of AMPK, thereby blocking the mTOR pathway and leading to the increased expression of LC3 [16]. These findings align closely with our own data, wherein we observe the upregulation of LC3II, suggesting an augmentation in the origination of the ATG12-ATG5 conjugate, a pivotal step in autophagosome biogenesis.

Under prolonged stress conditions, autophagy may also contribute to programmed cell death. ACGs induce cell cycle arrest in the G1/S phase [54–56] through the deregulation of various pathways such as MAPK [57] or Notch [18]. These pathways can increase the ROS levels [56], alter energy metabolism [17], and induce apoptosis, either in a caspase-dependent or caspase-independent manner [15,19]. We found a significant induction of programmed cell death in CRC cells following LAH treatment. LAH triggers apoptosis in CRC cells through multiple mechanisms. Firstly, we observed an increase in DNA DSBs, as shown by the upregulation of phosphorylated γ-H2AX, a well-established marker of DNA damage and a key component of the DNA damage response (DDR) [58]. γ-H2AX formation occurs at sites of DNA DSBs, where it serves as a recruitment platform for various DDR proteins involved in repair and signaling processes [59]. Previously, it was shown that the natural compound, resveratrol, which inhibits complex I of the ETC [60], sensitized radioresistant prostate cancer cells by increasing ATM phosphorylation and its target protein γ-H2AX, resulting in cell cycle arrest and subsequently cell death [61].

DDR activation initiates a cascade of events aimed at repairing the damaged DNA or triggering apoptotic cell death if repair is not feasible. The increased γ-H2AX signal observed in our study reflects the cellular response to the genotoxic stress inflicted by LAH, highlighting the effectiveness of LAH in inducing DNA damage and activating apoptotic pathways in CRC cells. Furthermore, our study revealed a cascade of events following the induction of DNA DSBs, notably the activation of caspase cascades. The observed increase in caspase-3 activation corroborates the initiation of the apoptotic signaling pathways triggered by LAH-induced DNA damage. This coordinated response underscores the potency of LAH in inducing apoptotic cell death in CRC cells through the activation of both the DNA damage response and apoptotic pathways. These results are similar to those reported by our group [10], who demonstrated that LAH induces cell death via apoptosis in a murine cancer colon model, correlating these results with decreased migration and a reduction in tumor volume (10). Similarly, LAH exhibits greater efficacy in decreasing tumor volume compared to doxorubicin [9].

As is well known, working with natural products presents certain limitations. The principal concerns include the bioavailability and access to the primary source, which in this case was the *A. macroprophyllata* tree. Our research group addressed these issues by enlisting an expert botanist to ensure the collection of sufficient fruit for laherradurin extraction.

The chemical complexity of acetogenins provides them with a diverse range of bioactivity, making them promising candidates for the development of anticancer agents. However, the isolation and characterization of these metabolites pose additional challenges. Improving the extraction method and synthesizing these compounds will be crucial to meet the demand for chemotherapeutic agents in cancer treatment and to ensure the safety of these compounds. Furthermore, the toxicity of acetogenins represents another area that requires further investigation; additional preclinical tests must be conducted to eventually progress to clinical trials in humans.

The discovery of drugs from natural products has proven to be a successful and reliable approach for proposing new structures to combat various illnesses. In this article, we demonstrate for the first time the versatility of laherradurin in inducing cancer cell death in colon cancer cell lines, revealing autophagy induction and mitochondrial dysfunction as mechanisms of action.

LAH exerts a range of effects on CRC cells, including significant alterations in mitochondrial function, metabolic reprogramming, and the induction of apoptosis. Our study demonstrates that LAH disrupts mitochondrial function by inhibiting the key components of the electron transport chain, leading to an increased reliance on glycolysis and subsequent changes in cellular energy metabolism. This metabolic shift not only affects tumor cell viability but also enhances the autophagic processes, which may further influence LAH's antitumor efficacy.

Future research should focus on elucidating how LAH interacts with specific metabolic pathways and signaling networks within CRC cells. Investigating the molecular details of LAH-induced mitochondrial damage, its impact on cellular energetics, and the precise role of autophagy and mitophagy in LAH's therapeutic effects will be essential. Furthermore, exploring LAH's effects in diverse in vivo models and clinical trials will be crucial for assessing its potential as a novel anticancer agent. Understanding these aspects could significantly advance the development of targeted therapies for CRC, addressing the metabolic vulnerabilities and potentially improving patient outcomes. By translating these findings into clinical practice, we may uncover new strategies to combat CRC and enhance the effectiveness of the existing treatments.

5. Conclusions

Our study provides compelling evidence for the therapeutic potential of LAH in CRC treatment. Our findings reveal that LAH exerts its anticancer effects through the alteration of mitochondrial function via the inhibition of OXPHOS complexes, accompanied by increased glycolysis and mitochondrial fragmentation. The disruption of mitochondrial dynamics and bioenergetics contributes to cellular stress and the induction of apoptosis, as evidenced by DNA DSBs and the activation of apoptotic pathways. In addition, LAH downregulates mTORC1 signaling and induces autophagy. In summary, LAH is emerging as a promising therapeutic agent against CRC. Further clarification of the precise molecular mechanisms underlying its effects, along with their validation in preclinical and clinical settings, will be crucial for their translation into clinical practice. Such clarification deserves future studies.

Supplementary Materials: The following supporting information can be downloaded at https://www.mdpi.com/article/10.3390/cells13191649/s1.

Author Contributions: Conceptualization, N.J.-H., I.D.-W., and C.P.P.; methodology, I.D.-W., J.C.-H., E.P.-A., and E.A.P.-Y.; software, I.D.-W. and A.L.-S. ; validation, I.D.-W., J.C.-H., Y.A.L.-B., E.P.-A., and E.A.P.-Y.; formal analysis, I.D.-W., E.P.-A., C.P.P., and N.J.-H.; investigation, S.D. and I.D.-W.; resources, S.D., N.J.-H., and C.P.P.; writing—original draft preparation, N.J.-H., I.D.-W., M.M.-V., and C.P.P.; supervision, N.J.-H., C.P.P., and M.M.-V. ; project administration, N.J.-H. and C.P.P.; funding acquisition, N.J.-H. and C.P.P. All authors have read and agreed to the published version of the manuscript.

Funding: This research was funded by CONAHCYT, Mexico, under grant number CB-2016-285884.

Institutional Review Board Statement: Not applicable.

Data Availability Statement: All data is available on request to Nadia Jacobo-Herrera (nadia.jacobo@gmail.com, nadia.jacoboh@incmnsz.mx) and Carlos Perez-Plasencia (carlos.pplas@gmail.com).

Acknowledgments: This paper is part of the requirements for obtaining a doctoral degree at the Posgrado en Ciencias Biológicas, UNAM, of ID-W. ID-W has received a scholarship from CONAHCyT (779672). Financing was granted by CONAHCyT, Mexico, grant number CB-2016-285884.The authors thank Instituto Nacional de Cancerología-Advanced Microscopy Applications Unit (ADMiRA) RRID:SCR_022788.

Conflicts of Interest: The authors declare no conflicts of interest.

References

1. Wolpin, B.M.; Mayer, R.J. Systemic Treatment of Colorectal Cancer. *Gastroenterology* **2008**, *134*, 1296. https://doi.org/10.1053/J.GASTRO.2008.02.098.
2. Fakhri, S.; Moradi, S.Z.; Farzaei, M.H.; Bishayee, A. Modulation of Dysregulated Cancer Metabolism by Plant Secondary Metabolites: A Mechanistic Review. *Semin. Cancer Biol.* **2022**, *80*, 276–305. https://doi.org/10.1016/J.SEMCANCER.2020.02.007.
3. Shin, S.A.; Moon, S.Y.; Kim, W.-Y.; Paek, S.M.; Park, H.H.; Lee, C.S. Structure-Based Classification and Anti-Cancer Effects of Plant Metabolites. *Int. J. Mol. Sci.* **2018**, *19*, 2651, https://doi.org/10.3390/ijms19092651.
4. Teoh, E.S. Secondary Metabolites of Plants. *Medicinal Orchids of Asia* **2016**, *1*, 59–73. https://doi.org/10.1007/978-3-319-24274-3_5.
5. Maher, T.; Raus, R.A.; Daddiouaissa, D.; Ahmad, F.; Adzhar, N.S.; Latif, E.S.; Abdulhafiz, F.; Mohammed, A. Medicinal Plants with Anti-Leukemic Effects: A Review. *Molecules* **2021**, *26*, 2741 https://doi.org/10.3390/MOLECULES26092741.
6. Sharifi-Rad, J.; Quispe, C.; Patra, J.K.; Singh, Y.D.; Panda, M.K.; Das, G.; Adetunji, C.O.; Michael, O.S.; Sytar, O.; Polito, L.; et al. Paclitaxel: Application in Modern Oncology and Nanomedicine-Based Cancer Therapy. *Oxidative Med. Cell. Longev.* **2021**, *2021*, 3687700. https://doi.org/10.1155/2021/3687700.
7. Winer, E.S.; DeAngelo, D.J. A Review of Omacetaxine: A Chronic Myeloid Leukemia Treatment Resurrected. *Oncol. Ther.* **2018**, *6*, 9. https://doi.org/10.1007/S40487-018-0058-6.
8. Blessing, L.D.T.; Ramos, J.; Diaz, S.; Ben Altabef, A.; Bardón, A.; Brovetto, M.; Seoane, G.; Neske, A. Insecticidal Properties of Annonaceous Acetogenins and Their Analogues. Interaction with Lipid Membranes. *Nat. Prod. Commun.* **2012**, *7*, 1215–1218. https://doi.org/10.1177/1934578x1200700929.
9. Schlie-Guzmán, M.A.; García-Carrancá, A.; González-Esquinca, A.R. In Vitro and in Vivo Antiproliferative Activity of Laherradurin and Cherimolin-2 of Annona Diversifolia Saff. *Phytother. Res.* **2009**, *23*, 1128–1133. https://doi.org/10.1002/PTR.2760.
10. Rendón-Barrón, M.J.; Pérez-Arteaga, E.; Delgado-Waldo, I.; Coronel-Hernández, J.; Pérez-Plasencia, C.; Rodríguez-Izquierdo, F.; Linares, R.; González-Esquinca, A.R.; Álvarez-González, I.; Madrigal-Bujaidar, E.; et al. Laherradurin Inhibits Tumor Growth in an Azoxymethane/Dextran Sulfate Sodium Colorectal Cancer Model In Vivo. *Cancers (Basel)* **2024**, *16*, *573*. https://doi.org/10.3390/CANCERS16030573.
11. Nakanishi, S.; Abe, M.; Yamamoto, S.; Murai, M.; Miyoshi, H. Bis-THF Motif of Acetogenin Binds to the Third Matrix-Side Loop of ND1 Subunit in Mitochondrial NADH-Ubiquinone Oxidoreductase. *Biochim. Biophys. Acta.* **2011**, *1807*, 1170–1176. https://doi.org/10.1016/J.BBABIO.2011.05.012.
12. Liu, Y.; Sun, Y.; Guo, Y.; Shi, X.; Chen, X.; Feng, W.; Wu, L.L.; Zhang, J.; Yu, S.; Wang, Y.; et al. An Overview: The Diversified Role of Mitochondria in Cancer Metabolism. *Int. J. Biol. Sci.* **2023**, *19*, 897. https://doi.org/10.7150/IJBS.81609.
13. Chen, Q.; Ruan, D.; Shi, J.; Du, D.; Bian, C. The Multifaceted Roles of Natural Products in Mitochondrial Dysfunction. *Front. Pharmacol.* **2023**, *14*, 1093038. https://doi.org/10.3389/FPHAR.2023.1093038/BIBTEX.
14. De Pedro, N.; Cautain, B.; Melguizo, A.; Vicente, F.; Genilloud, O.; Peláez, F.; Tormo, J.R. Mitochondrial Complex I Inhibitors, Acetogenins, Induce HepG2 Cell Death through the Induction of the Complete Apoptotic Mitochondrial Pathway. *J. Bioenerg. Biomembr.* **2013**, *45*, 153–164. https://doi.org/10.1007/S10863-012-9489-1.
15. Han, B.; Wang, T.D.; Shen, S.M.; Yu, Y.; Mao, C.; Yao, Z.J.; Wang, L.S. Annonaceous Acetogenin Mimic AA005 Induces Cancer Cell Death via Apoptosis Inducing Factor through a Caspase-3-Independent Mechanism. *BMC Cancer* **2015**, *15*, 139. https://doi.org/10.1186/S12885-015-1133-0.
16. Liu, Y.Q.; Cheng, X.; Guo, L.X.; Mao, C.; Chen, Y.J.; Liu, H.X.; Xiao, Q.C.; Jiang, S.; Yao, Z.J.; Zhou, G.B. Identification of an Annonaceous Acetogenin Mimetic, AA005, as an AMPK Activator and Autophagy Inducer in Colon Cancer Cells. *PLoS ONE* **2012**, *7*, e47049. https://doi.org/10.1371/JOURNAL.PONE.0047049.
17. Yu, B.B.; Yuan, H.; Chen, Y.C.; Zhou, D.X.; Gan, Z.J.; Wang, J.; Li, J.X.; Yao, Z.J. Annonaceous Acetogenin Mimic AA005 Inhibits the Growth of TNBC MDA-MB-468 Cells by Altering Cell Energy Metabolism. *Chembiochem* **2022**, *23*, e202200250. https://doi.org/10.1002/CBIC.202200250.
18. Li, Y.; Ye, J.; Chen, Z.; Wen, J.; Li, F.; Su, P.; Lin, Y.; Hu, B.; Wu, D.; Ning, L.; et al. Annonaceous Acetogenins Mediated Up-Regulation of Notch2 Exerts Growth Inhibition in Human Gastric Cancer Cells in Vitro. *Oncotarget* **2017**, *8*, 21140–21152. https://doi.org/10.18632/ONCOTARGET.15502.
19. Han, B.; Cao, Y.X.; Li, Z.M.; Wu, Z.X.; Mao, Y.Q.; Chen, H.L.; Yao, Z.J.; Wang, L.S. Annonaceous acetogenin mimic AA005 suppresses human colon cancer cell growth in vivo through downregulation of Mcl-1. *Acta Pharmacol. Sin.* **2018**, *40*, 231–242. https://doi.org/10.1038/s41401-018-0025-7.
20. Bouyahya, A.; El Allam, A.; Aboulaghras, S.; Bakrim, S.; El Menyiy, N.; Alshahrani, M.M.; Al Awadh, A.A.; Benali, T.; Lee, L.H.; El Omari, N.; et al. Targeting MTOR as a Cancer Therapy: Recent Advances in Natural Bioactive Compounds and Immunotherapy. *Cancers (Basel)* **2022**, *14*, 5520. https://doi.org/10.3390/CANCERS14225520.
21. Vichai, V.; Kirtikara, K. Sulforhodamine B Colorimetric Assay for Cytotoxicity Screening. *Nat. Protoc.* **2006**, *1*, 1112–1116. https://doi.org/10.1038/NPROT.2006.179.
22. Alberghina, L. The Warburg Effect Explained: Integration of Enhanced Glycolysis with Heterogeneous Mitochondria to Promote Cancer Cell Proliferation. *Int. J. Mol. Sci.* **2023**, *24*, 15787. https://doi.org/10.3390/IJMS242115787.
23. Ashton, T.M.; Gillies McKenna, W.; Kunz-Schughart, L.A.; Higgins, G.S. Oxidative Phosphorylation as an Emerging Target in Cancer Therapy. *Clin. Cancer Res.* **2018**, *24*, 2482–2490. https://doi.org/10.1158/1078-0432.CCR-17-3070.

24. Ren, L.; Meng, L.; Gao, J.; Lu, M.; Guo, C.; Li, Y.; Rong, Z.; Ye, Y. PHB2 Promotes Colorectal Cancer Cell Proliferation and Tumorigenesis through NDUFS1-Mediated Oxidative Phosphorylation. *Cell Death Dis.* **2023**, *14*, 1–11. https://doi.org/10.1038/s41419-023-05575-9.
25. Kojima, N.; Abe, M.; Suga, Y.; Ohtsuki, K.; Tanaka, T.; Iwasaki, H.; Yamashita, M.; Miyoshi, H. Critical Role of a Methyl Group on the γ-Lactone Ring of Annonaceous Acetogenins in the Potent Inhibition of Mitochondrial Complex I. *Bioorg. Med. Chem. Lett.* **2013**, *23*, 1217–1219. https://doi.org/10.1016/J.BMCL.2013.01.018.
26. Greene, J.; Segaran, A.; Lord, S. Targeting OXPHOS and the Electron Transport Chain in Cancer; Molecular and Therapeutic Implications. *Semin. Cancer Biol.* **2022**, *86*, 851–859. https://doi.org/10.1016/J.SEMCANCER.2022.02.002.
27. Qian, W.; Van Houten, B. Alterations in Bioenergetics Due to Changes in Mitochondrial DNA Copy Number. *Methods* **2010**, *51*, 452–457. https://doi.org/10.1016/J.YMETH.2010.03.006.
28. Ozsvari, B.; Sotgia, F.; Simmons, K.; Trowbridge, R.; Foster, R.; Lisanti, M.P. Mitoketoscins: Novel Mitochondrial Inhibitors for Targeting Ketone Metabolism in Cancer Stem Cells (CSCs). *Oncotarget* **2017**, *8*, 78340–78350. https://doi.org/10.18632/ONCOTARGET.21259.
29. Cheng, G.; Zielonka, J.; McAllister, D.M.; Mackinnon, A.C.; Joseph, J.; Dwinell, M.B.; Kalyanaraman, B. Mitochondria-Targeted Vitamin E Analogs Inhibit Breast Cancer Cell Energy Metabolism and Promote Cell Death. *BMC Cancer* **2013**, *13*, 285. https://doi.org/10.1186/1471-2407-13-285.
30. Zhao, F.; Vakhrusheva, O.; Markowitsch, S.D.; Slade, K.S.; Tsaur, I.; Cinatl, J.; Michaelis, M.; Efferth, T.; Haferkamp, A.; Juengel, E. Artesunate Impairs Growth in Cisplatin-Resistant Bladder Cancer Cells by Cell Cycle Arrest, Apoptosis and Autophagy Induction. *Cells* **2020**, *9*, 1–19. https://doi.org/10.3390/CELLS9122643.
31. Wu, Z.; Xiao, C.; Long, J.; Huang, W.; You, F.; Li, X. Mitochondrial Dynamics and Colorectal Cancer Biology: Mechanisms and Potential Targets. *Cell Commun. Signal.* **2024**, *22*, 1–14. https://doi.org/10.1186/S12964-024-01490-4/FIGURES/4.
32. Chen, W.; Zhao, H.; Li, Y. Mitochondrial Dynamics in Health and Disease: Mechanisms and Potential Targets. *Signal Transduct. Target. Ther.* 2023 8:1 **2023**, *8*, 1–25. https://doi.org/10.1038/s41392-023-01547-9.
33. Adebayo, M.; Singh, S.; Singh, A.P.; Dasgupta, S. Mitochondrial Fusion and Fission: The Fine-Tune Balance for Cellular Homeostasis. *FASEB J.* **2021**, *35*, e21620. https://doi.org/10.1096/FJ.202100067R.
34. Kim, I.; Rodriguez-Enriquez, S.; Lemasters, J.J. Selective Degradation of Mitochondria by Mitophagy. *Arch. Biochem. Biophys.* **2007**, *462*, 245–253. https://doi.org/10.1016/J.ABB.2007.03.034.
35. Boulton, D.P.; Caino, M.C. Mitochondrial Fission and Fusion in Tumor Progression to Metastasis. *Front. Cell Dev. Biol.* **2022**, *10*, 849962. https://doi.org/10.3389/FCELL.2022.849962/BIBTEX.
36. Wang, H.; Luo, W.; Chen, H.; Cai, Z.; Xu, G. Mitochondrial Dynamics and Mitochondrial Autophagy: Molecular Structure, Orchestrating Mechanism and Related Disorders. *Mitochondrion* **2024**, *75*, 101847. https://doi.org/10.1016/J.MITO.2024.101847.
37. Filadi, R.; Pendin, Di.; Pizzo, P. Mitofusin 2: From Functions to Disease. *Cell Death Dis.* **2018**, *9*, 1–13. https://doi.org/10.1038/s41419-017-0023-6.
38. Li, G.B.; Fu, R.Q.; Shen, H.M.; Zhou, J.; Hu, X.Y.; Liu, Y.X.; Li, Y.N.; Zhang, H.W.; Liu, X.; Zhang, Y.H.; et al. Polyphyllin I Induces Mitophagic and Apoptotic Cell Death in Human Breast Cancer Cells by Increasing Mitochondrial PINK1 Levels. *Oncotarget* **2017**, *8*, 10359. https://doi.org/10.18632/ONCOTARGET.14413.
39. Morita, M.; Prudent, J.; Basu, K.; Goyon, V.; Katsumura, S.; Hulea, L.; Pearl, D.; Siddiqui, N.; Strack, S.; McGuirk, S.; et al. MTOR Controls Mitochondrial Dynamics and Cell Survival via MTFP1. *Mol. Cell* **2017**, *67*, 922-935.e5. https://doi.org/10.1016/J.MOLCEL.2017.08.013.
40. Fu, W.; Liu, Y.; Yin, H. Mitochondrial Dynamics: Biogenesis, Fission, Fusion, and Mitophagy in the Regulation of Stem Cell Behaviors. *Stem Cells Int.* **2019**, *2019*, 1-15. https://doi.org/10.1155/2019/9757201.
41. Punter, K.B.; Chu, C.; Chan, E.Y.W. Mitochondrial Dynamics and Oxidative Phosphorylation as Critical Targets in Cancer. *Endocr. Relat. Cancer* **2023**, *30*, e220229. https://doi.org/10.1530/ERC-22-0229.
42. Cao, K.; Riley, J.S.; Heilig, R.; Montes-Gómez, A.E.; Vringer, E.; Berthenet, K.; Cloix, C.; Elmasry, Y.; Spiller, D.G.; Ichim, G.; et al. Mitochondrial Dynamics Regulate Genome Stability via Control of Caspase-Dependent DNA Damage. *Dev. Cell* **2022**, *57*, 1211-1225.e6. https://doi.org/10.1016/J.DEVCEL.2022.03.019.
43. Ježek, J.; Cooper, K.F.; Strich, R. Reactive Oxygen Species and Mitochondrial Dynamics: The Yin and Yang of Mitochondrial Dysfunction and Cancer Progression. *Antioxidants* **2018**, 7, 13. https://doi.org/10.3390/ANTIOX7010013.
44. Huang, Q.; Zhan, L.; Cao, H.; Li, J.; Lyu, Y.; Guo, X.; Zhang, J.; Ji, L.; Ren, T.; An, J.; et al. Increased Mitochondrial Fission Promotes Autophagy and Hepatocellular Carcinoma Cell Survival through the ROS-Modulated Coordinated Regulation of the NFKB and TP53 Pathways. *Autophagy* **2016**, *12*, 999. https://doi.org/10.1080/15548627.2016.1166318.
45. Bernard, G.; Bellance, N.; James, D.; Parrone, P.; Fernandez, H.; Letellier, T.; Rossignol, R. Mitochondrial Bioenergetics and Structural Network Organization. *J. Cell Sci.* **2007**, *120*, 838–848. https://doi.org/10.1242/JCS.03381.
46. Wai, T.; Langer, T. Mitochondrial Dynamics and Metabolic Regulation. *Trends Endocrin. Met.* **2016**, *27*, 105–117. https://doi.org/10.1016/J.TEM.2015.12.001.
47. Das, R.; Chakrabarti, O. Mitochondrial Hyperfusion: A Friend or a Foe. *Biochem Soc. Trans.* **2020**, *48*, 631–644. https://doi.org/10.1042/BST20190987.
48. Zorova, L.D.; Popkov, V.A.; Plotnikov, E.Y.; Silachev, D.N.; Pevzner, I.B.; Jankauskas, S.S.; Babenko, V.A.; Zorov, S.D.; Balakireva, A.V.; Juhaszova, M.; et al. Mitochondrial Membrane Potential. *Anal. Biochem.* **2018**, *552*, 50–59. https://doi.org/10.1016/J.AB.2017.07.009.

49. Sukumar, M.; Liu, J.; Mehta, G.U.; Patel, S.J.; Roychoudhuri, R.; Crompton, J.G.; Klebanoff, C.A.; Ji, Y.; Li, P.; Yu, Z.; et al. Mitochondrial Membrane Potential Identifies Cells with Enhanced Stemness for Cellular Therapy. *Cell Metab.* **2016**, *23*, 63–76. https://doi.org/10.1016/J.CMET.2015.11.002.
50. Francipane, M.G.; Lagasse, E. MTOR Pathway in Colorectal Cancer: An Update. *Oncotarget* **2014**, *5*, 49. https://doi.org/10.18632/ONCOTARGET.1548.
51. Wang, X.W.; Zhang, Y.J. Targeting MTOR Network in Colorectal Cancer Therapy. *World J. Gastroenterol.* **2014**, *20*, 4178. https://doi.org/10.3748/WJG.V20.I15.4178.
52. Leiphrakpam, P.D.; Are, C. PI3K/Akt/mTOR Signaling Pathway as a Target for Colorectal Cancer Treatment. *Int. J. Mol. Sci.* **2024**, *25*, 3178. https://doi.org/10.3390/ijms25063178.
53. Panwar, V.; Singh, A.; Bhatt, M.; Tonk, R.K.; Azizov, S.; Raza, A.S.; Sengupta, S.; Kumar, D.; Garg, M. Multifaceted role of mTOR (mammalian target of rapamycin) signaling pathway in human health and disease. *Signal Transduct. Target. Ther.* **2023**, *8*, 1–25. https://doi.org/10.1038/s41392-023-01608-z.
54. Lee, C.C.; Lin, Y.H.; Chang, W.H.; Lin, P.C.; Wu, Y.C.; Chang, J.G. Squamocin Modulates Histone H3 Phosphorylation Levels and Induces G1 Phase Arrest and Apoptosis in Cancer Cells. *BMC Cancer* **2011**, *11*, 58. https://doi.org/10.1186/1471-2407-11-58.
55. Gomes, I.N.F.; Silva-Oliveira, R.J.; Silva, V.A.O.; Rosa, M.N.; Vital, P.S.; Barbosa, M.C.S.; dos Santos, F.V.; Junqueira, J.G.M.; Severino, V.G.P.; Oliveira, B.G.; et al. Annona coriacea Mart. Fractions Promote Cell Cycle Arrest and Inhibit Autophagic Flux in Human Cervical Cancer Cell Lines. *Molecules* **2019**, *24*, 3963. https://doi.org/10.3390/molecules24213963.
56. Xue, J.Y.; Zhou, G.X.; Chen, T.; Gao, S.; Choi, M.Y.; Wong, Y.S. Desacetyluvaricin Induces S Phase Arrest in SW480 Colorectal Cancer Cells through Superoxide Overproduction. *J. Cell Biochem.* **2014**, *115*, 464–475. https://doi.org/10.1002/JCB.24680.
57. Yuan, F.; Bai, G.; Miao, Y.; Chen, Y.; Li, X.; Chen, J. Annosquacin B Induces Mitochondrial Apoptosis in Multidrug Resistant Human Breast Cancer Cell Line MCF-7/ADR through Selectively Modulating MAPKs Pathways. *Pharm. Biol.* **2016**, *54*, 3040–3045. https://doi.org/10.1080/13880209.2016.1200634.
58. Collins, P.L.; Purman, C.; Porter, S.I.; Nganga, V.; Saini, A.; Hayer, K.E.; Gurewitz, G.L.; Sleckman, B.P.; Bednarski, J.J.; Bassing, C.H.; et al. DNA Double-Strand Breaks Induce H2Ax Phosphorylation Domains in a Contact-Dependent Manner. *Nat. Commun.* **2020**, *11*, 1-9. https://doi.org/10.1038/S41467-020-16926-X.
59. Firsanov, D.V.; Solovjeva, L.V.; Svetlova, M.P. H2AX Phosphorylation at the Sites of DNA Double-Strand Breaks in Cultivated Mammalian Cells and Tissues. *Clin. Epigenetics* **2011**, *2*, 283. https://doi.org/10.1007/S13148-011-0044-4.
60. Desquiret-Dumas, V.; Gueguen, N.; Leman, G.; Baron, S.; Nivet-Antoine, V.; Chupin, S.; Chevrollier, A.; Vessières, E.; Ayer, A.; Ferré, M.; et al. Resveratrol Induces a Mitochondrial Complex I-Dependent Increase in NADH Oxidation Responsible for Sirtuin Activation in Liver Cells. *J. Biol. Chem.* 2013, *288*, 36662–36675. https://doi.org/10.1074/JBC.M113.466490.
61. Chen, Y.A.; Lien, H.M.; Kao, M.C.; Lo, U.G.; Lin, L.C.; Lin, C.J.; Chang, S.J.; Chen, C.C.; Hsieh, J.T.; Lin, H.; et al. Sensitization of Radioresistant Prostate Cancer Cells by Resveratrol Isolated from Arachis Hypogaea Stems. *PLoS ONE* 2017, 12, e0169204. https://doi.org/10.1371/JOURNAL.PONE.0169204.

Disclaimer/Publisher's Note: The statements, opinions and data contained in all publications are solely those of the individual author(s) and contributor(s) and not of MDPI and/or the editor(s). MDPI and/or the editor(s) disclaim responsibility for any injury to people or property resulting from any ideas, methods, instructions or products referred to in the content.

16. Anexo II (Artículos adicionales realizados durante los estudios de doctorado)

Nota: Los artículos presentados en esta tesis se incluyen en su versión completa, ya que las revistas en las que fueron publicados no tienen restricciones de publicación que impidan su reproducción en este documento.

cancers

MDPI

Article

Laherradurin Inhibits Tumor Growth in an Azoxymethane/Dextran Sulfate Sodium Colorectal Cancer Model In Vivo

Michael Joshue Rendón-Barrón [1,2], Eduardo Pérez-Arteaga [1], Izamary Delgado-Waldo [1], Jossimar Coronel-Hernández [3], Carlos Pérez-Plasencia [3,4], Frida Rodríguez-Izquierdo [3], Rosa Linares [5], Alma Rosa González-Esquinca [6], Isela Álvarez-González [2], Eduardo Madrigal-Bujaidar [2] and Nadia Judith Jacobo-Herrera [1,*]

1 Unidad de Bioquímica, Instituto Nacional de Ciencias Médicas y Nutrición Salvador Zubiran, Av. Vasco de Quiroga 15, Col. Belisario Domínguez Sección XVI, Tlalpan, Ciudad de México 14080, Mexico; mrendonb2101tmp@alumnoguinda.mx (M.J.R.-B.); eduardo.arteaga@comunidad.unam.mx (E.P.-A.); mybtondgomita@comunidad.unam.mx (I.D.-W.)
2 Unidad Profesional Adolfo López Mateos, Laboratorio de Genética, Instituto Politécnico Nacional, Escuela Nacional de Ciencias Biológicas, Zacatenco, Av. Wilfrido Massieu Esq Cda. Miguel Stampa S/N, Alcaldía Gustavo A. Madero, Ciudad de México 07738, Mexico; ralvarezg@ipn.mx (I.Á.-G.); emadrigalb@ipn.mx (E.M.-B.)
3 Unidad de Investigación Biomédica en Cancer, Instituto Nacional Nacional de Cancerología, Av. San Fernando 22, Belisario Domínguez Secc 16, Tlalpan, Ciudad de México 14080, Mexico; jossithunders@gmail.com (J.C.-H.); carlos.pplas@campus.iztacala.unam.mx (C.P.-P.); fridaizquierdo19@gmail.com (F.R.-I.)
4 Unidad de Investigación en Biomedicina, Laboratorio de Genómica, Facultad de Estudios Superiores Iztacala, Av. De los Barrios 1, Los Reyes Ixtacala, Tlalnepantla 54090, Mexico
5 Unidad de Investigación en Biología de la Reproducción, Laboratorio de Endocrinología, Facultad de Estudios Superiores Zaragoza, Batalla 5 de Mayo S/N, Ejército de Oriente Zona Peñon, Iztapalapa, Ciudad de México 09230, Mexico; rosa.linares@zaragoza.unam.mx
6 Laboratorio de Fisiología y Química Vegetal, Instituto de Ciencias Biológicas, Universidad de Ciencias y Artes de Chiapas, Libramiento Norte Poniente 1150, Lajas Maciel, Tuxtla Gutiérrez 29039, Mexico; aesquinca@unicach.mx
* Correspondence: nadia.jacoboh@incmnsz.mx

check for updates

Citation: Rendón-Barrón, M.J.; Pérez-Arteaga, E.; Delgado-Waldo, I.; Coronel-Hernández, J.; Pérez-Plasencia, C.; Rodríguez-Izquierdo, F.; Linares, R.; González-Esquinca, A.R.; Álvarez-González, I.; Madrigal-Bujaidar, E.; et al. Laherradurin Inhibits Tumor Growth in an Azoxymethane/Dextran Sulfate Sodium Colorectal Cancer Model In Vivo. *Cancers* **2024**, *16*, 573. https://doi.org/10.3390/cancers16030573

Academic Editor: Jesus Garcia-Foncillas

Received: 1 December 2023
Revised: 24 January 2024
Accepted: 26 January 2024
Published: 29 January 2024

Copyright: © 2024 by the authors. Licensee MDPI, Basel, Switzerland. This article is an open access article distributed under the terms and conditions of the Creative Commons Attribution (CC BY) license (https://creativecommons.org/licenses/by/4.0/).

Simple Summary: The complexity of the tumor cell, its ability to evade death, and its capacity to proliferate and conquer new tissues and organs make its treatment a challenge. Major challenges posed by therapeutic agents include their toxicity and consequences for patients after chemotherapy. Natural products provide a fundamental basis for the development of chemoagents. Our research aimed to test in vivo the antitumor activity of laherradurin in CRC and to measure its toxic effect. Our findings show that laherradurin inhibits growth and decreases the size of tumors in the colon compared with cisplatin. In addition, blood tests show no hepatic or renal damage or damage at the immunological level. Likewise, the disease activity index shows that those animals treated with laherradurin had diminished signs of disease. In our work, we provide new and conclusive evidence on the antitumor effect of laherradurin and measure its toxic activity under different criteria.

Abstract: Colorectal cancer (CRC) is the third most common neoplasia in the world. Its mortality rate is high due to the lack of specific and effective treatments, metastasis, and resistance to chemotherapy, among other factors. The natural products in cancer are a primary source of bioactive molecules. In this research, we evaluated the antitumor activity of an acetogenin (ACG), laherradurin (LH), isolated from the Mexican medicinal plant *Annona macroprophyllata* Donn.Sm. in a CRC murine model. The CRC was induced by azoxymethane–dextran sulfate sodium (AOM/DSS) in Balb/c mice and treated for 21 days with LH or cisplatin. This study shows for the first time the antitumor activity of LH in an AOM/DSS CRC model. The acetogenin diminished the number and size of tumors compared with cisplatin; the histologic studies revealed a recovery of the colon tissue, and the blood toxicity data pointed to less damage in animals treated with LH. The TUNEL assay indicated cell death by

apoptosis, and the in vitro studies exhibited that LH inhibited cell migration in HCT116 cells. Our study provides strong evidence of a possible anticancer agent for CRC.

Keywords: acetogenins; antitumoral activity; apoptosis; cell migration; colon cancer; in vivo model; laherradurin

1. Introduction

Colorectal cancer is a health problem worldwide, being the third most diagnosed type of cancer, with more than 1.9 million new cases and 900 thousand reported deaths per year since 2020, being the second leading cause of cancer-related death [1,2]. Current treatments consist of surgery and preoperative radiotherapy for patients in early and intermediate stages, while in stage III and metastatic patients, chemotherapy is mainly used [3,4]. The chemotherapy used in CRC includes 5-fluorouracil, capecitabine, irinotecan, oxaliplatin, trifluridine, and tipiracil [5]; however, they have severe side effects in patients, such as neurological damage, cytopenia, and mucositis [6–9]. Moreover, the high mortality rate is related to drug resistance and late diagnosis [10].

The search for molecules from natural products is not new and throughout history has been a successful approach to developing drugs for various diseases, including cancer [11]. Some specialized pharmacologically active plant metabolites are lignans, glycosides, diterpenes, steroids, fatty acids, flavonoids, and acetogenins (ACGs) [12,13]. The latter is selectively toxic to several types of cancer cells and multidrug-resistant cell lines [14,15], which interest our group. ACGs are compounds found in species of the Annonaceae family, particularly in the *Annona* genus; the fruits of these plants are employed in traditional medicine for various ailments, such as fever, rheumatism, diarrhea, arthritis, diabetes, headaches and insomnia, and cancer treatment [16,17]. The leading studies focus on ACGs from *A. muricata*, reporting their anti-inflammatory, pesticidal, antimicrobial, and mainly antitumor activities [18]. Therefore, it is necessary to study ACGs in other species of the *Annona* genus, such as *A. macroprophyllata* Donn. Sm., which is traditionally employed in Mexico for the treatment of skin cancer and gastric tumors [19,20], in addition to reporting the presence of LH (Figure 1). LH is a cytotoxic acetogenin proven effective against cervical and colon tumor lines [21]; even so, studies in vivo of its antineoplastic potential are limited. Therefore, in this work, we evaluated the anticancer effect of LH in vivo in a colon cancer model by chemical induction with AOM and DSS.

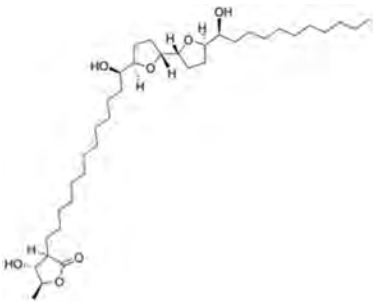


Figure 1. Chemical structure of laherradurin.

2. Results

2.1. Acute Toxicity (LD_{50})

To formulate safe doses to be used in animals, we performed an acute toxicity test based on the OECD criteria (Section 4). Animals administered 55 and 175 mg/Kg LH presented high toxicity since none of the experimental groups survived. As for the dose of 17.5 mg/Kg, only one death was recorded, while the mice treated with 5.5 mg/Kg survived the LH. Based on the above and the formula described, the LD_{50} was 11.5 mg/Kg. This dose was employed to determine the doses used in the AOM/DSS model (Section 2.2.).

2.2. AOM/DSS Model

2.2.1. Weight and Disease Activity Index (DAI)

Toxicity in new anticancer drugs is vital and key to the possibility of using them in clinical settings. Our research evaluated the toxicity of LH from two different and complementary perspectives: the macroscopic level, measuring weight and signs of illness (DAI) during the 16 weeks of the in vivo trial, and blood tests (Section 2.2.2.). Figure 2A depicts the average weight of each experimental group. In general, mice gained between 1.5 and 2.5 g compared with the negative control group (NC). However, from week 12 (start of LH treatment) until the end of the trial, weight recovery was observed in the groups treated with LH. Depending on the doses, the percentage of weight recovery was low (17.6%), medium (36.37%), high (46.10%), and high twice weekly (51.74%). In the cisplatin group, the weight recovery was 38.11%. Figure 2B shows the DAI results. The groups treated with AOM/DSS at week 11 presented values of 1.5 and 1.8 compared with the NC group. By week 16, the positive control group (PC) presented the highest value, with more severe disease symptoms (bloody diarrhea and anal prolapse). Groups treated with LH displayed fewer disease symptoms, given in percentages (DAI values). As the dose and frequency of administration were increased, the animals treated with LH saw improved effects of the drugs on cancer symptoms, as follows: low dose (30.8%), medium dose (56.4%), high dose (92.4%), and the twice-a-week high dose (90.6%). As for cisplatin-treated mice, the DAI values decreased by 53.1%. These data suggest lower toxicity compared with cisplatin.

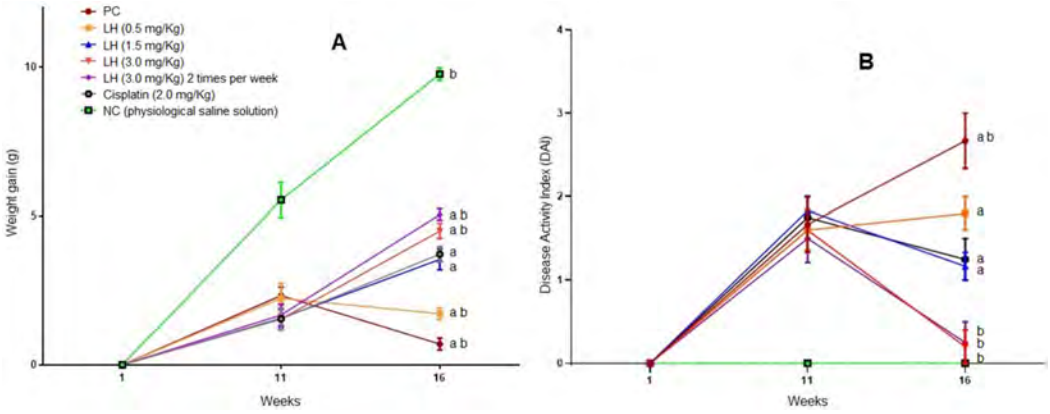


Figure 2. AOM/DSS toxicity data. (**A**) Variations in weight. (**B**) Disease Activity Index data. Data shown are the mean ± SE of six mice per group. a, significant differences against the negative control; b, significant differences against cisplatin. Anova and post hoc Newman–Keuls ($p < 0.05$).

2.2.2. Blood Analysis

Continuing with the toxicity analyses, we conducted blood tests when treatments finished as an end-point experiment. Table 1 shows the results of the biochemical blood analysis of the AOM/DSS model. The CP group presented a decrease in the levels of erythrocytes, hemoglobin, leukocytes, and ALT, as well as in the percentages of hematocrit, lymphocytes, and neutrophils. Moreover, the urea and glucose values increased compared with the negative control, presenting significant differences ($p < 0.05$). Regarding the groups treated with LH, remarkably, in those groups treated with the high dose (3 mg/Kg) either one or two times per week, the values of erythrocytes, hemoglobin, hematocrit, ALT, urea, and glucose were similar to those in the CN group. In the group treated with cisplatin, significant differences ($p < 0.05$) were observed in the levels of erythrocytes, hemoglobin, and ALT and the percentage of hematocrit. Our data support the benefits of LH over cisplatin in terms of the effects of toxicity on our AOM/DSS model.

Table 1. Toxicity analyses in blood in Balb/c mice treated with LH.

Biochemical Analysis	NC	PC	Cisplatin (2.0 mg/Kg)	LH			
				0.5 mg/Kg	1.5 mg/Kg	3.0 mg/Kg	3.0 mg/Kg (Double)
Erythrocytes ($\times 10^{12}$/L)	9.59 ± 0.34	5.42 ± 0.066 *	5.99 ± 1.65 *	5.29 ± 1.87 *	8.64 ± 1.22	8.86 ± 0.78	8.99 ± 0.18
Leukocytes ($\times 10^{9}$/L)	7.75 ± 0.77	3.93 ± 0.15 *	3.45 ± 0.77 *	4.2 ± 2.82 *	4 ± 0.7 *	4.26 ± 0.141 *	3.83 ± 0.30 *
Hematocrit (%)	51.1 ± 1.2	27.2 ± 1.6 *	31.2 ± 8.45 *	34 ± 10.3 *	38.66 ±6.57	43.92 ± 3.36	45.6 ± 1.21
Lymphocytes (%)	61.33 ± 6.11	85.33 ± 5.5 *	74.66 ± 3.05 *	86.5 ± 2.12 *	86 ± 8.12 *	82.175 ± 0.82 *	85.66 ± 1.52 *
Neutrophils (%)	34.66 ± 3.5	10.66 ± 7.23 *	23.33 ± 1.15 *	19.33 ± 10.21 *	16 ± 8.5 *	15 ± 1.15 *	13.33 ± 0.57 *
Hemoglobin (g/L)	157 ± 5.2	87.6 ± 4.1 *	98.6 ± 21.7 *	93.6 ± 23 *	120.3 ± 18.4	136 ± 10.7	144 ± 9.5
Glucose (g/L)	1.19 ± 0.09	2.07 ± 0.14 *	0.94 ± 0.09	1.65 ± 0.07 *	1.19 ± 0.09	1.01 ± 0.04	1.08 ± 0.1
Urea (g/L)	0.44 ± 0.02	0.58 ± 0.15 *	0.4 ± 0.06	0.4 ± 0.04	0.41 ± 0.03	0.36 ± 0.02	0.35 ± 0.01
Creatinine (mg/dL)	0.0056 ± 0.00049	0.0064 ± 0.00041	0.0055 ± 0.0007	0.006 ± 0.001	0.005 ± 0.00011	0.0057 ± 0.0012	0.0055 ± 0.0007
Alanine transferase U/I	132.7 ± 0.56	50.86 ± 11 *	89.5 ± 3.5 *	63 ± 2.8 *	110.45 ± 1.76 *	132 ± 3.6	126.33 ± 5.03

NC: negative control (physiological saline solution); PC: positive control (AOM/DSS); LH: laherradurin; Double: two times per week. Data shown are the mean ± SD of three mice per group. * shows statistically significant difference against the negative control. Anova and post hoc Newman–Keuls ($p < 0.05$). Kruskal–Wallis and post hoc Student Newman–Keuls ($p < 0.05$) for results in percentage (hematocrit, lymphocytes, and neutrophils).

2.2.3. Macroscopic Analysis of the Colon of Balb/c Mice

To complete the macroscopic examination of the colon, we considered the number and size of tumors, as well as the length of the colon. Figure 3 shows pictures of the colons of each of the experimental groups. Figure 3A depicts a healthy colon, whereas Figure 3B illustrates the AOM/DSS group (presence of tumors). The groups treated with LH (Figure 3C–F) exhibited fewer and smaller tumors. The cisplatin group (Figure 3G) displayed similarities to the group treated with the medium dose of LH (Figure 3D).

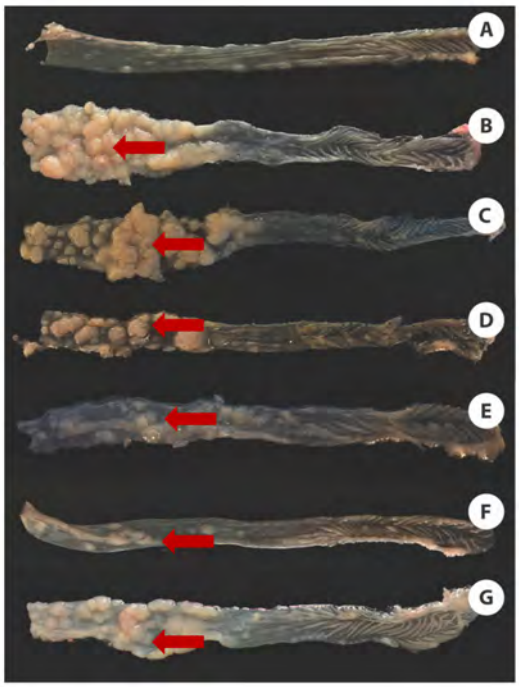


Figure 3. Photos of the colon after AOM/DSS scheme and treatments. (**A**): CN (healthy colon); (**B**): CP (AOM/DSS); (**C**): treatment with LH 0.5 mg/Kg; (**D**): treatment with LH 1.5 mg/Kg; (**E**): treatment with LH 3.0 mg/Kg; (**F**): treatment with LH 3.0 mg/Kg twice a week; (**G**): treatment with cisplatin 2.0 mg/Kg. All groups were administered LH or cisplatin once a week, except those indicated in the Methodology section. Red arrows point to tumors. The pictures are representative of the experimental groups.

Figure 4A displays the results for the number of tumors, where the PC presented an average of 33 tumors. The groups treated with LH showed decreases in the tumor index of 13.6%, 45%, 66.6%, and 69.7% for the low, medium, and high doses once and twice a week, respectively. The group administered cisplatin showed a decrease of 40.16% compared with the PC. Figure 4B presents the results for tumor size, where the same behavior can be observed, since the highest percentages of reduction were observed in the groups administered the high dose of LH (3 mg/Kg) once and twice a week, showing decreases of 72.5% and 78.34%, respectively. Regarding colon size (Figure 4C), the PC group presented a 35% decrease in length with respect to the NC, while the groups treated with the medium and high doses of LH one and two times per week avoided shortening, as there were decreases of 28%, 14.5%, and 14%, respectively. The group treated with cisplatin showed a decrease of 27%, showing similarity to the group administered the 1.5 mg/Kg dose of LH. The size of the colon and the significant reduction in tumors suggest the antitumor effect of LH in vivo.

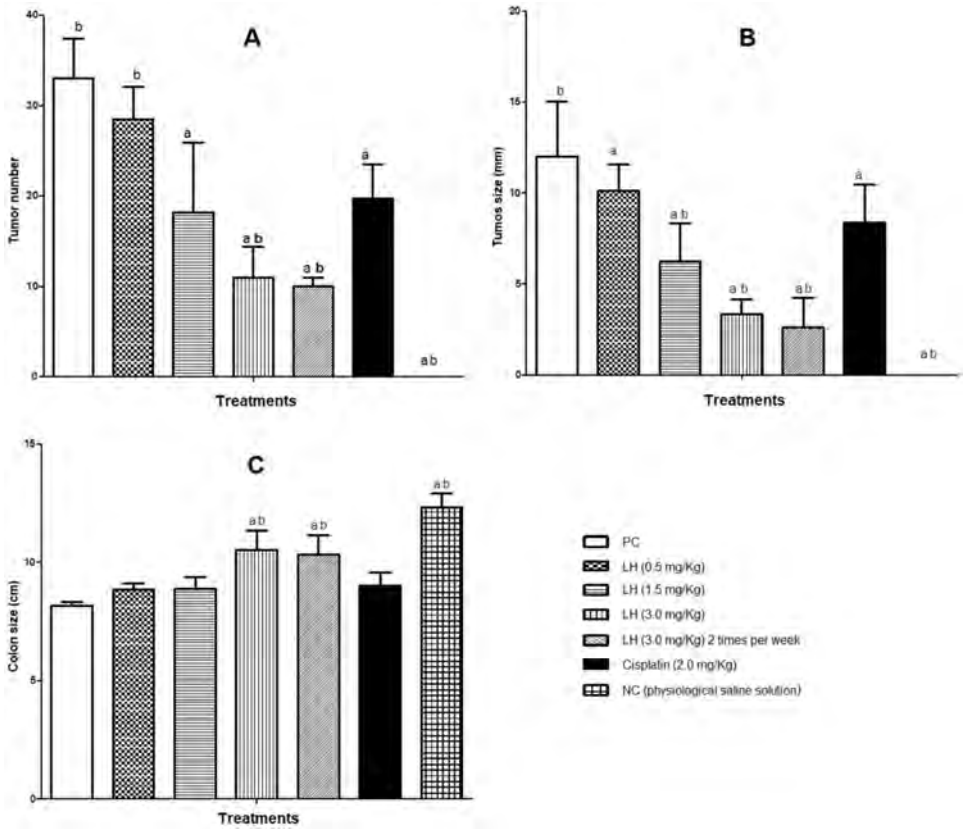


Figure 4. Quantitative analyses of the colon after treatment with LH and cisplatin. (**A**) tumor number, (**B**) tumor size, and (**C**) colon size. Data shown are the mean ± SD of six mice per group. a, significant differences against the positive control; b, significant differences against cisplatin. Anova and post hoc Newman–Keuls ($p < 0.05$).

2.2.4. Histology Image Analysis

Figure 5A shows a longitudinal section of the colon of a healthy animal. It is characterized by a muscular layer with circular and longitudinal fibers, a mucosal layer composed of glands, which form the crypts and connective tissue between them, and the lamina propria, which gives way to the submucosal layer. At 400× magnification, the surface epithelium and the crypt epithelium can be appreciated. On the contrary, in the AOM/DSS colon tissue that was not treated (Figure 5B), tumor cells are in the form of tubular adenomas with a high degree of dysplasia, loss of a healthy crypt organization, and the absence of a simple columnar epithelium observed. In animals treated with LH at 0.5 mg/Kg (Figure 5C), the image shows the presence of tumor cells and the loss of the mucosa layer, the surface epithelial tissue, and the crypts. Figure 5D depicts a longitudinal section of the colon treated with LH at 1.5 mg/Kg. In this image, the mucosal layer can be seen to be recovered, together with the presence of glands forming the crypts, although still without epithelial tissue inside them (magnification at 400×). Recovery of the lamina propria, a muscular layer with circular muscle fibers, and surface epithelial tissue can also be seen. In the experimental groups treated with LH at 3 mg/Kg once or twice a week (Figure 5E,F), a rearranging of the epithelial tissue (head of the arrow) of the crypts and the mucosa was observed. The mucosa is composed of glands with connective tissue between them and the lamina propria. At the end of this layer is the submucosa, formed of connective tissue, and the muscular layer with circular and longitudinal muscle fibers. Finally, cisplatin treatment restored the epithelial tissue, crypts, mucosa, and submucosa (Figure 5G).

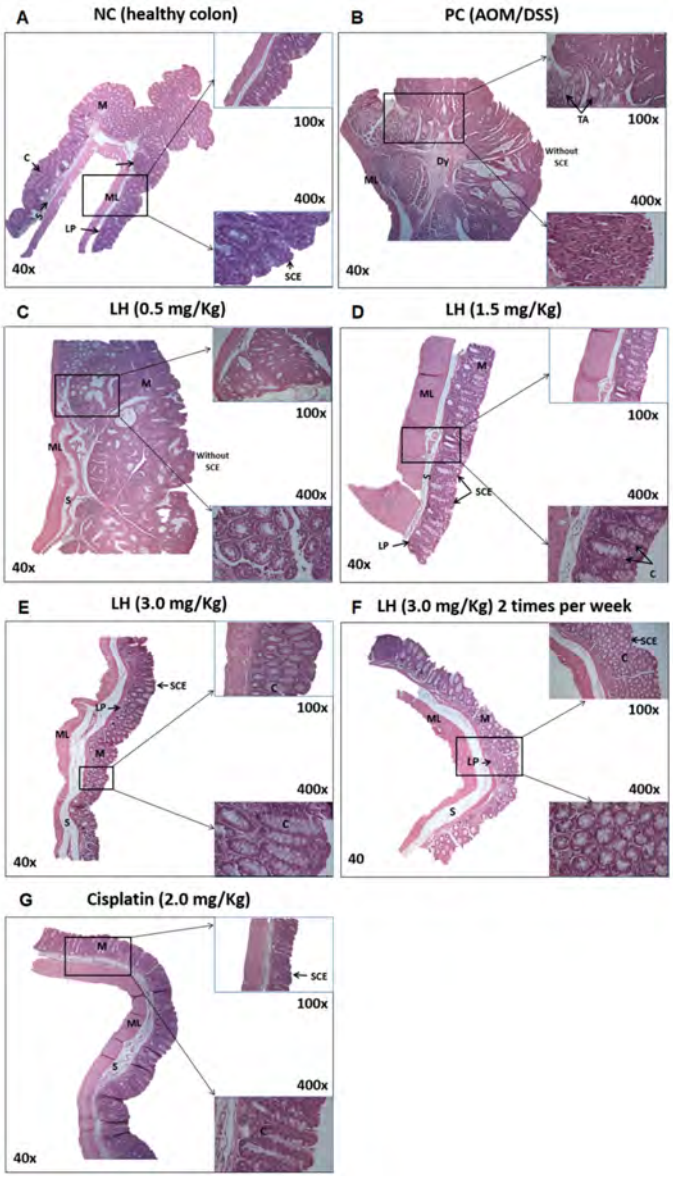


Figure 5. Histology image of the colon (H&E). NC: physiological saline solution, PC: positive control. ML: muscular layer, Dy: dysplasia, TAs: tubular adenomas, LP: lamina propria, SCE: simple columnar epithelium, M: mucosa, S: submucosa, C: crypts. Magnifications 40×, 100×, and 400× were used to amplify the selected section of the tissue cut for examination. Images were taken with a Nikon Eclipse E400 microscope.

2.2.5. Apoptosis Induction by LH

Apoptosis evasion is one of the hallmarks of cancer. Thus, searching for cell death induction is a goal of cancer treatment. For this research, we evaluated the presence of apoptotic bodies in the tumors extracted from the colon after being treated with LH or cisplatin. The LH-induced DNA fragmentation was visualized by confocal microscopy using a TUNEL assay. Figure 6 depicts the colon tissue. In the PC group (saline solution), in the third column, no apoptotic bodies were found. On the other hand, the LH-treated groups (columns 5–8) showed DNA fragmentation in different regions of the tissue. The apoptotic bodies' presence depends on the doses; the greater the dose, the greater the apoptosis induction. Our results show the ability of LH to induce cell death by apoptosis in the AOM/DSS CRC model.

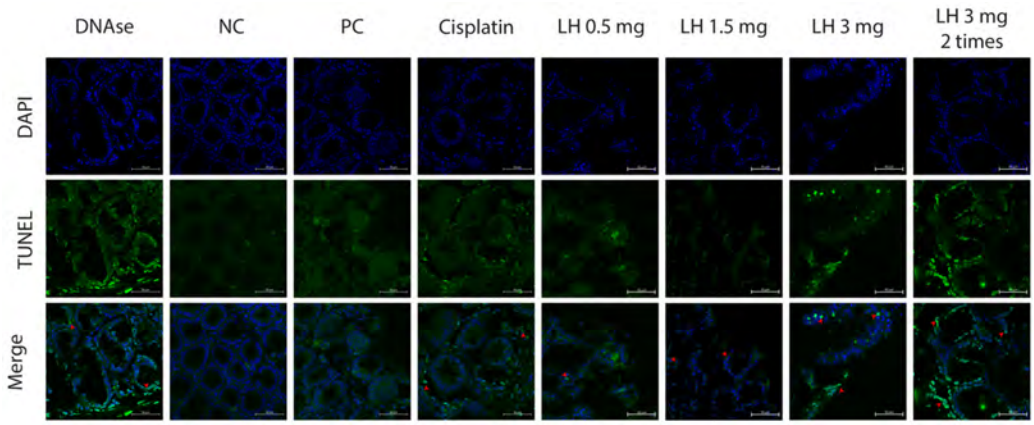


Figure 6. Apoptosis induction by LH (TUNEL assay). Green spots indicate DNA fragmentation and blue spots indicate DAPI staining nuclei. The images were acquired with a confocal microscope with the 40× objective (Zeiss LSM 710 DUO Inverted confocal laser scanning microscope, Oberkochen, Baden-Wurttemberg, Germany). Scale: 50 µm. DNAse corresponds to the positive control of the TUNEL assay. Photos shown are representative of at least three independent experiments. LH concentrations are in mg/Kg.

2.2.6. Inhibition of Migration (Wound Healing Assay)

As known, metastasis is one of the major complications for cancer patients. Thus, we evaluated another probable effect of LH on one of the hallmarks of cancer cells, migration to other tissues or organs. To this end, we carried out a wound healing assay in vitro on the CRC cell line HCT116. Figure 7A shows the panel of photos of the cells, while Figure 7B shows the graph of the migration percentages of each experimental group. After 24 h post-stimulus, the LH-treated group inhibited cell migration by preventing wound closure (14.60%) compared with the untreated group (SFB 10%), where wound closure by cell migration was 41.13%. Such results indicate another possible target for LH due to its capacity to stop cells from migrating to other tissues. However, more experiments should be performed to confirm and strengthen such findings.

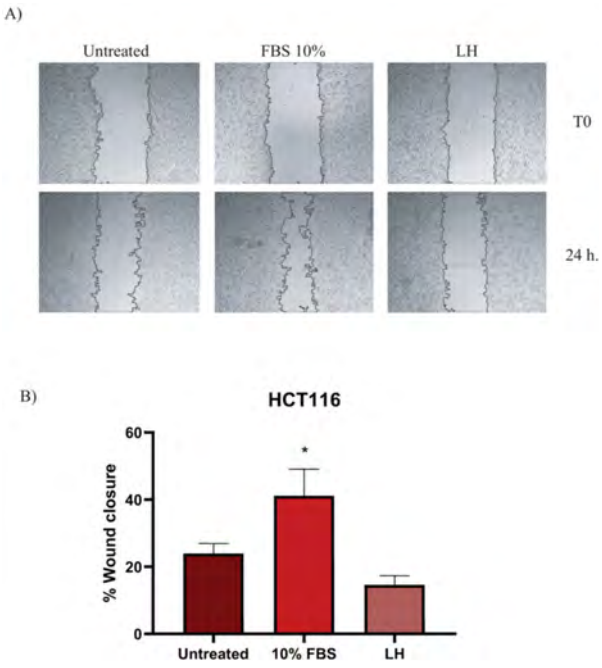


Figure 7. Migration assay in HCT116 cells treated with LH. (**A**) Wound healing assay of cells treated with LH or FBS or not treated at 24 h. (**B**) Percentage of migration at 24 h. * Significant differences against non-treated group. Kruskal–Wallis and post hoc Student Newman–Keuls ($p < 0.05$).

3. Discussion

Throughout history, people have used nature to alleviate different ailments, with plants and their secondary metabolites playing a central role [22] due to their biological activity and ability to improve human health [23]. Currently, 24% of drugs prescribed are derived from plant species [24], mostly from medicinal plants. Such is the relevance of traditional medicine that the World Health Organization, in the year 2022 in India, established the WHO World Center for Traditional Medicines with the objective of linking modern science with the traditional health system and fostering its evolution in favor of health, preserving natural resources, and respect for local heritage, among other factors (WHO, 2023) [25]. In addition, the First WHO World Summit on Traditional Medicinal Products was held in August of this year. In this scenario, the current importance of the use of medicinal plants in different societies is supported, either as a first line of treatment or as a complement to therapies, which is why evaluating the properties of specialized metabolites, extracts, and herbal combinations is of relevance to validate their use, evaluate their toxicity, determine their mechanisms of action, propose the repositioning of their use in other diseases, and formulate new drugs. Several studied specialized plant metabolites have antineoplastic activity. Among them, acetogenins are of particular importance, as they are selectively toxic to several types of cancer cells and to cell lines resistant to multiple drugs [15,26–32].

Regarding the antitumor activity of ACGs in vivo, to our knowledge, it has only been reported in xenograft models as an inhibitor of tumor growth [15,21,33–35]. In this work, the antineoplastic activity of LH isolated from the seeds of *A. macroprophyllata* was evaluated for the first time in an AOM/DSS-induced colon carcinogenesis model. Toxicity in cancer patients is a priority concern, as oncological drugs produce severe side effects that weaken the patient and can trigger other complications that delay recovery [36–38]. In this study, we determined the LD_{50} of LH to define its toxicity, obtaining a concentration of 11.5 mg/Kg, which is classified as moderate toxicity according to the OECD [39]. Based on this concentration, the experimental doses for the carcinogenesis assay were established. Toxicity studies in complete organisms are necessary to assess the parameters of damage at the systemic level of new possible anticancer agents. Little is known about the toxicity of ACGs, although the extract of A. *macroprophyllata* is cytotoxic at very low doses [40], and in species such as *A. muricata* and *A. squamosa*, they exhibit neurotoxicity [16,41,42]. Another indicator of toxicity is weight monitoring in experimental animals. Malnutrition is a common problem in CRC patients due to intestinal obstruction and cachexia [43] and has been associated with overexpression of cytokines such as interleukin-6 and tumor necrosis factor-alpha (TNF-α), as well as hormones that induce lack of appetite, and it has direct catabolic effects on skeletal muscle [44–46]. In a recent study, weight loss of more than 20% was observed in a colon cancer model induced with AOM/DSS [47], which is consistent with our results since the PC group presented a 31% decrease compared with the negative control. In addition to weight loss in animals, this model has been associated with other symptoms, such as severe colitis, diarrhea with bleeding, and the development of tumors in the colon [48]. Therefore, the DAI score allowed us to evaluate the progression and severity of the disease during a 16-week trial, where our results show that the AOM/DSS-treated groups presented symptoms of diarrhea and bleeding compared with the NC group. DSS in mouse models causes chronic inflammation and ulceration of the colon due to macrophage dysfunction, changes in intestinal microflora, and a toxic effect on the intestinal epithelium [49–52].

Concerning blood tests, we observed that the groups treated with AOM/DSS presented statistically significant changes in the levels of hemoglobin, erythrocytes, leukocytes, lymphocytes, hematocrit, ALT, urea, and glucose compared with the group of healthy mice. However, the groups administered LH showed less toxicity than the groups treated with cisplatin. Our results for weight loss and the decrease in hemoglobin levels could be related to the development of anemia in the animals. Bone marrow involvement, tumor-associated blood loss, and iron deficiency due to overexpression of cytokines such as IL-6 have been

shown to cause the occurrence of chronic anemia in cancer patients [53–55]. On the other hand, blood data could act as biomarkers in evaluating and predicting gastric cancer [54]. The antineoplastic effect of LH was macroscopically assessed by considering the number of tumors, their size, and the colon length of each of our experimental groups. The results in Figure 5A indicate that the groups administered 3 mg/Kg LH once or twice weekly demonstrated significant decreases in the tumor index of 66.6% and 69.7%, respectively, compared with the drug cisplatin with a 40.16% decrease. Similar results were observed for the reduction in tumor size, with the dose of 3.0 mg/Kg being more effective than cisplatin. Other works report that mice administered AOM/DSS show colon shortening, changes in morphology, and tissue stiffness [47,56,57], agreeing with our results since the groups with induced CRC showed a decrease in colon length compared with the group of healthy mice. The histopathology results obtained by hematoxylin–eosin staining suggest that those mice administered LH displayed restoration of the damaged mucosa layer, recovery of the lamina propria, and the absence of adenoma and intramucosal carcinoma. In addition, hyperchromatic epithelial regeneration was observed in the crypts. Such results are similar to the effect caused by cisplatin. It is still not known how ACGs inhibit morphological changes in the tumor cell; however, the upregulation of pro-inflammatory cytokines can control tumor formation in the colon [57,58].

According to the abovementioned results, we observed that the dose of 3 mg/kg presented a greater antineoplastic effect in comparison with cisplatin, with significant differences ($p < 0.05$). In addition, our results indicate a decrease in toxicity at the macroscopic level in the animals and in the blood tests, which were evaluated with liver and renal damage enzymes. The evaluation of LH toxicity is needed because drugs used as antineoplastic agents have adverse effects. Such is the case of cisplatin, which causes mainly nephrotoxic damage, with over 30% of patients presenting acute and chronic renal lesions [59]. Moreover, cisplatin could induce neurotoxicity, hepatotoxicity, ototoxicity, and testicular damage [60–63].

The neurotoxicity of acetogenins is reported in several works [64–67]. Some works demonstrated neural cell death and a change in the intracellular distribution of tau in primary cultures produced by annonacin. When the protein tau accumulates in cell bodies, it induces neurodegenerative problems called tauopathies [66]. These studies point out the neurotoxicity of the acetogenin annonacin and the neuronal damage caused in a tropical community where the consumption of this plant is a common practice [64,65]. However, it is necessary to investigate the form of preparation, the frequency of ingestion, and whether the damage caused is the same as that observed in other pathologies, such as cancer. Therefore, the antecedents of toxicity in acetogenins deter us from the possibility of inducing brain damage, and further studies are necessary.

Acetogenin cytotoxicity is explained by the inhibition of the mitochondrial NADH-ubiquinone reductase complex (complex I) of the electron transport chain involved in ATP synthesis. This complex could be a potential target in cancer treatment, given that cancer cells have a higher demand for ATP than normal cells [18,68,69]. Furthermore, several authors have found that ACGs induce cell death by apoptosis [70–72]. For instance, annonacin and squamocin induce apoptosis in several types of cancer throughout the upregulated expression of caspase 3, 8, and 9, and in turn, the downregulation of Bcl-2 [33,73–75], which is in agreement with De Pedro et al. (2013) [76], who observed an increase in caspase 9 activations in LH-treated cell lines. In this work, a TUNEL assay was carried out to determine whether LH induced apoptosis. The LH-treated groups showed gradual DNA fragmentation, with the high double dose inducing the most apoptosis. This result confirms the capacity of LH to induce cell death in vivo by apoptosis as a mechanism of action.

On the other hand, we report for the first time in this work the capacity of LH as an inhibitor of HCT116 tumor cell migration in vitro. This result suggests that it is possible to use this acetogenin to prevent tumor cells from colonizing tissues and organs to generate metastasis. In CRC, the most frequent organ of metastasis is the liver; 50% of patients

develop it in the course of the disease [77], and those patients with gastrointestinal tumors (including the colon) have a lower probability of survival if they develop metastasis to other organs [78]. Regarding the genus *Annona*, the extract of the species *A. muricata* was the only one reported to have antimetastatic properties in an orthotopic model of pancreatic tumor cells [15]. The process of metastasis is complex, involving not only genetic aberrations, vascular growth, metabolic reprogramming, and resistance to therapy but also factors involving the pro-inflammatory microenvironment in CRC [77]. Our migration results are not definitive but suggest the possibility of using LH as an antimetastatic drug.

4. Materials and Methods

4.1. Chemicals

Dextran sulfate sodium (DSS PM. 36,000–50,000 M W) MP Biomedicals (Irvine, CA, USA), antibiotic Capricorn Scientific (Ebsdorfergrund, Germany), silica gel column 60 HF Merck® (Darmstadt, Germany) were used in this study. The substances purchased from Sigma-Aldrich (St. Louis, MO, USA) included Azoxymethane CAS 25843-45-2 (AOM), phosphate-buffered saline P3813-10PAK (PBS), and trypsin. Fetal bovine serum (FBS) and RPMI 1640 medium were obtained from Gibco™ (Billings, MT, USA), and organic solvents (hexane, ethyl acetate, and methanol) were obtained from Baker®, Phillipsburg, NJ, USA.

4.2. Isolation and Identification of LH

LH was isolated from the seeds of *A. macroprophyllata* Donn.Sm. and compared with the original LH isolated from the seeds of the same species [21]. The plant was collected in Chiapas, Mexico, and identified with number 352 in the Eizi Matuda Herbarium of the Universidad de Ciencias y Artes de Chiapas, Mexico. Once dried, continuous extractions of the dried seeds were obtained using Soxhlet equipment with hexane (8 h/3 times) and methanol (8 h/3 times) to obtain the hexane and methanolic extracts. The latter was fractionated on a silica gel column (14 × 6 cm, extract/SiO_2 1:15, flow rate 20 mL/min). Organic solvents were used with an increasing polarity gradient of Hex, as follows: AcOEt, AcOEt, AcOEt, MeOH, and MeOH. The identification and purity of the LH were determined by high-performance liquid chromatography (HPLC), thin-layer chromatography (TLC), and melting point identification. The chemical characterization of LH was carried out by HPLC (HPLC 200, Perkin Elmer, Norwalk, CT, USA) at 220 nm, with a retention time of 4.2 min, a mobile phase methanol/acetonitrile/water ratio of 10/80/10, and a silica column, Spheri-5 RP-18 (100 × 4.6 mm, 5 µm), at 30 °C, and nuclear magnetic resonance analysis. LH had a melting point of 66–67 °C.

4.3. Acute Toxicity Determination of the Mean Lethal Dose (LD_{50})

The LD_{50} was obtained based on OECD criterion 423 in order to establish the experimental doses for subsequent in vivo tests. Balb/c mice were administered doses ordered with a factor of 3.2 (1.75, 5.5, 17.5, 55, 175, 550, and 2000 mg/Kg). The trial was initiated with the 175 mg/Kg dose and terminated when all three animals survived at each dose used. LH was administered intraperitoneally (i.p.). Three organisms were used for each experimental dose (OECD, 2002) [39].

The LD_{50} was calculated according to the criteria of Chinedu et al. (2013) [79] following the formula:

$LD_{50} = [M_0 + M_1]/2$;
M_0 = highest dose without mortality;
M_1 = lowest dose with at least one deceased.

4.4. In Vivo Model of Colon Cancer

4.4.1. Animals

Forty-two male Balb/c mice, 6 to 8 weeks old and with an average weight of 20 to 25 g, were used and kept in the INCMNSZ animal facilities with appropriate conditions (housing in polypropylene cages, light and dark cycles (12/12 h), temperature of 23 ± 2 °C,

water and food ad libitum, following international recommendations related to animal care and handling reported in the ARRIVE 2.0 guidelines [80]. The research protocol was approved by the Animal Ethics Committee of the National Nutrition Institute of Mexico (CICUAL No. BQO-1932-19-21-1).

4.4.2. Induction of Colon Cancer by AOM/DSS

The induction of carcinogenesis was modified from the inflammatory model proposed by Modesto et al. in 2022 [52]. Firstly, mice received a single dose of azoxymethane (AOM) at 12. 5 mg/Kg i.p. Subsequently, the mice received three cycles of sodium dextran sulfate (DSS) at 2% dilution in their drinking water. Each cycle lasted seven days, and there were two weeks of rest between each cycle (Figure 8A).

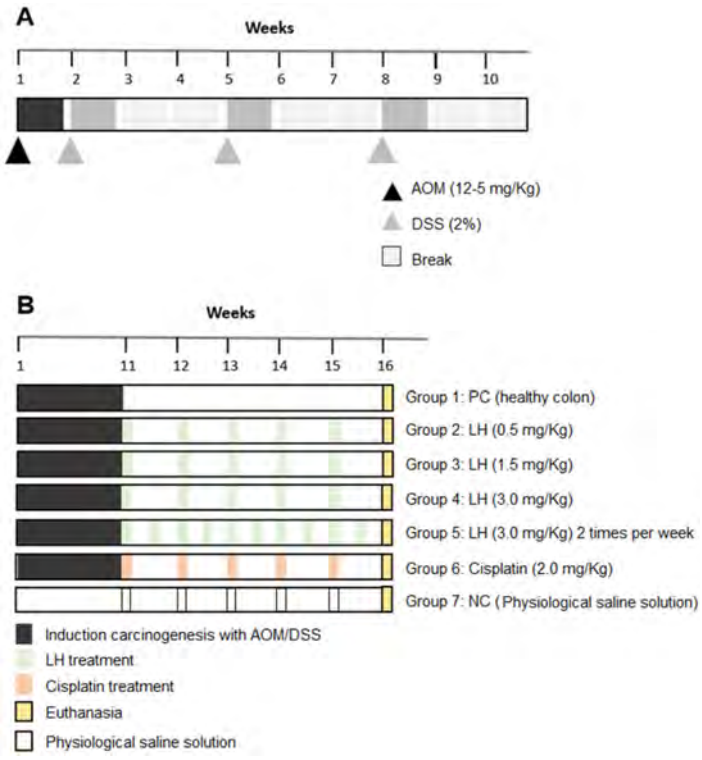


Figure 8. Timeline of the AOM/DSS model. (**A**) Carcinogenesis induction by AOM/DSS. (**B**) Experimental groups treated with LH and cisplatin, NC: negative control, PC: positive control.

Animals were randomly organized into seven experimental groups of six individuals each. After induction of carcinogenesis by AOM/DSS, LH treatment started with weekly administration for five weeks (Figure 8B). Group 1, positive control, no treatment; Group 2, LH at 0.5 mg/Kg; Group 3, LH at 1.5 mg/Kg; Group 4, LH at 3.0 mg/Kg; Group 5, LH at 3.0 mg/Kg twice a week; Group 6, cisplatin (reference drug) at 2 mg/Kg; and Group 7, healthy animals for colon reference. The experimental doses of LH were established according to its LD_{50}. During the whole experiment, the weight of the animals was recorded weekly and graphed on weeks 11 and 16. DAI data followed the scale values 0: solid feces; 1: soft feces (diarrhea); 2: normal feces with visible blood; and 3: bloody diarrhea [81].

4.4.3. Blood Test and Colon Macroscopic Analysis

One week after the last LH administration, blood collection by cardiac puncture was performed to carry out blood biometry and biochemistry at the Divet Laboratory, Mexico. Afterward, the mice were sacrificed to obtain the colon. The number and size of tumors and the length of the colon were recorded.

4.5. Histology and Immunohistochemical Analysis

4.5.1. Hematoxylin–Eosin Staining

To find histological alterations, the colon was examined using 5 mm thick sections with serial sections up to 200 mm and stained with hematoxylin/eosin. The sections were observed with the help of a Nikon Eclipse E400 microscope (Nikon, Tokyo, Japan), a digital Nikon DS-U2 camera (Nikon, Tokyo, Japan), and the software NIS-Elements version 3.0. Histology classification was performed according to recommended nomenclature for intestinal neoplasms in murine models [82].

4.5.2. Terminal Deoxynucleotide Transferase-Mediated Deoxy-UTP Nick End Labeling (TUNEL) Analysis

A TUNEL assay was executed to identify apoptotic cells in the colon tissues of LH-treated mice. Tissue sections were deparaffinized and rehydrated. DNA fragmentation was determined by catalytic incorporation of fluorescein-12-dUTP(a) into the 3′-OH ends of DNA using recombinant terminal deoxynucleotidyl transferase (rTdT) enzyme, according to the manufacturer's protocol (Dead End Fluorometric TUNEL System, Promega Part # TB235). Finally, the slides were washed with double-distilled water and cover-slipped using a Vecta Sheeld mounting medium (Vector Laboratories, Newark, CA, USA). Images were taken on a Zeiss LSM 880 confocal microscope.

4.6. Wound Healing Assay

To evaluate migration inhibition by LH, a wound closure assay was performed in vitro, according to Grada et al. (2017) [83]. In a 6-well plate, 2 mm adhesive tape was placed, and the HTC116 colon cancer cells were seeded at a density of 1.5×10^6 per well. The plates were incubated for 24 h in an atmosphere of 5% CO_2, 95% humidity, and 37 °C. Subsequently, the tapes were removed, and the cells were treated with LH at a concentration of 8 μM for 24 h. Treated cells were supplemented with SFB at 2%, and control cells with 10% SFB. The experiment was performed in triplicate. Photos of each well were taken with the Nikon TS100 microscope and analyzed with the help of the software ImageJ version 1.53k.

4.7. Statistics

Results are presented as the mean ± ES, weight and DAI, and blood and tumor analyses of each experimental group. One-way analysis of variance (Anova) and Kruskal–Wallis with a Newman–Keuls post hoc comparison test ($p < 0.05$) were performed, with the results given as percentages (hematocrit, lymphocyte, and neutrophil blood tests).

5. Conclusions

The high rate of CCR in the world population, the mortality numbers, and the lack of efficient treatment, chemoresistance, and metastasis are issues for public health discussion. Natural products are a source of chemical structures with varying bioactivity, presenting an opportunity for developing new drugs. Our research demonstrates the antitumor capacity of the acetogenin laherradurin in a CCR model in vivo. The LH reduced the number and size of the tumors and showed less toxicity at macroscopic and blood levels compared with the reference drug, cisplatin. Moreover, LH induced cell death by apoptosis in vivo and inhibited cell migration in HCT colon cancer cells. Also, those animals treated with LH manifested less toxicity, as indicated by the weight recovery and reduced disease signs compared with animals treated with cisplatin. These results bring new and worthwhile information regarding the potential of laherradurin as an anticancer drug for CCR. The study of this molecule is not over, as questions arising from our results about its activity, other mechanisms of action, possible therapeutic combinations, additional toxicity assays, and signaling pathways involved are under investigation by our research group.

Author Contributions: Conceptualization, N.J.J.-H., M.J.R.-B. and E.P.-A.; methodology, M.J.R.-B., E.P.-A., I.D.-W., J.C.-H. and F.R.-I.; software, M.J.R.-B., E.P.-A., R.L. and F.R.-I.; validation, I.Á.-G., E.M.-B., R.L., C.P.-P., N.J.J.-H. and A.R.G.-E.; formal analysis, N.J.J.-H., M.J.R.-B., C.P.-P. and J.C.-H.; investigation, M.J.R.-B., N.J.J.-H., A.R.G.-E. and I.D.-W.; resources, N.J.J.-H., E.M.-B. and A.R.G.-E.; data curation, N.J.J.-H. and M.J.R.-B.; writing—original draft preparation, M.J.R.-B., N.J.J.-H. and I.Á.-G.; writing—review and editing, N.J.J.-H., E.M.-B., I.Á.-G., R.L., C.P.-P., J.C.-H. and A.R.G.-E.; supervision, N.J.J.-H., E.M.-B. and I.Á.-G.; writing—original draft preparation, M.J.R.-B., N.J.J.-H. and I.Á.-G.; writing—review and editing, N.J.J.-H., E.M.-B., I.Á.-G. and R.L.; project administration, N.J.J.-H., C.P.-P., M.J.R.-B. and I.Á.-G.; funding acquisition, N.J.J.-H. All authors have read and agreed to the published version of the manuscript.

Funding: This research was funded by CONAHCYT, Mexico, under grant number CB-2016-285884.

Institutional Review Board Statement: The animal study protocol was approved by the Institutional Animal Ethics Committee of the National Nutrition Institute of Mexico Salvador Zubirán (INCMNSZ) (protocol code BQO-1932-19-21-1, 26 September 2018).

Informed Consent Statement: Not applicable.

Data Availability Statement: Data are contained within the article.

Acknowledgments: M.J.R.-B. acknowledges CONAHCYT, Mexico, for financially supporting this study via a studentship from Escuela Nacional de Ciencias Biológicas-Instituto Politécnico Nacional (ENCB-IPN). The authors are grateful to the team of the Animal Facilities (Vivarium) of the Instituto Nacional de Ciencias Médicas y Nutrición Salvador Zubirán, Mexico.

Conflicts of Interest: The authors declare no conflicts of interest. The funders had no role in the design of the study; in the collection, analyses, or interpretation of data; in the writing of the manuscript; or in the decision to publish the results.

References

1. Sung, H.; Ferlay, J.; Siegel, R.L.; Laversanne, M.; Soerjomataram, I.; Jemal, A.; Bray, F. Global Cancer Statistics 2020: GLOBOCAN Estimates of Incidence and Mortality Worldwide for 36 Cancers in 185 Countries. *CA Cancer J. Clin.* **2021**, *71*, 209–249. [CrossRef]
2. Zhu, G.; Pei, L.; Xia, H.; Tang, Q.; Bi, F. Role of oncogenic KRAS in the prognosis, diagnosis and treatment of colorectal cancer. *Mol. Cancer* **2021**, *20*, 143. [CrossRef]
3. Dekker, E.; Tanis, P.J.; Vleugels, J.L.; Kasi, P.M.; Wallace, M.B. Colorectal cancer. *Lancet* **2019**, *394*, 1467–1480. [CrossRef]
4. Modest, D.P.; Pant, S.; Sartore-Bianchi, A. Treatment sequencing in metastatic colorectal cancer. *Eur. J. Cancer* **2019**, *109*, 70–83. [CrossRef]
5. Diasio, R.B.; Innocenti, F.; Offer, S.M. Pharmacogenomic-Guided Therapy in Colorectal Cancer. *Clin. Pharmacol. Ther.* **2021**, *110*, 616–625. [CrossRef]
6. Latchman, J.; Guastella, A.; Tofthagen, C. 5-fluorouracil toxicity and dihydropyrimidine dehydrogenase enzyme: Implications for practice. *Clinical J. Oncol. Nurs.* **2014**, *18*, 581–585.
7. Zhang, L.; Xing, X.; Meng, F.; Wang, Y.; Zhong, D. Oral fluoropyrimidine versus intravenous 5-fluorouracil for the treatment of advanced gastric and colorectal cancer: Meta-analysis. *J. Gastroenterol. Hepatol.* **2018**, *33*, 209–225. [CrossRef]
8. Vodenkova, S.; Buchler, T.; Cervena, K.; Veskrnova, V.; Vodicka, P.; Vymetalkova, V. 5-fluorouracil and other fluoropyrimidines in colorectal cancer: Past, present and future. *Pharmacol. Ther.* **2020**, *206*, 107447. [CrossRef] [PubMed]
9. Paulík, A.; Nekvindová, J.; Filip, S. Irinotecan toxicity during treatment of metastatic colorectal cancer: Focus on pharmacogenomics and personalized medicine. *Tumori* **2020**, *106*, 87–94. [CrossRef] [PubMed]
10. Karthika, C.; Sureshkumar, R.; Zehravi, M.; Akter, R.; Ali, F.; Ramproshad, S.; Mondal, B.; Kundu, M.K.; Dey, A.; Rahman, M.H.; et al. Multidrug Resistance in Cancer Cells: Focus on a Possible Strategy Plan to Address Colon Carcinoma Cells. *Life* **2022**, *12*, 811. [CrossRef] [PubMed]
11. Newman, D.J. Natural products and drug discovery. *Natl. Sci. Rev.* **2022**, *9*, nwac206. [CrossRef]
12. Alonso-Castro, A.J. Use of medicinal fauna in Mexican traditional medicine. *J. Ethnopharmacol.* **2014**, *152*, 53–70. [CrossRef]
13. Jacobo-Herrera, N.J.; Jacobo-Herrera, F.E.; Zentella-Dehesa, A.; Andrade-Cetto, A.; Heinrich, M.; Pérez-Plasencia, C. Medicinal plants used in Mexican traditional medicine for the treatment of colorectal cancer. *J. Ethnopharmacol.* **2016**, *179*, 391–402. [CrossRef]
14. Tormo, J.R.; Royo, I.; Gallardo, T.; Zafra-Polo, M.C.; Hernández, P.; Cortes, D.; Peláez, F. In vitro antitumor structure-activity relationships of threo/trans/threo mono-tetrahydrofuranic acetogenins: Correlations with their inhibition of mitochondrial complex I. *Oncol. Res.* **2003**, *14*, 147–154. [CrossRef] [PubMed]
15. Torres, M.P.; Rachagani, S.; Purohit, V.; Pandey, P.; Joshi, S.; Moore, E.D.; Johansson, S.L.; Singh, P.K.; Ganti, A.K.; Batra, S.K. Graviola: A novel promising natural-derived drug that inhibits tumorigenicity and metastasis of pancreatic cancer cells in vitro and in vivo through altering cell metabolism. *Cancer Lett.* **2012**, *323*, 29–40. [CrossRef] [PubMed]

16. Moghadamtousi, S.Z.; Fadaeinasab, M.; Nikzad, S.; Mohan, G.; Ali, H.M.; Kadir, H.A. Annona muricata (Annonaceae): A Review of Its Traditional Uses, Isolated Acetogenins and Biological Activities. *Int. J. Mol. Sci.* **2015**, *16*, 15625–15658. [CrossRef] [PubMed]
17. Savithramma, N.; Rao, M.L.; Suhrulatha, D. Screening of medicinal plants for secondary metabolites. *MEJSR* **2011**, *8*, 579–584.
18. Durán, A.G.; Gutiérrez, M.T.; Mejías, F.J.R.; Molinillo, J.M.G.; Macías, F.A. An Overview of the Chemical Characteristics, Bioactivity and Achievements Regarding the Therapeutic Usage of Acetogenins from *Annona cherimola* Mill. *Molecules* **2021**, *26*, 2926. [CrossRef] [PubMed]
19. Alonso-Castro, A.J.; Villarreal, M.L.; Salazar-Olivo, L.A.; Gomez-Sanchez, M.; Dominguez, F.; Garcia-Carranca, A. Mexican medicinal plants used for cancer treatment: Pharmacological, phytochemical and ethnobotanical studies. *J. Ethnopharmacol.* **2011**, *133*, 945–972. [CrossRef] [PubMed]
20. Brindis, F.; González-Trujano, M.E.; González-Andrade, M.; Aguirre-Hernández, E.; Villalobos-Molina, R. Aqueous extract of Annona macroprophyllata: A potential α-glucosidase inhibitor. *Biomed. Res. Int.* **2013**, *2013*, 591313. [CrossRef] [PubMed]
21. Schlie-Guzmán, M.A.; García-Carrancá, A.; González-Esquinca, A.R. In vitro and in vivo antiproliferative activity of laherradurin and cherimolin-2 of Annona diversifolia Saff. *Phytother. Res.* **2009**, *23*, 1128–1133. [CrossRef] [PubMed]
22. Yuan, H.; Ma, Q.; Ye, L.; Piao, G. The Traditional Medicine and Modern Medicine from Natural Products. *Molecules* **2016**, *21*, 559. [CrossRef] [PubMed]
23. Li, Y.; Kong, D.; Fu, Y.; Sussman, M.R.; Wu, H. The effect of developmental and environmental factors on secondary metabolites in medicinal plants. *Plant Physiol. Biochem.* **2020**, *148*, 80–89. [CrossRef] [PubMed]
24. Sen, T.; Samanta, S.K. Medicinal plants, human health and biodiversity: A broad review. *Adv. Biochem. Eng. Biotechnol.* **2015**, *147*, 59–110.
25. World Health Organization. WHO Global Centre for Traditional Medicine. Available online: https://www.who.int/initiatives/who-global-centre-for-traditional-medicine (accessed on 6 November 2023).
26. Tormo, J.R.; De Pedro, N.; Royo, I.; Barrachina, I.; Zafra-Polo, M.C.; Cuadrillero, C.; Hernández, P.; Cortes, D.; Peláez, F. In vitro antitumor structure-activity relationships of threo/trans/threo/trans/erythro bis-tetrahydrofuranic acetogenins: Correlations with their inhibition of mitochondrial complex I. *Oncol. Res.* **2005**, *15*, 129–138. [CrossRef] [PubMed]
27. Tantithanaporn, S.; Wattanapiromsakul, C.; Itharat, A.; Keawpradub, N. Cytotoxic activity of acetogenins and styryl lactones isolated from Goniothalamus undulatus Ridl. root extracts against a lung cancer cell line (COR-L23). *Phytomedicine* **2011**, *18*, 486–490. [CrossRef] [PubMed]
28. Yuan, F.; Bai, G.; Chen, Y.; Miao, Y.; Chen, J.; Li, X. Structure-activity relationships of diverse ACGs against multidrug resistant human lung cancer cell line A549/Taxol. *Bioorg Med. Chem. Lett.* **2015**, *25*, 787–790. [CrossRef] [PubMed]
29. Qian, J.Q.; Sun, P.; Pan, Z.Y.; Fang, Z.Z. Annonaceous acetogenins reverse drug resistance of human hepatocellular carcinoma BEL-7402/5-FU and HepG2/ADM cell lines. *Int. J. Clin. Exp. Pathol.* **2015**, *8*, 11934–11944.
30. Chen, Y.; Chen, J.W.; Wang, Y.; Xu, S.S.; Li, X. Six cytotoxic annonaceous acetogenins from Annona squamosa seeds. *Food Chem.* **2012**, *135*, 960–966. [CrossRef]
31. Dai, Y.; Hogan, S.; Schmelz, E.M.; Ju, Y.H.; Canning, C.; Zhou, K. Selective growth inhibition of human breast cancer cells by graviola fruit extract in vitro and in vivo involving downregulation of EGFR expression. *Nutr. Cancer* **2011**, *63*, 795–801. [CrossRef]
32. Griggs, N.D.; Phillips, A.J. A concise and modular synthesis of pyranicin. *Org. Lett.* **2008**, *10*, 4955–4957. [CrossRef]
33. Ko, Y.M.; Wu, T.Y.; Wu, Y.C.; Chang, F.R.; Guh, J.Y.; Chuang, L.Y. Annonacin induces cell cycle-dependent growth arrest and apoptosis in estrogen receptor-α-related pathways in MCF-7 cells. *J. Ethnopharmacol.* **2011**, *37*, 1283–1290. [CrossRef]
34. Chen, Y.; Chen, J.; Xu, S.; Wang, Y.; Li, X.; Cai, B. Antitumor activity of annonaceous acetogenins in HepS and S180 xenografts bearing mice. *Bioorg. Med. Chem. Lett.* **2012**, *22*, 2717–2719. [CrossRef]
35. Yang, C.; Gundala, S.R.; Mukkavilli, R.; Vangala, S.; Reid, M.D.; Aneja, R. Synergistic interactions among flavonoids and acetogenins in Graviola (*Annona muricata*) leaves confer protection against prostate cancer. *Carcinogenesis* **2015**, *36*, 656–665. [CrossRef] [PubMed]
36. Livshits, Z.; Rao, R.B.; Smith, S.W. An approach to chemotherapy-associated toxicity. *Emerg. Med. Clin. N. Am.* **2014**, *32*, 167–203. [CrossRef] [PubMed]
37. Simkens, L.H.J.; Koopman, M.; Punt, C.J.A. Optimal duration of systemic treatment in metastatic colorectal cancer. *Curr. Opin. Oncol.* **2014**, *26*, 448–453. [CrossRef] [PubMed]
38. Ma, W.W.; Saif, M.W.; El-Rayes, B.F.; Fakih, M.G.; Cartwright, T.H.; Posey, J.A.; King, T.R.; Von Borstel, R.W.; Bamat, M.K. Emergency use of uridine triacetate for the prevention and treatment of life-threatening 5-fluorouracil and capecitabine toxicity. *Cancer* **2017**, *123*, 345–356. [PubMed]
39. OECD iLibrary. OECD Guidelines for the Testing of Chemicals, Section 4. Available online: https://www.oecd-ilibrary.org/environment/test-no-423-acute-oral-toxicity-acute-toxic-class-method_9789264071001-en (accessed on 12 October 2023).
40. Durán-Ruiz, C.A.; Cruz-Ortega, R.; Zaldívar-Riverón, A.; Zavaleta-Mancera, H.A.; De-la-Cruz-Chacón, I.; González-Esquinca, A.R. Ontogenic synchronization of Bephratelloides cubensis, Annona macroprophyllata seeds and acetogenins from Annonaceae. *J. Plant Res.* **2019**, *132*, 81–91. [CrossRef] [PubMed]
41. Ma, C.; Chen, Y.; Chen, J.; Li, X.; Chen, Y.A. Review on Annona squamosa L.: Phytochemicals and Biological Activities. *Am. J. Chin. Med.* **2017**, *45*, 933–964. [CrossRef]

42. Mutakin, M.; Fauziati, R.; Fadhilah, F.N.; Zuhrotun, A.; Amalia, R.; Hadisaputri, Y.E. Pharmacological Activities of Soursop (*Annona muricata* Lin.). *Molecules* **2022**, *27*, 1201. [CrossRef] [PubMed]
43. Wu, J.; Yeung, S.J.; Liu, S.; Qdaisat, A.; Jiang, D.; Liu, W.; Cheng, Z.; Liu, W.; Wang, H.; Li, L.; et al. Cyst(e)ine in nutrition formulation promotes colon cancer growth and chemoresistance by activating mTORC1 and scavenging ROS. *Signal Transduct. Target. Ther.* **2021**, *6*, 188. [CrossRef] [PubMed]
44. Tisdale, M.J. Catabolic mediators of cancer cachexia. *Curr. Opin. Support. Palliat. Care* **2008**, *2*, 256–261. [CrossRef] [PubMed]
45. Biswas, A.K.; Acharyya, S. Understanding cachexia in the context of metastatic progression. *Nat. Rev. Cancer* **2020**, *20*, 274–284. [CrossRef] [PubMed]
46. Brown, L.R.; Laird, B.J.A.; Wigmore, S.J.; Skipworth, R.J.E. Understanding Cancer Cachexia and Its Implications in Upper Gastrointestinal Cancers. *Curr. Treat. Options Oncol.* **2022**, *23*, 1732–1747. [CrossRef] [PubMed]
47. Cid-Gallegos, M.S.; Jiménez-Martínez, C.; Sánchez-Chino, X.M.; Madrigal-Bujaidar, E.; Vásquez-Garzón, V.R.; Baltiérrez-Hoyos, R.; Álvarez-González, I. Chemopreventive Effect of Cooked Chickpea on Colon Carcinogenesis Evolution in AOM/DSS-Induced Balb/c Mice. *Plants* **2023**, *12*, 2317. [CrossRef]
48. Sun, W.; Gao, J.; Yang, B.; Chen, X.; Kang, N.; Liu, W. Protocol for colitis-associated colorectal cancer murine model induced by AOM and DSS. *STAR Protoc.* **2023**, *4*, 102105. [CrossRef]
49. Jialing, L.; Yangyang, G.; Jing, Z.; Xiaoyi, T.; Ping, W.; Liwei, S.; Simin, C. Changes in serum inflammatory cytokine levels and intestinal flora in a self-healing dextran sodium sulfate-induced ulcerative colitis murine model. *Life Sci.* **2020**, *263*, 118587. [CrossRef]
50. Wang, J.; Zhang, C.; Guo, C.; Li, X. Chitosan Ameliorates DSS-Induced Ulcerative Colitis Mice by Enhancing Intestinal Barrier Function and Improving Microflora. *Int. J. Mol. Sci.* **2019**, *20*, 5751. [CrossRef]
51. Eichele, D.D.; Kharbanda, K.K. Dextran sodium sulfate colitis murine model: An indispensable tool for advancing our understanding of inflammatory bowel diseases pathogenesis. *World J. Gastroenterol.* **2017**, *33*, 6016–6029. [CrossRef]
52. Modesto, R.; Estarreja, J.; Silva, I.; Rocha, J.; Pinto, R.; Mateus, V. Chemically Induced Colitis-Associated Cancer Models in Rodents for Pharmacological Modulation: A Systematic Review. *J. Clin. Med.* **2022**, *11*, 2739. [CrossRef]
53. Weiss, G.; Goodnough, L.T. Anemia of chronic disease. *N. Engl. J. Med.* **2005**, *352*, 1011–1023. [CrossRef]
54. Huang, X.Z.; Yang, Y.C.; Chen, Y.; Wu, C.C.; Lin, R.F.; Wang, Z.N.; Zhang, X. Preoperative Anemia or Low Hemoglobin Predicts Poor Prognosis in Gastric Cancer Patients: A Meta-Analysis. *Dis. Markers* **2019**, *2019*, 7606128. [CrossRef]
55. Wilson, M.J.; van Haaren, M.; Harlaar, J.J.; Park, H.C.; Bonjer, H.J.; Jeekel, J.; Zwaginga, J.J.; Schipperus, M. Long-term prognostic value of preoperative anemia in patients with colorectal cancer: A systematic review and meta-analysis. *Surg. Oncol.* **2017**, *26*, 96–104. [CrossRef]
56. Ju, J.; Lee, G.Y.; Kim, Y.S.; Chang, H.K.; Do, M.S.; Park, K.Y. Bamboo salt suppresses colon carcinogenesis in C57BL/6 mice with chemically induced colitis. *J. Med. Food* **2016**, *19*, 1015–1022. [CrossRef]
57. Kim, H.Y.; Seo, J.E.; Lee, H.; Bae, C.H.; Ha, K.T.; Kim, S. *Rumex japonicus* Houtt. Extract Suppresses Colitis-Associated Colorectal Cancer by Regulating Inflammation and Tight-Junction Integrity in Mice. *Front. Pharmacol.* **2022**, *5*, 946909. [CrossRef] [PubMed]
58. Chou, Y.C.; Suh, J.H.; Wang, Y.; Pahwa, M.; Badmaev, V.; Ho, C.T.; Pan, M.H. Boswellia serrata resin extract alleviates azoxymethane (AOM)/dextran sodium sulfate (DSS)-induced colon tumorigenesis. *Mol. Nutr. Food Res.* **2017**, *61*, 1600984. [CrossRef] [PubMed]
59. Iskander, A.; Yan, L.J. Cisplatin-Induced Kidney Toxicity: Potential Roles of Major NAD^+-Dependent Enzymes and Plant-Derived Natural Products. *Biomolecules* **2022**, *12*, 1078. [CrossRef] [PubMed]
60. Yaegashi, A.; Yoshida, K.; Suzuki, N.; Shimada, I.; Tani, Y.; Saijo, Y.; Toyama, A. A case of severe hepatotoxicity induced by cisplatin and 5-fluorouracil. *Int. Cancer Conf. J.* **2019**, *9*, 24–27. [CrossRef]
61. Albers, J.W.; Chaudhry, V.; Cavaletti, G.; Donehower, R.C. Interventions for preventing neuropathy caused by cisplatin and related com-pounds. *Cochrane Database Syst. Rev.* **2014**, *3*, 1–79.
62. Callejo, A.; Sedó-Cabezón, L.; Juan, I.D.; Llorens, J. Cisplatin-Induced Ototoxicity: Effects, Mechanisms and Protection Strategies. *Toxics* **2015**, *3*, 268–293. [CrossRef]
63. Rahimi, A.; Asadi, F.; Rezghi, M.; Kazemi, S.; Soorani, F.; Memariani, Z. Natural products against cisplatin-induced male reproductive toxicity: A comprehensive review. *J. Biochem. Mol. Toxicol.* **2022**, *36*, e22970. [CrossRef]
64. Champy, P.; Höglinger, G.U.; Féger, J.; Gleye, C.; Hocquemiller, R.; Laurens, A.; Guérineau, V.; Laprévote, O.; Medja, F.; Lombès, A.; et al. Annonacin, a lipophilic inhibitor of mitochondrial complex I, induces nigral and striatal neurodegeneration in rats: Possible relevance for atypical parkinsonism in Guadeloupe. *J. Neurochem.* **2004**, *88*, 63–69. [CrossRef] [PubMed]
65. Champy, P.; Melot, A.; Guérineau Eng, V.; Gleye, C.; Fall, D.; Höglinger, G.U.; Ruberg, M.; Lannuzel, A.; Laprévote, O.; Laurens, A.; et al. Quantification of acetogenins in Annona muricata linked to atypical parkinsonism in guadeloupe. *Mov. Disord.* **2005**, *20*, 1629–1633. [CrossRef] [PubMed]
66. Escobar-Khondiker, M.; Höllerhage, M.; Muriel, M.P.; Champy, P.; Bach, A.; Depienne, C.; Respondek, G.; Yamada, E.S.; Lannuzel, A.; Yagi, T.; et al. Annonacin, a natural mitochondrial complex I inhibitor, causes tau pathology in cultured neurons. *J. Neurosci.* **2007**, *27*, 7827–7837. [CrossRef]
67. Le Ven, J.; Schmitz-Afonso, I.; Lewin, G.; Brunelle, A.; Touboul, D.; Champy, P. Identification of the environmental neurotoxins annonaceous acetogenins in an Annona cherimolia Mill. Alcoholic Beverage Using HPLC-ESI-LTQ-Orbitrap. *J. Agric. Food Chem.* **2014**, *62*, 8696–8704. [CrossRef] [PubMed]

68. Degli Esposti, M.; Ghelli, A.; Ratta, M.; Cortes, D.; Estornell, E. Natural substances (acetogenins) from the family Annonaceae are powerful inhibitors of mitochondrial NADH dehydrogenase (Complex I). *Biochem. J.* **1994**, *301*, 161–167. [CrossRef]
69. Chang, F.R.; Wu, Y.C. Novel cytotoxic annonaceous acetogenins from *Annona muricata*. *J. Nat. Prod.* **2001**, *64*, 925–931. [CrossRef] [PubMed]
70. Han, B.; Wang, T.D.; Shen, S.M.; Yu, Y.; Mao, C.; Yao, Z.J.; Wang, L.S. Annonaceous acetogenin mimic AA005 induces cancer cell death via apoptosis inducing factor through a caspase-3-independent mechanism. *BMC Cancer* **2015**, *15*, 139. [CrossRef] [PubMed]
71. Gaviria-Calle, M.M.; Posada-Arias, S.; Mira-Hernández, J. Acetogeninas, alternativa en el tratamiento de cáncer en caninos. *Rev. CES Med. Zootec.* **2018**, *13*, 157–172. [CrossRef]
72. Mangal, M.; Mhod, I.K.; Subhash, M.A. Acetogenins as Potential Anticancer Agents. *Anticancer. Agents Med. Chem.* **2016**, *16*, 138–159. [CrossRef]
73. Yap, C.V.; Subramaniam, K.S.; Khor, S.W.; Chung, I. Annonacin Exerts Antitumor Activity through Induction of Apoptosis and Extracellular Signal-regulated Kinase Inhibition. *Pharmacogn. Res.* **2017**, *9*, 378–383.
74. Yuan, S.S.; Chang, H.L.; Chen, H.W.; Kuo, F.C.; Liaw, C.C.; Su, J.H.; Wu, Y.C. Selective cytotoxicity of squamocin on T24 bladder cancer cells at the S-phase via a Bax-, Bad-, and caspase-3-related pathways. *Life Sci.* **2006**, *78*, 869–874. [CrossRef]
75. Jacobo-Herrera, N.; Pérez-Plasencia, C.; Castro-Torres, V.A.; Martínez-Vázquez, M.; González-Esquinca, A.R.; Zentella-Dehesa, A. Selective Acetogenins and Their Potential as Anticancer Agents. *Front. Pharmacol.* **2019**, *10*, 783. [CrossRef] [PubMed]
76. De Pedro, N.; Cautain, B.; Melguizo, A.; Vicente, F.; Genilloud, O.; Peláez, F.; Tormo, J.R. Mitochondrial complex I inhibitors, acetogenins, induce HepG2 cell death through the induction of the complete apoptotic mitochondrial pathway. *J. Bioenerg. Biomembr.* **2013**, *45*, 153–164. [CrossRef]
77. Tsilimigras, D.I.; Ntanasis-Stathopoulos, I.; Pawlik, T.M. Molecular Mechanisms of Colorectal Liver Metastases. *Cells* **2023**, *12*, 1657. [CrossRef] [PubMed]
78. Kim, S.K.; Lee, N.H.; Son, C.G. A Review of Herbal Resources Inducing Anti-Liver Metastasis Effects in Gastrointestinal Tumors via Modulation of Tumor Microenvironments in Animal Models. *Cancers* **2023**, *15*, 3415. [CrossRef] [PubMed]
79. Chinedu, E.; Arome, D.; Ameh, F.S. A new method for determining acute toxicity in animal models. *Toxicol. Int.* **2013**, *20*, 224–226. [CrossRef] [PubMed]
80. Percie du Sert, N.; Hurst, V.; Ahluwalia, A.; Alam, S.; Avey, M.T.; Baker, M.; Browne, W.J.; Clark, A.; Cuthill, I.C.; Dirnagl, U.; et al. The ARRIVE guidelines 2.0: Updated guidelines for reporting animal research. *PLoS Biol.* **2020**, *18*, e3000410.
81. Cuellar-Nuñez, M.L.; Luzardo-Ocampo, I.; Campos-Vega, R.; Gallegos-Corona, M.A.; González de Mejía, E.; Loarca-Piña, G. Physicochemical and nutraceutical properties of moringa (*Moringa oleifera*) leaves and their effects in an in vivo AOM/DSS-induced colorectal carcinogenesis model. *Food Res. Int.* **2018**, *105*, 159–168. [CrossRef]
82. Boivin, G.P.; Washington, K.; Yang, K.; Ward, J.M.; Pretlow, T.P.; Russell, R.; Besselsen, D.G.; Godfrey, V.L.; Doetschman, T.; Dove, W.F.; et al. Pathology of mouse models of intestinal cancer: Consensus report and recommendations. *Gastroenterology* **2003**, *124*, 762–777. [CrossRef]
83. Grada, A.; Otero-Vinas, M.; Prieto-Castrillo, F.; Obagi, Z.; Falanga, V. Research Techniques Made Simple: Analysis of Collective Cell Migration Using the Wound Healing Assay. *J. Investig. Dermatol.* **2017**, *137*, e11–e16. [CrossRef] [PubMed]

Disclaimer/Publisher's Note: The statements, opinions and data contained in all publications are solely those of the individual author(s) and contributor(s) and not of MDPI and/or the editor(s). MDPI and/or the editor(s) disclaim responsibility for any injury to people or property resulting from any ideas, methods, instructions or products referred to in the content.

frontiers | Frontiers in Oncology

TYPE Original Research
PUBLISHED 08 May 2023
DOI 10.3389/fonc.2023.1106667

Check for updates

OPEN ACCESS

EDITED BY
Mohamed Hassan,
Institut National de la Santé et de la Recherche Médicale (INSERM), France

REVIEWED BY
Fahad Khan,
Noida Institute of Engineering and Technology (NIET), India
Chandra Sekhar Bhol,
National Institute of Technology Rourkela, India

*CORRESPONDENCE
Nadia Judith Jacobo-Herrera
nadia.jacobo@gmail.com
Carlos Pérez-Plasencia
carlos.pplas@gmail.com

RECEIVED 24 November 2022
ACCEPTED 28 March 2023
PUBLISHED 08 May 2023

CITATION
Delgado-Waldo I, Contreras-Romero C, Salazar-Aguilar S, Pessoa J, Mitre-Aguilar I, García-Castillo V, Pérez-Plasencia C and Jacobo-Herrera NJ (2023) A triple-drug combination induces apoptosis in cervical cancer-derived cell lines.
Front. Oncol. 13:1106667.
doi: 10.3389/fonc.2023.1106667

COPYRIGHT
© 2023 Delgado-Waldo, Contreras-Romero, Salazar-Aguilar, Pessoa, Mitre-Aguilar, García-Castillo, Pérez-Plasencia and Jacobo-Herrera. This is an open-access article distributed under the terms of the Creative Commons Attribution License (CC BY). The use, distribution or reproduction in other forums is permitted, provided the original author(s) and the copyright owner(s) are credited and that the original publication in this journal is cited, in accordance with accepted academic practice. No use, distribution or reproduction is permitted which does not comply with these terms.

A triple-drug combination induces apoptosis in cervical cancer-derived cell lines

Izamary Delgado-Waldo[1,2], Carlos Contreras-Romero[2,3], Sandra Salazar-Aguilar[4], João Pessoa[5], Irma Mitre-Aguilar[1], Verónica García-Castillo[6], Carlos Pérez-Plasencia[3,6]* and Nadia Judith Jacobo-Herrera[1]*

[1]Unidad de Bioquímica Guillermo Soberón Acevedo, Instituto de Ciencias Médicas y Nutrición Salvador Zubirán, Tlalpan, Mexico, [2]Posgrado en Ciencias Biológicas, Universidad Nacional Autónoma de México. Copilco Universidad, Coyoacán, Mexico, [3]Laboratorio de Genómica, Instituto Nacional de Cancerología, Tlalpan, Mexico, [4]Laboratorio de Hematopoiesis y Leucemia, Unidad de Investigación, Diferenciación Celular y Cáncer, Facultad de Estudios Superiores Zaragoza, Universidad Nacional Autónoma de México, Iztapalapa, Mexico, [5]CNC - Center for Neuroscience and Cell Biology, CIBB - Center for Innovative Biomedicine and Biotechnology, University of Coimbra, Coimbra, Portugal, [6]Laboratorio de Genómica Funcional, Unidad de Biomedicina, FES-IZTACALA, Universidad Nacional Autónoma de México, Tlalnepantla, Mexico

Introduction: Cervical cancer is a worldwide health problem due to the number of deaths caused by this neoplasm. In particular, in 2020, 30,000 deaths of this type of tumor were reported in Latin America. Treatments used to manage patients diagnosed in the early stages have excellent results as measured by different clinical outcomes. Existing first-line treatments are not enough to avoid cancer recurrence, progression, or metastasis in locally advanced and advanced stages. Therefore, there is a need to continue with the proposal of new therapies. Drug repositioning is a strategy to explore known medicines as treatments for other diseases. In this scenario, drugs used in other pathologies that have antitumor activity, such as metformin and sodium oxamate, are analyzed.

Methods: In this research, we combined the drugs metformin and sodium oxamate with doxorubicin (named triple therapy or TT) based on their mechanism of action and previous investigation of our group against three CC cell lines.

Results: Through flow cytometry, Western blot, and protein microarray experiments, we found TT-induced apoptosis on HeLa, CaSki, and SiHa through the caspase 3 intrinsic pathway, including the critical proapoptotic proteins BAD, BAX, cytochrome-C, and p21. In addition, mTOR and S6K phosphorylated proteins were inhibited in the three cell lines. Also, we show an anti-migratory activity of the TT, suggesting other targets of the drug combination in the late CC stages.

Discussion: These results, together with our former studies, conclude that TT inhibits the mTOR pathway leading to cell death by apoptosis. Our work provides new evidence of TT against cervical cancer as a promising antineoplastic therapy.

KEYWORDS

cervical cancer, apoptosis, combinatorial therapy, repurposing drugs, mTOR pathway

1 Introduction

Despite early detection programs, cervical cancer (CC) is a public health problem that still needs to be solved. Although its incidence has decreased by approximately 40% in the last decade, it currently remains the second leading cause of cancer-related deaths in women, accounting for an estimated 270,000 women's lives annually (1). The use of cervical cancer screening has helped in an early diagnosis of this disease; however, there is still a large population in which the disease is diagnosed in locally advanced stages (2). In such a scenario, the clinical response rates to conventional treatment based on radiation therapy and/or surgery, chemotherapy (3), and immunotherapy (4) are poor. These therapies have systemic side effects on patients (5), high costs (6), and rapid development of drug resistance (7–10), which are some of the limitations that reduce their effectiveness (11).

Warburg's research in the 1920s proved that tumor cells require a high income of glucose to maintain their extremely demanded metabolism activity independently of the oxygen levels, a process known as the Warburg effect or aerobic glycolysis (12–14). In contrast to the normal cell, the tumor cell produces vast amounts of extracellular lactate *via* aerobic glycolysis (15) and consequently generates several disturbances in other cells and the tumor microenvironment (16), leading to hypoxia, promotion of angiogenesis, and distant metastasis (17, 18). The high rate of glucose consumption allows the tumor cell to obtain biosynthetic precursors necessary for the biosynthesis of nucleotides, proteins, and lipids to achieve increased proliferation, survival, and progression of tumor characteristics (19–23).

Drug repositioning is a current strategy for new anticancer treatments (24) in terms of safety, side effects, and mechanisms of action (25). In this scenario, our research group successfully proved that the combination of the known drugs metformin, doxorubicin, and sodium oxamate (named triple therapy or TT) inhibited tumor growth in cell lines derived from breast and colon cancers and in two different murine models (17, 26, 27). Metformin is widely used to treat type 2 diabetes mellitus (28). Besides it is an antitumor candidate due to its ability to inhibit respiratory-chain complex I (29), activate the protein AMPK, and inhibit the mTOR activation (30). Such events stop cell proliferation and the production of proteins, lipids, and carbohydrates (31–34). The second drug, oxamate, is a competitive inhibitor of lactate dehydrogenase A (LDH-A), an enzyme that catalyzes the pyruvate to lactate in aerobic glycolysis (35–38). Finally, doxorubicin is a well-known drug used to treat several types of cancer (39). It induces cell death in three different ways: topoisomerase II inhibition, inhibition of DNA synthesis, and induction of oxidative stress (39–41).

Previously, we have shown that the TT leads to apoptosis by the upregulation of PARP-1 and the caspase 3 cleavage, as well as mTOR and LDH-A inhibition. Additionally, in murine models, the TT was even more efficient than the doxorubicin treatment and did not present visible toxicity in organs or tissues, and the animals had a longer survival rate than those under the control drug treatment (17, 26, 27). In the present work, we aimed to establish the apoptosis pathway induced by the TT in CC cell lines as a novel proposal to treat CC patients. Hence, we showed that the TT triggered tumor cell death by apoptosis through the caspase 3 intrinsic pathway. These results indicate that the combination of drugs that inhibit different tumor pathways, in this case aerobic glycolysis, nucleic acid synthesis, and complex I of the respiratory chain, has evident antitumor effects. The use of radio- and chemotherapy affects tumor cells with high proliferative rates. Therefore, inhibition of multiple pathways, including aberrant tumor metabolism in cancer therapy, should be considered.

2 Materials and methods

2.1 Reagents and cell culture

Doxorubicin (Doxolem® RU, 10 mg/5 ml) (Dox), metformin (Met) (1-1dimethylbiguanidine hydrochloride; sc-202000A, Santa Cruz Biotech, USA), and sodium oxamate (Ox) (sc-215880, Santa Cruz Biotech, USA) were diluted with DMEM/F12 medium (GIBCO, USA) supplemented with 2% FBS (ATCC 30-2020), with the following concentrations *in vitro*: 1.5 µM/25 mM/20 mM for dox/met/ox respectively, for 12 h, and 1 µM/20 mM/15 mM for dox/met/ox, respectively, for 24 h.

The human cervical cancer cell lines Hela, SiHa, and CaSki were purchased from the American Type Culture Collection (ATCC). All cells were cultured in DMEM/F12 medium supplemented with 10% FBS and 1% penicillin–streptomycin at 37°C in a humidified atmosphere of 95% air plus 5% CO_2, as recommended by ATCC.

2.2 Cytotoxicity assay

Cell viability was determined using the sulforhodamine (SRB) cell protein stain (42). Cancer cells were seeded in 96-well plates at a density of 10,000 cells/well and allowed to adhere overnight (24 h). After 24 h of incubation, the cells were treated with different doses of metformin (15, 20, 25, 30, 40 mM), sodium oxamate (10, 15, 20, 25, 30 mM), and doxorubicin (0.5, 1, 2, 3, 4 µM) in combination for 12 and 24 h. Cells were fixed with cold trichloroacetic acid 10% (TCA) (MERCK, USA) at 4°C for 1 h and then washed four times with tap water, followed by staining with 100 µl of 0.5% SRB (S9012-5G Sigma-Aldrich) in 1% acetic acid for 30 min at room temperature (RT). Excess stain was washed four times with 1% acetic acid. The stained cells were resuspended in 200 µl of 10 mM Tris, pH 10. The optical density at 510 nm was determined using an Epoch microplate spectrophotometer (BioTek). All the experiments were done in triplicate.

2.3 Apoptosis antibody array and Western blot

The Human Apoptosis Antibody Array Kit (RayBiotech, Inc., Norcross, USA) was used to evaluate the apoptotic protein expression according to the manufacturer's instructions. The

membranes were soaked in blocking buffer at RM for 30 min. Extracted protein (1 mg/ml) from HeLa cells with treatment at 12 h was added into each well containing the membranes and was left overnight at 4°C for incubation. The membrane was added with a biotinylated antibody cocktail and subsequently with HRP-streptavidin for incubation overnight at 4°C for incubation. A total of 500 µl of the detection buffer was pipetted onto the membrane for 5 min at RM. The membranes were transferred and exposed to a chemiluminescence C-DiGit scanner employing the Image Studio (LICOR, USA) software, then they were used to quantify the intensity of each array dot and then normalized to the internal control. All incubations and washes were performed under rotation (~0.5–1 cycle/s).

In order to determine specific proteins, Western blot analysis was done; briefly, cells were collected and lysed with RIPA buffer (Santa Cruz Biotechnology sc-24948) containing protease inhibitors for 30 min on ice and then centrifuged at 13,000*g* at 4°C for 25 min. The supernatant containing total protein was harvested. The concentration was detected using Bradford assay (Bio-Rad) according to the manufacturer's instructions. Thereafter, 25 µg of proteins was separated by 12% SDS-PAGE and transferred to polyvinylidene difluoride (PVDF) membranes (GE Healthcare, USA) in a semidry Trans-Blot Turbo chamber (Bio-Rad) at 25 V, 1 mA, for 30 min. The membranes were blocked with 5% non-fat milk in TBS containing 0.1% Tween 20 for 2 h. The membrane was incubated with specific primary antibodies Caspase-3 (1:3,000, sc-7148), Caspase-8 (1:2,000, sc-56070), and p21 (1:3,000, sc-397) from Santa Cruz Biotechnology; XIAP (1:1,000, ab28151) from Abcam; and BAX (1:1,000, 12105S) and BAK (1:1000, 5023S) from Cell Signaling Technology, overnight at 4°C on a rocking platform, washed, and then incubated with the corresponding secondary antibodies anti-mouse (1:5,000, sc-23719) and anti-rabbit (1:3,000, sc-2370) for 2 h at room temperature. The control for equal protein loading was assessed using an anti-β-actin antibody (1:5,000; sc-47778). The blot was visualized using the SuperSignal West Femto chemiluminescent substrate (Pierce) in the C-DiGit scanner (LICOR)™ employing the Image Studio (LI-COR) software. All the experiments were repeated in triplicate.

2.4 Flow cytometry: Annexin V-FITC apoptosis detection

Apoptosis was detected using Annexin V-FITC Apoptosis Detection Kit I (BD 556547) by flow cytometry according to the manufacturer's instructions. There are two distinct phases in the apoptotic process, termed early and late apoptosis, which can be distinguished with an intracellular staining assay. Annexin V (AV) and propidium iodide (IP) double staining can quantitatively distinguish viable cells from dead cells. Therefore, cells were distinguished into four groups in a scatter plot: viable cells (Annexin V-/IP-) in the lower-left quadrant, early apoptotic cells (Annexin V+/IP-) in the lower-right quadrant, late apoptotic cells together with secondary necrotic cells (Annexin V+/7-AAD+) in the upper-right quadrant, and necrotic cells (Annexin V-/IP+) in the upper-left quadrant. Cancer cells were seeded in six-well plates at a density of 500,000 cells/well and allowed to adhere overnight (24 h). Then, the cells were treated with the IC_{50} of TT for 12 and 24 h. Briefly, the treated cells were harvested by trypsin, washed with PBS, collected by centrifuging at 1,500*g* for 5 min, mixed with a binding buffer, and incubated with Annexin V-FITC and propidium iodide (PI) for 15 min at RT in the dark. Afterward, labeled cells were counted by flow cytometry within 30 min. All early apoptotic cells (Annexin V–positive, PI-negative), necrotic/late apoptotic cells (double positive), and living cells (double negative) were detected using a FACSCalibur flow cytometer and subsequently analyzed using CellQuest Pro software. All the experiments were performed in triplicate.

2.5 Terminal deoxynucleotidyl transferase dUTP nick end labelling assay

DNA damage is one of the main characteristics of apoptosis. The visualization of DNA damage is achieved with terminal deoxynucleotidyl transferase dUTP nick end labeling (TUNEL) staining, which is based on the ability of the enzyme deoxynucleotidyl transferase to catalyze the addition of nucleotide dUTP to the 3′ ends free of fragmented DNA. dUTPs that are FITC-labeled fluoresce when used, and apoptotic cells can be specifically identified. For this purpose, CC cell lines were used and kept in cover slides previously treated with polylysine in six-well plates with a density of 4 × 105 cells in each well with the conditions already mentioned and with 24 h of adherence. They were exposed to the pharmacological combination for 12 and 24 h. After the drug exposure time, the cells were fixed with 4% paraformaldehyde and, through the DeadEnd Fluorometric TUNEL System Cat. G3250 kit, apoptosis was evaluated according to the manufacturer's instructions. Finally, the cells were observed under a confocal microscope and the resulting images were analyzed using Illustrator software.

2.6 Wound healing assay

A wound healing assay was performed to assess migration. An adhesive tape was placed in six-well plates. The HeLa, SiHa, and CaSki cells were seeded (4×10^5 cells per well) and maintained with 2% FBS-supplemented medium to avoid cell proliferation at 37°C, and after 24 h of adhesion, the tape was removed to form the wound. These cells were treated with triple therapy or controls for 12 and 24 h. The cells were monitored at 0, 8, 12, and 24 h.

3 Results

3.1 TT-induced cytotoxicity against HeLa, SiHa, and CaSki cell lines

The triple therapy was evaluated at 12 and 24 h against the three CC cell lines at different concentrations. The time selected for this investigation was based on our previous research on colon and

breast cancers (26, 27), where the effect exerted by the TT inducing apoptosis and autophagy starts at short times (4 h). Moreover, in the breast cancer *in vivo* model, tumor reduction with the TT was initiated at 24 h (26). These results provided the timing used in this work. The percentage of cell growth inhibition (IC_{50}) depends on the concentration of the drug and is time-dependent (Figure 1). The IC_{50} values obtained for the three cell lines were 1.5 µM/25 mM/20 mM for dox/met/ox, respectively, in 12 h, and for 24 h, the IC_{50} values were 1 µM/20 mM/15 mM for dox/met/ox, respectively, and were employed for the other tests.

3.2 The apoptosis pathway is triggered by TT in HeLa cells

We first characterized the apoptotic response with the triple therapy using a protein profile involved in apoptosis carried out on HeLa cells. For this experiment, we detected the emission of light as a result of a chemical reaction (chemiluminescence) of each point that corresponds to a specific antibody. The microarray map of Figure 2A (untreated cells) and Figure 2B (cells treated with TT) shows the location of each protein. Figures 3C, D depict the overexpression of the pro-apoptotic proteins BAD, BAX, caspase 3, cytochrome C, CD40-R, CD40L, Fas-R, Fas-L, HTRA2, p21, p27, and SMAC. Also, anti-apoptotic proteins such as XIAP, survivin, HSP27, HSP60, and HASP70 were overexpressed after TT treatment for 12 h. The experiment was performed only at 12 h, time enough to demonstrate the apoptosis induction by the triple therapy. The other proteins had no change (Figure 3D). The signal intensity of the pro-apoptotic proteins p21, HTRA2, CD40-R, caspase-3, and Bax is remarkable (Figure 3D).

The next step was to corroborate the results obtained in the microarray by WB. Proteins involved in apoptosis were evaluated in the three CC cell lines. The IC_{50} values used were those detected for each time frame, as indicated in the Materials and Methods section. Figures 2A–C shows that the activity of caspase 3 is time-dependent, increasing to 24 h in all CC cell lines treated with TT. Such results could indicate the activation of the intrinsic pathway of apoptosis due to caspase 3 detection. Caspase 8 in HeLa had no change, corresponding to the data obtained in the microarray (Figure 3A). Contrarily, in SiHa an increase in caspase-8 detection is maintained from 8 to 24 h, whereas in CaSki, an increase in caspase-8 is observed up to 12 h and decreases at 24 h. Likewise, a rise of p21 in HeLa is observed (Figure 2). The detection of XIAP in the three cell lines decreases as the exposure time with TT expires, emphasizing the absence in HeLa and SiHa at 24 h.

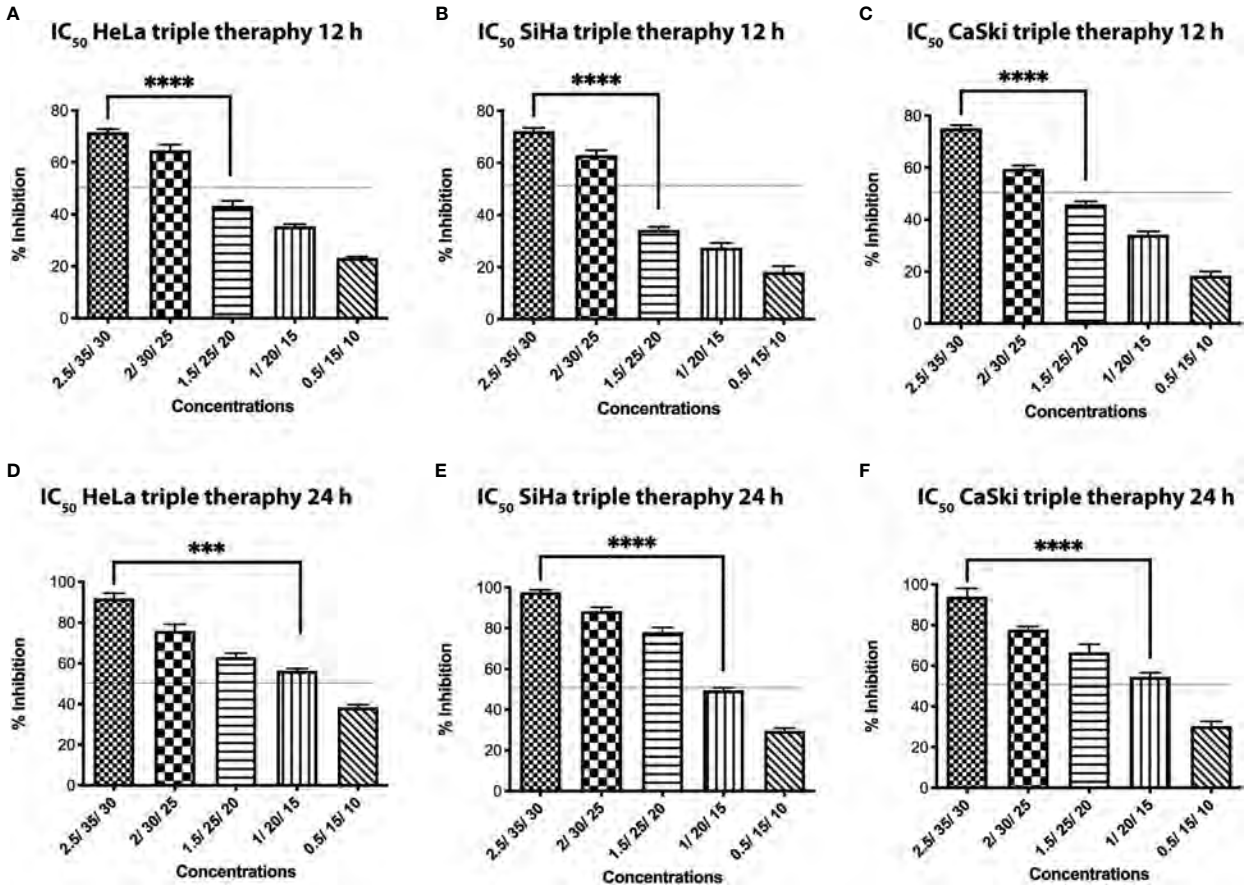


FIGURE 1
Inhibitory concentration of the TT at 12 **(A–C)** and 24 h **(D–F)** against Hela, SiHa, and CaSki cervical cancer cell lines. For all panels, *P* values were determined by the ANOVA test; ***P ≤ 0.001 ****P ≤ 0.0001.

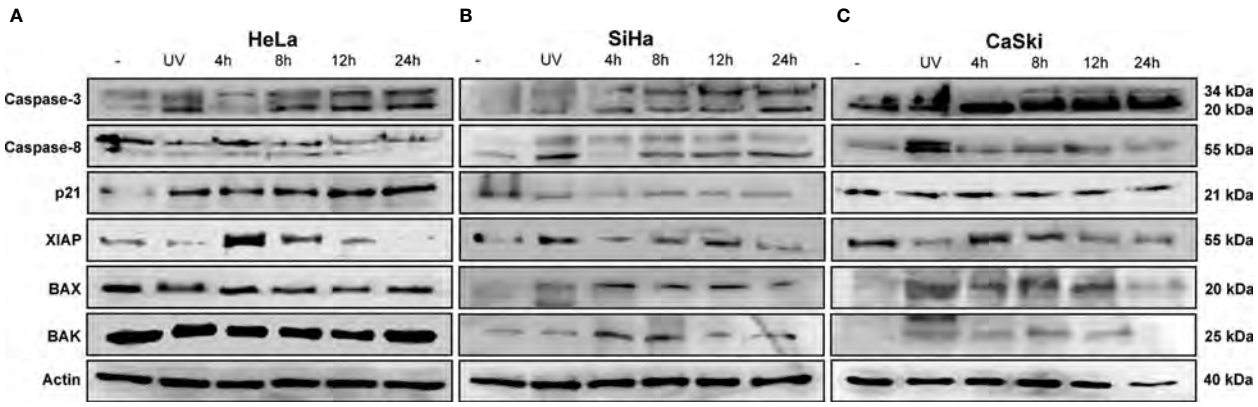


FIGURE 2
TT-induced intrinsic apoptosis by cleavage of caspase 3. **(A)** HeLa, **(B)** SiHa, and **(C)** CaSki CC cell lines. All cells were treated with the TT at 4, 8, 12, and 24 (h) UV radiation (positive control). The blots are a representative figure of at least three independent experiments.

Detection of BAX and BAK increased in the first hours of stimulation, although detection decreased after 24 h.

These findings together with the microarray assay and the Western blotting are complementary to each other. Information validates the proapoptotic proteins activated by the TT through caspase 3.

3.3 Early and late apoptoses are stimulated by the TT

The death of cervical cancer cells through the apoptotic pathway was analyzed by flow cytometry using the Annexin V/IP kit and the IC_{50} values previously mentioned. The TT produced late apoptosis in the three CC cell lines, above 60%, observed in the dot plots (Figure 4, right columns) compared with controls. In HeLa, the percentage of cells in apoptosis was 85.1% and 73.8% in 12 and 24 h, respectively. In SiHa, the apoptosis population corresponded to 76.6% and 84.4% in 12 and 24 h, respectively, whereas in CaSki late apoptosis was observed in 62.7% in 12 h and 54.1% in 24 h. Apoptosis induction by UV radiation over 50% was observed only in HeLa.

In summary, the TT requires 12 h to induce apoptosis in more than 60% of the three CC cell lines, keeping high percentages until 24 h over the positive control.

3.4 Morphological analysis revealed apoptotic bodies and DNA fragmentation due to the TT

Apoptosis is complex and implies many morphological changes for the cell, for example, membrane permeability, chromatin condensation, and cell shrinkage. The DNA fragmentation produced by the TT was visualized by confocal microscopy using the TUNEL assay. Figures 5A, B show the images of the cells taken after 12 and 24 h of TT stimulus. The formation of micronuclei, small extranuclear bodies that originate from fragments of chromatids and/or chromosomes that are left behind in the anaphase of dividing cells and are not included in the main nucleus during the telophase, is observed in TUNEL and MERGE marked with green. Likewise, DNA condensation is observed at the periphery of the nuclear membrane, forming a growing structure, whereas in the negative control, no DNA fragmentation is observed (Figure 5B MERGE).

In Figure 5B, for the three cell lines and the positive control (UV) in TUNEL and MERGE pictures, observed in green, the formation of apoptotic bodies and detection of fragmented DNA throughout the cell, characteristics of late apoptosis, is observed. Results are in congruence with the Annexin V/IP assay.

3.5 Triggering of intrinsic apoptosis is required for inhibition of the mTOR signaling pathway by triple therapy in cervical cancer cells

The master regulator, mTOR, plays a fundamental role in cell-cycle regulation, proliferation, apoptosis, and autophagy. To investigate the role of mTOR in triple therapy-induced apoptosis and autophagy, inhibition of mTOR and the substrate S6k was examined by Western blotting assay using phosphorylated antibodies. As shown in Figure 6, treatment with the triple therapy decreased the levels of phosphorylated mTOR and S6K in HeLa, SiHa, and CaSki cells. Our results displayed that the induction of intrinsic apoptosis through caspase-3 activation might be inhibiting the PI3K/AKT/mTOR signaling pathway. mTOR inhibition is an attractive therapeutic target in cancer due to its intervention in cellular functions such as cell survival or cell death (43), synthesis of biomolecules (44), and cell migration (45).

3.6 The TT suppressed the migration of cervical cancer cells *in vitro* at non-cytotoxic doses

Increasing evidence suggests that the mTOR pathway also plays a critical role in the regulation of cell migration. A wound healing

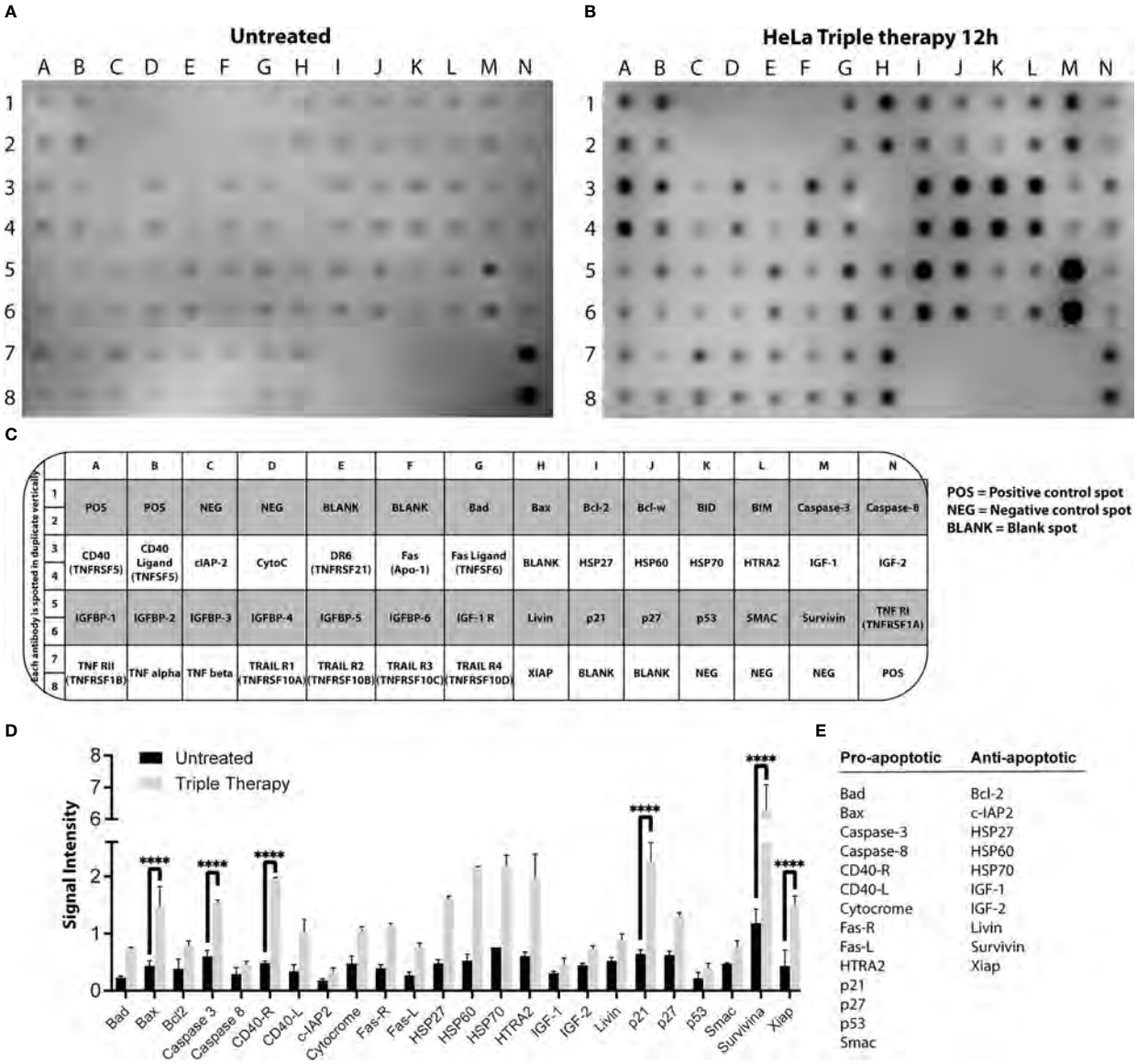


FIGURE 3
Profile of proteins involved in apoptosis in HeLa cells. Protein extracts of untreated cells **(A)** and treated cells **(B)** with the TT at 12 h of exposure. **(C)** Map array showing the location of apoptosis-related antibodies detected by the Apoptosis Kit. **(D)** Chemiluminescent intensities quantified by densitometry. A positive control was used to normalize the membrane results. **(E)** Proteins were selected and divided into two groups (pro-apoptotic or anti-apoptotic); *P* values were determined by two-way ANOVA test; ****P ≤ 0.0001.

assay was performed to test whether the triple therapy exerts an anti-migratory effect on cervical cancer cells. Cells were treated with the TT, doxorubicin, or untreated for 8, 12, and 24 h, respectively (Figure 7). Following treatment with the triple therapy for up to 24 h, cell migration was significantly inhibited, with a wound area of ~90.0% compared with the control of ~30% and doxorubicin in HeLa and CaSki ((Figure 7B). The control drug for this experiment was doxorubicin (positive control) to compare with the TT. These results suggest that the anti-migratory effects of the triple therapy may be potentially related to the induction of apoptosis and mTOR inhibition. In summary, the TT is a multitarget successful apoptosis-inducing combination.

4 Discussion

Cancer cells share several hallmarks that confer them a unique metabolism. However, the success of treatment not only depends on suppressing those characteristics but also on multifactorial events, such as sex, age, stage of disease, and response to treatment (43). The mentioned external factors establish different circumstances for treatment decisions turning the new therapeutic strategies into personal or individual medicine in the near future. In this context, our chemo design is optimistic. We propose a combination of three drugs targeting essential mechanisms of cell survival and proliferation, driving cancer cells to death in three

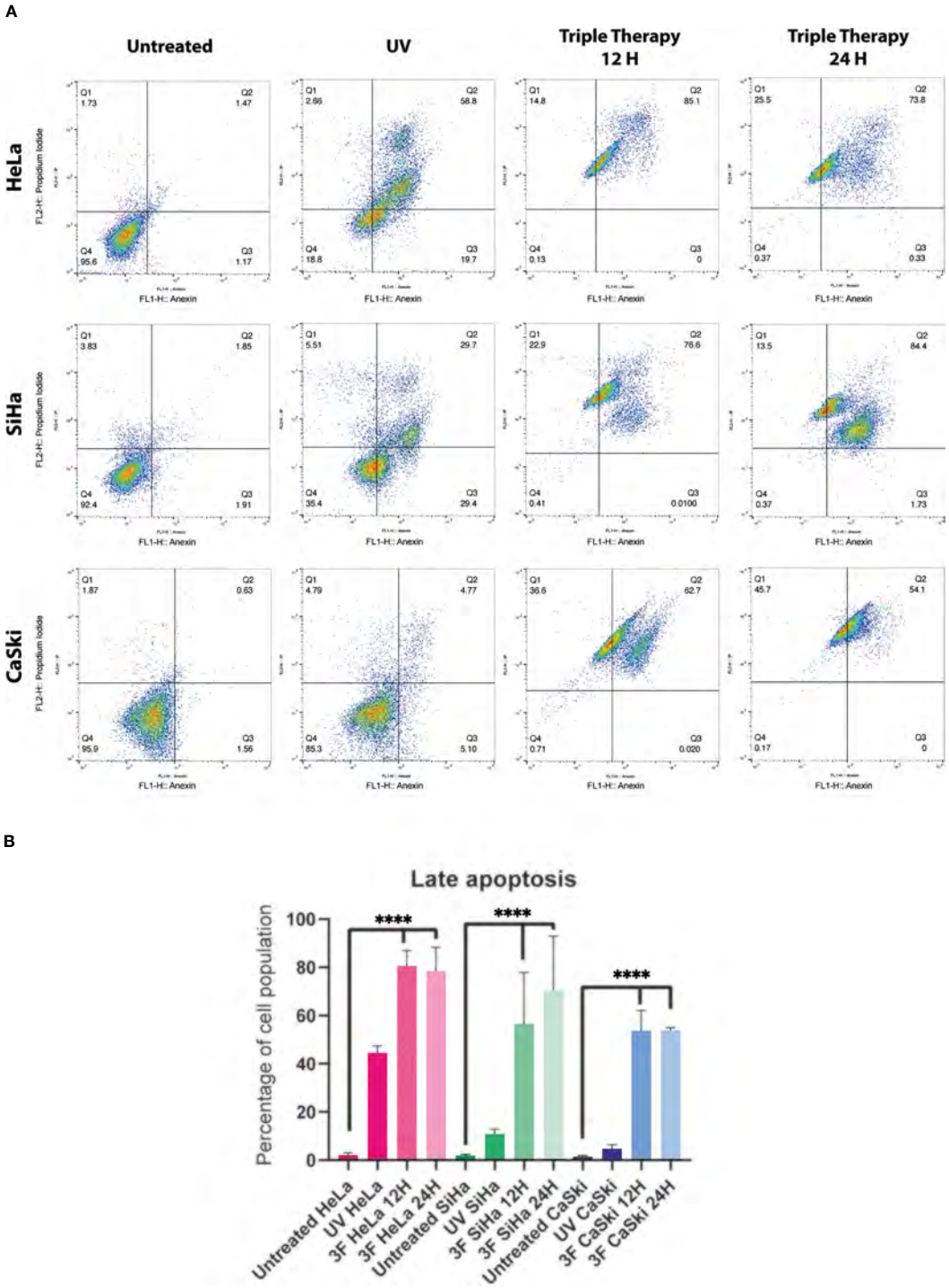


FIGURE 4
Dot plots from flow cytometry of Cervical cancer cells untreated, or treated with UV, or TT at 12 and 24 h of stimulation. **(A)** The dot plots are a representative image of at least three independent experiments. **(B)** The bar graph shows the percentage of cells undergoing apoptosis in response to triple therapy for 12 and 24 (h) *P* values were determined by ANOVA test; ****P ≤ 0.0001.

different CC cell lines. Hela cells correspond to the HPV-18 form, whereas SiHa and CaSki correspond to the HPV-16 genotype (44).

The mTOR pathway has been explored as a potential therapeutic target in cancer as it integrates two of the main signals in the regulation of cell growth activated by tyrosine kinase receptors and nutrients, including amino acids and glucose (45). One of the principal pathways leading to mTOR activation is PI3K/AKT (46), which plays an essential role in cancer progression. mTOR phosphorylates S6K, its major effector leading to protein synthesis and promoting cell survival by inhibiting the pro-apoptotic protein BAD. Furthermore, mTOR regulates autophagy characterized by the formation of autophagic vesicles and the

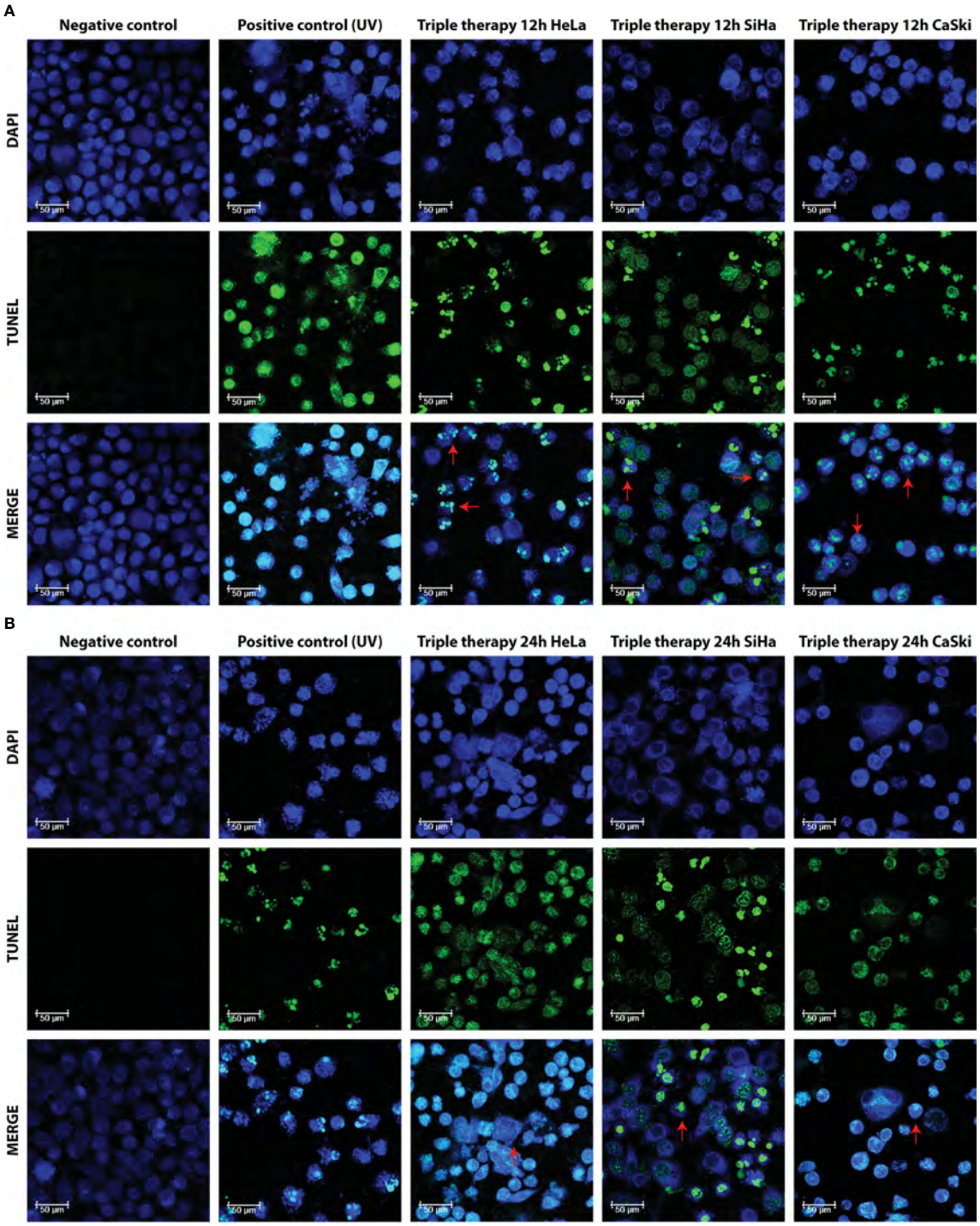


FIGURE 5
Morphological aspect of DNA fragmentation in HeLa, SiHa, and CaSki cells. Fluorescence images taken with LEICA confocal microscope at 63x with DAPI, TUNEL (dUTP cutoff marking of TUNEL deoxynucleotidyl transferase terminal), and MERGE markers in untreated cells (negative control), UV (positive control), and TT at 12 h **(A)** and 24 h **(B)** of exposure. Photos are representative of at least three independent experiments.

envelopment of organelles and proteins to recycle nutrients. Autophagy is activated mainly by the deprivation of nutrients such as glucose and amino acids. Therefore, the mTOR pathway is a sensor of the energy content of the cell, as it responds to AMP/ATP levels through AMPK, which inactivates mTOR when the AMP/ATP ratio increases. This event causes ULK1, ULK2, and Atg13 to be activated by phosphorylation leading to the initiation of autophagic vesicle conformation (47). Our findings indicate that TT involves the mTOR pathway to induce apoptosis in CC cell lines. Such an event is observed by the depletion of mTOR-activated levels when cells are stimulated with the TT (Figure 6, 12 h). According to these results and the previous ones obtained in colon

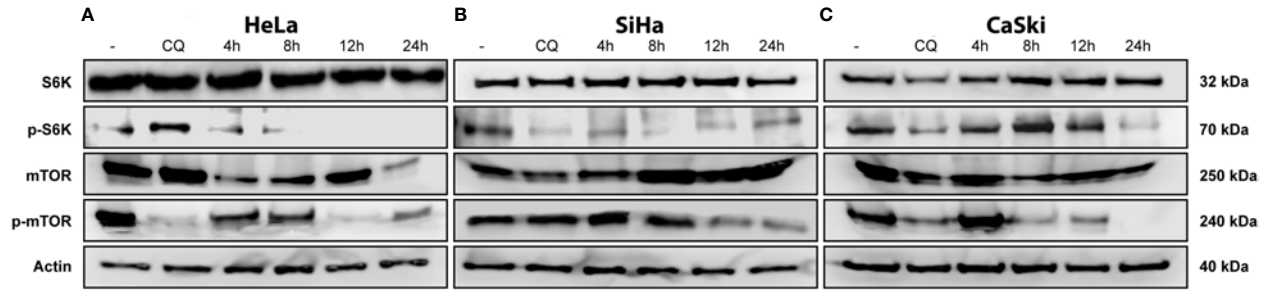


FIGURE 6
TT-induced suppression of the mTOR pathway. **(A)** HeLa, **(B)** SiHa, and **(C)** CaSki CC cell lines. All cells were treated with TT at 4, 8, 12, and 24 (h) Chloroquine (positive control). The blots are a representative figure of at least three independent experiments.

and breast cancers, we can suggest that the depletion of mTOR is due to the synergistic interaction of the drug combination. In summary, metformin induces apoptosis through inhibition of mTOR *via* AMPK activation (36, 48), sodium oxamate inhibits the lactate dehydrogenase enzyme and aerobic glycolysis (49), and doxorubicin interferes with DNA synthesis (50, 51). Each drug eventually triggers key cell pathways leading to cell death, assembling a novel and attractive therapeutic strategy for cancer treatment.

The mechanism of action of these drugs is based on the inhibition of the energy generation pathways of the tumor cell: glycolysis, the mTOR pathway, and DNA synthesis (29, 35, 39). Thus, the combined inhibition of the glycolytic pathway could lead to a complete depletion of cellular ATP and increment cell death (35, 45–49, 52). Metformin-induced activation of AMPK is associated with increased oxidative stress, cell-cycle arrest, and induction of apoptosis (53). The combination of phenformin (another biguanide) and oxamate increases the number of cells in late apoptosis in different cancer cells and increases ROS levels and DNA damage (35, 36, 45, 47–49). The mix of metformin and sodium oxamate induces cell death in 85% of cells in late apoptosis in melanoma cancer, (54) and there was a decrease in LDHA, lactate, and ATP levels (55). Our group (50) showed metformin and oxamate plus doxorubicin-induced late apoptosis, an increase of protein caspase-3, and a drop in PARP-1 in triple-negative breast cancer cells. In this study, we aimed to identify the apoptosis pathway activated by the three drugs in combination in cervical cancer. For this purpose, we performed flow cytometry, Western blot, and confocal microscopy as complementary techniques to settle the activation of apoptosis. Our results indicate that the TT induced late apoptosis (Figure 3).

The execution of intrinsic apoptosis is characterized by permeabilization of the mitochondrial outer membrane (MOMP), enabling the release of cytochrome C leading to apoptosome formation and subsequent cleavage and activation of effector caspases (3 and 7) (56); as observed with the triple-therapy treatment, there is an increase in the detection of cleaved caspase-3, but not cleavage caspase-8, which is involved in extrinsic apoptosis (57). Taken together, these data indicate that the triple therapy may trigger intrinsic apoptosis (Figure 2).

It was reported elsewhere that metformin (51) and oxamate (52, 58) induced the activation of proteins implicated in intrinsic apoptosis (59) (BAD, BAX, cytochrome-C, Apaf-1, caspase-9, caspase-3 and 7) and decreased antiapoptotic proteins such as Bcl-2 and XIAP. It has been demonstrated that in the presence of an apoptotic stimulus, mitochondrial survivin is released to the cytosol, (60) where it inhibits the activation of caspase-3 through its interaction with XIAP to continue proliferating (61); metformin decreases XIAP expression in colorectal cancer by STAT3 suppression (47).

The induction of early apoptosis is related to the activation of Bcl-2 family proteins, depolarization of mitochondria, and activation of caspases (62) and occurs approximately 30 min after the applied stimulus (63). In the case of late apoptosis, it occurs after caspase activation induces nuclear condensation and the formation of apoptotic bodies, in a time frame of 4 to 24 h depending on the stimulus (63). Our outcomes revealed that cells treated with the TT induce apoptosis by the intrinsic pathway *via* caspase 3. Based on our previous studies, this results in decreased glucose consumption, inhibition of cell growth, and proliferation signals by blocking the mTOR pathway, eventually inducing late apoptosis cell death (50, 64).

One strategy in the search for anticancer treatments is the use of drugs known to be utilized for other treatments whose mechanism of action is involved in some target of the tumor cell. This is known as drug repositioning (65, 66). Its advantages are its toxicological history, which helps in terms of safety, knowledge of collateral effects, effectiveness, and even reduction of costs. The success of the therapies will also depend on the multiple performances of the pharmacological proposal, in order to attack the tumor cell at several points simultaneously. Our research covers two main targets in cancer therapy, energy metabolism and the inhibition of cell proliferation, key steps to stop tumor growth, and subsequent invasion and metastasis.

The combination of Dox–Met–Ox is an excellent candidate for drug repositioning in cancer treatment. Together, they exerted *in vitro* apoptosis induction in cervix, colon, and breast cancer cell lines (50, 64). Moreover, their synergy showed tumor growth suppression and no accumulative or new detectable side effects *in vivo*. The drugs composing the TT are well characterized at therapeutically effective doses worthy of further study and go a step forward to clinical trials.

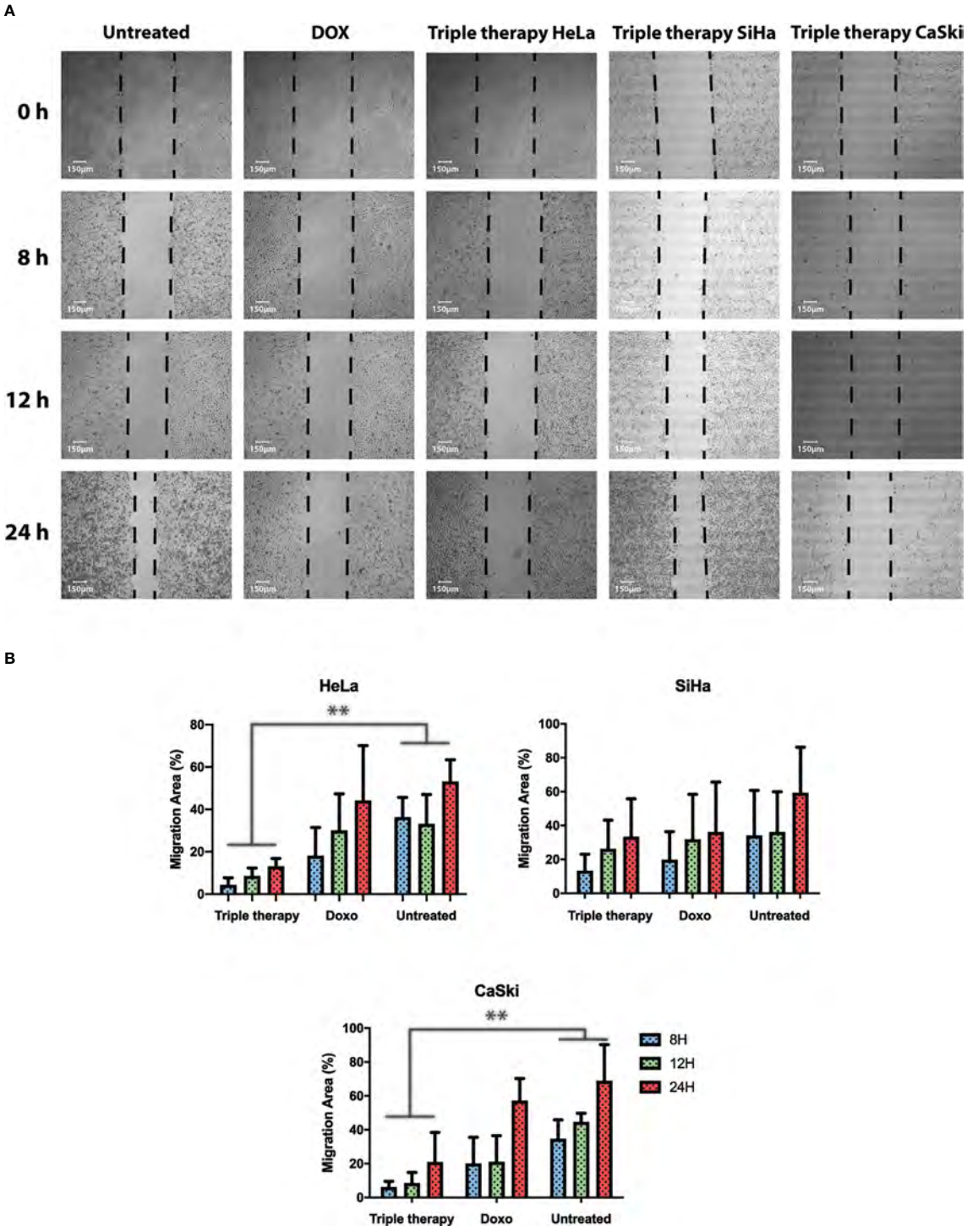


FIGURE 7
Triple therapy suppresses migration abilities in HeLa, SiHa, and CaSki cells compared with doxorubicin. A wound scratch assay was performed according to the procedure described in Materials and Methods in HeLa, SiHa, and CaSki. **(A)** Cell migration was observed at time 0 and 8, 12, and 24 h after scratching by photographs (magnification: 10×), and reduction of the initial scratch area was compared. **(B)** Quantitative analysis of the migration area was performed for HeLa, SiHa, and CaSki. All results are representative of three independent experiments. *P* values were determined by ANOVA test; **P ≤ 0.01.

All the backgrounds supporting the effectiveness and safety of metformin and oxamate, added to the metformin and doxorubicin success in the clinic, were taken together for our research group to propose them as a therapeutic option for a diverse of cancers.

Data availability statement

The original contributions presented in the study are included in the article/supplementary material. Further inquiries can be directed to the corresponding authors.

Author contributions

ID-W performed and analyzed *in vitro* experiments and participated in the discussion of the article. SS-A performed the microscopy experiments and analyzed results. CC, JP, IA and VG-C analyzed the results and NJ-H and CP-P were responsible for conceptualization, discussion, writing, and funding resources. All authors contributed to the article and approved the submitted version.

Funding

This work was supported by CONACYT, Mexico, project nos. CB-2016-285884 and UNAM/PAPIIT-IN231420.

Acknowledgments

This paper is part of the requirements for obtaining a doctoral degree at the Posgrado en Ciencias Biológicas, UNAM, of ID-W. Financing was granted by CONACYT for the scholarship no. 868414; NJ-H thanks CONACYT for the grant CB-2016-285884; C.P-P thanks UNAM/PAPIIT for the grant IN231420.

Conflict of interest

The authors declare that the research was conducted in the absence of any commercial or financial relationships that could be construed as a potential conflict of interest.

Publisher's note

All claims expressed in this article are solely those of the authors and do not necessarily represent those of their affiliated organizations, or those of the publisher, the editors and the reviewers. Any product that may be evaluated in this article, or claim that may be made by its manufacturer, is not guaranteed or endorsed by the publisher.

References

1. Siegel RL, Miller KD, Fuchs HE, Jemal A. Cancer statistics, 2022. *CA Cancer J Clin* (2022) 72(1):7–33. doi: 10.3322/caac.21708

2. Zhang H, Kong W, Chen S, Zhao X, Luo D, Xie Y. Surgical staging of locally advanced cervical cancer: current status and research progress. *Front Oncol* (2022) 12:3277. doi: 10.3389/fonc.2022.940807

3. Anand U, Dey A, Chandel AKS, Sanyal R, Mishra A, Pandey DK, et al. Cancer chemotherapy and beyond: current status, drug candidates, associated risks and progress in targeted therapeutics. *Genes Dis* (2022). doi: 10.1016/j.gendis.2022.02.007

4. Debela DT, Muzazu SG, Heraro KD, Ndalama MT, Mesele BW, Haile DC, et al. New approaches and procedures for cancer treatment: current perspectives. *SAGE Open Med* (2021) 9:205031212110343. doi: 10.1177/20503121211034366

5. Arunachalam SS, Shetty AP, Panniyadi N, Meena C, Kumari J, Rani B, et al. Study on knowledge of chemotherapy's adverse effects and their self-care ability to manage - the cancer survivors impact. *Clin Epidemiol Glob Health* (2021) 11:100765. doi: 10.1016/j.cegh.2021.100765

6. Pichler M, Steyrer J. Cost-effectiveness analysis of the use of immunotherapy in metastatic solid tumours in Austria by applying the ESMO-magnitude of clinical benefit scale (ESMO-MCBS) version 1.1. *ESMO Open* (2021) 6(4):100198. doi: 10.1016/j.esmoop.2021.100198

7. Alfarouk KO, Stock CM, Taylor S, Walsh M, Muddathir AK, Verduzco D, et al. Resistance to cancer chemotherapy: failure in drug response from ADME to p-gp. *Cancer Cell Int* (2015) 15(1):71. doi: 10.1186/s12935-015-0221-1

8. Bukowski K, Kciuk M, Kontek R. Mechanisms of multidrug resistance in cancer chemotherapy. *Int J Mol Sci* (2020) 21(9):3233. doi: 10.3390/ijms21093233

9. Wang X, Zhang H, Chen X. Drug resistance and combating drug resistance in cancer. *Cancer Drug Res* (2019) 2(2):141–60. doi: 10.20517/cdr.2019.10

10. Das T, Anand U, Pandey SK, Ashby CR, Assaraf YG, Chen ZS, et al. Therapeutic strategies to overcome taxane resistance in cancer. *Drug Resist Update* (2021) 55:100754. doi: 10.1016/j.drup.2021.100754

11. Maeda H, Khatami M. Analyses of repeated failures in cancer therapy for solid tumors: poor tumor-selective drug delivery, low therapeutic efficacy and unsustainable costs. *Clin Transl Med* (2018) 7(1):11. doi: 10.1186/s40169-018-0185-6

12. Chen Q, Cao HZ, Zheng PS, Chen Q, Cao HZ, Zheng PS. LGR5 promotes the proliferation and tumor formation of cervical cancer cells through the wnt/β-catenin signaling pathway. *Oncotarget* (2014) 5(19):9092–105. doi: 10.18632/oncotarget.2377

13. Coronel-Hernández J, Pérez-Yépez EA, Delgado-Waldo I, Contreras-Romero C, Jacobo-Herrera N, Cantú-De León D, et al. Aberrant metabolism as inductor of epigenetic changes in breast cancer: therapeutic opportunities. *Front Oncol* (2021) 11:3895. doi: 10.3389/fonc.2021.676562

14. Pavlova NN, Thompson CB. The emerging hallmarks of cancer metabolism. *Cell Metab* (2016) 23(1):27–47. doi: 10.1016/j.cmet.2015.12.006

15. Wang ZH, Peng WB, Zhang P, Yang XP, Zhou Q. Lactate in the tumour microenvironment: from immune modulation to therapy. *EBioMedicine* (2021) 73:103627. doi: 10.1016/j.ebiom.2021.103627

16. de la Cruz-López KG, Castro-Muñoz LJ, Reyes-Hernández DO, García-Carrancá A, Manzo-Merino J. Lactate in the regulation of tumor microenvironment and therapeutic approaches. *Front Oncol* (2019) 9:1143. doi: 10.3389/fonc.2019.01143

17. Salgado-García R, Coronel-Hernández J, Delgado-Waldo I, de León DC, García-Castillo V, López-Urrutia E, et al. Negative regulation of ulk1 by microrna-106a in autophagy induced by a triple drug combination in colorectal cancer cells *in vitro*. *Genes (Basel)* (2021) 12(2):1–14. doi: 10.3390/genes12020245

18. Sharma D, Singh M, Gupta R, Kumar V, Kumar V, Rani R. Intervention on lactate in cancer: a promising approach for the development of cancer therapeutics. *Adv Cancer Biol - Metastas* (2022) 5:100058. doi: 10.1016/j.adcanc.2022.100058

19. Koundouros N, Poulogiannis G. Reprogramming of fatty acid metabolism in cancer. *Br J Cancer* (2019) 122(1):4–22. doi: 10.1038/s41416-019-0650-z

20. Jeong DW, Lee S, Chun YS. How cancer cells remodel lipid metabolism: strategies targeting transcription factors. *Lipids Health Dis* (2021) 20(1):1–19. doi: 10.1186/s12944-021-01593-8

21. Schiliro C, Firestein BL. Mechanisms of metabolic reprogramming in cancer cells supporting enhanced growth and proliferation. *Cells* (2021) 10(5):1056. doi: 10.3390/cells10051056

22. Kılınç G, Sasani H, Erbaş O. The warburg effect on cancer formation and progression. *J Exp Bas Med Sci* (2022) 3(2):090–6. doi: 10.5606/jebms.2022.1014

23. Fukushi A, Kim H, Chang YC, Kim CH. Revisited metabolic control and reprogramming cancers by means of the warburg effect in tumor cells. *Int J Mol Sci* (2022) 23(17):10037. doi: 10.3390/ijms231710037

24. Hernández-Lemus E, Martínez-García M. Pathway-based drug-repurposing schemes in cancer: the role of translational bioinformatics. *Front Oncol* (2021) 10:2996. doi: 10.3389/fonc.2020.605680

25. Kirtonia A, Gala K, Fernandes SG, Pandya G, Pandey AK, Sethi G, et al. Repurposing of drugs: an attractive pharmacological strategy for cancer therapeutics. *Semin Cancer Biol* (2021) 68:258–78. doi: 10.1016/j.semcancer.2020.04.006

26. García-Castillo V, López-Urrutia E, Villanueva-Sánchez O, Ávila-Rodríguez MA, Zentella-Dehesa A, Cortés-González C, et al. Targeting metabolic remodeling in triple negative breast cancer in a murine model. *J Cancer* (2017) 8(2):178–89. doi: 10.7150/jca.16387

27. Figueroa-González G, García-Castillo V, Coronel-Hernández J, López-Urrutia E, León-Cabrera S, Arias-Romero LE, et al. Anti-inflammatory and antitumor activity of a triple therapy for a colitis-related colorectal cancer. *J Cancer* (2016) 7(12):1632–44. doi: 10.7150/jca.13123

28. Imai A, Ichigo S, Matsunami K, Takagi H, Yasuda K. Clinical benefits of metformin in gynecologic oncology. *Oncol Lett* (2015) 10(2):577–82. doi: 10.3892/ol.2015.3262

29. Fontaine E. Metformin-induced mitochondrial complex I inhibition: facts, uncertainties, and consequences. *Front Endocrinol (Lausanne)* (2018) 9:753. doi: 10.3389/fendo.2018.00753

30. Wu H, Huang D, Zhou H, Sima X, Wu Z, Sun Y, et al. Metformin: a promising drug for human cancers. *Oncol Lett* (2022) 24(1):204. doi: 10.3892/ol.2022.13325

31. Liu Y, Zhang Y, Jia K, Dong Y, Ma W. [Corrigendum] metformin inhibits the proliferation of A431 cells by modulating the PI3K/Akt signaling pathway. *Exp Ther Med* (2022) 24(1):1–1. doi: 10.3892/etm.2022.11372/abstract

32. Shen Z, Xue D, Wang K, Zhang F, Shi J, Jia B, et al. Metformin exerts an antitumor effect by inhibiting bladder cancer cell migration and growth, and promoting apoptosis through the PI3K/AKT/mTOR pathway. *BMC Urol* (2022) 22(1):1–10. doi: 10.1186/s12894-022-01027-2

33. Zheng Y, Zhang H, Sun H. Metformin inhibits the proliferation and invasion of ovarian cancer cells by suppressing tripartite motif-containing 37-induced tumor necrosis factor receptor-associated factor 2 ubiquitination. *Cancer Sci* (2022) 113 (11):3776–86. doi: 10.1111/cas.15524

34. Xu Y, Xu T, Xiong Y, Huang J. [Metformin inhibits proliferation and promotes apoptosis of HER-2 positive breast cancer cells possibly through the hippo-YAP pathway]. *Nan Fang Yi Ke Da Xue Xue Bao* (2022) 42(5):740–6. doi: 10.12122/j.issn.1673-4254.2022.05.16

35. Zhao Z, Han F, Yang S, Wu J, Zhan W. Oxamate-mediated inhibition of lactate dehydrogenase induces protective autophagy in gastric cancer cells: involvement of the akt-mTOR signaling pathway. *Cancer Lett* (2015) 358(1):17–26. doi: 10.1016/j.canlet.2014.11.046

36. Miskimins WK, Ahn HJ, Kim JY, Ryu S, Jung YS, Choi JY. Synergistic anti-cancer effect of phenformin and oxamate. *PloS One* (2014) 9(1):85576. doi: 10.1371/journal.pone.0085576

37. Yang Y, Su D, Zhao L, Zhang D, Xu J, Wan J, et al. Different effects of LDH-a inhibition by oxamate in non-small cell lung cancer cells. *Oncotarget* (2014) 5 (23):11886–96. doi: 10.18632/oncotarget.2620

38. Zhai X, Yang Y, Wan J, Zhu R, Wu Y. Inhibition of LDH-a by oxamate induces G2/M arrest, apoptosis and increases radiosensitivity in nasopharyngeal carcinoma cells. *Oncol Rep* (2013) 30(6):2983–91. doi: 10.3892/or.2013.2735

39. van der Zanden SY, Qiao X, Neefjes J. New insights into the activities and toxicities of the old anticancer drug doxorubicin. *FEBS J* (2021) 288(21):6095–111. doi: 10.1111/febs.15583

40. Kalyanaraman B. Teaching the basics of the mechanism of doxorubicin-induced cardiotoxicity: have we been barking up the wrong tree? *Redox Biol* (2020) 29:101394. doi: 10.1016/j.redox.2019.101394

41. Micallef I, Baron B. Doxorubicin: an overview of the anti-cancer and chemoresistance mechanisms. *Ann Clin Toxicol* (2020) 3(2):1031.

42. Vichai V, Kirtikara K. Sulforhodamine b colorimetric assay for cytotoxicity screening. *Nat Protoc* (2006) 1(3):1112–6. doi: 10.1038/nprot.2006.179

43. Zhu J, Wang H, Jiang X. mTORC1 beyond anabolic metabolism: regulation of cell death. *J Cell Biol* (2022) 221(12):221. doi: 10.1083/jcb.202208103

44. Yang M, Lu Y, Piao W, Jin H. The translational regulation in mTOR pathway. *Biomolecules* (2022) 12(6):802. doi: 10.3390/biom12060802

45. Huang S, Zhou H. Role of mTOR signaling in tumor cell motility, invasion and metastasis. *Curr Protein Pept Sci* (2011) 12(1):30–42. doi: 10.2174/138920311795659407

46. Zhang C, Zhang C, Wang Q, Li Z, Lin J, Wang H. Differences in stage of cancer at diagnosis, treatment, and survival by race and ethnicity among leading cancer types. *JAMA Netw Open* (2020) 3(4):e202950–e202950. doi: 10.1001/jamanetworkopen.2020.2950

47. Meissner JD. Nucleotide sequences and further characterization of human papillomavirus DNA present in the CaSki, SiHa and HeLa cervical carcinoma cell lines. *J Gen Virol* (1999) 80(7):1725–33. doi: 10.1099/0022-1317-80-7-1725

48. Inoki K, Corradetti MN, Guan KL. Dysregulation of the TSC-mTOR pathway in human disease. *Nat Genet* (2005) 37(1):19–24. doi: 10.1038/ng1494

49. Sekulić A, Hudson CC, Homme JL, Yin P, Otterness DM, Karnitz LM, et al. A direct linkage between the phosphoinositide 3-Kinase-AKT signaling pathway and the mammalian target of rapamycin in mitogen-stimulated and transformed Cells1. *Cancer Res | Am Assoc Cancer Res* (2000) 60(13):3504–13

50. Coronel-Hernández J, Salgado-García R, Cantú-De León D, Jacobo-Herrera N, Millan-Catalan O, Delgado-Waldo I, et al. Combination of metformin, sodium oxamate and doxorubicin induces apoptosis and autophagy in colorectal cancer cells via downregulation HIF-1α. *Front Oncol* (2021) 11:594200. doi: 10.3389/fonc.2021.594200

51. Shafiei-Irannejad V, Samadi N, Yousefi B, Salehi R, Velaei K, Zarghami N. Metformin enhances doxorubicin sensitivity via inhibition of doxorubicin efflux in p-gp-overexpressing MCF-7 cells. *Chem Biol Drug Des* (2018) 91(1):269–76. doi: 10.1111/cbdd.13078

52. Wu YT, Tan HL, Huang Q, Ong CN, Shen HM. Activation of the PI3K-Akt-mTOR signaling pathway promotes necrotic cell death via suppression of autophagy. *Autophagy* (2009) 5(6):824–34. doi: 10.4161/auto.9099

53. Dowling RJO, Zakikhani M, Fantus IG, Pollak M, Sonenberg N. Metformin inhibits mammalian target of rapamycin-dependent translation initiation in breast cancer cells. *Cancer Res* (2007) 67(22):10804–12. doi: 10.1158/0008-5472.CAN-07-2310

54. Chaube B, Malvi P, Singh SV, Mohammad N, Meena AS, Bhat MK. Targeting metabolic flexibility by simultaneously inhibiting respiratory complex I and lactate generation retards melanoma progression. *Oncotarget* (2015) 6(35):37281–99. doi: 10.18632/oncotarget.6134

55. Valvona CJ, Fillmore HL. Oxamate, but not selective targeting of LDH-a, inhibits medulloblastoma cell glycolysis, growth and motility. *Brain Sci* (2018) 8 (4):56. doi: 10.3390/brainsci8040056

56. Brentnall M, Rodriguez-Menocal L, De Guevara RL, Cepero E, Boise LH. Caspase-9, caspase-3 and caspase-7 have distinct roles during intrinsic apoptosis. *BMC Cell Biol* (2013) 14(1):1–9. doi: 10.1186/1471-2121-14-32

57. Beaudouin J, Liesche C, Aschenbrenner S, Hörner M, Eils R. Caspase-8 cleaves its substrates from the plasma membrane upon CD95-induced apoptosis. *Cell Death Differ* (2013) 20(4):599–610. doi: 10.1038/cdd.2012.156

58. Park JH, Kim Yh, Park EH, Lee SJ, Kim H, Kim A, et al. Effects of metformin and phenformin on apoptosis and epithelial-mesenchymal transition in chemoresistant rectal cancer. *Cancer Sci* (2019) 110(9):2834–45. doi: 10.1111/cas.14124

59. Chen H, Sun B, Sun H, Xu L, Wu G, Tu Z, et al. Bak instead of bax plays a key role in metformin-induced apoptosis s in HCT116 cells. *Cell Death Discov* (2021) 7 (1):1–9. doi: 10.1038/s41420-021-00755-y

60. Antonio Cheung CH, Huang CC, Tsai FY, Lee JYC, Cheng SM, Chang YC, et al. Survivin – biology and potential as a therapeutic target in oncology. *Onco Targets Ther* (2013) 6:1453. doi: 10.2147/OTT.S33374

61. Lu CC, Chiang JH, Tsai FJ, Hsu YM, Juan YN, Yang JS, et al. Metformin triggers the intrinsic apoptotic response in human AGS gastric adenocarcinoma cells by activating AMPK and suppressing mTOR/AKT signalling. *Int J Oncol* (2019) 54 (4):1271–81. doi: 10.3892/ijo.2019.4704/abstract

62. Rehm M, Huber HJ, Dussmann H, Prehn JHM. Systems analysis of effector caspase activation and its control by X-linked inhibitor of apoptosis protein. *EMBO J* (2006) 25(18):4338–49. doi: 10.1038/sj.emboj.7601295

63. Altinoz MA, Ozpinar A. Oxamate targeting aggressive cancers with special emphasis to brain tumors. *Biomed Pharmacother* (2022) 147:112686. doi: 10.1016/j.biopha.2022.112686

64. Qiao T, Xiong Y, Feng Y, Guo W, Zhou Y, Zhao J, et al. Inhibition of LDH-a by oxamate enhances the efficacy of anti-PD-1 treatment in an NSCLC humanized mouse model. *Front Oncol* (2021) 11:1033. doi: 10.3389/fonc.2021.632364

65. Lei Y, Yi Y, Liu Y, Liu X, Keller ET, Qian CN, et al. Metformin targets multiple signaling pathways in cancer. *Chin J Cancer* (2017) 36(1):1–9. doi: 10.1186/s40880-017-0184-9

66. Bouche G, Gedye C, Meheus L, Pantziarka P. Drug repurposing in oncology. *Lancet Oncol* (2020) 21(12):e542. doi: 10.1016/S1470-2045(20)30561-1